

# **Numerical Solution of Static and Dynamic Problems of Nanobeams and Nanoplates**

A THESIS

SUBMITTED FOR THE AWARD OF THE DEGREE

OF

**DOCTOR OF PHILOSOPHY**

**IN**

**MATHEMATICS**

*BY*

**LAXMI BEHERA**

**(Roll NO. 511MA105)**



**DEPARTMENT OF MATHEMATICS  
NATIONAL INSTITUTE OF TECHNOLOGY ROURKELA  
ROURKELA 769008, ODISHA, INDIA**

**AUGUST 2015**

# **Numerical Solution of Static and Dynamic Problems of Nanobeams and Nanoplates**

A THESIS

SUBMITTED FOR THE AWARD OF THE DEGREE

OF

**DOCTOR OF PHILOSOPHY  
IN  
MATHEMATICS**

*BY*

**LAXMI BEHERA**

**(Roll NO. 511MA105)**

**UNDER THE SUPERVISION OF**

**PROF. S. CHAKRAVERTY**



**DEPARTMENT OF MATHEMATICS  
NATIONAL INSTITUTE OF TECHNOLOGY ROURKELA  
ROURKELA 769008, ODISHA, INDIA**

**AUGUST 2015**



DEPARTMENT OF MATHEMATICS  
NATIONAL INSTITUTE OF TECHNOLOGY ROURKELA

## DECLARATION

I hereby declare that the work which is being presented in the thesis entitled “**Numerical Solution of Static and Dynamic Problems of Nanobeams and Nanoplates**” for the award of the degree of Doctor of Philosophy in Mathematics, submitted in the Department of Mathematics, National Institute of Technology Rourkela, Rourkela-769008, Odisha, India, is an authentic record of my own work carried out under the supervision of Prof. (Dr.) S. Chakraverty.

The matter embodied in this thesis has not been submitted by me for the award of any other degree.

Place: Rourkela

Date:

**LAXMI BEHERA**

(Roll No. 511MA105)

Department of Mathematics

Natioal Institute of Technology Rourkela

Rourkela 769008, Odisha, India



DEPARTMENT OF MATHEMATICS  
NATIONAL INSTITUTE OF TECHNOLOGY ROURKELA

## CERTIFICATE

It is certified that the thesis entitled “**Numerical Solution of Static and Dynamic Problems of Nanobeams and Nanoplates**” is being submitted by **Miss. Laxmi Behera** for the award of the degree of Doctor of Philosophy in Mathematics at National Institute of Technology Rourkela, Rourkela-769008, Odisha, India is a record of bonafide research work carried out by her under my supervision and guidance. Miss. Laxmi Behera has worked for four four years on the above problem in the Department of Mathematics, National Institute of Technology Rourkela and this thesis has reached the standard for fulfilling the requirements and the regulation relating to the degree. The contents of this thesis, in full or part, have not been submitted to any other university or institution for the award of any degree or diploma.

**Place:** Rourkela

**Date:**

**Dr. S. Chakraverty**

Professor, Department of Mathematics

National Institute of Technology Rourkela

Rourkela 769008, Odisha, India

*Dedicated*  
*to*  
*MY PARENTS and*  
*GOD*

# ACKNOWLEDGEMENTS

Completing the Ph.D. and writing this thesis was an amazing journey that would not have been without the support and encouragement of many outstanding people around me.

First and foremost, I would like to express my deep sense of gratitude and indebtedness to my supervisor Prof. S. Chakraverty, Professor, Department of Mathematics, National Institute of Technology Rourkela for his invaluable advice and guidance from the formative stage of this research and providing me extraordinary experiences throughout the work. His tireless working capacity, devotion towards research work as well as his clarity of presentation have strongly motivated me. Apart from the academic support, his friendly camaraderie even helps me to reach the divine feet of the almighty. I am also thankful to his family members for their continuous love, support and source of inspiration at all the time during my Ph.D. work.

I am grateful to Prof. S. K. Sarangi, Director, National Institute of Technology, Rourkela for providing excellent facilities in the Institute for carrying out research. Also I would like to thank the members of my doctoral scrutiny committee and all the faculty and staff members of the Department of Mathematics, National Institute of Technology Rourkela for their encouragement and suggestions during the preparation of this thesis.

Ministry of Human Resource Development (MHRD), Government of India is highly acknowledged for financial support through the Graduate Aptitude Test in Engineering (GATE).

I am indebted to my lab mates Diptiranjana, Smita, Sukant, Susmita, Karan, Deepti Moyi and Nisha Rani for their help and support during my stay in the laboratory and making it a memorable experience in my life.

I record my sincere apologies to those whose names I have inadvertently missed despite their meaningful contribution during the course of this work.

Most importantly, none of this would have been possible without the love and patience of my family. My family, to whom this dissertation is dedicated to, has been a constant source of love, concern, support and strength for all these four years. I would like to express my heartfelt gratitude to them.

I would like to thank all my friends and relatives for their co-operations and good wishes.

**Laxmi Behera**

# Contents

<b>Declaration</b>	<b>i</b>
<b>Certificate</b>	<b>ii</b>
<b>Acknowledgements</b>	<b>iv</b>
<b>Abstract</b>	<b>ix</b>
<b>1 Introduction</b>	<b>1</b>
1.1 Background . . . . .	1
1.2 Literature review . . . . .	5
1.2.1 Nanobeams . . . . .	5
1.2.2 Nanoplates . . . . .	8
1.3 Gaps . . . . .	9
1.4 Aims and objectives . . . . .	10
1.5 Organization of the thesis . . . . .	10
1.6 Preliminaries . . . . .	13
1.6.1 Review of nonlocal elasticity theory . . . . .	13
1.6.2 Beam theories . . . . .	13
1.6.3 Plate theory . . . . .	18
<b>2 Numerical methods</b>	<b>20</b>
2.1 Rayleigh-Ritz method . . . . .	20
2.1.1 Bending problems . . . . .	20
2.1.2 Vibration problems . . . . .	24
2.2 Plate theory . . . . .	25
2.2.1 Classical plate theory . . . . .	26
2.3 Differential quadrature method (DQM) . . . . .	29
2.3.1 Buckling problems . . . . .	29
2.3.2 Euler Bernoulli beam theory (EBT) . . . . .	30
2.3.3 Timoshenko beam theory (TBT) . . . . .	30
2.3.4 Reddy beam theory (RBT) . . . . .	30
2.3.5 Levinson beam theory (LBT) . . . . .	31
2.3.6 Vibration problems . . . . .	31
2.3.7 Euler-Bernoulli beam theory (EBT) . . . . .	31

2.3.8	Timoshenko beam theory (TBT)	31
2.3.9	Reddy beam theory (RBT)	32
2.3.10	Levinson beam theory (LBT)	32
<b>3</b>	<b>Bending and buckling of nanobeams</b>	<b>37</b>
3.1	Numerical results and discussions	39
3.1.1	Effect of aspect ratio	40
3.1.2	Effect of scale coefficient	40
3.1.3	Effect of boundary conditions	41
3.1.4	Deflection and rotation shapes	41
3.2	Numerical results and discussions	46
3.2.1	Convergence	46
3.2.2	Validation	47
3.2.3	Effect of small scale	49
3.2.4	Effect of non-uniform parameter	50
3.2.5	Effect of aspect ratio	51
3.2.6	Effect of various beam theories	52
3.2.7	Effect of boundary condition	53
3.3	Numerical results and discussions	58
3.3.1	Convergence	58
3.3.2	Validation	60
3.3.3	Effect of Winkler modulus parameter	61
3.3.4	Effect of Pasternak shear modulus parameter	63
3.3.5	Effect of temperature	65
3.3.6	Effect of aspect ratio	67
3.4	Conclusions	67
<b>4</b>	<b>Bending and buckling of nanoplates</b>	<b>69</b>
4.1	Numerical results and discussions	70
4.1.1	Convergence	70
4.1.2	Validation	70
4.1.3	Effect of aspect ratio	71
4.1.4	Effect of length	72
4.1.5	Effect of nonlocal parameter	72
4.2	Numerical results and discussions	74
4.2.1	Convergence	74
4.2.2	Validation	75
4.2.3	Effect of length	75
4.2.4	Effect of aspect ratio	76
4.2.5	Effect of stiffness ratio	77
4.2.6	Effect of nonlocal parameter	77
4.2.7	Effect of elastic foundation	78
4.3	Conclusions	79



<b>5</b>	<b>Vibration of nanobeams</b>	<b>80</b>
5.1	Numerical results and discussions . . . . .	81
5.2	Numerical results and discussions . . . . .	90
5.2.1	Convergence . . . . .	90
5.2.2	Validation . . . . .	90
5.2.3	Effect of nonlocal parameter . . . . .	92
5.2.4	Effect of various beam theories . . . . .	96
5.2.5	Effect of boundary conditions . . . . .	98
5.2.6	Effect of aspect ratio . . . . .	98
5.3	Conclusions . . . . .	99
<b>6</b>	<b>Vibration of nanobeams with complicating effects</b>	<b>100</b>
6.1	Numerical results and discussions . . . . .	102
6.1.1	Convergence . . . . .	102
6.1.2	Validation . . . . .	103
6.1.3	Effect of non-uniform parameter . . . . .	104
6.1.4	Effect of small scale parameter . . . . .	108
6.1.5	Effect of boundary condition . . . . .	109
6.1.6	Effect of aspect ratio . . . . .	109
6.1.7	Mode shapes . . . . .	110
6.2	EBT . . . . .	112
6.3	TBT . . . . .	113
6.4	RBT . . . . .	115
6.5	Numerical results and discussions . . . . .	116
6.5.1	Convergence . . . . .	116
6.5.2	Validation . . . . .	118
6.5.3	Effect of Winkler modulus parameter . . . . .	119
6.5.4	Effect of Pasternak shear modulus parameter . . . . .	121
6.5.5	Effect of temperature . . . . .	123
6.5.6	Effect of aspect ratio . . . . .	124
6.6	Conclusions . . . . .	125
<b>7</b>	<b>Vibration of nanoplates</b>	<b>126</b>
7.1	Numerical results and discussions . . . . .	127
7.1.1	Convergence . . . . .	127
7.1.2	Validation . . . . .	128
7.1.3	New results . . . . .	129
7.1.4	Effect of aspect ratio . . . . .	131
7.1.5	Effect of nonlocal parameter . . . . .	132
7.1.6	Effect of length . . . . .	133
7.1.7	Mode shapes . . . . .	134
7.2	Conclusions . . . . .	135

<b>8</b>	<b>Vibration of nanoplates with complicating effects</b>	<b>136</b>
8.1	Numerical results and discussions . . . . .	137
8.1.1	Convergence . . . . .	137
8.1.2	Validation . . . . .	138
8.1.3	Effect of non-uniform parameter . . . . .	139
8.1.4	Effect of length . . . . .	141
8.1.5	Effect of aspect ratio . . . . .	142
8.1.6	Effect of nonlocal parameter . . . . .	143
8.1.7	Effect of elastic foundation . . . . .	144
8.1.8	Mode shapes . . . . .	145
8.2	Conclusion . . . . .	146
<b>9</b>	<b>Conclusions and future directions</b>	<b>147</b>
9.1	Conclusions . . . . .	147
9.2	Future directions . . . . .	150
	<b>References</b>	<b>151</b>
	<b>List of publications</b>	<b>161</b>

# Abstract

Recently nanotechnology has become a challenging area of research. Accordingly, a new class of materials with revolutionary properties and devices with enhanced functionality has been developed by various researchers. Structural elements such as beams, membranes and plates in micro or nanoscale have a vast range of applications. Conducting experiments at nanoscale size is quite difficult and so development of appropriate mathematical models plays an important role. Among various size dependent theories, nonlocal elasticity theory pioneered by Eringen is being increasingly used for reliable and better analysis of nanostructures. Finding solutions for governing partial differential equations are the key factor in static and dynamic analyses of nanostructures. It is sometimes difficult to find exact or closed-form solutions for these differential equations. As such, few approximate methods have been developed by other researchers. But, the existing methods may not handle all sets of boundary conditions and sometimes those are problem dependent. Accordingly, computationally efficient numerical methods have been developed here for better understanding of static and dynamic behaviors of nanostructures. Also these numerical methods can handle all classical boundary conditions of the static and dynamic problems of nanobeams and nanoplates with ease.

It may be noted that application of numerical methods converts bending problem to system of equations while buckling and vibration problems to generalized eigen value problems. The present thesis first investigates bending of nanobeams and nanoplates. Next buckling and vibration of the above nanostructural members are studied by solving the corresponding partial differential equations. In the above regard, various beam and plate theories are considered for the analysis and corresponding results are reported after the convergence study and validation in special cases wherever possible. Finally, few complicating effects are also considered in some of the problems. As regards, structural members (nanobeams and nanoplates) with variable material properties are frequently used in engineering applications to satisfy various requirements. For efficient design of nanostructures, sometimes non-uniform material properties of the nano-components should also be studied. As such, we have considered here non-uniform material properties of nanobeams and nanoplates and investigated the deflection in static problems and vibration characteristics in vibration problems. Similarly, other complicating effects such as surrounding medium and temperature are important in the nanotechnology applications too. Accordingly, the effect of these complicating effects on the nanobeams and nanoplates have also been investigated in detail.

It is worth mentioning that Rayleigh-Ritz and differential quadrature methods have been used to solve the above said problems. In the Rayleigh-Ritz method, simple and boundary characteristic orthogonal polynomials have been used as shape functions. Use of boundary characteristic orthogonal polynomials in the Rayleigh-Ritz method has some advantages over other shape

functions. This is because of the fact that some of the entries of stiffness, mass and buckling matrices become either one or zero. On the other hand, Differential Quadrature (DQ) method is also a computationally efficient method which can be used to solve higher order partial differential equations that may handle all sets of classical boundary conditions. Accordingly DQ method has also been used in solving the problems of nanobeams with complicating effects.

In view of the above, systematic study of static and dynamic problems of nanobeams and nanoplates are done after reviewing the existing ones. Various new results of the above problems are reported in term of Figures and Tables. The new results obtained through the above mathematical models may serve as bench mark and those may certainly be used by design engineers and practitioners to validate their experimental work for better design of the related nanostructures.

**Keywords:** Boundary characteristic orthogonal polynomials, Chebyshev polynomials, vibration, buckling, bending, nanobeams, nanoplates, mode shapes, aspect ratio, length, nanostructures.

# **Chapter 1**

## **Introduction**

# Chapter 1

## Introduction

### 1.1 Background

Nanotechnology is concerned with the fabrication of functional materials and systems at the atomic and molecular levels. Recently, development of nanotechnology enables a new generation of materials with revolutionary properties and devices with enhanced functionality (Ansari and Sahmani 2011) having a vast range of applications, such as in medicine, electronics, biomaterials and energy production (Şimşek and Yurtcu 2013). Recently nanomaterials have encouraged the interest of the scientific researchers in mathematics, physics, chemistry and engineering. These nanomaterials have outstanding mechanical, chemical, electrical, optical and electronic properties. Because of these properties, the nanomaterials are perceived to be the components for various nanoelectromechanical systems and nanocomposites. Some of the common examples of these nanomaterials are nanoparticles, nanowires and nanotubes (viz. carbon nanotubes, ZnO nanotubes), etc. Nanomaterials are the basis material of many nanoscale objects which are referred to as nanostructures (Murmu and Adhikari 2010a). It is thus quite important to have proper knowledge of mechanical behavior for the development of nanostructures. Studying the behavior of structures at very small length scales has become one of new frontier of research in the area of computational nanomechanics (Ansari and Sahmani 2011). Structural elements such as beams, sheets and plates in micro or nanolength scale which are commonly used as components in microelectromechanical systems (MEMS) or nanoelectromechanical systems (NEMS) devices (Lu et al. 2007), present a significant challenge to researchers in nanomechanics (Mahmoud et al. 2012). Invention of carbon nanotubes (CNTs) by Ijima in 1991 has initiated a new era in nano-world (Danesh et al. 2012). Some of the excellent properties of CNTs are high stiffness, low density, very high aspect ratio, remarkable electronic properties, high conductivity and high strength (Ehteshami and Hajabasi 2011). Some of the applications of CNTs include atomic force microscopes (AFMs), field emitters, nanofillers for composite materials and nanoscale electronic devices. They are also used for the development of superconductive devices for microelectromechanical (MEM) and nano-

electromechanical (NEM) system applications (Wang and Varadan 2006). Therefore, research on CNTs may contribute to some new applications (Wang and Varadan 2006). Hence static and dynamic behaviors of CNTs have become one of the interesting topic in the past few years.

Similar to CNTs, nanoplates in the form of graphene sheets have aroused interest due to their unique superior properties. Graphene sheets are commonly used as components in MEMS/NEMS devices such as resonators, mass sensors and atomistic dust detectors (Farajpour et al. 2011). Nanoplates may be used as thin film elements, nanosheet resonators and paddle like resonators (Aksencer and Aydogdu 2012).

Conducting experiments at nanoscale size is quite difficult and expensive. In this regard, development of appropriate mathematical models for nanostructures (such as graphene, carbon nanotube, nanorod, nanofibre etc.) became an important concern (Pradhan and Phadikar 2009b). Generally three approaches such as atomistic, hybrid atomistic-continuum mechanics and continuum mechanics have been developed to model nanostructures (Narendar and Gopalakrishnan 2012). Some of atomistic approaches are classical Molecular Dynamics (MD), Tight Binding Molecular Dynamics (TBMD) and Density Functional Theory (DFT) (Wang and Varadan 2006). But the atomic methods are limited to systems with a small number of molecules and atoms. As such, it is restricted to the study of small scale modeling (Wang and Varadan 2006). Also this approach is computationally intensive and very expensive (Pradhan and Phadikar 2009a). Continuum mechanics results are found to be in good agreement with those obtained from atomistic and hybrid approaches (Narendar and Gopalakrishnan 2012).

Small scale of nanotechnology's makes the applicability of classical or local continuum models such as beam, shell and plate questionable. Classical continuum models do not admit intrinsic size dependence in the elastic solutions of inclusions and inhomogeneities. At nanoscale size, the material microstructure such as lattice spacing between individual atoms becomes increasingly important and the discrete structure of the material can no longer be homogenized into a continuum. It is therefore needed to extend continuum models for considering scale effect in nanomaterial studies. As the length scales are reduced, the influences of long range interatomic and intermolecular cohesive forces on the static and dynamic properties become significant and thus could not be neglected. Classical continuum mechanics exclude these effects and thus fail to capture the small scale effects when dealing with nanostructures. It is found that small size analysis using local theory over predicts the results. Therefore it is quite necessary to consider small effects for correct prediction of nanostructures (Narendar and Gopalakrishnan 2012). Small scale effects and the atomic forces must be incorporated in the realistic design of the nanostructures [viz., nanoresonators, nanoactuators, nanomachines and nanooptomechanical Systems] to achieve solutions with acceptable accuracy. Both experimental and atomistic simulation results show that when the dimensions of the structures become small then the size

effect has significant role in the mechanical properties (Murmu and Adhikari 2010a). Classical continuum models are scale free theory and it does not include the effects arising from the small scale (Murmu and Adhikari 2010a). As such, various size-dependent continuum models such as strain gradient theory (Nix and Gao 1998), couple stress theory (Hadjesfandiari and Dargush 2011), modified couple stress theory (Asghari et al. 2010) and nonlocal elasticity theory (Eringen 1997) came into existence. Among these theories, nonlocal elasticity theory pioneered by Eringen has been widely used by the researchers (Thai 2012). Recent literature shows that nonlocal elasticity theory is being increasingly used for reliable and better analysis of nanostructures (Murmu and Adhikari 2010a). Applications of nonlocal continuum mechanics include lattice dispersion of elastic waves, fracture mechanics, dislocation mechanics and wave propagation in composites (Aydogdu 2009). Generally, nonlocal elasticity theory is used in two forms that is nonlocal differential elasticity and nonlocal integral elasticity (Ghannadpour et al. 2013). But nonlocal differential elasticity is more popular due to its simplicity (Ghannadpour et al. 2013). In nonlocal elasticity theory, the stress at a point is a function of the strains at all points in the domain whereas in classical continuum models, the stress at a point is a function of the strains at that points in the domain (Murmu and Adhikari 2010a).

In the last few years, there has been extensive research on the bending, free vibration and buckling of nanostructures based on nonlocal elasticity theory. Vibration analysis of nanostructures include applications in structural engineering such as long span bridges, aerospace vehicles, automobiles and many other industrial usages. When nanostructure-elements are subjected to compressive inplane loads then, these structures may buckle (Emam 2013). It is well known fact that buckling of a nanostructure initiates instability. In this context, knowledge of buckling load is quite necessary. As such, proper understanding of the stability response under in plane loads for nanostructures is quite necessary.

Beam theories such as Euler-Bernoulli beam theory (EBT), Timoshenko beam theory (TBT), Reddy-Bickford beam theory (RBT), general exponential shear deformation beam theory (ABT), Levinson beam theory (LBT) and plate theories such as classical plate theory (CPT), first-order shear deformation plate theory (FSDT), third-order shear deformation plate theory (TSDT) etc. have been developed by various researchers (Wang et al. 2000).

In Euler-Bernoulli beam theory, both transverse shear and transverse normal strains are neglected. In Timoshenko beam theory, a constant state of transverse shear strain and also shear stress with respect to the thickness coordinate is included. Due to this constant shear stress assumption, shear correction factors are needed to compensate the error. Shear correction factors depend on the material and geometric parameters, the loading and boundary conditions. Next, we have different third order beam theories such as Reddy-Bickford beam theory (RBT), Levinson beam theory (LBT) etc. In these theories, shear correction factors are not needed



(Wang et al. 2000). Levinson derived equations of equilibrium using vector approach. As such, governing equations are same as those of Timoshenko beam theory. But Reddy derived equations of motion using the principle of virtual displacements. Thus Reddy (Reddy 1997) and Levinson beam theories have same displacement and strain fields with different equations of motion. One may also note that the equations of Levinson's beam theory cannot be derived from the principle of total potential energy (Reddy 2007).

In classical plate theory, both transverse shear and transverse normal strains are neglected. In FSDT, transverse shear strain is assumed to be constant with respect to the thickness coordinate. As such, shear correction factors are taken into consideration to compensate the error. Similar to third-order beam theories, shear correction factors are not needed in third-order plate theories (Wang et al. 2000).

Structural members with variable material properties are frequently used in engineering to satisfy various requirements. The literature reveals that previous studies done in nanobeams and nanoplates are mostly with constant parameters. But in actual practice, there may be a variation in these parameters. Hence for practical applications of nanobeams and nanoplates, one should investigate geometrically non-linearity model of nanostructures. Study of various aspects of nanotubes such as bending, buckling and thermal properties etc. has attracted considerable attentions among the researcher of nanotechnology. Thermal effects can induce an axial force within CNTs which may lead to bending and buckling (Lee and Chang 2009). Thermal vibration frequencies may be used to estimate Young's modulus of various nanotubes. Therefore, investigation of thermal effect is having great importance. Moreover, the surrounding elastic medium such as Winkler-type and Pasternak-type elastic foundation has also a great influence on the analysis of carbon nanotubes.

As mentioned in the above paragraphs, conducting experiments at nanoscale size is quite difficult to handle. In this regard, mathematical modeling of nanostructures is quite necessary. In all of the above said problems, differential equations play a vital role. These are solved by using analytical methods in simple cases and solutions have been given for few boundary conditions. Unfortunately, these analytical methods are not capable of handling all sets of boundary conditions. Also, exact or closed-form solutions for the governing differential equations may sometimes be difficult. In this regard, one may seek approximate solution of the above problems. Accordingly, computationally efficient numerical methods are developed here which may suit to investigate the static and dynamic behaviors of nanostructures (nanobeams and nanoplates) with all classical boundary conditions.

## 1.2 Literature review

In this section, we have discussed some of the relevant works that have been carried out by the previous authors. First we have discussed below bending, buckling and vibration of nanobeams and then the nanoplates.

### 1.2.1 Nanobeams

Here, we have shown some of the relevant works related to bending, buckling and vibration of nanobeams.

#### 1.2.1.1 Bending

Reddy (2007) reformulated various nonlocal beam theories such as Euler-Bernoulli, Timoshenko, Reddy and Levinson used for the study of bending, buckling and vibration of nanobeams. Equations of motion of the above beam theories are presented along with analytical solutions for simply-supported edge condition. In another work, Reddy and Pang (2008) presented analytical solutions for bending, buckling, and vibration of nanobeams subjected to four sets of boundary conditions. Aydogdu (2009) developed a general nonlocal beam theory to derive governing equations from which all the well known beam theories have been obtained. A nonlocal shear deformation beam theory has been proposed by Thai (2012) which has strong similarities with nonlocal Euler-Bernoulli beam theory with respect to the equations of motion, boundary conditions and stress resultant expressions. Analytical solutions have also been presented for a nonlocal sinusoidal shear deformation beam theory (Thai and Vo 2012). Şimşek and Yurtcu (2013) examined bending and buckling of a functionally graded (FG) nanobeam based on nonlocal Timoshenko and Euler-Bernoulli beam theories. Analytical solutions have been presented by Wang et al. (2006) for bending of nanobeams based on nonlocal Timoshenko beam theory. Some of the numerical methods such as Ritz and Differential Quadrature (Wang and Bert 1993; Janghorban and Zare 2011 ) have also been developed for bending analysis of nanobeams. Ghannadpour et al. (2013) applied Ritz method to study bending, buckling and vibration analyses of nonlocal Euler beams. Civalek and Demir (2011) used Differential Quadrature method to investigate buckling and bending analyses of cantilever carbon nanotubes based on Euler-Bernoulli beam theory. Alshorbagy et al. (2013) applied finite element method for static analysis of nanobeams based on nonlocal Euler-Bernoulli beam theory. Similarly, finite element method has also been applied by Eltahaer et al. (2013a) to analyse static and stability of functionally graded nanobeams. Civalek and Akgöz (2009) presented deflection shapes and bending moment for nonlocal Euler-Bernoulli beams subjected to different boundary conditions. Bending analysis of tapered nanowires with circular cross section has been investigated by Janghorban (2012).

### 1.2.1.2 Buckling

Buckling analysis of nano rods/tubes has been investigated analytically by Wang et al. (2006) based on nonlocal Euler-Bernoulli and Timoshenko beam theories. Static nonlinear postbuckling response of nanobeams has been studied analytically by Emam (2013) and the results show that as the nonlocal parameter increases, critical buckling load reduces. Some of the other studies based on analytical methods are: (Aydogdu 2009; Thai 2012; Reddy and Pang 2008; Kumar et al. 2008; Şimşek and Yurtcu 2013; Yang and Lim 2011). One of the numerical methods such as Rayleigh-Ritz method has been employed in some of the studies such as buckling analysis of single-walled carbon nanotubes in thermal environments (Ansari et al. 2011a, 2011b), bending, buckling and vibration problems of nonlocal Euler beams (Ghannadpour et al. 2013), buckling analysis of single-walled carbon nanotubes subjected to different boundary conditions (Ansari et al. 2011) etc. Differential transformation method has been applied by Pradhan and Reddy (2011) to predict the buckling behavior of Single Walled Carbon Nanotube (SWCNT) embedded in Winkler foundation. Ghannadpour and Mohammadi (2010) applied Chebyshev polynomials in the Rayleigh-Ritz method to investigate buckling analysis of nanorods based on Timoshenko beam theory. Sahmani and Ansari (2011) developed state-space method to study buckling of nanobeams based on Euler-Bernoulli, Timoshenko and Levinson beam theories. Effect of temperature on the buckling analysis of SWCNTs embedded in elastic medium has been investigated by Narendar and Gopalakrishnan (2011). Nonlocal shell model has been used by Yan et al. (2010) to study nonlocal effect on axially compressed buckling of triple walled carbon nanotubes under the influence of temperature. Some of the studies in context with buckling of single layered graphene sheets based on plate theories are: (Pradhan 2009; , Pradhan and Murmu 2010a; Pradhan 2012; Narendar 2011; Anjomshoa et al. 2014; Analooei et al. 2013). Buckling analysis of SWCNTs embedded in an elastic medium has been analyzed by Murmu and Pradhan (2009b) based on nonlocal Timoshenko beam theory. Differential quadrature method has been employed to study thermal buckling analysis of embedded SWCNTs subjected to various edge conditions ( Murmu and Pradhan 2010). Analytical solution of thermal buckling behavior of nanobeams has been analyzed by Tounsi et al. (2013) based on higher order beam theory.

### 1.2.1.3 Vibration

Integral equation approach has been employed by Xu (2006) to investigate free transverse vibration of nano-to-micron scale beams and the author found that the nonlocal effect on the natural frequencies and vibrating modes is negligible for microbeams while it plays a crucial role in nanobeams. Peddieson et al. (2003) formulated nonlocal version of Euler-Bernoulli beam theory. Free vibration of Euler-Bernoulli and Timoshenko nanobeams based on nonlocal continuum mechanics has been solved analytically by Wang et al. (2007). These authors have given the frequency parameters for different scaling effect parameters. They have given first

five mode shapes of clamped nanobeams based on nonlocal Timoshenko beam theory for various values of scaling effect parameter. Nonlocal elasticity model has been used by Loya et al. (2009) to study free transverse vibration of cracked Euler-Bernoulli nanobeams. Investigations have also been carried out for vibration of multiwalled carbon nanotubes. Ansari and Ramezanzhad (2011) studied nonlocal Timoshenko beam model for investigating the large amplitude vibrations of embedded multiwalled carbon nanotubes including thermal effects. Murmu and Adhikari (2010a) developed an analytical method to investigate transverse vibration of double-nanobeam systems based on nonlocal elasticity theory. One may find significant role of nonlocal effects in nanoscale devices (Lu et al. 2006). Some numerical methods like meshless (Roque et al. 2011), differential quadrature (Pradhan and Murmu 2010), finite element (Eltaher et al. 2013b) and Rayleigh-Ritz have also been applied in various studies related to vibration of nanobeams. It is not always possible to find analytical solutions for all set of boundary conditions at the edges. In this regard, Rayleigh-Ritz method (Bhat 1985, 1991; Chakraverty et al. 1999, 2007; Chakraverty 2009; Chakraverty and Petyt 1997; Dickinson 1978; Singh and Chakraverty 1994a, 1994b, 1992) is an efficient numerical method in handling all set of classical boundary conditions. Chebyshev polynomials and boundary characteristic orthogonal polynomials have been used in the Rayleigh-Ritz method to study vibration of Timoshenko nanobeams (Mohammadi and Ghannadpour 2011; Behera and Chakraverty 2014a, b). Previous authors have also considered various complicating effects in the vibration of nanobeams based on nonlocal elasticity theory. Zhang et al. (2005) investigated double walled carbon nanotubes to examine the influence of nonlocal parameter on the natural frequencies. Double nanobeam systems are useful in nano-optomechanical systems and sensor applications. Seeing practical applications, authors have studied vibration of double nanobeam systems and the study shows that small scale effects are higher with increasing nonlocal parameter in the in-phase vibration than in the out-of-phase vibration (Murmu and Adhikari 2010). A detailed study has also been conducted to analyze the influences of nonlocal parameter, length of the tubes, spring constant and end supports on the nonlinear free vibration characteristics of SWCNTs (Yang et al. 2010) and Double Walled Carbon NanoTubes (Ke et al. 2009). Eltaher et al. (2012) studied free vibration of functionally graded size dependent nanobeams. Free vibration of SWCNTs has been investigated based on nonlocal Levinson beam theory (Maachou et al. 2011) and Timoshenko beam theory (Zidour et al. 2012; Benzair et al. 2008) in thermal environment by employing analytical solution for simply supported edge condition. Authors found that vibration characteristics are strongly dependent on temperature change. Similar thermal effect may also be seen on the instability of SWCNTs conveying fluid (Wang et al. 2008). Thermal effect on the vibration of double-walled carbon nanotubes has been investigated analytically by Zhang et al. (2007) for simply supported edge condition. Differential quadrature method has also been employed by Murmu and Pradhan (2009a) to study thermo-mechanical vibration SWCNTs embedded in elastic medium. Murmu and Adhikari (2009) studied small scale effect on the vibration of nonuniform nanocantilever. Rafiei et al. (2012) investigated small-scale effect on

the vibration of non-uniform carbon nanotubes conveying fluid and embedded in viscoelastic medium. Phadikar and Pradhan (2010) developed finite element nonlocal elastic nanobeams and nanoplates.

## **1.2.2 Nanoplates**

In this section, we have discussed some of the previous work related to nanoplates.

### **1.2.2.1 Bending**

Analytical solution for bending of simply-supported rectangular nanoplate has been presented by Aghababaei and Reddy (2009) based on third-order shear deformation plate theory. Kananipour (2014) applied differential quadrature method (DQM) to investigate bending of two-dimensional rectangular nanoplates based on Kirchhoff and Mindlin plate theories. An analytical method as been adopted by Nami and Janghorban (2013) to solve the governing equations for static analysis of simply supported nanoplates based on trigonometric shear deformation theory in conjunction with nonlocal elasticity theory. Alibeigloo et al. (2013) studied bending of a simply supported rectangular graphene sheets based on three dimensional theory of elasticity. Bending analysis of rectangular nanoplates subjected to mechanical loading has been investigated by Nami and Janghorban (2014). Alzahrani et al. (2013) analyzed small scale effect on the bending of nanoplates embedded in two-parameter elastic medium and subjected to hygro-thermo-mechanical loading.

### **1.2.2.2 Buckling**

Stability analysis of of nanoplates subjected to both uniaxial and biaxial in-plane loadings has been studied by Naderi and Saidi (2014) based on modified nonlocal Mindlin plate theory. Analytical solution for the buckling analysis of rectangular nanoplates has been presented by Hashemi and Samaei (2011) based on the nonlocal Mindlin plate theory. Bedroud et al. (2013) investigated axisymmetric buckling analysis of moderately thick circular or annular Mindlin nanoplates under uniform radial compressive in-plane load. Ravari and Shahidi (2013) developed finite difference method to study axisymmetric buckling behavior of circular annular nanoplates and solid disks under uniform compression. Anjomshhoa (2012) presented Ritz solution for buckling analysis of embedded orthotropic circular and elliptical nanoplates based on nonlocal elasticity theory. Zenkour and Sobhy (2013) studied thermal buckling of single-layered graphene sheets lying on an elastic medium. Biaxial buckling behavior of single-layered graphene sheets (SLGSs) has been investigated by Ansari and Sahmani (2013) based on nonlocal plate models. Thermal buckling characteristic of orthotropic arbitrary straight-sided quadrilateral nanoplates embedded in an elastic medium has been investigated by Malekzadeh et al. (2011b)

### 1.2.2.3 Vibration

Differential quadrature method has been used by Malekzadeh and Shojaee (2013) to investigate free vibration nanoplates based on nonlocal two variable refined plate theory. Wang et al. (2011) applied Navier's approach to study vibration behaviors of simply supported Kirchhoff and Mindlin nanoscale plates with consideration of surface effects. Wang and Wang (2011) investigated mechanisms of nonlocal effect on the vibration of nanoplates. Again differential quadrature method has been used by Malekzadeh et al. (2011a) to examine free vibration of orthotropic arbitrary straight-sided quadrilateral nanoplate using first order shear deformation theory. Murmu and Pradhan (2009) investigated the effects of small scale on the free in-plane vibration of nanoplates. Adali (2012) developed semi-inverse method to derive variational principle for nonlocal continuum model of orthotropic graphene sheets embedded in an elastic medium. Rayleigh-Ritz method has also been applied by Chakraverty and Behera (2014) to study vibration of rectangular nanoplates. Pradhan and Phadikar (2009b) presented analytical solutions for vibration of nanoplates based on classical plate theory and first order shear deformation plate theory using Navier's approach. Aksencer and Aydogdu (2011) presented Levy type solution for vibration of nanoplates based on classical plate theory. Analooei et al. (2013) studied vibration of orthotropic nanoplates using spline finite strip method. Jomehzadeh and Saidi (2012) studied nonlinear vibration of nanoplates. Small-scale effect on the vibration of nanoplates subjected to a moving nanoparticle has been studied by Kiani (2011). Similarly, vibration of piezoelectric nanoplates has been investigated by Liu et al. (2013) based on the nonlocal theory.

## 1.3 Gaps

Nanotechnology is a recent development which enables a new generation of materials and devices. For design of nanostructures, one should have proper knowledge about their mechanical and physical behaviors. As such, few authors have investigated bending, buckling and vibration of nanobeams and nanoplates. Bending problems simplify to system of linear equations whereas buckling and vibration problems convert to eigen value problems. In this respect, previous authors have developed different methods for the solution of these problems. But, sometimes the existing methods are not computationally efficient and may not handle all sets of boundary conditions with ease. Also these methods may not handle the problems with complicating effects. It is revealed from literatures that a very little effort has been made for the problems of vibration and buckling analyses of Reddy and Levinson nanobeams. Moreover, structural elements with variable material properties are frequently used in practical applications. But, very few studies have been done for such types of nanobeams and nanoplates. It is also well known that computations become complex when nonlocal elasticity theory is introduced. Having these in mind one has to develop computationally efficient methods very

carefully to handle the above said problems. Accordingly, following are the broad aims and objectives of the present work.

## **1.4 Aims and objectives**

In view of the above gaps, our aim in this research is to develop numerical methods that may best suit to solve bending, buckling and vibration of nanobeams and nanoplates. Some of the complicating effects are also taken into consideration. As such, we include below the objectives related to the present research:

- development of numerical methods for solving the partial differential equations related to bending, buckling and vibration of nanobeams and nanoplates;
- bending analysis of nanobeams;
- buckling analysis of nanobeams with complicating effects such as non-uniformity, temperature and Winker as well as Pasternak foundations;
- bending and buckling of rectangular nanoplates;
- vibration of rectangular nanoplates subjected to various classical boundary conditions;
- vibration of rectangular nanoplates with complicating effects such as non-uniformity and Winkler as well as Pasternak foundations;

## **1.5 Organization of the thesis**

Present work deals with the solution of bending, buckling and vibration of nanobeams and nanoplates. Accordingly, this thesis consists of nine chapters which investigate numerical methods for the above problems. Various complicating effects such as non-uniformity, temperature and Winker as well as Pasternak foundations have also been considered. Recently, effort has been made by various researchers to solve these types of problems but a lot of important information is still missing in the existing literature. Further, some of the known methods are computationally expensive and may not handle all sets of classical boundary conditions. The purpose of the present work is to fill these gaps. Accordingly, the contents of the nine chapters are summarized below:

Chapter 1 includes a brief introduction of nanostructures and their applications. This chapter highlights advantage of small scale effect on the nanotechnology applications and importance of nonlocal elasticity theory. Various beam and plate theories have been discussed and related literatures are systematically reviewed. Gaps as well as aims and objectives of the present study

are included here. This chapter also addresses some of the preliminaries of nanostructures related to our problems.

Chapter 2 incorporates the details of the numerical methods such as Rayleigh-Ritz and differential quadrature that have been used in the present problems. Advantage of these numerical methods and systematic procedure for applying boundary conditions has also been highlighted.

Chapter 3 addresses bending and buckling analyses of nanobeams. Bending analysis has been carried out based on Euler-Bernoulli and Timoshenko nonlocal beam theories by using boundary characteristic orthogonal polynomials as shape functions in the Rayleigh-Ritz method. Differential quadrature method has been employed to study buckling analysis of non-uniform nanobeams based on four beam theories such as Euler-Bernoulli, Timoshenko, Reddy and Levinson. Buckling analysis of embedded nanobeams under the influence of temperature has also been investigated based on Euler-Bernoulli, Timoshenko and Reddy beam theories. In these problems, boundary characteristic and Chebyshev polynomials have been used in the Rayleigh-Ritz method respectively for Euler-Bernoulli and Timoshenko beam theories. Further, differential quadrature method has been employed for buckling analysis of nanobeams embedded in elastic foundations based on nonlocal Reddy beam theory. Effects of temperature and foundation parameters on the buckling load parameter have also been investigated.

Chapter 4 deals with bending and buckling problems of nanoplates based on classical plate theory in conjunction with nonlocal elasticity theory of Eringen. In this chapter, rectangular nanoplates are considered. Two-dimensional simple polynomials have been implemented in the Rayleigh-Ritz method to investigate these problems. Effects of length, nonlocal parameter and aspect ratio on the non-dimensional maximum deflection have been discussed. Similarly, effects of length, nonlocal parameter, aspect ratio, stiffness ratio and foundation parameters on the buckling loads have also been included.

In Chapter 5, vibration of nanobeams has been investigated. Rayleigh-Ritz method with simple polynomials and boundary characteristic orthogonal polynomials has been implemented to compute vibration characteristics of Euler-Bernoulli and Timoshenko nanobeams. Differential quadrature method has been used to investigate four types of nonlocal beam theories such as Euler-Bernoulli, Timoshenko, Reddy and Levinson. In these problems, differential equations are converted into single unknown variable and boundary conditions have been substituted in the coefficient matrices. Convergence study along with validation in special cases has been carried out. Effect of scaling effect parameter on the frequency parameter has been investigated for different boundary conditions. Mode shapes for some specified boundary conditions are presented for different values of scaling effect parameter. In particular, new results have been presented for Reddy and Levinson beam theories.



Chapter 6 presents numerical solution of vibration of nanobeams with complicating effects. The complicating effects such as non-uniformity, temperature and Winkler as well as Pasternak foundations have been taken into consideration. At first, Rayleigh-Ritz method with boundary characteristic orthogonal polynomials has been used to investigate vibration of non-uniform Euler-Bernoulli and Timoshenko nanobeams. Non-uniformity is assumed to arise due to linear and quadratic variations in Young's modulus and density with space coordinate. Comparisons have been made for uniform nanobeams with that of known results in special cases. Variation of non-uniform parameter on the frequency parameter is depicted in term of plots. Next, vibration analysis of embedded nanobeams with elastic foundations has been analyzed in the influence of temperature. The nanobeam is embedded in elastic foundations such as Winkler and Pasternak. Here, three types of nonlocal beam theories such as Euler-Bernoulli, Timoshenko and Reddy are taken into consideration. Rayleigh-Ritz method has been used with boundary characteristic orthogonal polynomials and Chebyshev polynomials as shape functions for Euler-Bernoulli and Timoshenko nonlocal beam theories respectively. On the other hand, differential quadrature method has been implemented for vibration analysis of embedded nanobeams with elastic foundation based on Reddy nonlocal beam theory. Effects of temperature, Winkler and Pasternak coefficients on the frequency parameter have also been investigated.

In Chapter 7, vibration of rectangular nanoplate has been studied based on classical plate theory in conjunction with nonlocal elasticity theory of Eringen. Here, two-dimensional simple polynomials have been used as shape functions in the Rayleigh-Ritz method. It may be noted that there are 24 possible sets of boundary conditions for rectangular nanoplate. Accordingly, new results have been presented in term of boundary conditions. Parametric studies such as effects of length, aspect ratio and nonlocal parameter on the frequency parameters have been carried out. Three-dimensional mode shapes have also been presented for some of the typical boundary conditions.

Chapter 8 describes solution of vibration of nanoplates with various complicating effects. Two-dimensional simple polynomials and boundary characteristic orthogonal polynomials have been used as shape functions in the Rayleigh-Ritz method. Complicating effects such as non-uniformity is assumed by taking linear and quadratic variations of Young's modulus and density along space coordinate. Comparison has been made in special cases. Investigation has also been done for the nanoplate when it is embedded in elastic foundation such as Winkler and Pasternak. Effects of non-uniform parameters and elastic foundation on the frequency parameter have also been depicted in term of plots.

Based on the present work, Chapter 9 summarizes the conclusions of the study and suggestions for future work.

## 1.6 Preliminaries

Next, we have discussed some of the preliminaries related to the bending, buckling and vibration of nanobeams and nanoplates based on nonlocal elasticity theory which will be frequently used in the subsequent chapters. Firstly, we have shown overview of nonlocal elasticity theory.

### 1.6.1 Review of nonlocal elasticity theory

According to nonlocal elasticity theory, the nonlocal stress tensor  $\sigma$  at a point  $x$  is expressed as (Murmu and Adhikari 2010a)

$$\sigma(x) = \int_V K(|x' - x|, \alpha) \tau dV(x') \quad (1.1)$$

where  $\tau$  is the classical stress tensor,  $K(|x' - x|, \alpha)$  the nonlocal modulus and  $|x' - x|$  the Euclidean distance. The volume integral is taken over the region  $V$  occupied by the body. Here  $\alpha$  is a material constant which depends on both internal and external characteristic lengths.

According to Hooke's law

$$\tau(x) = C(x) : \epsilon(x) \quad (1.2)$$

where  $C$  is the fourth-order elasticity tensor,  $\epsilon$  the classical strain tensor and  $:$  denotes double dot product.

Eq. (1.1) is the integral constitutive relation which is quite difficult to solve. Hence equivalent differential form of this equation may be written as (Murmu and Adhikari 2010a)

$$(1 - \alpha^2 L^2 \nabla^2) \sigma = \tau, \alpha = \frac{e_0 l_{int}}{L} \quad (1.3)$$

where  $\nabla^2$  the Laplace operator,  $e_0$  is a material constant which could be determined from experiments or by matching dispersion curves of plane waves with those of atomic lattice dynamics,  $l_{int}$  is an internal characteristic length such as lattice parameter, C-C bond length or granular distance while  $L$  is an external characteristic length which is usually taken as the length of the nanostructure. The term  $e_0 l_{int}$  is called the nonlocal parameter which reveals scale effect in models or it reveals the nanoscale effect on the response of structures.

### 1.6.2 Beam theories

In this section, we have discussed displacement fields, energies of the system and governing equations which are used for our problems. In all the beam theories (Reddy 2007),  $x, y, z$  coordinates are taken along the length, width and thickness (the height) of the beam respectively. All applied loads and geometry are such that the displacements  $(u_1, u_2, u_3)$  along the coordinates  $(x, y, z)$  are only functions of  $x$  and  $z$  coordinates as well as time  $t$ . A schematic diagram for nanobeams embedded within an elastic medium characterized by spring constant

$K_w$  and shear constant  $K_g$  has been shown in Fig. 1.1.

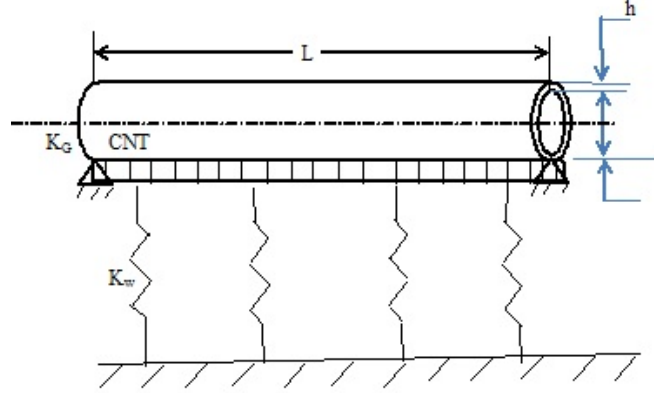


Fig. 1.1 Single-walled carbon nanotube embedded within an elastic medium

Next, we have discussed four types of beam theories viz. Euler-Bernoulli beam theory, Timoshenko beam theory, Reddy beam theory and Levinson beam theory. In all the beam theories, we have not considered axial displacement of the point  $(x, 0)$  on the mid-plane ( $z = 0$ ) of the beam. One may note that the notations  $M, P, Q, R$  which will be used in our subsequent paragraphs are defined as below:

$$M = \int_A z \sigma_{xx} dA, P = \int_A z^3 \sigma_{xx} dA, Q = \int_A \sigma_{xz} dA, R = \int_A z^2 \sigma_{xz} dA.$$

### 1.6.2.1 Euler-Bernoulli beam theory (EBT)

Based on Euler-Bernoulli beam theory, the displacement fields are given by (Reddy 2007)

$$\begin{aligned} u_1 &= -z \frac{\partial w}{\partial x} \\ u_2 &= 0 \\ u_3 &= w(x, t) \end{aligned} \quad (1.4)$$

where  $(u_1, u_2, u_3)$  are the displacements along  $x, y$  and  $z$  coordinates respectively and  $w$  is the transverse displacement of the point  $(x, 0)$  on the mid-plane ( $z = 0$ ) of the beam.

The only nonzero strain of the Euler-Bernoulli beam theory is written as

$$\varepsilon_{xx} = -z \frac{\partial^2 w}{\partial x^2} \quad (1.5)$$

Governing equation of Euler-Bernoulli nanobeams may be written as (Reddy 2007)

$$\frac{\partial^2 M}{\partial x^2} + q - \bar{N} \frac{\partial^2 w}{\partial x^2} = m_0 \frac{\partial^2 w}{\partial t^2} \quad (1.6)$$

where  $q$  is the transverse force per unit length,  $\bar{N}$  the applied axial compressive force and  $m_0$  is the mass inertia defined by  $m_0 = \int_A \rho dA = \rho A$  with  $A$  as the cross-sectional area of the beam.

According to Eringen's nonlocal theory (Eringen 1987), the constitutive relation for Euler-Bernoulli nanobeam is given by (Reddy 2007)

$$M - \mu \frac{\partial^2 M}{\partial x^2} = -EI \frac{\partial^2 w}{\partial x^2} \quad (1.7)$$

where  $E$  is the Young's modulus and  $I$  is the second moment of area about  $y$ - axis. It may be noted here that  $\mu = (e_0 l_{int})^2$  is the nonlocal parameter where  $e_0$  and  $l_{int}$  denote material constant and internal characteristic length respectively.

Using Eqs. (1.6) and (1.7), nonlocal form of  $M$  may be written as

$$M = -EI \frac{\partial^2 w}{\partial x^2} + \mu \left( \bar{N} \frac{\partial^2 w}{\partial x^2} - q + m_0 \frac{\partial^2 w}{\partial t^2} \right) \quad (1.8)$$

Governing equation in terms of displacement is rewritten as

$$-EI \frac{\partial^4 w}{\partial x^4} + \mu \frac{\partial^2}{\partial x^2} \left[ \bar{N} \frac{\partial^2 w}{\partial x^2} - q + m_0 \frac{\partial^2 w}{\partial t^2} \right] + q - \bar{N} \frac{\partial^2 w}{\partial x^2} = m_0 \frac{\partial^2 w}{\partial t^2} \quad (1.9)$$

### 1.6.2.2 Timoshenko beam theory (TBT)

The displacement fields are based on (Reddy 2007)

$$\begin{aligned} u_1 &= z\phi(x, t) \\ u_2 &= 0 \\ u_3 &= w(x, t) \end{aligned} \quad (1.10)$$

where  $\phi$  is the rotation of the cross-section.

The nonzero strains of the Timoshenko beam theory are given by

$$\epsilon_{xx} = z \frac{\partial \phi}{\partial x} \quad (1.11)$$

$$\gamma_{xz} = \phi + \frac{\partial w}{\partial x} \quad (1.12)$$

Constitutive relations for Timoshenko beam theory may be written as (Reddy 2007)

$$M - \mu \frac{\partial^2 M}{\partial x^2} = EI \frac{\partial \phi}{\partial x} \quad (1.13)$$

$$Q - \mu \frac{\partial^2 Q}{\partial x^2} = k_s GA \left( \phi + \frac{\partial w}{\partial x} \right) \quad (1.14)$$

where  $G$  is the shear modulus and  $k_s$  is the shear correction factor.

Governing equations of this beam theory are (Reddy 2007)

$$\frac{\partial M}{\partial x} - Q = m_2 \frac{\partial^2 \phi}{\partial t^2} \quad (1.15)$$

$$\frac{\partial Q}{\partial x} + q - \bar{N} \frac{\partial^2 w}{\partial x^2} = m_0 \frac{\partial^2 w}{\partial t^2} \quad (1.16)$$

Using Eqs. (1.13-1.16), nonlocal form of  $M$  and  $Q$  may be obtained as

$$M = EI \frac{\partial \phi}{\partial x} + \mu \left[ -q + \bar{N} \frac{\partial^2 w}{\partial x^2} + m_0 \frac{\partial^2 w}{\partial t^2} + m_2 \frac{\partial^3 \phi}{\partial x \partial t^2} \right] \quad (1.17)$$

$$Q = GAk_s \left( \phi + \frac{\partial w}{\partial x} \right) + \mu \frac{\partial}{\partial x} \left[ -q + \bar{N} \frac{\partial^2 w}{\partial x^2} + m_0 \frac{\partial^2 w}{\partial t^2} \right] \quad (1.18)$$

Using Eqs. (1.17-1.18) in Eqs. (1.15-1.16), we have the governing equations as

$$GAk_s \left( \frac{\partial \phi}{\partial x} + \frac{\partial^2 w}{\partial x^2} \right) + q - \bar{N} \frac{\partial^2 w}{\partial x^2} - \mu \left[ \frac{\partial^2 q}{\partial x^2} - \bar{N} \frac{\partial^4 w}{\partial x^4} \right] = m_0 \left( \frac{\partial^2 w}{\partial t^2} - \mu \frac{\partial^4 w}{\partial x^2 \partial t^2} \right) \quad (1.19)$$

$$EI \frac{\partial^2 \phi}{\partial x^2} - GAk_s \left( \phi + \frac{\partial w}{\partial x} \right) = m_2 \frac{\partial^2 \phi}{\partial t^2} - \mu m_2 \frac{\partial^4 \phi}{\partial x^2 \partial t^2} \quad (1.20)$$

### 1.6.2.3 Reddy beam theory (RBT)

Displacement fields for Reddy beam theory are based on (Reddy 2007)

$$\begin{aligned} u_1 &= z\phi(x, t) - c_1 z^3 \left( \phi + \frac{\partial w}{\partial x} \right) \\ u_2 &= 0 \\ u_3 &= w(x, t) \end{aligned} \quad (1.21)$$

where  $c_1 = \frac{4}{3h^2}$  with  $h$  as the height of the beam.

The nonzero strains of the Reddy beam theory are

$$\begin{aligned} \varepsilon_{xx} &= z(1 - c_1 z^2) \frac{\partial \phi}{\partial x} - c_1 z^3 \frac{\partial^2 w}{\partial x^2} \\ \gamma_{xz} &= (1 - c_2 z^2) \left( \frac{\partial w}{\partial x} + \phi \right) \end{aligned} \quad (1.22)$$

where  $c_2 = \frac{4}{h^2}$ .

Nonlocal constitutive equations take the following form in case of RBT

$$\begin{aligned}\hat{M} - \mu \frac{\partial^2 \hat{M}}{\partial x^2} &= E\hat{I} \frac{\partial \phi}{\partial x} + E\hat{J}(-c_1) \left( \frac{\partial \phi}{\partial x} + \frac{\partial^2 w}{\partial x^2} \right) \\ \hat{Q} - \mu \frac{\partial^2 \hat{Q}}{\partial x^2} &= G\bar{A} \left( \phi + \frac{\partial w}{\partial x} \right) + G\bar{I}(-c_2) \left( \phi + \frac{\partial w}{\partial x} \right) \\ P - \mu \frac{\partial^2 P}{\partial x^2} &= EJ \frac{\partial \phi}{\partial x} + EK(-c_1) \left( \frac{\partial \phi}{\partial x} + \frac{\partial^2 w}{\partial x^2} \right)\end{aligned}\quad (1.23)$$

where  $I, J$  and  $K$  are the second, fourth and sixth order moments of area respectively about the  $y$ - axis and are defined as  $(I, J, K) = \int_A (z^2, z^4, z^6) dA$ .

Also  $\hat{M} = M - c_1 P$ ,  $\hat{Q} = Q - c_2 R$ ,  $\hat{I} = I - c_1 J$ ,  $\hat{J} = J - c_1 K$ ,  $\bar{A} = A - c_2 I$ ,  $\bar{I} = I - c_2 J$ ,  $\bar{A} = \bar{A} - c_2 \bar{I}$ .

$\hat{M}$  and  $\hat{Q}$  are given by (Reddy 2007)

$$\hat{M} = E\hat{I} \frac{\partial \phi}{\partial x} - c_1 E\hat{J} \left( \frac{\partial \phi}{\partial x} + \frac{\partial^2 w}{\partial x^2} \right) + \mu \left[ -c_1 \frac{\partial^2 P}{\partial x^2} - q + \bar{N} \frac{\partial^2 w}{\partial x^2} + m_0 \frac{\partial^2 w}{\partial t^2} \right] \quad (1.24)$$

$$\hat{Q} = G\bar{A} \left( \phi + \frac{\partial w}{\partial x} \right) + \mu \left[ -c_1 \frac{\partial^3 P}{\partial x^3} + \bar{N} \frac{\partial^3 w}{\partial x^3} - \frac{\partial q}{\partial x} \right] + \mu m_o \frac{\partial^3 w}{\partial x \partial t^2} \quad (1.25)$$

As such, governing equations may be written as (Reddy 2007)

$$G\bar{A} \left( \frac{\partial \phi}{\partial x} + \frac{\partial^2 w}{\partial x^2} \right) - \bar{N} \frac{\partial^2 w}{\partial x^2} + q + \mu \left[ \bar{N} \frac{\partial^4 w}{\partial x^4} - \frac{\partial^2 q}{\partial x^2} \right] + c_1 EJ \frac{\partial^3 \phi}{\partial x^3} - c_1^2 EK \left( \frac{\partial^3 \phi}{\partial x^3} + \frac{\partial^4 w}{\partial x^4} \right) = m_0 \left( \frac{\partial^2 w}{\partial t^2} - \mu \frac{\partial^4 w}{\partial x^2 \partial t^2} \right) \quad (1.26)$$

$$E\hat{I} \frac{\partial^2 \phi}{\partial x^2} - c_1 E\hat{J} \left( \frac{\partial^2 \phi}{\partial x^2} + \frac{\partial^3 w}{\partial x^3} \right) - G\bar{A} \left( \phi + \frac{\partial w}{\partial x} \right) = 0 \quad (1.27)$$

It may be noted here that in our problems, we have neglected the higher order inertias i.e.  $m_2, m_4$  and  $m_6$ .

#### 1.6.2.4 Levinson beam theory (LBT)

Levinson beam theory is based on the following displacement fields (Reddy 2007)

$$\begin{aligned}u_1 &= z\phi(x, t) - c_1 z^3 \left( \phi + \frac{\partial w}{\partial x} \right) \\ u_2 &= 0 \\ u_3 &= w(x, t)\end{aligned}\quad (1.28)$$

It may be noted that displacement and strain fields of the Levinson beam theory is the same as that of Reddy beam theory.

Governing equations are given as follows (Reddy 2007)

$$\begin{aligned}\frac{\partial Q}{\partial x} + q - \bar{N} \frac{\partial^2 w}{\partial x^2} &= m_0 \frac{\partial^2 w}{\partial t^2} \\ \frac{\partial M}{\partial x} - Q &= m_2 \frac{\partial^2 \phi}{\partial t^2}\end{aligned}\quad (1.29)$$

Nonlocal constitutive relations may be expressed as (Reddy 2007)

$$\begin{aligned}M - \mu \frac{\partial^2 M}{\partial x^2} &= EI \frac{\partial \phi}{\partial x} + EJ(-c_1) \left( \frac{\partial \phi}{\partial x} + \frac{\partial^2 w}{\partial x^2} \right) \\ Q - \mu \frac{\partial^2 Q}{\partial x^2} &= GA \left( \phi + \frac{\partial w}{\partial x} \right) + GI(-c_2) \left( \phi + \frac{\partial w}{\partial x} \right)\end{aligned}\quad (1.30)$$

Using Eqs. (1.29) and (1.30),  $M$  and  $Q$  are obtained as

$$M = EI \frac{\partial \phi}{\partial x} - c_1 EJ \left( \frac{\partial \phi}{\partial x} + \frac{\partial^2 w}{\partial x^2} \right) + \mu \left[ -q + \bar{N} \frac{\partial^2 w}{\partial x^2} + m_0 \frac{\partial^2 w}{\partial t^2} + m_2 \frac{\partial^3 \phi}{\partial x \partial t^2} \right] \quad (1.31)$$

$$Q = G\bar{A} \left( \phi + \frac{\partial w}{\partial x} \right) + \mu \left[ \bar{N} \frac{\partial^3 w}{\partial x^3} - \frac{\partial q}{\partial x} + m_0 \frac{\partial^3 w}{\partial x \partial t^2} \right] \quad (1.32)$$

Utilizing Eqs. (1.31)- (1.32), governing differential equations may be transformed to

$$G\bar{A} \left( \frac{\partial \phi}{\partial x} + \frac{\partial^2 w}{\partial x^2} \right) + q - \bar{N} \frac{\partial^2 w}{\partial x^2} + \mu \left[ \bar{N} \frac{\partial^4 w}{\partial x^4} - \frac{\partial^2 q}{\partial x^2} \right] = m_0 \left( \frac{\partial^2 w}{\partial t^2} - \mu \frac{\partial^4 w}{\partial^2 x \partial t^2} \right) \quad (1.33)$$

$$EI \frac{\partial^2 \phi}{\partial x^2} - c_1 EJ \left( \frac{\partial^2 \phi}{\partial x^2} + \frac{\partial^3 w}{\partial x^3} \right) - G\bar{A} \left( \phi + \frac{\partial w}{\partial x} \right) = m_2 \left( \frac{\partial^2 \phi}{\partial t^2} - \mu \frac{\partial^4 \phi}{\partial^2 x \partial t^2} \right) \quad (1.34)$$

### 1.6.3 Plate theory

In this section, we have shown some of the preliminaries related to classical plate theory. Fig. 1.2 shows the coordinate system used for nanoplate. The  $x$ ,  $y$ ,  $z$  coordinates are taken along the length, width and thickness of the plate respectively and origin is chosen at one corner of the mid-plane of the plate.

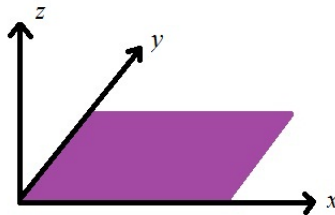


Fig. 1.2 Schematic of single layered nanoplate

### 1.6.3.1 Classical plate theory (CLPT)

Based on classical plate theory, the displacement fields  $(u_1, u_2, u_3)$  at time  $t$  are written as (Pradhan and Phadikar 2009b)

$$\begin{aligned} u_1 &= u(x, y, t) - z \frac{\partial w}{\partial x} \\ u_2 &= v(x, y, t) - z \frac{\partial w}{\partial y} \\ u_3 &= w(x, y, t) \end{aligned} \quad (1.35)$$

where  $u, v, w$  denote displacement of the point  $(x, y, 0)$  along  $x, y, z$  directions respectively.

The strain components are expressed as

$$\varepsilon_{xx} = \frac{\partial u}{\partial x} - z \frac{\partial^2 w}{\partial x^2}, \varepsilon_{yy} = \frac{\partial v}{\partial y} - z \frac{\partial^2 w}{\partial y^2}, \varepsilon_{xy} = \frac{1}{2} \left( \frac{\partial u}{\partial y} + \frac{\partial v}{\partial x} - 2z \frac{\partial^2 w}{\partial x \partial y} \right), \varepsilon_{zz} = \varepsilon_{xz} = \varepsilon_{yz} = 0$$

Nonlocal constitutive relations take the form

$$\begin{aligned} M_{xx} - \mu \nabla^2 M_{xx} &= -D \left( \frac{\partial^2 w}{\partial x^2} + \nu \frac{\partial^2 w}{\partial y^2} \right) \\ M_{yy} - \mu \nabla^2 M_{yy} &= -D \left( \frac{\partial^2 w}{\partial y^2} + \nu \frac{\partial^2 w}{\partial x^2} \right) \\ M_{xy} - \mu \nabla^2 M_{xy} &= -D(1 - \nu) \frac{\partial^2 w}{\partial x \partial y} \end{aligned} \quad (1.36)$$

where  $(M_{xx}, M_{yy}, M_{xy})$  are moment resultants,  $\nabla^2$  the Laplacian operator in 2-D cartesian coordinate system and  $D = \frac{Eh^3}{12(1-\nu^2)}$  denotes bending rigidity of the plate.

In the expression of bending rigidity,  $h$  is the thickness of the plate,  $E$  the Young's modulus and  $\nu$  is the Poisson's ratio.

Governing equation in terms of the displacement is written as (Pradhan and Phadikar 2009b)

$$-D \nabla^4 w + (1 - \mu \nabla^2) \left[ q + N_{xx} \frac{\partial^2 w}{\partial x^2} + N_{yy} \frac{\partial^2 w}{\partial y^2} + 2N_{xy} \frac{\partial^2 w}{\partial x \partial y} - m_0 \frac{\partial^2 w}{\partial t^2} + m_2 \left( \frac{\partial^4 w}{\partial x^2 \partial t^2} + \frac{\partial^4 w}{\partial y^2 \partial t^2} \right) \right] = 0 \quad (1.37)$$

where  $q$  is the transverse distributed load and  $(N_{xx}, N_{xy}, N_{yy})$  are in-plane force resultants. Also  $m_0$  and  $m_2$  are mass moments of inertia which are defined as

$$m_0 = \int_{-\frac{h}{2}}^{\frac{h}{2}} \rho dz, \quad m_2 = \int_{-\frac{h}{2}}^{\frac{h}{2}} \rho h^2 dz \quad \text{with } \rho \text{ as the density of the material.}$$

It may be noted here that in all of the above beam and plate theories if  $\mu = 0$ , then we obtain expressions for local beam and plate theories.



# **Chapter 2**

## **Numerical methods**

# Chapter 2

## Numerical methods

Two important numerical methods such as Rayleigh-Ritz and differential quadrature have been applied to investigate bending, buckling and vibration of nanobeams and nanoplates. The novelty of the methods is that boundary conditions may easily be handled. In this chapter, we have discussed elaborately about these methods.

### 2.1 Rayleigh-Ritz method

Rayleigh-Ritz method has been implemented in the bending, buckling and free vibration of nanobeams based on Euler-Bernoulli and Timoshenko beam theories. We have also applied Rayleigh-Ritz method in the bending, buckling and free vibration of nanoplates based on classical plate theory. As such, we have discussed Rayleigh-Ritz method for the above said problems.

One may note that subsequent notations have been defined in the preliminaries of Chapter 1.

#### 2.1.1 Bending problems

We have investigated bending of nanobeams based on Euler-Bernoulli and Timoshenko beam theories. Boundary characteristic orthogonal polynomials have used as shape functions in the Rayleigh-Ritz method. As such, we have discussed below the procedure of application of Rayleigh-Ritz method in the bending of nanobeams.

##### 2.1.1.1 Euler-Bernoulli beam theory

The strain energy  $U$  may be given as (Wang et al. 2000)

$$U = -\frac{1}{2} \int_0^L M \frac{d^2 w}{dx^2} dx \quad (2.1)$$

where  $M$  may be obtained from Eq. (1.8) by setting  $\bar{N}$  and all time derivatives to zero. As such,

$$M = -EI \frac{d^2 w}{dx^2} - \mu q \quad (2.2)$$

The potential energy of the transverse force  $q$  may be given as (Ghannadpour et al. 2013)

$$V = - \int_0^L q w dx \quad (2.3)$$

The total energy  $U_T$  of the system is written as

$$U_T = \frac{1}{2} \int_0^L \left( EI \left( \frac{d^2 w}{dx^2} \right)^2 + \mu q \frac{d^2 w}{dx^2} - q w \right) dx \quad (2.4)$$

It is important to note that in all of the problems in subsequent chapters, the domain has been transformed from  $[0, L]$  to  $[0, 1]$  by using the relation  $X = \frac{x}{L}$ . As such, we discussed the methods taking the domain as  $[0, 1]$ .

To apply Rayleigh-Ritz method, the displacement function ( $w$ ) can be represented in the form of a series

$$w(X) = \sum_{k=1}^n c_k \varphi_k \quad (2.5)$$

where  $n$  is the number of terms needed in the series and  $c_k$ 's are unknowns. Here  $\varphi_k$  are polynomials which are consisting of a boundary polynomial specifying support conditions (essential boundary conditions) multiplied by one-dimensional simple polynomials. That is  $\varphi_k = f f_k$  with  $f_k = X^{k-1}$ ,  $k = 1, 2, \dots, n$  and  $f = X^u(1 - X)^v$  where  $u$  and  $v$  takes the values 0, 1 and 2 respectively for free (F), simply supported (S) and clamped (C) edge conditions respectively.

If instead of simple polynomials, Chebyshev polynomials ( $T_k$ ) are used then  $\varphi_k = f T_k$ . These Chebyshev polynomials are well known and we have  $T_0 = 1, T_1 = X$  and then  $T_{n+1}$  may be obtained by the recurrence relation  $T_{(n+1)}(X) = 2X T_n(X) - T_{n-1}(X)$ .

When  $\varphi_k$  are orthogonal polynomials then Gram-Schmidt process as discussed below may be used to obtain these polynomials from set of linearly independent functions  $F_k = f f_k$ . Then orthonormal polynomials  $\hat{\varphi}_k$  may be obtained from orthogonal polynomials  $\varphi_k$  if we divide  $\varphi_k$  by the norm of  $\varphi_k$ . Below, we have included detailed procedure to obtain orthogonal and orthonormal polynomials.

$$\varphi_1 = F_1, \varphi_k = F_k - \sum_{j=1}^{k-1} \beta_{kj} \varphi_j \quad (2.6)$$

where

$$\beta_{kj} = \frac{\langle F_k, \varphi_j \rangle}{\langle \varphi_j, \varphi_j \rangle}, \quad k = 2, 3, \dots, n, j = 1, 2, \dots, k-1.$$

and  $\langle, \rangle$  denotes inner product of two functions.

We define inner product of two functions, say,  $\varphi_i$  and  $\varphi_k$  as

$$\langle \varphi_i, \varphi_k \rangle = \int_0^1 \varphi_i(X) \varphi_k(X) dX, \quad i = 1, 2, \dots, n \quad (2.7)$$

Here we have taken weight function as 1.

Similarly, norm of the function  $\varphi_k$  is defined as

$$\|\varphi_k\| = \langle \varphi_k, \varphi_k \rangle^{\frac{1}{2}}$$

As such, normalized functions  $\hat{\varphi}_k$  may be obtained by using

$$\hat{\varphi}_k = \frac{\varphi_k}{\|\varphi_k\|}$$

In the bending problem (Chapter 3), we have considered orthonormal polynomials ( $\hat{\varphi}_k$ ) in Eq. (2.5). As such, substituting Eq. (2.5) in Eq. (2.4) and minimizing  $U_T$  as a function of  $c_j$ 's, one may obtain the following system of linear equation

$$\sum_{j=1}^n a_{ij}c_j = P_c b_i \quad (2.8)$$

where  $a_{ij}$ ,  $b_i$  and  $P_c$  are defined in Chapter 3.

### 2.1.1.2 Timoshenko beam theory

In this beam theory, the strain energy may be expressed as (Wang et al. 2007)

$$U = \frac{1}{2} \int_0^L \left( M \frac{d\phi}{dx} + Q \left( \phi + \frac{dw}{dx} \right) \right) dx \quad (2.9)$$

where bending moment  $M$  and shear force  $Q$  may be obtained by setting  $\bar{N}$  and all time derivatives to zero respectively in Eqs. (1.17) and (1.18). As such,

$$M = EI \frac{d\phi}{dx} - \mu q \quad (2.10)$$

$$Q = k_s GA \left( \phi + \frac{dw}{dx} \right) - \mu \frac{dq}{dx} \quad (2.11)$$

The potential energy of the transverse force  $q$  may be given as (Ghannadpour et al. 2013)

$$V = - \int_0^L q w dx \quad (2.12)$$

As such, the total energy  $U_T$  of the system is then written as

$$U_T = \frac{1}{2} \int_0^L \left( EI \left( \frac{d\phi}{dx} \right)^2 - \mu q \frac{d\phi}{dx} + k_s GA \left( \phi + \frac{dw}{dx} \right)^2 - \mu \frac{dq}{dx} \left( \phi + \frac{dw}{dx} \right) - q w \right) dx \quad (2.13)$$

For applying Rayleigh-Ritz method, each of the unknown functions  $w$  and  $\phi$  may now be expressed as the sum of series of polynomials viz.

$$w(X) = \sum_{k=1}^n c_k \varphi_k \quad (2.14)$$

$$\phi(X) = \sum_{k=1}^n d_k \psi_k \quad (2.15)$$

where  $n$  is the number of terms needed in the series and  $c_k$ 's and  $d_k$ 's are unknowns. Here  $\varphi_k$  and  $\psi_k$  are polynomials which are consisting of boundary polynomial specifying support conditions (essential boundary conditions) multiplied by one-dimensional simple polynomials viz.  $\varphi_k = f_w X^{k-1}$  and  $\psi_k = f_\phi X^{k-1}$ . It may be noted that  $f_w$  and  $f_\phi$  are the boundary functions corresponding to unknown functions  $w$  and  $\phi$  respectively which are given in Table 2.1 for some of the boundary conditions. Similarly, one may find boundary functions for other boundary conditions also.

If instead of simple polynomials, Chebyshev polynomials ( $T_k$ ) are used then  $\varphi_k = f_w T_k$  and  $\psi_k = f_\phi T_k$ .

When  $\varphi_k$  and  $\psi_k$  are orthogonal polynomials then Gram-Schmidt process may similarly be used as discussed in section 2.1.1.1 in order to obtain these polynomials from the set of linearly independent functions  $F_k$  and  $G_k$  where  $F_k = f_w f_k$  and  $G_k = f_\phi f_k$  with  $f_k = X^{k-1}$ ,  $k = 1, 2, \dots, n$ . Then orthonormal polynomials  $\hat{\varphi}_k$  may be obtained as in previous section 2.1.1.1 from orthogonal polynomials  $\varphi_k$ . Similarly,  $\hat{\psi}_k$  may also be obtained.

Table 2.1 Boundary functions used for different edge conditions (TBT)

Boundary condition	$f_w$	$f_\phi$
S-S	$X(1 - X)$	1
C-S	$X(1 - X)$	$X$
C-C	$X(1 - X)$	$X(1 - X)$
C-F	$X$	$X$

In the bending analysis of Timoshenko nanobeams (Chapter 3), we have used  $\hat{\varphi}_k$  and  $\hat{\psi}_k$  in Eqs. (2.14) and (2.15) respectively. As such, substituting Eqs. (2.14) and (2.15) in Eq. (2.13) and then minimizing  $U_T$  as a function of constants, one may find the following system of linear equations for Timoshenko beam theory

$$[K]\{Z\} = P_c\{B\} \quad (2.16)$$

where  $Z$  is a column vector of constants,  $[K]$ ,  $\{B\}$  and  $P_c$  are defined in Chapter 3.

## 2.1.2 Vibration problems

We have analyzed vibration of nanobeams based on Euler-Bernoulli and Timoshenko beam theories. In this problem, we have considered one-dimensional simple polynomials and boundary characteristic orthogonal polynomials as shape functions in the Rayleigh-Ritz method. As such, we present below the procedure for handling the above problems.

### 2.1.2.1 Euler-Bernoulli beam theory

For free vibration, we assume displacement function as harmonic type viz.

$$w(x, t) = w_0(x) \sin \omega t \quad (2.17)$$

where  $w_0$  is amplitude of the displacement component of free vibration of nanobeam and  $\omega$  denotes natural frequency of vibration.

As such, maximum strain energy  $U_{max}$  may be given as

$$U_{max} = -\frac{1}{2} \int_0^L M \frac{d^2 w_0}{dx^2} dx \quad (2.18)$$

where  $M$  may be obtained from Eq. (1.8) by setting  $\bar{N}$  and  $q$  to zero. As such,  $M$  may be given by

$$M = -EI \frac{d^2 w_0}{dx^2} + \mu (-\rho A \omega^2 w_0) \quad (2.19)$$

Here we have taken  $m_0 = \rho A$ .

Maximum kinetic energy is expressed as

$$T_{max} = \frac{1}{2} \int_0^L \rho A \omega^2 w_0^2 dx \quad (2.20)$$

where  $\rho$  denotes the density of beams.

Rayleigh Quotient  $\lambda^2$  may be obtained by equating maximum kinetic and strain energies which is given in Chapter 5.

In the vibration of Euler-Bernoulli nanobeams (Chapter 5), simple polynomials ( $\varphi_k$ ) and orthonormal polynomials ( $\hat{\varphi}_k$ ) are used in Eq. (2.5). As such, substituting Eq. (2.5) in the Rayleigh Quotient and minimizing Rayleigh Quotient with respect to the constant coefficients, a generalized eigen value problem will be obtained as

$$[K] \{Z\} = \lambda^2 [M_a] \{Z\} \quad (2.21)$$

where  $Z$  is a column vector of constants and the matrices  $[K]$  as well as  $[M_a]$  are the stiffness and mass matrices which are defined in respective Chapters.

### 2.1.2.2 Timoshenko beam theory

Here also, we have considered free harmonic motion viz.  $w(x, t) = w_0(x)\sin\omega t$  and  $\phi(x, t) = \phi_0(x)\sin\omega t$ .

Maximum strain energy may be given as (Wang et al. 2007)

$$U_{max} = \frac{1}{2} \int_0^L \left( M \frac{d\phi_0}{dx} + Q \left( \phi_0 + \frac{dw_0}{dx} \right) \right) dx \quad (2.22)$$

Bending moment  $M$  and shear force  $Q$  may be obtained by setting  $\bar{N}$  and  $q$  to zero respectively in Eqs. (1.17) and (1.18). As such, we have

$$M = EI \frac{d\phi_0}{dx} + \mu \left[ -\rho A \omega^2 w_0 - \rho I \omega^2 \frac{d\phi_0}{dx} \right] \quad (2.23)$$

$$Q = GAK_s \left( \phi_0 + \frac{dw_0}{dx} \right) - \mu \rho A \omega^2 \frac{dw_0}{dx} \quad (2.24)$$

Maximum kinetic energy is written as (Wang et al. 2007)

$$T_{max} = \frac{1}{2} \int_0^L (\rho A \omega^2 w_0^2 + \rho I \omega^2 \phi_0^2) dx \quad (2.25)$$

Equating maximum kinetic and strain energies, one may obtain Rayleigh Quotient ( $\lambda^2$ ) which is given in Chapter 5.

In the vibration of Timoshenko nanobeams (Chapter 5), we have used simple polynomials ( $\varphi_k$  and  $\psi_k$ ) and orthonormal polynomials ( $\hat{\varphi}_k$  and  $\hat{\psi}_k$ ) in Eqs. (2.14) and (2.15).

Substituting Eqs. (2.14) and (2.15) in the Rayleigh-Quotient and minimizing  $\lambda^2$  with respect to the unknown coefficients  $c_j$  and  $d_j$ , the following generalized eigen value problem will be obtained

$$[K] \{Z\} = \lambda^2 [M_a] \{Z\} \quad (2.26)$$

where  $Z$  is a column vector of constants and the matrices  $[K]$  as well as  $[M_a]$  are stiffness and mass matrices which are given in Chapter 5.

## 2.2 Plate theory

Here we have discussed the procedure for applying Rayleigh-Ritz method in the bending, buckling and vibration analyses of nanoplates based on classical plate theory. Consider a rectangular nanoplate with the domain  $a \leq x \leq b$ ,  $a \leq y \leq b$  in  $xy$ - plane where  $a$  and  $b$  are the length and the breadth of the nanoplate respectively. The  $x$ - and  $y$ - axes are taken along the edges of

the nanoplate and  $z$ - axis is perpendicular to the  $xy$ - plane. The middle surface being  $z = 0$  and origin (O) is at one of the corners of the nanoplate (Fig. 2.1).

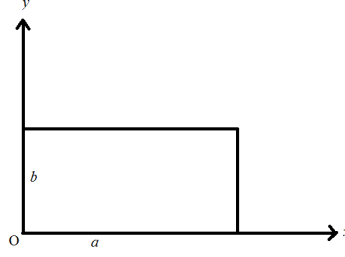


Fig. 2.1 Geometry of the nanoplate

## 2.2.1 Classical plate theory

### 2.2.1.1 Bending problem

To apply Rayleigh-Ritz method, one should have knowledge about energies of the system. As such, we have shown below energies of orthotropic nanoplates embedded in elastic foundations such as Winkler and Pasternak.

The strain energy ( $U$ ) of orthotropic nanoplates may be given by (Anjomshoa 2013)

$$\begin{aligned}
 U = & \frac{1}{2} \int_0^a \int_0^b \left\{ D_{11} \left( \frac{\partial^2 w}{\partial x^2} \right)^2 + 2D_{12} \left( \frac{\partial^2 w}{\partial x^2} \frac{\partial^2 w}{\partial y^2} \right) + D_{22} \left( \frac{\partial^2 w}{\partial y^2} \right)^2 + 4D_{33} \left( \frac{\partial^2 w}{\partial x \partial y} \right)^2 \right. \\
 & + k_w \left[ w^2 + \mu \left( \left( \frac{\partial w}{\partial x} \right)^2 + \left( \frac{\partial w}{\partial y} \right)^2 \right) \right] \\
 & \left. + k_p \left[ \left( \frac{\partial w}{\partial x} \right)^2 + \left( \frac{\partial w}{\partial y} \right)^2 + \mu \left( \left( \frac{\partial^2 w}{\partial x^2} \right)^2 + 2 \left( \frac{\partial^2 w}{\partial x \partial y} \right)^2 + \left( \frac{\partial^2 w}{\partial y^2} \right)^2 \right) \right] \right\} dx dy \quad (2.27)
 \end{aligned}$$

where  $w$  is the displacement and  $\mu = (e_0 l_{int})^2$  is the nonlocal parameter with  $e_0$  as material constant and  $l_{int}$  as internal characteristic length of the system (lattice parameter, granular distance, distance between C-C bonds). Here  $k_w$  and  $k_p$  denote the Winkler and Pasternak coefficients of the elastic foundation respectively and  $D_{ij}$  are flexural rigidities of the nanoplate which are defined as

$$D_{11} = \frac{E_x h^3}{12(1-\nu_x \nu_y)}, \quad D_{12} = \frac{\nu_y E_x h^3}{12(1-\nu_x \nu_y)} = \frac{\nu_x E_y h^3}{12(1-\nu_x \nu_y)}, \quad D_{22} = \frac{E_y h^3}{12(1-\nu_x \nu_y)} \quad \text{and} \quad D_{33} = \frac{G_{xy} h^3}{12}$$

In the expression of flexural rigidities,  $h$  is the height of the nanoplate,  $E_x$  and  $E_y$  the Young's moduli,  $\nu_x$  and  $\nu_y$  the Poisson's ratios and  $G_{xy}$  the shear modulus of the nanoplate.



In case of isotropic nanolates, the potential energy (Eq. 2.27) reduces to

$$\begin{aligned}
 U = & \frac{1}{2}D \int_0^a \int_0^b \left\{ \left( \frac{\partial^2 w}{\partial x^2} \right)^2 + 2\nu \left( \frac{\partial^2 w}{\partial x^2} \frac{\partial^2 w}{\partial y^2} \right) + \left( \frac{\partial^2 w}{\partial y^2} \right)^2 + 2(1-\nu) \left( \frac{\partial^2 w}{\partial x \partial y} \right)^2 \right. \\
 & + k_w \left[ w^2 + \mu \left( \left( \frac{\partial w}{\partial x} \right)^2 + \left( \frac{\partial w}{\partial y} \right)^2 \right) \right] \\
 & \left. + k_p \left[ \left( \frac{\partial w}{\partial x} \right)^2 + \left( \frac{\partial w}{\partial y} \right)^2 + \mu \left( \left( \frac{\partial^2 w}{\partial x^2} \right)^2 + 2 \left( \frac{\partial^2 w}{\partial x \partial y} \right)^2 + \left( \frac{\partial^2 w}{\partial y^2} \right)^2 \right) \right] \right\} dx dy \quad (2.28)
 \end{aligned}$$

where  $D = \frac{Eh^3}{12(1-\nu^2)}$  is flexural rigidity for isotropic nanoplate.

The potential energy of the transverse force  $q$  may be given by (Anjomshoa 2013)

$$V = -q \left[ w - \mu \left( \frac{\partial^2 w}{\partial x^2} + \frac{\partial^2 w}{\partial y^2} \right) \right] \quad (2.29)$$

The total energy  $U_T$  of the system may be written as

$$U_T = U + V \quad (2.30)$$

Displacement function  $w$  may be expressed as the sum of series of polynomials. As such,

$$w(X) = \sum_{k=1}^n c_k \varphi_k \quad (2.31)$$

where  $n$  is the number of terms needed in the series and  $c_k$ 's are unknowns. Here  $\varphi_k$  are the polynomials which are consisting of a boundary polynomial specifying support conditions (essential boundary conditions) multiplied by two-dimensional simple polynomials viz.  $\varphi_k = f f_k$  where  $f_k$  are two-dimensional simple polynomials and  $f = X^u(1-X)^v Y^{u_1}(1-Y)^{v_1}$ . Here  $u = 0, 1, \text{ or } 2$  as the edge  $X = 0$  is free, simply supported or clamped. Same justification can be given to  $v, u_1$  and  $v_1$  for the edges  $X = 1, Y = 0$  and  $Y = 1$ . The edge conditions are taken in anticlockwise direction starting at the edge  $X = 0$  and obtained by assigning various values to  $u, v, u_1$  and  $v_1$  as 0, 1, 2 for free, simply supported and clamped edge conditions respectively. Fig. 2.2 shows the handling of using S-C-S-C boundary condition. Similarly other boundary conditions may also be handled.

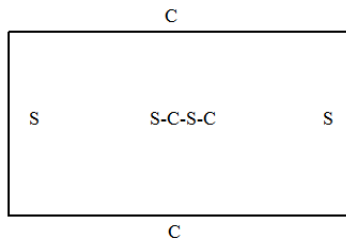


Fig. 2.2 Boundary condition

When  $\varphi_k$  are orthogonal polynomials then Gram-Schmidt process as discussed in section 2.1.1.1 has been used to obtain these polynomials respectively from set of linearly independent functions  $F_k$  where  $F_k = f f_k$ . Then orthonormal polynomials  $\hat{\varphi}_k$  may be obtained from orthogonal polynomials  $\varphi_k$  as discussed in section 2.1.1.1.

Substituting Eq. (2.31) in Eq. (2.30) and then minimizing total energy of the system as a function of constants, one may obtain following system of linear equation.

$$\sum_{j=1}^n a_{ij} c_j = P_c b_i \quad (2.32)$$

where  $a_{ij}$ ,  $P_c$  and  $b_i$  are given in Chapter 4.

### 2.2.1.2 Buckling problem

For this problem, we have the strain energy same as that of Eq. (2.27).

The potential energy due to axial compressive force is written as (Anjomshoa 2013)

$$V_a = \frac{1}{2} N_{xx} \int_0^a \int_0^b \left\{ \left( \frac{\partial w}{\partial x} \right)^2 + \mu \left( \left( \frac{\partial^2 w}{\partial x^2} \right)^2 + \left( \frac{\partial^2 w}{\partial x \partial y} \right)^2 \right) + \frac{N_{yy}}{N_{xx}} \left[ \left( \frac{\partial w}{\partial y} \right)^2 + \mu \left( \left( \frac{\partial^2 w}{\partial y^2} \right)^2 + \left( \frac{\partial^2 w}{\partial x \partial y} \right)^2 \right) \right] \right. \\ \left. + \frac{2 N_{xy}}{N_{xx}} \left[ \frac{\partial w}{\partial x} \frac{\partial w}{\partial y} + \mu \left( \frac{\partial^2 w}{\partial x^2} \frac{\partial^2 w}{\partial x \partial y} + \frac{\partial^2 w}{\partial y^2} \frac{\partial^2 w}{\partial x \partial y} \right) \right] \right\} dx dy \quad (2.33)$$

For uniform in-plane compression, we have used the relations  $N_{xx} = N_{yy} = -N$ ,  $N_{xy} = 0$ .

Accordingly, Eq. (2.33) reduces to

$$V_a = \frac{1}{2} N_{xx} \int_0^a \int_0^b \left\{ \left( \frac{\partial w}{\partial x} \right)^2 + \mu \left( \left( \frac{\partial^2 w}{\partial x^2} \right)^2 + \left( \frac{\partial^2 w}{\partial x \partial y} \right)^2 \right) + \left( \frac{\partial w}{\partial y} \right)^2 + \mu \left( \left( \frac{\partial^2 w}{\partial y^2} \right)^2 + \left( \frac{\partial^2 w}{\partial x \partial y} \right)^2 \right) \right\} dx dy$$

Equating above energies of the system, one may get Rayleigh-quotient ( $\bar{N}^0$ ) which is given in Chapter 4.

Substituting Eq. (2.31) into Rayleigh-quotient, we get a generalized eigen value problem as

$$[K] \{Z\} = \bar{N}^0 [B_c] \{Z\} \quad (2.34)$$

where  $K$  and  $B_c$  are the stiffness and buckling matrices given in Chapter 4 and  $Z$  is a column vector of constants.

### 2.2.1.3 Vibration Problem

In this case, we have considered free harmonic motion.

As such, maximum strain energy for isotropic nanoplate is given by

$$\begin{aligned}
 U_{max} = & \frac{1}{2}D \int_0^a \int_0^b \left\{ \left( \frac{\partial^2 w_0}{\partial x^2} \right)^2 + 2\nu \left( \frac{\partial^2 w_0}{\partial x^2} \frac{\partial^2 w_0}{\partial y^2} \right) + \left( \frac{\partial^2 w_0}{\partial y^2} \right)^2 + 2(1-\nu) \left( \frac{\partial^2 w_0}{\partial x \partial y} \right)^2 \right. \\
 & + k_w \left[ w_0^2 + \mu \left( \left( \frac{\partial w_0}{\partial x} \right)^2 + \left( \frac{\partial w_0}{\partial y} \right)^2 \right) \right] \\
 & \left. + k_p \left[ \left( \frac{\partial w_0}{\partial x} \right)^2 + \left( \frac{\partial w_0}{\partial y} \right)^2 + \mu \left( \left( \frac{\partial^2 w_0}{\partial x^2} \right)^2 + 2 \left( \frac{\partial^2 w_0}{\partial x \partial y} \right)^2 + \left( \frac{\partial^2 w_0}{\partial y^2} \right)^2 \right) \right] \right\} dx dy \quad (2.35)
 \end{aligned}$$

Maximum kinetic energy ( $T_{max}$ ) is given by (Anjomshoa 2013)

$$T_{max} = \frac{1}{2} m_0 \omega^2 \int_0^a \int_0^b \left\{ w_0^2 + \mu \left( \left( \frac{\partial w_0}{\partial x} \right)^2 + \left( \frac{\partial w_0}{\partial y} \right)^2 \right) \right\} dx dy \quad (2.36)$$

Equating maximum kinetic and strain energies, one may obtain the Rayleigh-quotient ( $\lambda^2$ ).

Substituting Eq. (2.31) into Rayleigh-quotient ( $\lambda^2$ ), we get a generalized eigen value problem as

$$[K] \{Z\} = \lambda^2 [M_a] \{Z\} \quad (2.37)$$

where  $K$  and  $M_a$  are respectively the stiffness and mass matrices which are given in Chapter 7.

## 2.3 Differential quadrature method (DQM)

We have used differential quadrature method in the buckling and vibration analyses of nanobeams. As such, we have first shown governing equations which are then converted to single variable.

### 2.3.1 Buckling problems

We have shown below governing differential equations for buckling analyses of nanobeams based on four types of beam theories such as Euler-Bernoulli, Timoshenko, Reddy and Levinson.

### 2.3.2 Euler Bernoulli beam theory (EBT)

Following governing equation for buckling analysis may be obtained from Eq. (1.9) by setting  $q$  and all time derivatives as zero

$$-EI \frac{d^4 w}{dx^4} + \mu \bar{N} \frac{d^4 w}{dx^4} - \bar{N} \frac{d^2 w}{dx^2} = 0 \quad (2.38)$$

### 2.3.3 Timoshenko beam theory (TBT)

For this theory, governing equation is obtained from Eqs. (1.19) and (1.20) by setting  $q$  and all time derivatives as zero and is written as

$$GAK_s \left( \frac{d\phi}{dx} + \frac{d^2 w}{dx^2} \right) - \bar{N} \frac{d^2 w}{dx^2} + \mu \bar{N} \frac{d^4 w}{dx^4} = 0 \quad (2.39)$$

$$EI \frac{d^2 \phi}{dx^2} - GAK_s \left( \phi + \frac{dw}{dx} \right) = 0 \quad (2.40)$$

Eliminating  $\phi$  from Eqs. (2.39) and (2.40), governing equations can be written in terms of one variable as

$$-EI \frac{d^4 w}{dx^4} + EI \frac{\bar{N}}{k_s GA} \frac{d^4 w}{dx^4} - \mu EI \frac{\bar{N}}{k_s GA} \frac{d^6 w}{dx^6} - \bar{N} \frac{d^2 w}{dx^2} + \mu \bar{N} \frac{d^4 w}{dx^4} = 0 \quad (2.41)$$

### 2.3.4 Reddy beam theory (RBT)

Governing equation for RBT may be obtained from Eqs. (1.26) and (1.27) by setting  $q$  and all time derivatives as zero

$$G\tilde{A} \left( \frac{d\phi}{dx} + \frac{d^2 w}{dx^2} \right) - \bar{N} \frac{d^2 w}{dx^2} + \mu \bar{N} \frac{d^4 w}{dx^4} + c_1 EJ \frac{d^3 \phi}{dx^3} - c_1^2 EK \left( \frac{d^3 \phi}{dx^3} + \frac{d^4 w}{dx^4} \right) = 0 \quad (2.42)$$

$$EI \frac{d^2 \phi}{dx^2} - c_1 EJ \left( \frac{d^2 \phi}{dx^2} + \frac{d^3 w}{dx^3} \right) - G\tilde{A} \left( \phi + \frac{dw}{dx} \right) = 0 \quad (2.43)$$

Again eliminating  $\phi$  from Eqs. (2.42) and (2.43), governing equations is obtained in terms of displacement as

$$\frac{105}{84} G\tilde{A} \frac{d^4 w}{dx^4} - \frac{1}{105} EI \frac{d^6 w}{dx^6} = -\frac{105}{84EI} G\tilde{A} \bar{N} \frac{d^2 w}{dx^2} + \frac{105}{84EI} \mu G\tilde{A} \bar{N} \frac{d^4 w}{dx^4} + \frac{68}{84} \bar{N} \frac{d^4 w}{dx^4} - \frac{68}{84} \mu \bar{N} \frac{d^6 w}{dx^6} \quad (2.44)$$

### 2.3.5 Levinson beam theory (LBT)

In this case, governing equation is obtained from Eqs. (1.33) and (1.34) by again setting  $q$  and all time derivatives as zero

$$G\bar{A} \left( \frac{d\phi}{dx} + \frac{d^2w}{dx^2} \right) - \bar{N} \frac{d^2w}{dx^2} + \mu\bar{N} \frac{d^4w}{dx^4} = 0 \quad (2.45)$$

$$EI \frac{d^2\phi}{dx^2} - c_1 EJ \left( \frac{d^2\phi}{dx^2} + \frac{d^3w}{dx^3} \right) - G\bar{A} \left( \phi + \frac{dw}{dx} \right) = 0 \quad (2.46)$$

Eliminating  $\phi$  from Eqs. (2.45) and (2.46), the reduced governing differential equation is

$$\frac{4}{5} EI \frac{\bar{N}}{G\bar{A}} \frac{d^4w}{dx^4} - EI \frac{d^4w}{dx^4} - \frac{4}{5} EI \mu \frac{\bar{N}}{G\bar{A}} \frac{d^6w}{dx^6} - \bar{N} \frac{d^2w}{dx^2} + \mu\bar{N} \frac{d^4w}{dx^4} = 0 \quad (2.47)$$

### 2.3.6 Vibration problems

Here, we have shown governing equations for free vibration analysis based on four beam theories such as Euler-Bernoulli, Timoshenko, Reddy and Levinson. Here free harmonic motion has been assumed. Also we have used the relations  $m_0 = \rho A$  and  $m_2 = \rho I$ .

### 2.3.7 Euler-Bernoulli beam theory (EBT)

For EBT, the governing equation for vibration analysis may be obtained from Eq. (1.9) by setting  $q$  and  $\bar{N}$  to zero and is written as

$$EI \frac{d^4w_0}{dx^4} + \mu\rho A\omega^2 \frac{d^2w_0}{dx^2} = \rho A\omega^2 w_0 \quad (2.48)$$

### 2.3.8 Timoshenko beam theory (TBT)

In this case, governing equation may be obtained from Eqs. (1.19) and (1.20) by setting  $q$  and  $\bar{N}$  to zero and we have

$$GAK_s \left( \frac{d\phi_0}{dx} + \frac{d^2w_0}{dx^2} \right) = \rho A\omega^2 \left( -w_0 + \mu \frac{d^2w_0}{dx^2} \right) \quad (2.49)$$

$$EI \frac{d^2\phi_0}{dx^2} - GAK_s \left( \phi_0 + \frac{dw_0}{dx} \right) = \rho I\omega^2 \left( -\phi_0 + \mu \frac{d^2\phi_0}{dx^2} \right) \quad (2.50)$$

Eliminating  $\phi_0$  from Eqs. (2.49-2.50) and neglecting coefficient of  $\omega_n^4$ , governing equations can be transformed to

$$-EI \frac{d^4w_0}{dx^4} = \frac{EI}{k_s GA} \rho A\omega^2 \left( \frac{d^2w_0}{dx^2} - \mu \frac{d^4w_0}{dx^4} \right) + \rho I\omega^2 \left( \frac{d^2w_0}{dx^2} - \mu \frac{d^4w_0}{dx^4} \right) - \rho A\omega^2 \left( w_0 - \mu \frac{d^2w_0}{dx^2} \right) \quad (2.51)$$

### 2.3.9 Reddy beam theory (RBT)

Governing equation for RBT may be obtained from Eqs. (1.26) and (1.27) by setting  $q$  and  $\bar{N}$  to zero and is obtained as

$$G\bar{A} \left( \frac{d\phi_0}{dx} + \frac{d^2w_0}{dx^2} \right) + c_1EJ \frac{d^3\phi_0}{dx^3} - c_1^2EK \left( \frac{d^3\phi_0}{dx^3} + \frac{d^4w_0}{dx^4} \right) = -\rho A\omega^2 \left( w_0 - \mu \frac{d^2w_0}{dx^2} \right) \quad (2.52)$$

$$EI \frac{d^2\phi_0}{dx^2} - c_1EJ \left( \frac{d^2\phi_0}{dx^2} + \frac{d^3w_0}{dx^3} \right) - G\bar{A} \left( \phi_0 + \frac{dw_0}{dx} \right) = 0 \quad (2.53)$$

Eliminating  $\phi_0$  from Eqs. (2.52) and (2.53), governing equations may be obtained in terms of  $w_0$  as

$$G\bar{A} \frac{5}{4} \frac{d^4w_0}{dx^4} - \frac{1}{105} EI \frac{d^6w_0}{dx^6} = -\frac{17}{21} \rho A\omega^2 \frac{d^2w_0}{dx^2} + \frac{17}{21} \mu \rho A\omega^2 \frac{d^4w_0}{dx^4} + G\bar{A} \frac{105}{84EI} \rho A\omega^2 \left( w_0 - \mu \frac{d^2w_0}{dx^2} \right) \quad (2.54)$$

### 2.3.10 Levinson beam theory (LBT)

For this beam theory, governing equations may be obtained from Eqs. (1.33) and (1.34) by setting  $q$  and  $\bar{N}$  to zero and is written as

$$G\bar{A} \left( \frac{d\phi_0}{dx} + \frac{d^2w_0}{dx^2} \right) = -\rho A\omega^2 \left( w_0 - \mu \frac{d^2w_0}{dx^2} \right) \quad (2.55)$$

$$EI \frac{d^2\phi_0}{dx^2} - c_1EJ \left( \frac{d^2\phi_0}{dx^2} + \frac{d^3w_0}{dx^3} \right) - G\bar{A} \left( \phi_0 + \frac{dw_0}{dx} \right) = -\rho I\omega^2 \left( \phi_0 - \mu \frac{d^2\phi_0}{dx^2} \right) \quad (2.56)$$

Eliminating  $\phi_0$  from Eqs. (2.55) and (2.56) and neglecting coefficient of  $\omega_n^4$ , the governing differential equation reduces to

$$\left( -\rho A\omega^2 \frac{d^2w_0}{dx^2} + \rho A\mu\omega^2 \frac{d^4w_0}{dx^4} - G\bar{A} \frac{d^4w_0}{dx^4} \right) \left( \frac{EI}{G\bar{A}} - \frac{c_1EJ}{G\bar{A}} \right) - c_1EJ \frac{d^4w_0}{dx^4} + \rho A\omega^2 \left( w_0 - \mu \frac{d^2w_0}{dx^2} \right) = \rho I\omega^2 \left( \frac{d^2w_0}{dx^2} - \mu \frac{d^4w_0}{dx^4} \right) \quad (2.57)$$

Next, we have briefly explained the procedure for applying differential quadrature method in the above equations. We have considered the function  $w(X)$  in the domain  $[0, 1]$  with  $n$  discrete

grid points. First derivative at point  $i$ ,  $w_i' = \frac{dw}{dX}$  at  $X = X_i$  is given by (Wang and Bert 1993)

$$\begin{aligned}
 w_i' &= \sum_{j=1}^n A_{ij} w_j \\
 w_i'' &= \sum_{j=1}^n B_{ij} w_j \\
 w_i''' &= \sum_{j=1}^n C_{ij} w_j \\
 w_i^{IV} &= \sum_{j=1}^n D_{ij} w_j
 \end{aligned} \tag{2.58}$$

where  $i = 1, 2, \dots, n$  and  $n$  is the number of discrete grid points.

Here  $A_{ij}$ ,  $B_{ij}$ ,  $C_{ij}$  and  $D_{ij}$  are the weighting coefficients of the first, second, third and fourth derivatives respectively.

#### *Determination of Weighting coefficients*

Computation of weighting coefficient matrix  $A = (A_{ij})$  is the key step in the DQM. In the present investigation, we have used Quan and Chang's (1989) approach to compute weighting coefficients  $A_{ij}$ . As per this approach, matrix  $A = (A_{ij})$  may be computed by the following procedure.

$$A_{ij} = \frac{1}{X_j - X_i} \prod_{\substack{k \neq i \\ k \neq j \\ k=1}}^n \frac{X_i - X_k}{X_j - X_k}, \quad i \neq j, \quad i = 1, 2, \dots, n \quad j = 1, 2, \dots, n \tag{2.59}$$

$$A_{ii} = \sum_{\substack{k \neq i \\ k=1}}^n \frac{1}{X_i - X_k}, \quad i = 1, 2, \dots, n \tag{2.60}$$

Once weighting coefficients of first order derivatives are computed, weighting coefficients of higher order derivatives may be obtained by simply matrix multiplication as follow.

$$B = B_{ij} = \sum_{k=1}^n A_{ik} A_{kj} \tag{2.61}$$

$$C = C_{ij} = \sum_{k=1}^n A_{ik} B_{kj} \tag{2.62}$$

$$D = D_{ij} = \sum_{k=1}^n A_{ik} C_{kj} = \sum_{k=1}^n B_{ik} B_{kj} \quad (2.63)$$

*Selection of mesh point distribution*

We assume that the domain  $0 \leq X \leq 1$  is divided into  $(n - 1)$  intervals with coordinates of the grid points given as  $X_1, X_2, \dots, X_n$ . These  $X_i$ 's have been computed by using Chebyshev-Gauss-Lobatto grid points. That is

$$X_i = \frac{1}{2} \left[ 1 - \cos \left( \frac{i-1}{n-1} \cdot \Pi \right) \right]$$

*Application of boundary condition*

Above matrices  $A, B, C$  and  $D$  are converted into modified weighting coefficient matrices  $\bar{A}, \bar{B}, \bar{C}$  and  $\bar{D}$  as per the boundary condition. First, we denote

$$\bar{A}_1 = \begin{bmatrix} 0 & A_{1,2} & \cdots & A_{1,n} \\ 0 & A_{2,2} & \cdots & A_{2,n} \\ \cdots & \cdots & \cdots & \cdots \\ 0 & A_{n,2} & \cdots & A_{n,n} \end{bmatrix}, \bar{A}_2 = \begin{bmatrix} A_{1,1} & A_{1,2} & \cdots & A_{1,n-1} & 0 \\ A_{2,1} & A_{2,2} & \cdots & A_{2,n-1} & 0 \\ \cdots & \cdots & \cdots & \cdots & \cdots \\ A_{n,1} & A_{n,2} & \cdots & A_{n-1,n-1} & 0 \end{bmatrix}$$

In view of the above, we now illustrate the procedure for finding modified weighting coefficient matrices as per the considered boundary conditions and are discussed below:

### **simply supported-simply supported (S-S)**

For this boundary condition, Eq. (2.58) may be rewritten in matrix form as

$$A = \begin{bmatrix} A_{1,1} & A_{1,2} & \cdots & A_{1,n-1} & A_{1,n} \\ A_{2,1} & A_{2,2} & \cdots & A_{2,n-1} & A_{2,n} \\ \vdots & \vdots & & \vdots & \vdots \\ A_{n,1} & A_{n,2} & \cdots & A_{n,n-1} & A_{n,n} \end{bmatrix} \begin{Bmatrix} w_1 \\ w_2 \\ \vdots \\ w_n \end{Bmatrix} = \begin{Bmatrix} w_1' \\ w_2' \\ \vdots \\ w_n' \end{Bmatrix} \quad (2.64)$$

Firstly, to apply boundary condition  $w_1 = w_n = 0$ , Eq. (2.64) becomes

$$\begin{bmatrix} 0 & A_{1,2} & \cdots & A_{1,n-1} & 0 \\ 0 & A_{2,2} & \cdots & A_{2,n-1} & 0 \\ \vdots & \vdots & & \vdots & \vdots \\ 0 & A_{n,2} & \cdots & A_{n,n-1} & 0 \end{bmatrix} \begin{Bmatrix} w_1 \\ w_2 \\ \vdots \\ w_n \end{Bmatrix} = \begin{Bmatrix} w_1' \\ w_2' \\ \vdots \\ w_n' \end{Bmatrix} \quad (2.65)$$



or

$$[\bar{A}]\{w\} = \{w'\} \quad (2.66)$$

For the second derivative, one has

$$\{w''\} = [A]\{w'\} \quad (2.67)$$

Using Eq. (2.66), one may obtain

$$\begin{aligned} \{w''\} &= [A][\bar{A}]\{w\} \\ &= [\bar{B}]\{w\} \end{aligned} \quad (2.68)$$

where  $\bar{B} = [A][\bar{A}]$ .

Now, since  $w''_1 = w''_n = 0$ , we have third order derivative as

$$\{w'''\} = [\bar{A}]\{w''\} \quad (2.69)$$

Using Eq. (2.68), one obtains

$$\begin{aligned} \{w'''\} &= [\bar{A}][\bar{B}]\{w\} \\ &= [\bar{C}]\{w\} \end{aligned} \quad (2.70)$$

where  $[\bar{C}] = [\bar{A}][\bar{B}]$ .

Similarly, for fourth order derivative, we have

$$\begin{aligned} \{w^{IV}\} &= [A]\{w'''\} \\ &= [A][\bar{C}]\{w\} \\ &= [\bar{B}][\bar{B}]\{w\} \\ &= [\bar{D}]\{w\} \end{aligned} \quad (2.71)$$

where  $[\bar{D}] = [\bar{B}][\bar{B}]$  or  $[\bar{D}] = [A][\bar{C}]$ .

Proceeding in the similar fashion as that of simply supported-simply supported, we have following modified coefficient matrices for other boundary conditions.

### **clamped-simply supported (C-S)**

$$\{w'\} = [\bar{A}]\{w\}$$

$$\{w''\} = [\bar{A}_1]\{w'\} = [\bar{A}_1][\bar{A}]\{w\} = [\bar{B}]\{w\} \text{ with } [\bar{B}] = [\bar{A}_1][\bar{A}].$$

$$\{w'''\} = [\bar{A}_2]\{w''\} = [\bar{A}_2][\bar{B}]\{w\} = [\bar{C}]\{w\} \text{ with } [\bar{C}] = [\bar{A}_2][\bar{B}]$$

$$\{w^{IV}\} = [A]\{w'''\} = [A][\bar{C}]\{w\} = [\bar{D}]\{w\} \text{ with } [\bar{D}] = [A][\bar{C}].$$

### clamped-clamped (C-C)

$$\{w'\} = [\bar{A}]\{w\}$$

$$\{w''\} = [\bar{A}]\{w'\} = [\bar{A}][\bar{A}]\{w\} = [\bar{B}]\{w\} \text{ with } [\bar{B}] = [\bar{A}][\bar{A}]$$

$$\{w'''\} = [A]\{w''\} = [A][\bar{B}]\{w\} = [\bar{C}]\{w\} \text{ with } [\bar{C}] = [A][\bar{B}]$$

$$\{w^{IV}\} = [A]\{w'''\} = [A][\bar{C}]\{w\} = [\bar{D}]\{w\} \text{ with } [\bar{D}] = [A][\bar{C}].$$

### clamped-free (C-F)

$$\{w'\} = [\bar{A}_1]\{w\}$$

$$\{w''\} = [\bar{A}_1]\{w'\} = [\bar{A}_1][\bar{A}_1]\{w\} = [\bar{B}]\{w\} \text{ with } [\bar{B}] = [\bar{A}_1][\bar{A}_1]$$

$$\{w'''\} = [\bar{A}_2]\{w''\} = [\bar{A}_2][\bar{B}]\{w\} = [\bar{C}]\{w\} \text{ with } [\bar{C}] = [\bar{A}_2][\bar{B}]$$

$$\{w^{IV}\} = [\bar{A}_2]\{w'''\} = [\bar{A}_2][\bar{C}]\{w\} = [\bar{D}]\{w\} \text{ with } [\bar{D}] = [\bar{A}_2][\bar{C}]$$

It may be noted that while substituting values of the derivatives in the governing differential equations, one has to use  $[\bar{A}]$ ,  $[\bar{B}]$ ,  $[\bar{C}]$ ,  $[\bar{D}]$  as per the specified boundary conditions.

Substituting Eq. (2.58) in any of the Eqs. (2.38, 2.41, 2.44, 2.47) depending upon the beam theories, a generalized eigen value problem for buckling problem obtained as

$$[K]\{W\} = \bar{N}^0 [B_c]\{W\} \quad (2.72)$$

where  $K$  is the stiffness matrix,  $B_c$  is the buckling matrix.

Substituting Eq. (2.58) in any of the Eqs. (2.48, 2.51, 2.54, 2.57) depending upon the beam theories, a generalized eigen value problem obtained for vibration problem as

$$[K]\{W\} = \lambda^2 [M_a]\{W\} \quad (2.73)$$

where  $K$  is the stiffness matrix,  $M_a$  is the mass matrix and  $\lambda^2$  is the frequency parameter.

# **Chapter 3**

## **Bending and buckling of nanobeams**

The contents of this chapter have been communicated for publication.

## Chapter 3

# Bending and buckling of nanobeams

As discussed in Chapter 1 that bending and buckling analyses of nanostructures play an important role. As such, this chapter is concerned with bending and buckling of nanobeams. Bending analysis has been carried out based on Euler-Bernoulli and Timoshenko beam theories in conjunction with nonlocal elasticity theory of Eringen (Eringen 1972). Boundary characteristic orthogonal polynomials have been used as shape functions in the Rayleigh-Ritz method. Various parametric studies have been carried out and shown. Deflection and rotation shapes of nanobeams with specified boundary conditions have also been presented.

Next, differential quadrature method has been applied for buckling of non-uniform nanobeams based on four beam theories such as Euler-Bernoulli, Timoshenko, Reddy and Levinson. Here, we have also investigated buckling of nanobeams embedded in elastic medium such as Winkler and Pasternak under the influence of temperature. Boundary characteristic orthogonal polynomials and Chebyshev polynomials have been applied in the Rayleigh-Ritz method to investigate buckling of embedded nanobeams based on Euler-Bernoulli and Timoshenko beam theories respectively. Also, differential quadrature method has been employed to study buckling of embedded nanobeams based on Reddy beam theory. Here also, various parametric studies have been carried out and have been shown graphically.

## Bending of nanobeams

It is already discussed in Chapter 2 that non-dimensionalisation may be done by introducing variable  $X$  as

$$X = \frac{x}{L}$$

In this problem, we have considered uniform transverse distributed load viz. ( $q(X) = q_0$ ). Both Euler-Bernoulli and Timoshenko beam theories are considered. Rayleigh-Ritz method with boundary characteristic orthogonal polynomials as shape functions have been applied. Application of the method converts bending problem to system of linear equations as discussed in section 2.1.1.1. In the system of linear equation for EBT [Eq. (2.8)], the notations  $a_{ij}$ ,  $b_i$  and  $P_c$  are defined as follows:

$$P_c = \frac{q_0 L^4}{EI}$$

$$a_{ij} = \int_0^1 \hat{\varphi}_i'' \hat{\varphi}_j'' dX$$

$$b_i = \int_0^1 (\hat{\varphi}_i - \frac{\mu}{L^2} \hat{\varphi}_i'') dX$$

where  $i = 1, 2, \dots, n$  and  $j = 1, 2, \dots, n$ .

Similarly, in the system of linear equation for TBT [Eq. (2.16)], the notations  $K$  and  $B$  are given as

$$B = \begin{Bmatrix} b_1 \\ b_2 \end{Bmatrix} \text{ where}$$

$$b_1 = \begin{Bmatrix} \int_0^1 \varphi_1 dX \\ \vdots \\ \int_0^1 \varphi_i dX \end{Bmatrix}, b_2 = \begin{Bmatrix} \int_0^1 \mu q L \varphi_1' \\ \vdots \\ \int_0^1 \mu q L \varphi_1' dX \end{Bmatrix}$$

$$K = \begin{bmatrix} k_1 & k_2 \\ k_3 & k_4 \end{bmatrix} \text{ where } k_1, k_2, k_3 \text{ and } k_4 \text{ are submatrices which are given by}$$

$$k_1(i, j) = \int_0^1 2k_s GA \hat{\varphi}_i' \hat{\varphi}_j' dX$$

$$k_2(i, j) = \int_0^1 2k_s GAL \hat{\varphi}_i' \hat{\psi}_j dX$$

$$k_3(i, j) = \int_0^1 2k_s GAL \hat{\psi}_i \hat{\psi}_j' dX$$

$$k_4(i, j) = \int_0^1 (2k_s GAL^2 \hat{\psi}_i \hat{\psi}_j + 2EI \hat{\psi}_i' \hat{\psi}_j') dX$$

### 3.1 Numerical results and discussions

The parameters used in this investigation are (Alshorbagy et al. 2013; Reddy 2007):  $E = 30 \times 10^6$ ,  $h = 1$ ,  $k_s = \frac{5}{6}$ ,  $nu = 0.3$ . A uniformly distributed load ( $q_0 = 1$ ) has been taken into consideration. System of linear equations have been solved by using MATLAB. It is well known fact that non-dimensional maximum deflection is evaluated at the center of the beam which is given by  $W_{max} = -w \times 10^2 \left( \frac{EI}{q_0 L^4} \right)$ . At first, convergence study has been carried out to find minimum number of terms required for computation. As such, Fig. 3.1 shows convergence of EBT nanobeams for  $\frac{L}{h} = 10$  and  $\mu = 1.5nm^2$  with C-S support. One may note that  $n = 4$  is sufficient for obtaining converged results. Next, the obtained results are compared with available literature and is shown below (Table 3.1). One may find close agreement of the results.

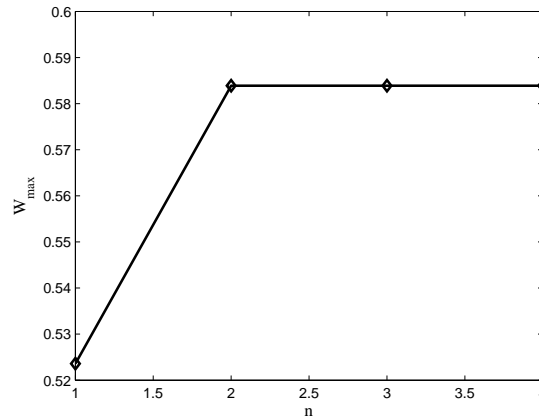


Fig. 3.1 Convergence of non-dimensional maximum center deflection for EBT

Table 3.1 Comparison of non-dimensional maximum center deflection ( $W_{max}$ ) for C-S and C-C boundary conditions

	C-S		C-C	
	Present	Ref.*	Present	Ref.*
0	0.50	0.52	0.24	0.0.26
1	0.52	0.58	0.24	0.26
2	0.59	0.61	0.24	0.26
3	0.60	0.64	0.24	0.26

\* Alshorbagy et al. (2012)

Next, we have carried out some of the parametric studies which are discussed below. It is noted here that unless mentioned deflection and rotation would denote non-dimensional maximum center deflection and non-dimensional maximum center rotation respectively.

### 3.1.1 Effect of aspect ratio

Fig. 3.2 illustrates effect of aspect ratio on the deflection of nanobeams. Here, we have shown variation of deflection with aspect ratio for both local and nonlocal cases. The figure is plotted for both EBT and TBT beam theories. Nonlocal results have been computed for  $\mu = 1nm^2$ . Aspect ratio ( $\frac{L}{h}$ ) varies from 10 to 50 with the consideration of C-S boundary condition. One may observe that in case of local EBT, aspect ratio has no effect on the beam deflection whereas in nonlocal EBT, deflection is dependent on the aspect ratio. It may also be noticed that in case of both local and nonlocal TBT, deflection is dependent on the aspect ratio. The dependency of the responses on the aspect ratio for local TBT is unique due to the effect of shear deformation. As aspect ratio decreases, the difference between the solutions of EBT and TBT becomes highly important.

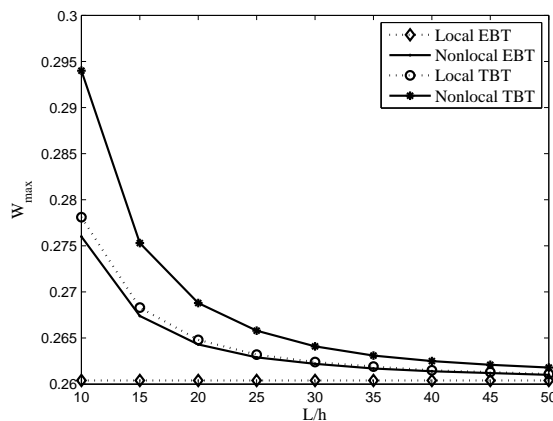


Fig. 3.2 Effect of the aspect ratio on the deflection

### 3.1.2 Effect of scale coefficient

Effect of scale coefficient on the bending response of nanobeams has been demonstrated in Fig. 3.3 for different values of  $\frac{L}{h}$ . Results have been given for TBT nanobeams with  $\frac{L}{h} = 10$  and C-S edge condition. It is seen from the figure that bending responses vary nonlinearly with the scale coefficient. One may also observe that bending responses of nanobeams with lower aspect ratios are strongly affected by the scale coefficient than those of nanobeams with relatively higher aspect ratios. Hence, one may conclude that local beam model may not be suitable for adequate approximation for the nanosized structures.

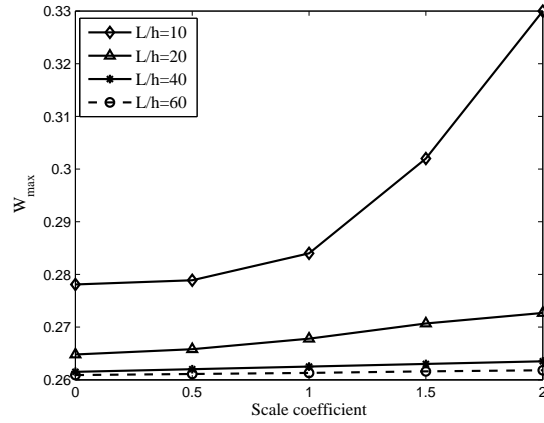


Fig. 3.3 Effect of the scale coefficient on the deflection

### 3.1.3 Effect of boundary conditions

Non-dimensional maximum center deflection of nanobeams under uniform load have been computed for different boundary conditions and have been shown graphically in Fig. 3.4. It is observed that C-C is having smallest deflection for a particular value of nonlocal parameter. One may note that in case of C-C edge condition, there is no effect of the nonlocal parameter on the deflection whereas in case of S-S and C-S supports, deflection increases with increase in nonlocal parameter. Hence effect of nonlocal parameter on the deflection is inconsistent for different boundary conditions.

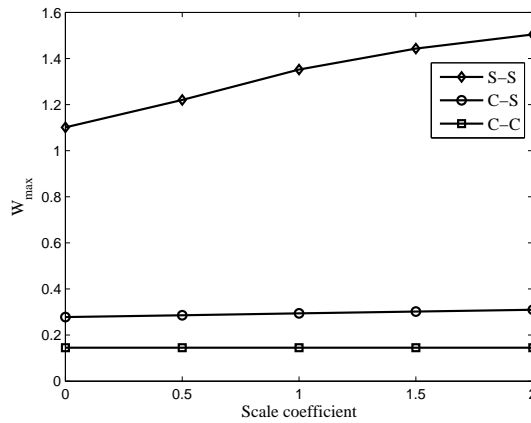


Fig. 3.4 Effect of the scale coefficient on the deflection for different boundary conditions

### 3.1.4 Deflection and rotation shapes

In this subsection, we have examined the behavior of deflection and rotation shapes of nanobeams along its length for different boundary conditions. Figs 3.5-3.7 show variation of deflection with length for S-S, C-S and C-C edge conditions respectively. It is observed from the figures that deflection of S-S and C-S nanobeams increases with increase in nonlocal parameter. It is



due to the fact that increasing nonlocal parameter causes increase in bonding force of atoms and this force is constraint from its boundaries which increases deflection (Alshorbagy et al. 2013 ). Another observation is seen that nonlocal parameter has no effect on the deflection of C-C nanobeams because of its constrained nature. Next, we have shown variation of rotation with length for S-S, C-S and C-C edge conditions respectively in Figs. 3.8-3.10. It may be noticed that rotation behaves differently than that of deflection. Increasing nonlocal parameter decreases rotation of S-S and C-C nanobeams upto mid length and after wards increase in nonlocal parameter increases rotation. One may also notice that nonlocal parameter has no effect on the rotation of C-C nanobeams.

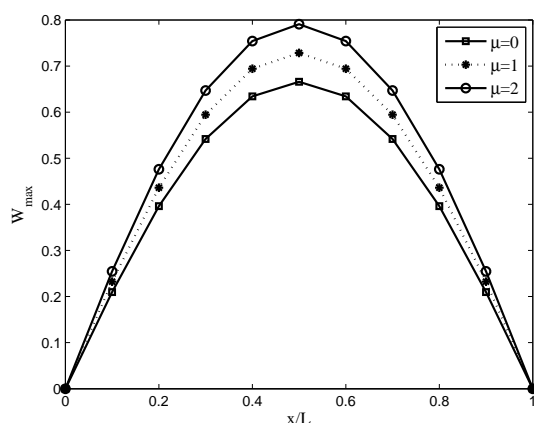


Fig. 3.5 Static deflection of S-S nanobeams for different nonlocal parameters

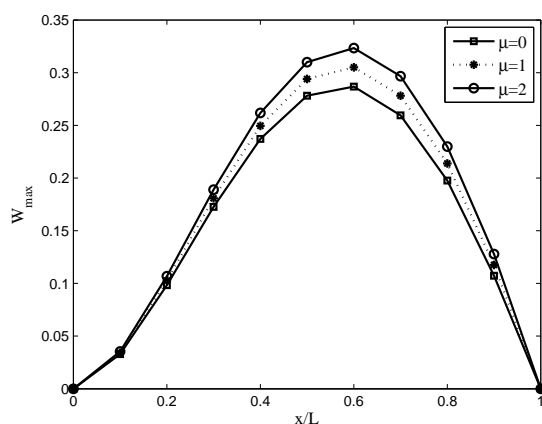


Fig. 3.6 Static deflection of C-S nanobeams for different nonlocal parameters

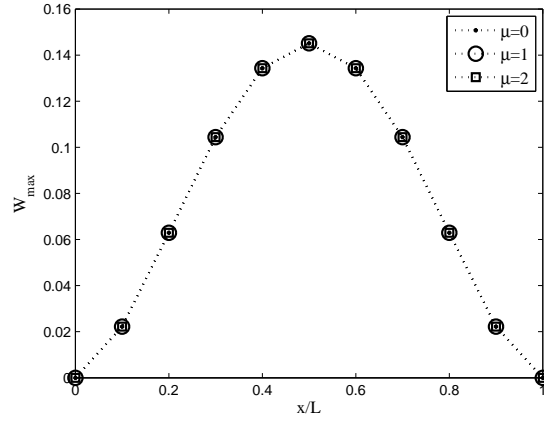


Fig. 3.7 Static deflection of C-C nanobeams for different nonlocal parameters

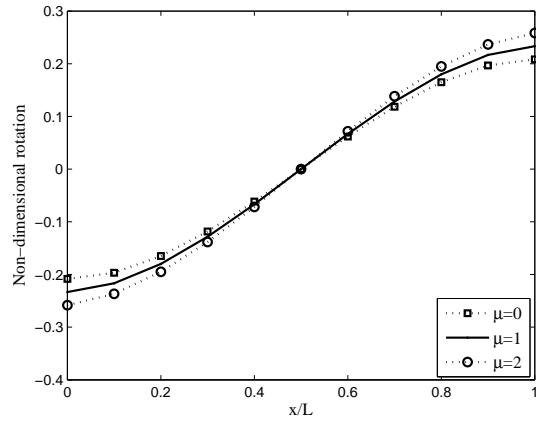


Fig. 3.8 Static rotation of S-S nanobeams for different nonlocal parameters

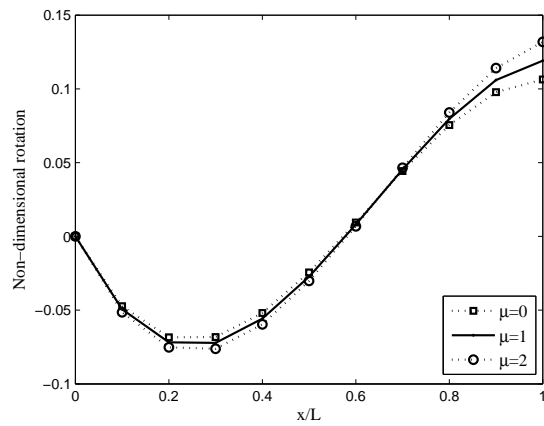


Fig. 3.9 Static rotation of C-S nanobeams for different nonlocal parameters

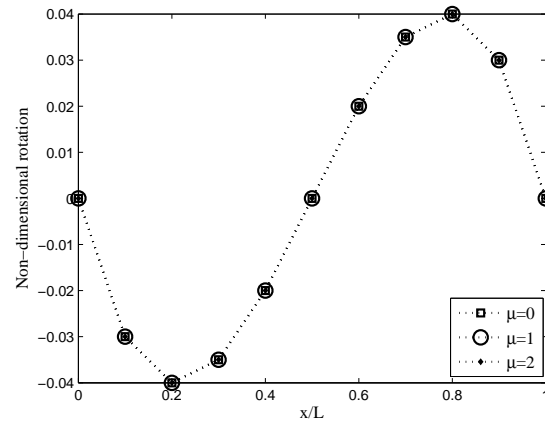


Fig. 3.10 Static rotation of C-C nanobeams for different nonlocal parameters

## Buckling of non-uniform nanobeams

As we have discussed in the Chapter 1 that study of non-uniform nanobeams play a vital role for the design of nanodevices. As such, we have investigated buckling of non-uniform nanobeams having exponentially varying stiffness. Four types beam theories have been taken into consideration. Differential quadrature method has been employed and the boundary conditions are substituted in the coefficient matrices. Some of the new results in terms of boundary conditions have also been shown.

In this problem, we have assumed exponential variation of the flexural stiffness ( $EI$ ) as:

$$EI = EI_0 e^{-\eta X}$$

where  $I_0$  is the second moment of area at the left end and  $\eta$  is the positive constant.

Here, following non-dimensional terms have been used

$$\begin{aligned} X &= \frac{x}{L} \\ W &= \frac{w}{L} \\ \alpha &= \frac{e_0 a}{L} = \text{scaling effect parameter} \\ \bar{N}^0 &= \frac{\bar{N} L^2}{EI_0} = \text{buckling load parameter} \\ \Omega &= \frac{EI_0}{k_s G A L^2} \\ \bar{\Omega} &= \frac{G \tilde{A} L^2}{EI_0} \\ \hat{\Omega} &= \frac{EI_0}{G \bar{A} L^2} \end{aligned}$$

Below we have shown the non-dimensionalized forms of the governing differential equations for EBT, TBT, RBT and LBT in Eqs. (3.1-3.4) respectively.

$$e^{-\eta X} \frac{d^4 W}{dX^4} = \bar{N}^0 \left( \alpha^2 \frac{d^4 W}{dX^4} - \frac{d^2 W}{dX^2} \right) \quad (3.1)$$

$$e^{-\eta X} \frac{d^4 W}{dX^4} = \bar{N}^0 \left( \Omega e^{-\eta X} \frac{d^4 W}{dX^4} - \Omega e^{-\eta X} \alpha^2 \frac{d^6 W}{dX^6} - \frac{d^2 W}{dX^2} + \alpha^2 \frac{d^4 W}{dX^4} \right) \quad (3.2)$$

$$\frac{105}{84}\bar{\Omega}\frac{d^4W}{dx^4} - \frac{1}{105}e^{-\eta x}\frac{d^6W}{dx^6} = \bar{N}^0 \left( -\frac{105}{84}\bar{\Omega}e^{\eta x}\frac{d^2W}{dX^2} + \frac{105}{84}\bar{\Omega}e^{\eta x}\alpha^2\frac{d^4W}{dX^4} + \frac{68}{84}\frac{d^4W}{dX^4} - \frac{68}{84}\alpha^2\frac{d^6W}{dX^6} \right) \quad (3.3)$$

$$e^{-\eta x}\frac{d^4W}{dX^4} = \bar{N}^0 \left( \frac{4}{5}\hat{\Omega}e^{-\eta x}\frac{d^4W}{dX^4} - \frac{4}{5}\hat{\Omega}e^{-\eta x}\alpha^2\frac{d^6W}{dX^6} - \frac{d^2W}{dX^2} + \alpha^2\frac{d^4W}{dX^4} \right) \quad (3.4)$$

By the application of differential quadrature method, one may obtain generalized eigen value problem as

$$[K] \{W\} = \bar{N}^0 [B_c] \{W\} \quad (3.5)$$

where  $K$  is the stiffness matrix and  $B_c$  is the buckling matrix.

## 3.2 Numerical results and discussions

In this section, numerical results have been computed by solving Eq. (3.5) using MATLAB program developed by the authors. Differential quadrature method has been employed and boundary conditions are implemented in the coefficient matrices. Here unless mentioned, buckling load would denote the critical buckling load parameter (first eigen value). It may be noted that the following parameters are taken for the computation (Sahmani and Ansari 2011; Reddy 2007):  $E = 70Gpa$ ,  $\nu = 0.23$ ,  $h = 1$ ,  $k_s = 5/6$ .

### 3.2.1 Convergence

To find the minimum number of grid points for obtaining desired results, a convergence study has been carried out for EBT and TBT nanobeams. To show how the solution is being affected by grid points, variation of critical buckling load parameter with number grid points ( $n$ ) has been shown in Fig. 3.11. In this figure, we have taken  $e_0a = 1nm$ , non-uniform parameter ( $\eta$ ) = 0.2 and  $L = 10nm$ . The convergence has been shown for simply supported edge condition only. From this figure, one may observe that convergence is achieved as we increase number of grid points. It may be noted that eleven grid points are sufficient to compute the results.

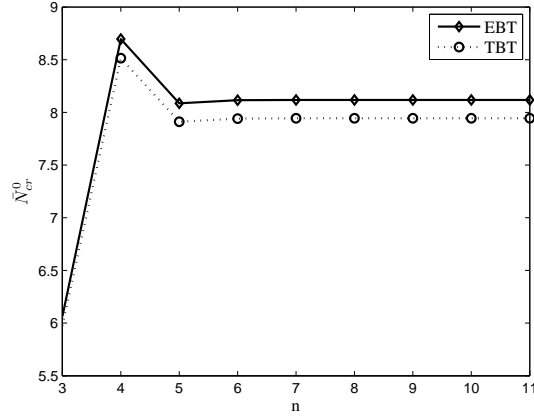


Fig. 3.11 Variation of  $\bar{N}_{cr}^0$  with grid points

### 3.2.2 Validation

To validate the present results, we compare our results with that of available in the literatures. For the validation purpose, we consider an uniform ( $\eta = 0$ ) nanobeam. To compare our results of EBT and TBT nanobeams with Wang et al. (2006), we have considered a beam of diameter  $d = 1nm$ , Young's modulus  $E = 1Tpa$  and Poisson's ratio  $\nu = 0.19$ . The comparison has been shown in Table 3.2 for three types of boundary conditions such as S-S, C-S and C-C. In this table, critical buckling load parameter (in nN) for EBT and TBT nanobeams with  $L/d=10$  have been presented for various values of scale coefficients ( $0nm, 0.5nm, 1nm$ ). Similarly, buckling load of RBT and LBT nanobeams have been compared respectively with Emam (2013) and Sahmani and Ansari (2011) in Table 3.3. It may be noted that comparison for RBT nanobeams has been made with aspect ratio ( $\frac{L}{h}$ ) as 10 and nonlocal parameter ( $\mu$ ) as  $0nm^2, 1nm^2, 2nm^2, 3nm^2$  while comparison for LBT nanobeams has been done with  $\frac{L}{h} = 50$  and  $\mu = 0nm^2, 0.5nm^2, 1nm^2, 1.5nm^2$ . In this table, we have considered S-S and C-C edge conditions. It is seen that critical buckling load parameter ( $\bar{N}_{cr}^0$ ) decreases with increase in nonlocal parameter. From these tables, one may observe close agreement of results with that of available in the literatures.

Table 3.2 Comparison of critical buckling load parameter  $\bar{N}_{cr}^0$  (nN) for EBT and TBT nanobeams

		EBT		TBT	
$L/d$	$e_0a$	Present	Ref.*	Present	Ref.*
S-S					
10	0	4.8447	4.8447	4.7835	4.7670
	0.5	4.7280	4.7281	4.6683	4.654
	1	4.4095	4.4095	4.3534	4.3450
C-S					
10	0	9.91109	9.9155	9.5580	9.5605
	0.5	9.4348	9.4349	9.1934	9.1179
	1	8.2461	8.2461	8.0356	8.0055
C-C					
10	0	19.3789	19.379	18.4342	18.192
	0.5	17.6381	17.6381	16.7783	16.649
	1	13.8939	13.8939	13.2165	13.273

\*Wang et al. (2006)

Table 3.3 Comparison of critical buckling load parameter ( $\bar{N}_{cr}^0$ ) for RBT and LBT nanobeams

		RBT			
		S-S		C-C	
$L/h$	$\mu$	Present	Ref.*	Present	Ref.*
10	0	9.6228	9.6228	35.8075	35.8075
	1	8.7583	8.7583	25.6724	25.6724
	2	8.0364	8.0364	20.0090	20.0090
	3	7.4245	7.4245	16.3927	16.3927
LBT					
		S-S		C-C	
$L/h$	$\mu$	Present	Ref.**	Present	Ref.**
50	0	9.8595	9.8616	39.4170	39.4457
	0.5	9.8401	9.8422	39.3589	39.3899
	1	9.8207	9.8228	38.2958	39.3118
	1.5	9.8014	9.8036	38.2072	39.2351

\*Emam (2013)

\*\*Sahmani and Ansari (2011)

### 3.2.3 Effect of small scale

In this paragraph, the significance of scale coefficient has been highlighted. First, we define buckling load ratio as  $\frac{\bar{N}^0 \text{ calculated using nonlocal theory}}{\bar{N}^0 \text{ calculated using local theory}}$ . This buckling load ratio serves as an index to estimate quantitatively the small scale effect on the buckling solution. To state the importance of scale coefficient, variation of buckling load ratio (associated with first mode) with scale coefficient ( $e_0 l_{int}$ ) has been shown in Figs. 3.12-3.15. It may be noted that Figs. 3.12 and 3.13 present graphical results for RBT nanobeams with guided and simply supported-guided respectively. Similarly, Figs. 3.14 and 3.15 illustrate results for LBT nanobeams with guided and simply supported-guided respectively. In these figures, we have taken non-uniform parameter ( $\eta$ ) as 0.4. Results have been shown for different values of aspect ratio ( $\frac{L}{h}$ ). It is noticed from the figures that buckling load ratios are less than unity. This implies that application of local beam model for the buckling analysis of carbon nanotubes would lead to over prediction of the buckling load if the small length scale effect between the individual carbon atoms is neglected. As the scale coefficient ( $e_0 l_{int}$ ) increases, buckling loads obtained by nonlocal beam model become smaller than those of its local counterpart. In other words, buckling load parameter obtained by local beam theory is more than that obtained by nonlocal beam theory. So, presence of nonlocal parameter in the constitutive equation is significant in the field of nanomechanics. It is also observed that the small scale effect is affected by  $\frac{L}{h}$ . This observation is explained as: When  $\frac{L}{h}$  increases, buckling load ratio comes closer to one. This implies that buckling load parameter obtained by nonlocal beam model comes closer to that furnished by local beam model. Hence small scale effect is negligible for a very slender carbon nanotube (CNT) while it is significant for short carbon nanotubes (CNTs). This implies that if we compare magnitude of small scale effect with length of the slender tube, the small scale (internal characteristic length) is so small that it can be regarded as zero.



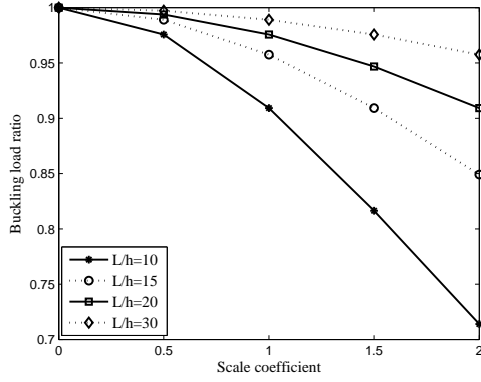


Fig. 3.12 Variation of buckling load ratio with  $e_0 l_{int}$

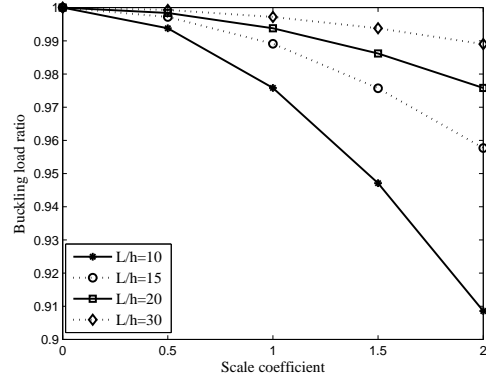


Fig. 3.13 Variation of buckling load ratio with  $e_0 l_{int}$

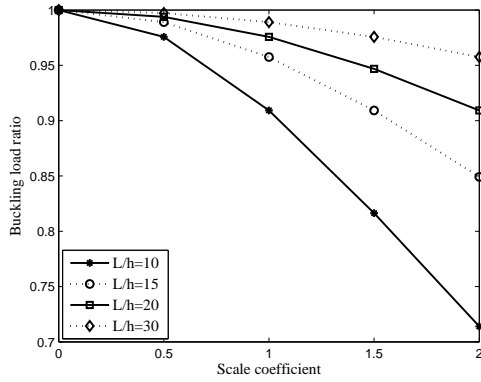


Fig. 3.14 Variation of buckling load ratio with  $e_0 l_{int}$

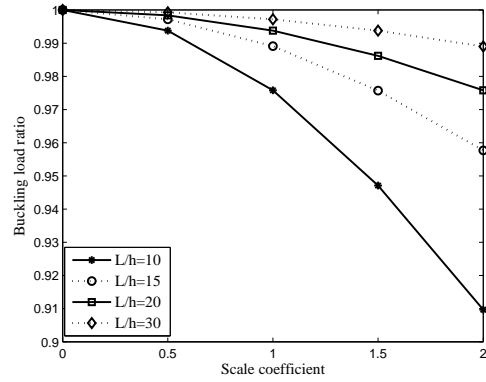


Fig. 3.15 Variation of buckling load ratio with  $e_0 l_{int}$

### 3.2.4 Effect of non-uniform parameter

In this subsection, effect of non-uniformity ( $\eta$ ) on the critical buckling load parameter is illustrated. This analysis will help design engineers in their design to have an idea of the values of critical buckling load parameter. Fig. 3.16 shows the variation of critical buckling load parameter ( $\bar{N}_{cr}^0$ ) with non-uniform parameter  $\eta$ . In this graph, we have considered EBT nanobeam with C-S edge condition having  $L = 50nm$ . Results have been shown for different values of scale coefficients. It is observed that with increase in non-uniform parameter, critical buckling load parameter decreases. This decrease is attributed to the decrease of stiffness of the beam. It is also observed that with increase in nonlocal parameter, critical buckling load parameter decreases. This shows that local beam theory ( $\mu = 0$ ) over predicts buckling load parameter. Hence, for better predictions of buckling load parameter, one should consider nonlocal theory. Next, to investigate the influence of non-uniform parameter on the higher buckling modes, variation of buckling load parameter ( $\bar{N}^0$ ) with non-uniform parameter ( $\eta$ ) has been presented in Fig. 3.17. Here we have considered LBT nanobeams with S-S edge condition having  $\mu = 2nm^2$  and  $L = 15nm$ . It is seen from figure that buckling load parameters decrease with increase in non-uniform parameter and this decrease is more significant in case of higher modes.

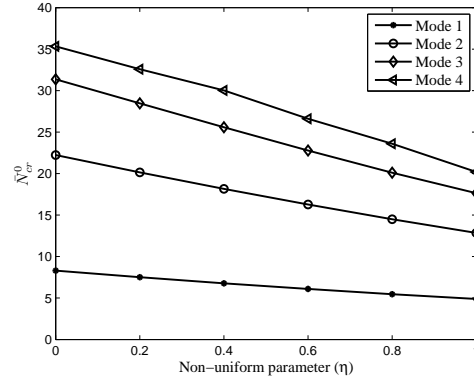
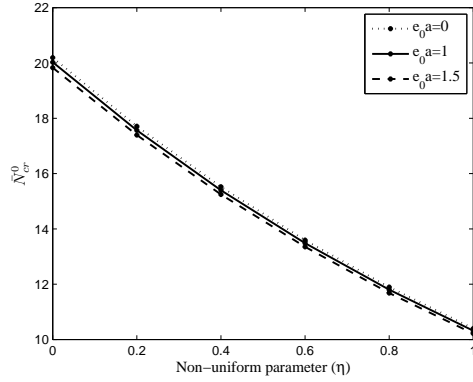


Fig. 3.16 Variation of  $\bar{N}_{cr}^0$  with non-uniform parameter Fig. 3.17 Variation of  $\bar{N}^0$  with non-uniform parameter

### 3.2.5 Effect of aspect ratio

One of the another important factor that design engineers should keep in mind, that is the effect of aspect ratio. To investigate the effect of aspect ratio ( $\frac{L}{h}$ ) on the critical buckling load parameter, variation of critical buckling load parameter with  $\frac{L}{h}$  has been shown in Figs. 3.18-3.21. Results have been shown for different values of scale coefficients ( $0.5nm, 1nm, 1.5nm$ ). In these graphs, we have considered EBT and TBT nanobeams with edge conditions such as C-S and C-C. Numerical values have been obtained by taking  $\eta = 0.5$ . It is observed that buckling load increases with increase in  $\frac{L}{h}$ . It is also noticed that buckling load decreases with increase in scale coefficient. Hence one should incorporate nonlocal theory in the buckling analysis of nanobeams. One may also notice that for a particular value of  $\frac{L}{h}$ , results obtained by TBT nanobeams are less as compared to EBT nanobeams. This is due to the absence of transverse shear stress and strain in EBT nanobeams. One may say TBT nanobeams predict better prediction of buckling load than EBT nanobeams.

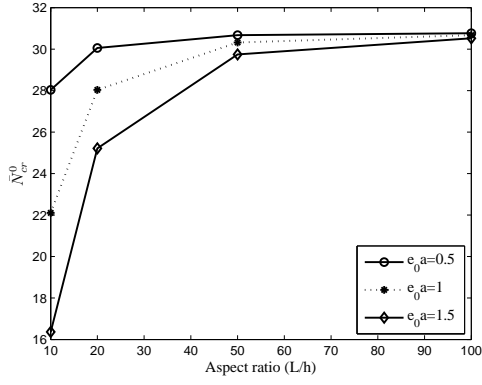


Fig. 3.18 Variation of  $\bar{N}_{cr}^0$  with  $\frac{L}{h}$  (EBT C-C)

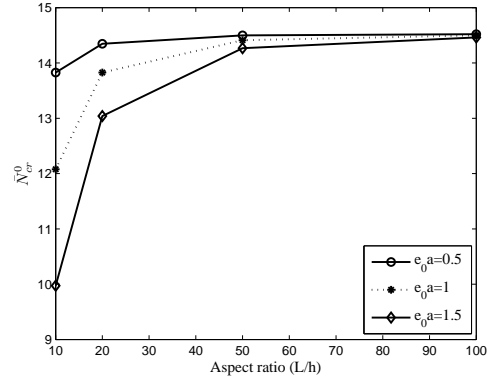


Fig. 3.19 Variation of  $\bar{N}_{cr}^0$  with  $\frac{L}{h}$  (EBT C-S)

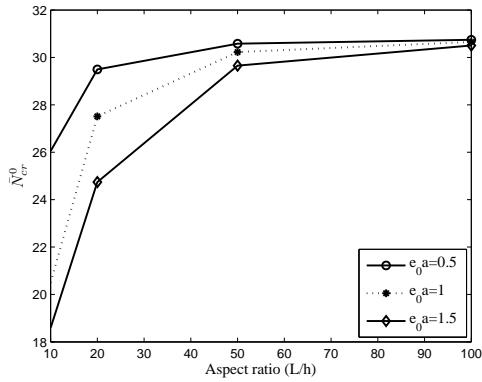


Fig. 3.20 Variation of  $\bar{N}_{cr}^0$  with  $\frac{L}{h}$  (TBT C-C)

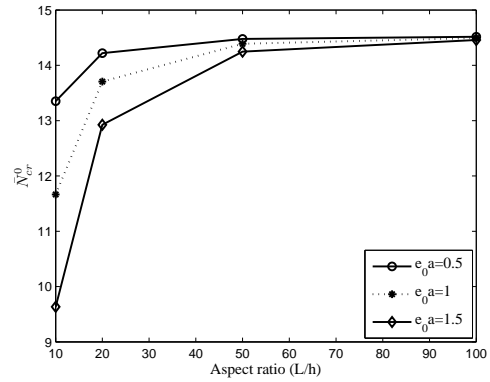


Fig. 3.21 Variation of  $\bar{N}_{cr}^0$  with  $\frac{L}{h}$  (TBT C-S)

### 3.2.6 Effect of various beam theories

Modeling of nanostructures based on beam theories is one of the important area in the field of nanotechnology. To investigate the effect of various beam theories such as EBT, TBT, RBT and LBT on the buckling load parameter, variation of critical buckling load parameter with scale coefficient has been shown in Fig. 3.22 for various types of beam theories. In this figure, C-S boundary condition is taken into consideration with  $L = 10nm$  and  $\eta = 0.5$ . It is seen from the figure that EBT predicts higher buckling load than other types of beam theories. It is due to the fact that in EBT, transverse shear and transverse normal strains are not considered. It is also noted that beam theories such as TBT, RBT and LBT predict approximately same results.

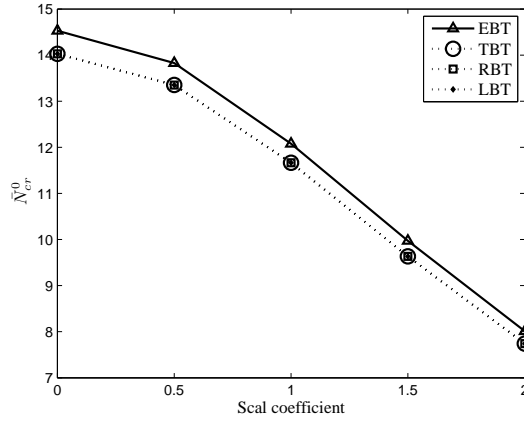


Fig. 3.22 Variation of  $\bar{N}_{cr}^0$  with scale coefficient

### 3.2.7 Effect of boundary condition

For designing engineering structures, one must have proper knowledge about boundary conditions. It will help engineers to have an idea without carrying out detail investigation. Therefore, analysis of boundary conditions is quite important. In this subsection, we have considered the effect of boundary condition on the critical buckling load parameter. Fig. 3.23 depicts variation of critical buckling load parameter of TBT nanobeam with scale coefficient for different boundary conditions. This graph is plotted with  $L = 10nm$  and  $\eta = 0.2$ . It is observed from the figure that C-C nanobeams are having highest critical buckling load parameter and simply supported-guided nanobeams are having lowest critical buckling load parameter.

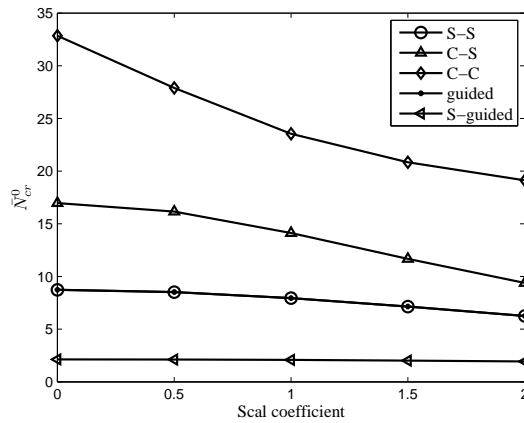


Fig. 3.23 Variation of  $\bar{N}_{cr}^0$  with scale coefficient

## Buckling of embedded nanobeams

Here, we have investigated buckling of embedded nanobeams in thermal environments based on EBT, TBT and RBT beam theories. The nanobeam is embedded in elastic foundations such as Winkler and Pasternak. Rayleigh-Ritz has been applied in EBT and TBT with shape functions as boundary characteristic orthogonal polynomials and Chebyshev polynomials respectively. Differential quadrature method has been employed in buckling of embedded nanobeams based on RBT.

For simplicity and convenience in mathematical formulation, following non-dimensional parameters have been introduced here

$$X = \frac{x}{L}, W = \frac{w}{L}, \alpha = \frac{e_0 a}{L}, \hat{N} = \frac{\bar{N}L^2}{EI}, \tau = \frac{I}{AL^2}, \Omega = \frac{EI}{k_s GAL^2}, \bar{\Omega} = \frac{G\bar{A}L^2}{EI}, K_g = \frac{k_g L^2}{EI},$$

$$K_w = \frac{k_w L^4}{EI}, \hat{N}_\theta = \frac{N_\theta L^2}{EI}, \hat{N}_m = \frac{N_m L^2}{EI}$$

### 3.2.7.1 Euler-Bernoulli beam theory

The strain energy may be written as Eq. (2.1).

The potential energy due to the axial force may be expressed as (Amirian et al. 2013)

$$V_a = \frac{1}{2} \int_0^L \left\{ \bar{N} \left( \frac{dw}{dx} \right)^2 + f_e w \right\} dx \quad (3.6)$$

where  $\bar{N}$  is the axial force and is expressed as  $\bar{N} = N_m + N_\theta$ . Here  $N_m$  is the axial force due to the mechanical loading prior to buckling and  $N_\theta$  is the axial force due to the influence of temperature change which is defined by  $N_\theta = -\frac{EA}{1-2\nu} \alpha_x \theta$ .

In this expression,  $E$  is the Young's modulus,  $A$  the cross sectional area,  $\nu$  the Poisson's ratio,  $\alpha_x$  the coefficient of thermal expansion in the direction of  $x$  axis and  $\theta$  is the change in temperature. Also  $f_e$  is the density of reaction force of elastic foundation which is expressed as  $f_e = k_w w - k_g \frac{d^2 w}{dx^2}$  where  $k_w$  denotes Winkler modulus and  $k_g$  denotes shear modulus of the elastic medium.

Using Hamilton's principle and setting coefficient of  $\delta w$  to zero, we obtain following governing equation of motion

$$\frac{d^2 M}{dx^2} + \bar{N} \frac{d^2 w}{dx^2} - k_w w + k_g \frac{d^2 w}{dx^2} = 0 \quad (3.7)$$

Using Eqs. (3.7) and (1.7),  $M$  in nonlocal form may be written as

$$M = -EI \frac{d^2 w}{dx^2} + \mu \left[ -\bar{N} \frac{d^2 w}{dx^2} + k_w w - k_g \frac{d^2 w}{dx^2} \right]$$

Let us substitute  $N_m = -P_b$

Equating energies of the system, we may obtain Rayleigh-quotient ( $\bar{N}^0$ ) from the following eigen equation in non-dimensional form

$$\bar{N}^0 \left[ \left( \frac{dW}{dX} \right)^2 + \alpha^2 \left( \frac{d^2 W}{dX^2} \right)^2 \right] = \left( \frac{d^2 W}{dX^2} \right)^2 - K_w \alpha^2 W \frac{d^2 W}{dX^2} + K_g \alpha^2 \left( \frac{d^2 W}{dX^2} \right)^2 + K_w W^2 - K_g W \frac{d^2 W}{dX^2} + \hat{N}_\theta \left( \frac{dW}{dX} \right)^2 + \hat{N}_\theta \alpha^2 \left( \frac{d^2 W}{dX^2} \right)^2 \quad (3.8)$$

where  $\bar{N}^0 = \frac{P_b L^2}{EI}$  is the non-dimensional buckling load parameter.

Here, we have used orthonormal polynomials ( $\hat{\varphi}_k$ ) in Eq. (2.5). Substituting Eq. (2.5) in Eq. (3.8) and minimizing  $\bar{N}^0$  with respect to constant coefficients, the following eigenvalue value problem may be obtained as

$$[K] \{Z\} = \bar{N}^0 [B_c] \{Z\} \quad (3.9)$$

where  $Z$  is a column vector of constants, stiffness matrix  $K$  and buckling matrix  $B_c$  are given as below:

$$K(i, j) = \int_0^1 \left( (2 + 2K_g \alpha^2 + 2\hat{N}_\theta \alpha^2) \hat{\varphi}_i'' \hat{\varphi}_j'' - K_w \alpha^2 \hat{\varphi}_i'' \hat{\varphi}_j - K_w \alpha^2 \hat{\varphi}_i \hat{\varphi}_j'' + 2K_w \hat{\varphi}_i \hat{\varphi}_j - K_g \hat{\varphi}_i'' \hat{\varphi}_j - K_g \hat{\varphi}_i \hat{\varphi}_j'' + 2\hat{N}_\theta \alpha^2 \hat{\varphi}_i' \hat{\varphi}_j' \right) dX$$

$$B_c(i, j) = \int_0^1 (2\hat{\varphi}_i' \hat{\varphi}_j' + 2\alpha^2 \hat{\varphi}_i'' \hat{\varphi}_j'') dX$$

### 3.2.7.2 Timoshenko beam theory

The strain energy may be given as Eq. (2.9).

The potential energy due to the axial force may be expressed as Eq. (3.6).

Using Hamilton's principle, governing equations are obtained as

$$\frac{dM}{dx} - Q = 0 \quad (3.10)$$

$$\frac{dQ}{dx} + \bar{N} \frac{d^2 w}{dx^2} - f_e = 0 \quad (3.11)$$

Using Eqs. (3.10-3.11) and Eqs. (1.13-1.14), one may obtain bending moment  $M$  and shear force  $Q$  in nonlocal form as

$$M = EI \frac{d\phi}{dx} + \mu \left[ -\bar{N} \frac{d^2 w}{dx^2} + f_e \right] \quad (3.12)$$

$$Q = k_s GA \left( \phi + \frac{dw}{dx} \right) + \mu \left[ -\bar{N} \frac{d^3 w}{dx^3} + k_w \frac{dw}{dx} - k_g \frac{d^3 w}{dx^3} \right] \quad (3.13)$$

Equating energies of the system, one may obtain following expressions for TBT nanobeams in non-dimensional form as

$$\begin{aligned} \bar{N}^0 \left[ \left( \frac{dW}{dX} \right)^2 - \alpha^2 \frac{d\phi}{dX} \frac{d^2 W}{dX^2} - \alpha^2 \frac{d^3 W}{dX^3} \left( \phi + \frac{dW}{dX} \right) \right] &= \left( \frac{d\phi}{dX} \right)^2 - \hat{N}_\theta \alpha^2 \frac{d\phi}{dX} \frac{d^2 W}{dX^2} - K_w \alpha^2 W \frac{d\phi}{dX} \\ &\quad - K_g \alpha^2 \frac{d^2 W}{dX^2} \frac{d\phi}{dX} + \frac{1}{\Omega} \left( \phi + \frac{dW}{dX} \right)^2 \\ &\quad - \hat{N}_\theta \alpha^2 \frac{d^3 W}{dX^3} \left( \phi + \frac{dW}{dX} \right) + K_w \alpha^2 \frac{dW}{dX} \left( \phi + \frac{dW}{dX} \right) \\ &\quad - K_g \alpha^2 \frac{d^3 W}{dX^3} \left( \phi + \frac{dW}{dX} \right) + \hat{N}_\theta \left( \frac{dW}{dX} \right)^2 \\ &\quad + K_w W^2 - K_g W \frac{d^2 W}{dX^2} \end{aligned} \quad (3.14)$$

In this problem, we have used Chebyshev polynomials in the Rayleigh-Ritz method. As such, we introduce another independent variable  $\xi$  as  $\xi = 2X - 1$  which transforms the range  $0 \leq X \leq 1$  into the applicability range  $-1 \leq \xi \leq 1$ .

Substituting  $N_m = -P_b$  and equating energies of the system, one may obtain Rayleigh Quotient ( $\bar{N}^0$ ) from following equation

$$\begin{aligned} \bar{N}^0 \left[ 4 \left( \frac{dW}{d\xi} \right)^2 - 8\alpha^2 \frac{d\phi}{d\xi} \frac{d^2 W}{d\xi^2} - 8\alpha^2 \frac{d^3 W}{d\xi^3} \left( \phi + 2 \frac{dW}{d\xi} \right) \right] &= 4 \left( \frac{d\phi}{d\xi} \right)^2 - 8\hat{N}_\theta \alpha^2 \frac{d\phi}{d\xi} \frac{d^2 W}{d\xi^2} + 2K_w \alpha^2 W \frac{d\phi}{d\xi} - \\ &\quad 8K_g \alpha^2 \frac{d^2 W}{d\xi^2} \frac{d\phi}{d\xi} + \frac{1}{\Omega} \left( \phi + 2 \frac{dW}{d\xi} \right)^2 + K_w W^2 \\ &\quad - 8\hat{N}_\theta \alpha^2 \frac{d^3 W}{d\xi^3} \left( \phi + 2 \frac{dW}{d\xi} \right) + 4\hat{N}_\theta \left( \frac{dW}{d\xi} \right)^2 \\ &\quad + K_w \alpha^2 \frac{dW}{d\xi} \left( \phi + 2 \frac{dW}{d\xi} \right) - 4K_g W \frac{d^2 W}{d\xi^2} \\ &\quad - 8K_g \alpha^2 \frac{d^3 W}{d\xi^3} \left( \phi + 2 \frac{dW}{d\xi} \right) \end{aligned} \quad (3.15)$$

where  $\bar{N}^0 = \frac{P_b L^2}{EI}$  is the buckling load parameter.

Substituting Eqs. (2.14) and (2.15) in Eq. (3.15) and minimizing  $\bar{N}^0$  with respect to the constant coefficients, the following eigenvalue problem is obtained

$$[K] \{Z\} = \bar{N}^0 [B_c] \{Z\} \quad (3.16)$$

where  $Z$  is a column vector of constants. Here  $K$  and  $B_c$  are the stiffness and buckling matrices for TBT nanobeams which are given by

$$K = \begin{bmatrix} k_1 & k_2 \\ k_3 & k_4 \end{bmatrix} \text{ where } k_1, k_2, k_3, k_4 \text{ are submatrices and are given as}$$

$$k_1(i, j) = \int_{-1}^1 (8(\frac{1}{\Omega} + K_w \alpha^2 + \hat{N}_\theta) \varphi_i' \varphi_j' - 16(\hat{N}_\theta \alpha^2 + K_g \alpha^2) \varphi_i''' \varphi_j' - 16(\hat{N}_\theta \alpha^2 + K_g \alpha^2) \varphi_i' \varphi_j''' + 2K_w \varphi_i \varphi_j - 4K_g \varphi_i'' \varphi_j - 4K_g \varphi_i \varphi_j'') d\xi$$

$$k_2(i, j) = \int_{-1}^1 (-8\hat{N}_\theta \alpha^2 \varphi_i'' \psi_j' + 2K_w \alpha^2 \varphi_i \psi_j' - 8K_g \alpha^2 \varphi_i'' \psi_j' + 4\frac{1}{\Omega} \varphi_i' \psi_j - (8\hat{N}_\theta \alpha^2 + 8K_g \alpha^2) \varphi_i''' \psi_j + 2K_w \alpha^2 \varphi_i' \psi_j) d\xi$$

$$k_3(i, j) = \int_{-1}^1 (-8\hat{N}_\theta \alpha^2 \psi_i' \varphi_j'' + 2K_w \alpha^2 \psi_i' \varphi_j - 8K_g \alpha^2 \psi_i' \varphi_j'' + 4\frac{1}{\Omega} \psi_i \varphi_j' - 8\hat{N}_\theta \alpha^2 \psi_i \varphi_j''' + 2K_w \alpha^2 \psi_i \varphi_j' - 8K_g \alpha^2 \psi_i \varphi_j''') d\xi$$

$$k_4(i, j) = \int_{-1}^1 (8\psi_i' \psi_j' + 2\frac{1}{\Omega} \psi_i \psi_j) d\xi$$

$$B_c = \begin{bmatrix} B_1 & B_2 \\ B_3 & B_4 \end{bmatrix}$$

where  $B_1, B_2, B_3, B_4$  are submatrices and are given as

$$B_1(i, j) = \int_{-1}^1 (8\varphi_i' \varphi_j' - 16\alpha^2 \varphi_i' \varphi_j''' - 16\alpha^2 \varphi_i''' \varphi_j') d\xi$$

$$B_2(i, j) = \int_{-1}^1 (-8\alpha^2 \varphi_i'' \psi_j' - \alpha^2 \varphi_i''' \psi_j) d\xi$$

$$B_3(i, j) = \int_{-1}^1 (-8\alpha^2 \psi_i' \varphi_j'' - 8\alpha^2 \psi_i \varphi_j''') d\xi$$

$$B_4(i, j) = 0$$

### 3.2.7.3 Reddy beam theory (RBT)

Governing equations of embedded nanobeams based on Reddy beam theory may be written as (Reddy 2007)

$$G\tilde{A} \left( \frac{d\phi}{dx} + \frac{d^2 w}{dx^2} \right) - \tilde{N} \frac{d^2 w}{dx^2} - k_w w + k_g \frac{d^2 w}{dx^2} + \mu \left[ \tilde{N} \frac{d^4 w}{dx^4} + k_w \frac{d^2 w}{dx^2} - k_g \frac{d^4 w}{dx^4} \right] + c_1 E J \frac{d^3 \phi}{dx^3} - c_1^2 E K \left( \frac{d^3 \phi}{dx^3} + \frac{d^4 w}{dx^4} \right) = 0 \quad (3.17)$$

$$E\hat{I} \frac{d^2 \phi}{dx^2} - c_1 E \hat{J} \left( \frac{d^2 \phi}{dx^2} + \frac{d^3 w}{dx^3} \right) - G\tilde{A} \left( \phi + \frac{dw}{dx} \right) = 0 \quad (3.18)$$



Eliminating  $\phi$  from Eqs. (3.17) and (3.18), governing equations may be obtained in terms of displacement as

$$\begin{aligned} -\left(\frac{68}{84}\bar{N} + \frac{105}{84EI}G\tilde{A}\mu\bar{N}\right)\frac{d^4w}{dx^4} + \frac{105}{84EI}G\tilde{A}\bar{N}\frac{d^2w}{dx^2} + \frac{68}{84}\mu\bar{N}\frac{d^6w}{dx^6} &= \left(\frac{68}{84}\mu k_g + \frac{1}{105}EI\right)\frac{d^6w}{dx^6} - \frac{105}{84EI}G\tilde{A}k_w w \\ -\left(\frac{68}{84}k_g + \frac{68}{84}\mu k_w + \frac{105}{84EI}G\tilde{A}\mu k_g + \frac{21}{84}G\tilde{A}\right)\frac{d^4w}{dx^4} &+ \left(\frac{68}{84}k_w + \frac{105}{84EI}G\tilde{A}k_g + \frac{105}{84EI}G\tilde{A}\mu k_w\right)\frac{d^2w}{dx^2} \end{aligned} \quad (3.19)$$

Substituting  $N_m = -P_b$ , governing equation in non-dimensional form is obtained as

$$\begin{aligned} \bar{N}^0 \left[ \left( \frac{68}{84} - \frac{105}{84}\bar{\Omega}\alpha^2 \right) \frac{d^4W}{dX^4} - \frac{105}{84}\bar{\Omega}\frac{d^2W}{dX^2} - \frac{68}{84}\alpha^2\frac{d^6W}{dX^6} \right] &= \left( \frac{68}{84}\alpha^2 K_g + \frac{1}{105} + \frac{68}{84}\alpha^2\hat{N}_\theta \right) \frac{d^6W}{dX^6} + \\ \left( -\frac{68}{84}K_g - \frac{68}{84}\alpha^2 K_w - \frac{105}{84}\bar{\Omega}\alpha^2 K_g - \frac{21}{84}\bar{\Omega} - \hat{N}_\theta \frac{68}{84} + \frac{105}{84}\bar{\Omega}\alpha^2\hat{N}_\theta \right) \frac{d^4W}{dX^4} &- \frac{105}{84}\bar{\Omega}K_w \\ + \left( \frac{68}{84}K_w + \frac{105}{84}\bar{\Omega}K_g + \frac{105}{84}\bar{\Omega}\alpha^2 K_w + \frac{105}{84}\bar{\Omega}\hat{N}_\theta \right) \frac{d^2W}{dX^2} \end{aligned} \quad (3.20)$$

where  $\bar{N}^0 = \frac{P_b L^2}{EI}$  is the buckling load parameter.

Application of differential quadrature method in Eq. (3.20), one may obtain generalized eigen value problem as

$$[K] \{W\} = \bar{N}^0 [B_c] \{W\} \quad (3.21)$$

where  $K$  is the stiffness matrix and  $B_c$  is the buckling matrix.

### 3.3 Numerical results and discussions

Buckling of single-walled carbon nanotubes (SWCNTs) embedded in elastic medium including thermal effect has been investigated. The elastic medium is modeled as Winkler-type and Pasternak-type foundations. The effective properties of SWCNTs are taken as follows (Benzair et al. 2008; Murmu and Pradhan 2009b): Young's modulus ( $E$ ) = 1000 GPa, Poisson's ratio ( $\nu$ ) = 0.19, shear correction factor ( $k_s$ ) = 0.877,  $\alpha_x = -1.6 \times 10^{-6} K^{-1}$  for room or low temperature and  $\alpha_x = 1.1 \times 10^{-6} K^{-1}$  for high temperature. A computer code is developed by the authors in MATLAB based on Eq. (3.9), (3.16) and (3.21).

#### 3.3.1 Convergence

First of all, convergence test has been performed to find minimum number of terms required for computation. As such, Figs. 3.24 and 3.25 illustrate convergence of critical buckling load

parameter ( $\bar{N}_{cr}^0$ ) respectively for EBT and RBT. In Fig. 3.24, we have considered C-S edge condition with  $\frac{L}{h} = 20, e_0a = 1nm, K_w = 60, K_g = 4, \theta = 10K$  and in Fig. 3.25, we have taken  $K_w = 50, K_g = 2, \theta = 20K, e_0a = 1.5nm, \frac{L}{h} = 20$  with C-S support. Similarly Table 3.4 shows convergence of critical buckling load parameter of nanobeams based on TBT. In this table, we have taken  $K_w = 50, K_g = 2, \theta = 10K, e_0a = 1nm, \frac{L}{h} = 10$  and C-S edge condition. One may note that convergence test has been performed in low temperature environment. Above convergence patterns show that ten grid points are sufficient to obtain results in the present analysis.

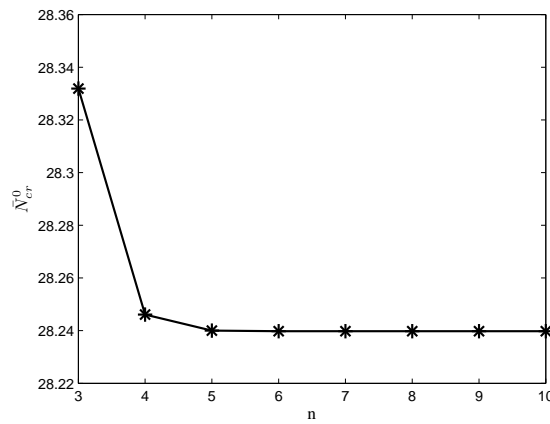


Fig. 3.24 Convergence of critical buckling load parameter (EBT)

Table 3.4 Convergence of first three buckling load parameters (TBT)

$n$	First	Second	Third
4	22.2348	39.7800	65.3622
5	22.1742	38.0072	51.6357
6	22.1711	37.6160	49.2176
7	22.1600	37.6100	47.9400
8	22.1616	37.4205	43.5535
9	22.1500	35.8300	37.7600
9	22.1500	35.8300	37.7600

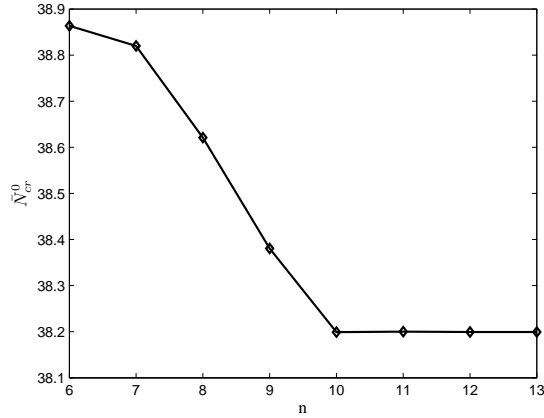


Fig. 3.25 Convergence of critical buckling load parameter (RBT)

### 3.3.2 Validation

To validate the present results, a comparison study has been carried out with the results of Wang et al. (2006). For this comparison, we have taken  $K_w = 0, K_g = 0$  and  $\theta = 0K$ . As such, Figs. 3.26-3.27 show graphical comparisons of EBT and TBT nanobeams respectively. In Fig. 3.26, we have considered C-S support with  $\frac{L}{d} = 14$  and in Fig. 3.27, we have considered S-S support with  $\frac{L}{d} = 10$ . Similarly, tabular comparison has been tabulated in Table 3.5 for RBT nanobeams with that of Emam (2013) for  $\frac{L}{h} = 10$ . For this comparison, we have taken same parameters as that of Emam (2013). One may find a close agreement of the results. This shows the suitability and reliability of the present method for the buckling analyses of SWCNTs.

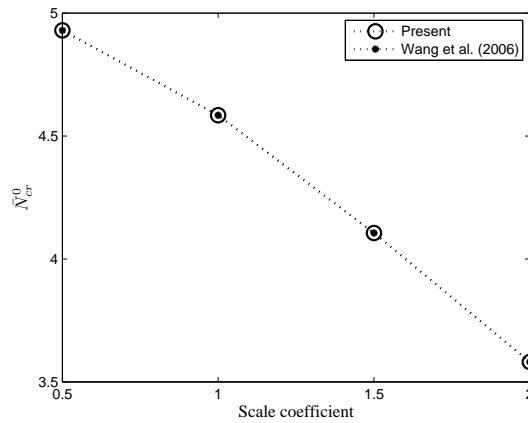


Fig. 3.26 Comparison of critical buckling load parameter (EBT)

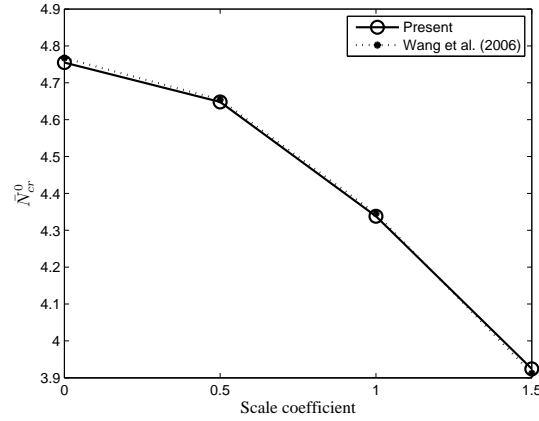


Fig. 3.27 Comparison of critical buckling load parameter (TBT)

Table 3.5 Comparison of critical buckling load parameter (RBT)

$L/h$	$\mu$	S-S		C-C	
		Present	Ref.*	Present	Ref.*
10	0	9.6228	9.6228	35.8075	35.8075
	1	8.7583	8.7583	25.6724	25.6724
	2	8.0364	8.0364	20.0090	20.0090
	3	7.6149	7.4245	16.3927	16.3927

\*Emam (2013)

### 3.3.3 Effect of Winkler modulus parameter

In this subsection, we have investigated the influence of surrounding medium on the buckling of SWCNTs. The elastic medium is modeled as Winkler-type and Pasternak-type foundations. Figs. 3.28-3.30 illustrate effect of Winkler modulus parameter on the buckling solutions based on EBT, TBT and RBT respectively. We have shown these graphical results in low temperature environment with  $K_g = 0$ . Numerical values taken for this computation are  $\theta = 30K$ ,  $\frac{L}{h} = 10$  in Fig. 3.28 with C-F support whereas in Fig. 3.29, we have taken  $\theta = 10K$ ,  $\frac{L}{h} = 20$  with S-S support and in Fig. 3.30, we have taken  $\theta = 10K$ ,  $\frac{L}{h} = 30$  with C-C support. In these figures, results have been shown for various values of scale coefficients. The Winkler modulus parameter is taken in the range of 0-400. It is observed from these figures that critical buckling load parameter ( $\bar{N}_{cr}^0$ ) decreases with increase in scale coefficient. It may be noted that results associated with  $e_0a = 0nm$  correspond to those of local beam theory. One may observe that results obtained by local beam theory are over predicted than that of obtained by nonlocal beam theory. Therefore, nonlocal theory should be considered for buckling analysis of structures at nanoscale. It is seen that critical buckling load increases with increase in Winkler modulus

parameter. This is because that the nanotube becomes stiffer when elastic medium constant is increased. In addition, it is also observed that critical buckling loads show nonlinear behavior with respect to stiffness of surrounding matrix for higher  $e_0 l_{int}$  values. This may be due to the fact that increase of the Winkler modulus causes CNT to be more rigid.

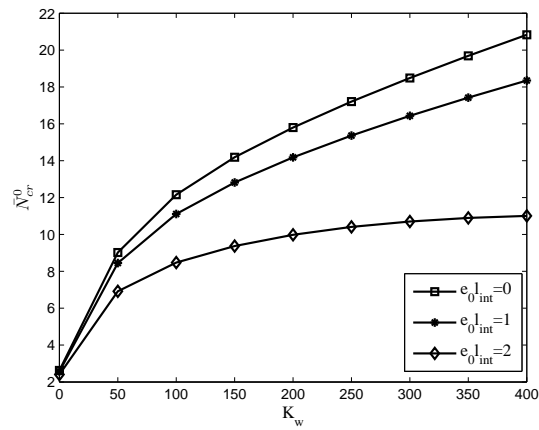


Fig. 3.28 Effect of the Winkler modulus parameter on critical buckling load parameter (EBT)

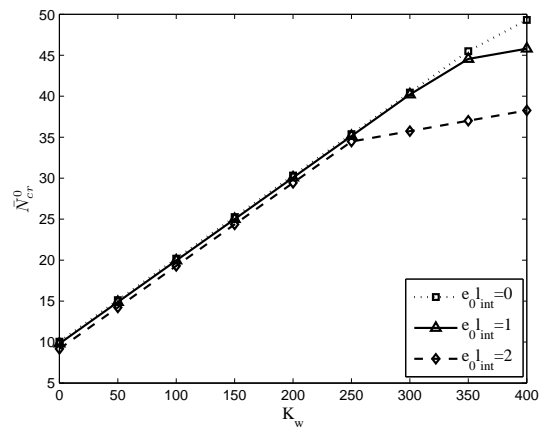


Fig. 3.29 Effect of the Winkler modulus parameter on critical buckling load parameter (TBT)

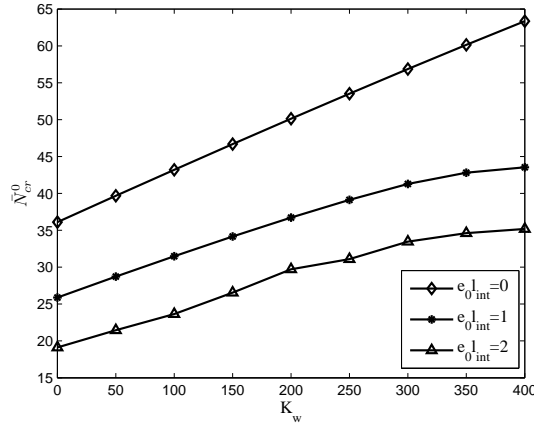


Fig. 3.30 Effect of the Winkler modulus parameter on critical buckling load parameter (RBT)

### 3.3.4 Effect of Pasternak shear modulus parameter

In this subsection, effect of Pasternak shear modulus parameter on the buckling has been examined. As such, Figs. 3.31-3.33 show the distribution of critical buckling load parameter against Pasternak shear modulus for EBT, TBT and RBT respectively in low temperature environment. Numerical values of parameters are chosen as  $K_w = 0, \theta = 10K, \frac{L}{h} = 40$  with C-S support in Fig. 3.31 whereas in Fig. 3.32, we have taken  $K_w = 50, \theta = 10K, \frac{L}{h} = 20$  with C-S support and in Fig. 3.33, we have taken  $K_w = 0, \theta = 10K, \frac{L}{h} = 20$  with S-S edge condition. Graph is plotted for various values of scale coefficients with Pasternak shear modulus parameter ranging from 0-10. It is observed from the figures that critical buckling load parameter associated increases with Pasternak shear modulus parameter. This increase is influenced by small scale coefficient. With increase in scale coefficient, critical buckling load parameter for a particular Pasternak shear modulus parameter decreases. Here it is also observed that unlike Winkler foundation model, the increase of critical buckling load parameter with Pasternak foundation is linear in nature. This is due to the domination of elastic medium modeled as the Pasternak type foundation model. Same observation has also been reported in Murmu and Pradhan (2009b). Next, we have analyzed the effect of Pasternak foundation model over Winkler foundation model. As such, Fig. 3.34 illustrates the critical buckling load parameter of RBT nanobeams as a function of small scale coefficient in low temperature environment with  $\frac{L}{h} = 10$  and C-C edge condition. It may be observed that critical buckling load parameter obtained from Pasternak foundation model is relatively larger than those obtained from the Winkler foundation model.

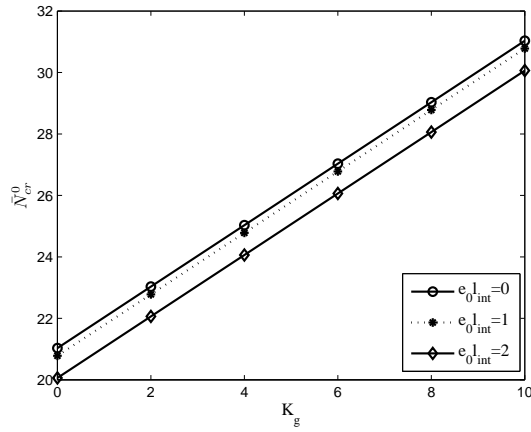


Fig. 3.31 Effect of Pasternak shear modulus parameter on critical buckling load parameter (EBT)

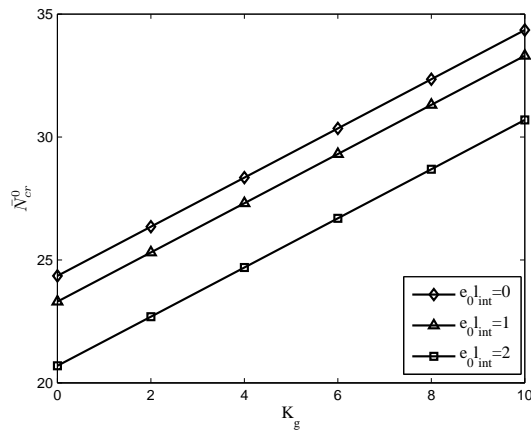


Fig. 3.32 Effect of Pasternak shear modulus parameter on critical buckling load parameter (TBT)

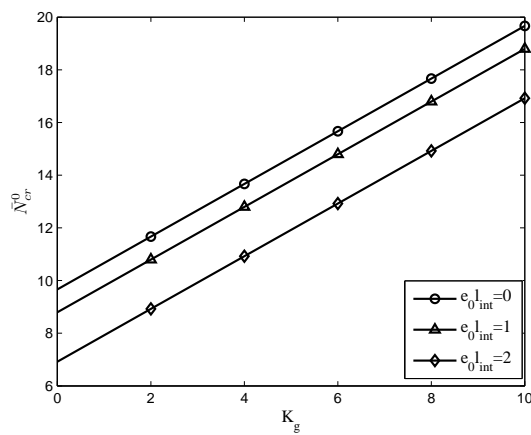


Fig. 3.33 Effect of Pasternak shear modulus parameter on critical buckling load parameter (RBT)

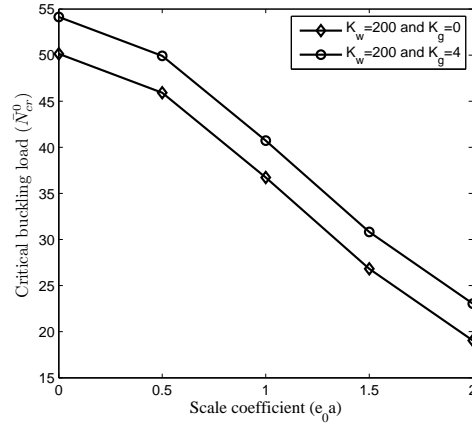


Fig. 3.34 Variation of  $\bar{N}_{cr}^0$  with  $e_0 a$

### 3.3.5 Effect of temperature

Here, effect of temperature on the buckling of nanobeams embedded in elastic medium has been investigated. As such, Figs. 3.35-3.37 show variation of thermal load ratio (associated with first mode) with change in temperature ( $\theta$ ) respectively for EBT, TBT and RBT. In Fig. 3.35, we have taken S-S nanobeam with  $\frac{L}{h} = 20$ ,  $e_0 a = 2nm$ ,  $K_w = 50$ ,  $K_g = 2$ . Similarly, we have taken  $\frac{L}{h} = 50$ ,  $e_0 a = 0.5nm$ ,  $K_w = 50$ ,  $K_g = 2$  with C-C support in Fig. 3.36 and  $\frac{L}{h} = 10$ ,  $e_0 a = 1.5nm$ ,  $K_w = 50$ ,  $K_g = 2$  with C-C support in Fig. 3.37.

Here, we define thermal load ratio ( $\chi_{thermal}$ ) as  $\chi_{thermal} = \frac{\text{Buckling load with thermal effect}}{\text{Buckling load without thermal effect}}$ .

It is noticed that in low temperature environment, thermal load ratios are more than unity. This implies that buckling load parameter considering thermal effect is larger than ignoring influence of temperature change. Whereas in high temperature environment, thermal load ratios are less than unity. This implies that buckling load parameter considering thermal effect is smaller than excluding influence of temperature change. In other words, critical buckling load parameter increases with increase in temperature in low temperature environment while they decrease with increase in temperature in high temperature environment. Same observation have also been noted in Refs. (Murmu and Pradhan 2009a; Zidour et al. 2012; Maachou et al. 2011; Murmu and Pradhan 2010).



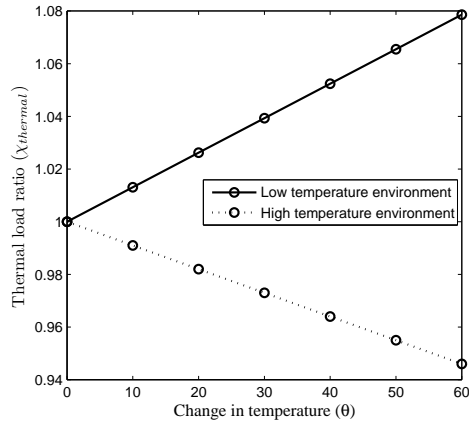


Fig. 3.35 Change of thermal load ratio with change in temperature (EBT)

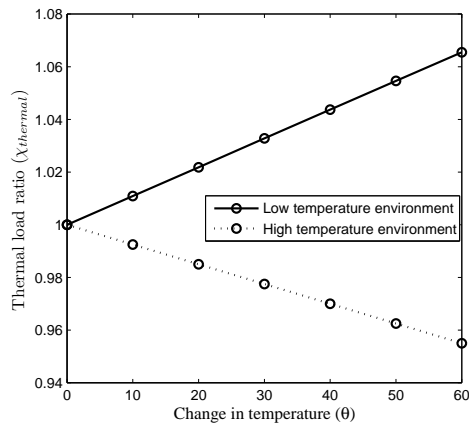


Fig. 3.36 Change of thermal load ratio with change in temperature (TBT)

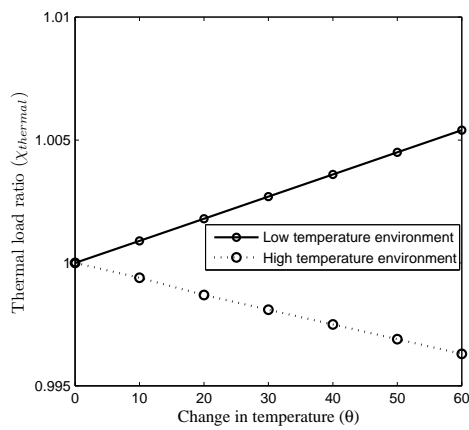


Fig. 3.37 Change of thermal load ratio with change in temperature (RBT)

### 3.3.6 Effect of aspect ratio

To illustrate the effect of aspect ratio on the critical buckling load parameter, variation of buckling load ratio with the aspect ratio ( $\frac{L}{h}$ ) has been shown in Fig. 3.38 for different magnitudes of temperature change. Results have been shown for TBT nanobeam with  $K_w = 50$ ,  $K_g = 2$ ,  $e_0 a = 1nm$  and S-S edge condition. It is observed that buckling load ratio (associated with first mode) increases with increase in aspect ratio. In addition, it is also seen that critical load is also dependent on temperature change ( $\theta$ ). The differences in magnitudes of buckling load ratio for different temperature changes are larger in low aspect ratios while the differences in magnitudes of buckling load ratio for different temperature changes are smaller for large aspect ratios. It is also seen that for larger temperature change, the rate of increase of buckling load ratio is less compared to smaller temperature change. One may note that same observation may also be seen in case of EBT and RBT beam theories.

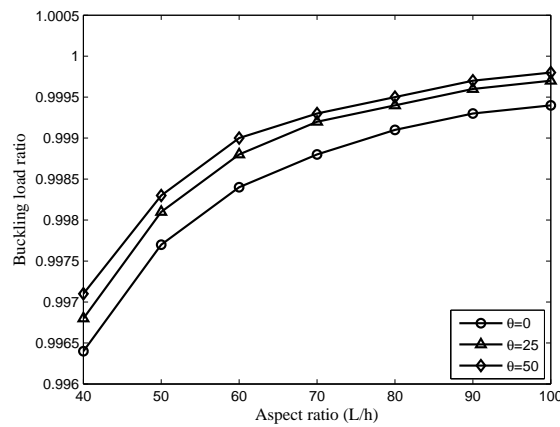


Fig. 3.38 Change of buckling load ratio with aspect ratio

## 3.4 Conclusions

Rayleigh-Ritz method has been used for bending of nanobeams based on both Euler-Bernoulli and Timoshenko beam theories in conjunction with nonlocal elasticity of Eringen. Nonlocal parameter has no effect on the deflection of C-C nanobeams whereas in case of S-S and C-S supports, deflection increases with increase in nonlocal parameter. Again, Rayleigh-Ritz method has been applied to investigate thermal effect on the buckling of nanobeams embedded in elastic medium. Application of Rayleigh-Ritz method converts bending problems to system of linear equations and buckling to generalized eigen value problem.

Differential quadrature method has been employed for buckling analysis of non-uniform nanobeams based on four different beam theories such as EBT, TBT, RBT and LBT. Non-uniform material properties are assumed by taking exponentially varying stiffness. New results have been shown for two types of boundary conditions such as guided and simply supported-guided. Similarly,

differential quadrature method has also been applied to investigate thermal effect on the buckling of nanobeams embedded in elastic medium based on nonlocal Reddy beam theory. Theoretical formulations include effects of small scale , elastic medium and temperature change. It is seen that results obtained based on local beam theory are over estimated. Critical buckling load parameter increase with increase in Winkler and Pasternak coefficients of elastic foundation. It may again be observed that thermal load ratio is more than unity in case of low temperature environment while thermal load ratio is less than unity in case of high temperature environment.

# **Chapter 4**

## **Bending and buckling of nanoplates**

The contents of this chapter have been communicated for publication.

# Chapter 4

## Bending and buckling of nanoplates

In this chapter, we have discussed bending and buckling of nanoplates based on classical plate theory in conjunction with nonlocal elasticity theory of Eringen. Two-dimensional simple polynomials have been used as shape functions in the Rayleigh-Ritz method. Complicating effects such as Winkler and pasternak foundation models have been considered.

### Bending of nanoplates

We have investigated bending of nanoplates in the absence of elastic foundation. As such, the strain energy may be obtained from Eq. (2.28) by setting  $k_w = k_p = 0$ .

$$U = \frac{1}{2}D \int_0^a \int_0^b \left\{ \left( \frac{\partial^2 w}{\partial x^2} \right)^2 + 2\nu \left( \frac{\partial^2 w}{\partial x^2} \frac{\partial^2 w}{\partial y^2} \right) + \left( \frac{\partial^2 w}{\partial y^2} \right)^2 + 2(1-\nu) \left( \frac{\partial^2 w}{\partial x \partial y} \right)^2 \right\} dx dy \quad (4.1)$$

Similarly, the potential energy of the transverse force  $q$  may be given by Eq. (2.29).

We have introduced the non-dimensional variables  $X = \frac{x}{a}$  and  $Y = \frac{y}{b}$ .

The total potential energy  $U_T$  of the system may be written in non-dimensional form as

$$U_T = u_s + u_v \quad (4.2)$$

where

$$u_s = \frac{1}{2} \int_0^1 \int_0^1 \left\{ \frac{D}{a^4} \left[ \left( \frac{\partial^2 w}{\partial X^2} \right)^2 + 2\nu R^2 \left( \frac{\partial^2 w}{\partial X^2} \frac{\partial^2 w}{\partial Y^2} \right) + R^4 \left( \frac{\partial^2 w}{\partial Y^2} \right)^2 + 2(1-\nu) R^2 \left( \frac{\partial^2 w}{\partial X \partial Y} \right)^2 \right] \right\} dX dY \quad (4.3)$$

$$u_v = - \int_0^1 \int_0^1 q \left[ w - \frac{\mu}{a^2} \left( \frac{\partial^2 w}{\partial X^2} + R^2 \frac{\partial^2 w}{\partial Y^2} \right) \right] dX dY \quad (4.4)$$

Here  $R = \frac{a}{b}$  is the aspect ratio.

Substituting Eq. (2.31) in Eq. (4.4) and then minimizing  $U_T$  as a function of constants, one may obtain following system of linear equation

$$\sum_{j=1}^n a_{ij}c_j = P_c b_i \quad (4.5)$$

where  $a_{ij} = \int_0^1 \int_0^1 [\varphi_i^{XX} \varphi_j^{XX} + R^4 \varphi_i^{YY} \varphi_j^{YY} + \nu R^2 (\varphi_i^{XX} \varphi_j^{YY} + \varphi_i^{YY} \varphi_j^{XX}) + 2(1-\nu)R^2 \varphi_i^{XY} \varphi_j^{XY}] dXdY$

$$b_i = \int_0^1 \int_0^1 (\varphi_i - \frac{\mu}{a^2} (\varphi_i^{XX} + R^2 \varphi_i^{YY})) dXdY \text{ and } P_c = \frac{qa^4}{D}.$$

## 4.1 Numerical results and discussions

Above system of linear equation has been solved by using MATLAB. It should be noted that present study is subjected to uniformly distributed loading ( $q(X) = q_0$ ). Non-dimensional maximum center deflection ( $W_{max}$ ) is given by (Aghababaei and Reddy 2009)  $-w \times \left(\frac{Eh^2}{q_0 a^4}\right) \times 100$ .

### 4.1.1 Convergence

First of all, convergency has been carried out to find the minimum number of terms required for computation. As such, Fig. 4.1 shows convergence of simply supported nanoplates with  $\mu = 0.5nm^2$ ,  $R = 1$  and  $a = 10nm$ . One may find from this figure that convergency is attained at  $n = 7$ .

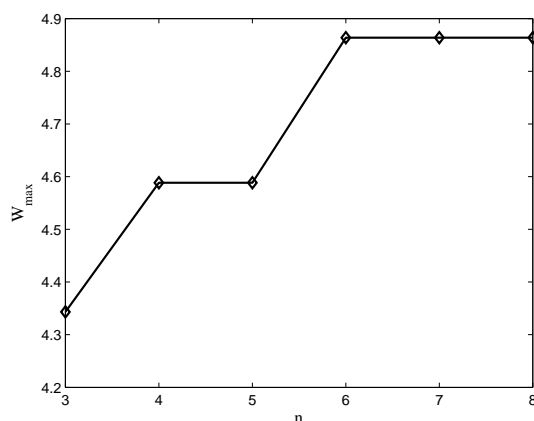


Fig. 4.1 Variation of non-dimensional maximum center deflection ( $W_{max}$ ) with  $n$

### 4.1.2 Validation

Next, to show the reliability and accuracy of the present method, our numerical results are compared with those available in literature for simply supported nanoplates. As such, tabular

comparison has been given in Table 4.1 with Aghababaei and Reddy (2009). For this comparison, same parameters as that of Aghababaei and Reddy (2009) have been used. One can see that our results are in a good agreement with analytical solutions. It is noted that S-S-S-S would denote simply supported-simply supported-simply supported-simply supported boundary condition.

Table 4.1 Comparison of non-dimensional maximum center deflection of S-S-S-S nanoplate

	$\mu = 0$	$\mu = 0.5$	$\mu = 1$	$\mu = 1.5$	$\mu = 2$	$\mu = 2.5$	$\mu = 3$
Present	4.0673	4.3637	4.7601	5.0565	5.4530	5.8094	6.1058
Ref.*	4.0083	4.3702	4.7322	5.0942	5.4561	5.8181	6.1800

\*Aghababaei et al. (2009)

In the following paragraphs, we have investigated some of the parametric studies.

### 4.1.3 Effect of aspect ratio

To investigate the effect of aspect ratio on the deflection, variation of deflection ratio with aspect ratio has been illustrated in Fig. 4.2 for F-S-F-S nanoplate with  $a = 5nm$ . Here, we define deflection ratio as

$$\text{deflection ratio} = \frac{\text{deflection calculated by nonlocal theory}}{\text{deflection calculated using local theory}}$$

One may notice that deflection ratio increases with increase in aspect ratio. In other words, increasing aspect ratio will decrease non-dimensional maximum center deflection. Same observation has also been reported in Aghababaei and Reddy (2009). It is noticed that deflection ratio increases with increase in nonlocal parameter. From the above graph, one may notice that that nonlocal effect on the deflection ratio is more in higher values of aspect ratio.

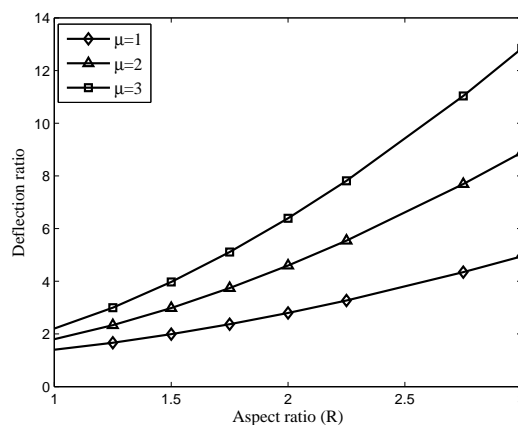


Fig. 4.2 Variation of deflection ratio with aspect ratio

#### 4.1.4 Effect of length

Next, Fig. 4.3 depicts effect of length on the non-dimensional maximum center deflection. Results have been shown for different nonlocal parameters with  $R = 1$  and S-C-S-C edge condition. It is figured out that non-dimensional maximum center deflection decreases with increase in length. It is also noticed that for each length of the nanoplates, the non-dimensional maximum center deflection increases with increase in the nonlocal parameter. Again, One may see that as the length of nanoplates increases, the non-dimensional maximum center deflection increases for each value of the nonlocal parameter. This is due to the fact that size-dependency plays a vital role in the nonlocal elasticity theory.

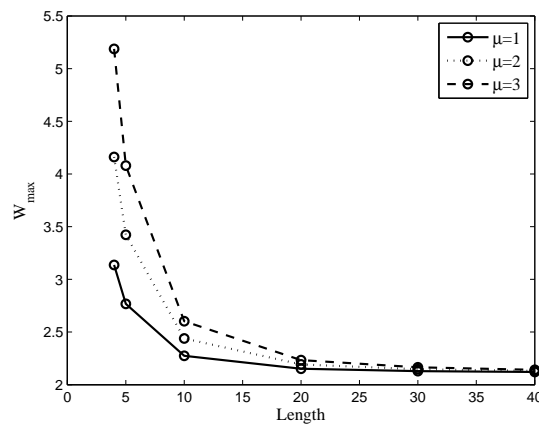


Fig. 4.3 Variation of  $W_{max}$  with length

#### 4.1.5 Effect of nonlocal parameter

To illustrate effect of nonlocal parameter on the deflection, Fig. 4.4 illustrates variation of nonlocal parameter with non-dimensional maximum center deflection. In this figure, we have taken  $a = 10nm$ ,  $R = 2$  with F-C-F-C edge condition. One may find increase in nonlocal parameter will increase deflection.



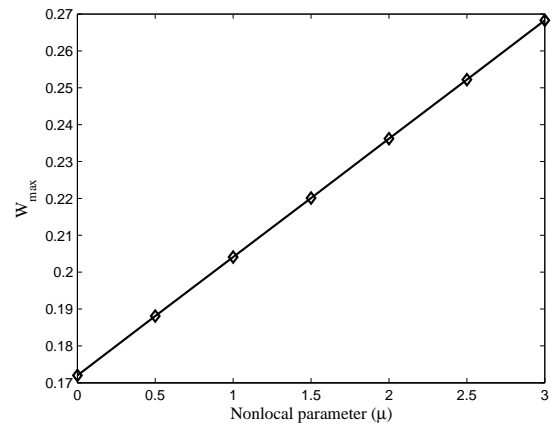


Fig. 4.4 Variation of  $W_{max}$  with nonlocal parameter

## Buckling of nanoplates

In this analysis, we have considered orthotropic nanoplates embedded in elastic medium such as Winkler and Pasternak.

As such, one may obtain Rayleigh-quotient in non-dimensional form as

$$\bar{N}^0 = \frac{U_b}{V_b} \quad (4.6)$$

where

$$\begin{aligned} U_b = & \frac{1}{2} \int_0^1 \int_0^1 \left\{ \frac{E_1}{E_2} \left( \frac{\partial^2 W}{\partial X^2} \right)^2 + 2\nu_x R^2 \left( \frac{\partial^2 W}{\partial X^2} \frac{\partial^2 W}{\partial Y^2} \right) + R^4 \left( \frac{\partial^2 W}{\partial Y^2} \right)^2 + 4 \frac{G_{xy}}{E_2} (1 - \nu_x \nu_y) R^2 \left( \frac{\partial^2 W}{\partial X \partial Y} \right)^2 \right. \\ & + K_g \left[ \left( \frac{\partial W}{\partial X} \right)^2 + R^2 \left( \frac{\partial W}{\partial Y} \right)^2 + \frac{\mu}{a^2} \left( \left( \frac{\partial^2 W}{\partial X^2} \right)^2 + R^2 \left( \frac{\partial^2 W}{\partial X \partial Y} \right)^2 \right) + \frac{\mu}{b^2} \left( \left( \frac{\partial^2 W}{\partial X \partial Y} \right)^2 + R^2 \left( \frac{\partial^2 W}{\partial Y^2} \right)^2 \right) \right] \\ & \left. + K_w \left[ W^2 + \frac{\mu}{a^2} \left( \left( \frac{\partial W}{\partial X} \right)^2 + R^2 \left( \frac{\partial W}{\partial Y} \right)^2 \right) \right] \right\} dX dY \end{aligned}$$

$$\begin{aligned} V_b = & \frac{1}{2} \int_0^1 \int_0^1 \left\{ \left( \frac{\partial W}{\partial X} \right)^2 + \frac{\mu}{a^2} \left( \left( \frac{\partial^2 W}{\partial X^2} \right)^2 + R^2 \left( \frac{\partial^2 W}{\partial X \partial Y} \right)^2 \right) + R^2 \left( \frac{\partial W}{\partial Y} \right)^2 \right. \\ & \left. + \frac{\mu}{b^2} \left( \left( \frac{\partial^2 W}{\partial X \partial Y} \right)^2 + R^2 \left( \frac{\partial^2 W}{\partial Y^2} \right)^2 \right) \right\} dX dY \end{aligned}$$

Here  $\bar{N}^0 = \frac{N_{xx} a^2}{E_2 h^3}$  is the non-dimensional buckling load parameter.

Substituting Eq. (2.31) into Rayleigh-quotient, we get a generalized eigen value problem as discussed in Chapter 2. In the generalized eigen value problem [Eq. (2.34)], stiffness matrix ( $K$ ) and buckling matrix ( $B_c$ ) are given as

$$K(i, j) = \int_0^1 \int_0^1 \left[ \frac{E_1}{E_2} \varphi_i^{XX} \varphi_j^{XX} + R^4 \varphi_i^{YY} \varphi_j^{YY} + \nu_x R^2 (\varphi_i^{XX} \varphi_j^{YY} + \varphi_i^{YY} \varphi_j^{XX}) + 4 \frac{G_{xy}}{E_2} (1 - \nu_x \nu_y) R^2 \varphi_i^{XY} \varphi_j^{XY} \right] dX dY$$

$$B_c(i, j) = \int_0^1 \int_0^1 \left( \varphi_i^X \varphi_j^X + \frac{\mu}{a^2} (\varphi_i^{XX} \varphi_j^{XX} + R^2 \varphi_i^{XY} \varphi_j^{XY}) + R^2 \varphi_i^Y \varphi_j^Y + \frac{\mu}{b^2} (\varphi_i^{XY} \varphi_j^{XY} + R^2 \varphi_i^{YY} \varphi_j^{YY}) \right) dX dY$$

## 4.2 Numerical results and discussions

### 4.2.1 Convergence

Convergence study has been carried out in order to establish the required degree of the polynomial set for desired results and is presented in Fig. 4.5. In this figure, we have taken stiffness

ratio ( $\frac{E_1}{E_2}$ )= 10, nonlocal parameter ( $\mu$ ) =  $1nm^2$ , length ( $a$ ) =  $10nm$  and aspect ratio ( $R$ ) = 1. Results have been shown for  $K_w = 50$  and  $K_p = 2$  with S-S-S-S edge condition. one may see from this figure that  $n = 25$  is sufficient in the present analysis.

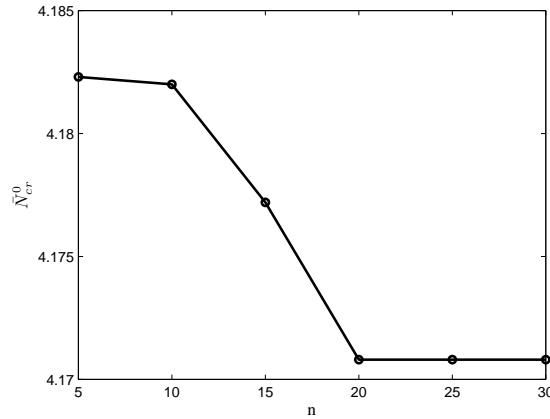


Fig. 4.5 Variation of  $\bar{N}_{cr}$  with grid points

## 4.2.2 Validation

To validate the present results, a comparison study has been carried out in Table 4.2 with Thai and Kim (2011). For this, same parameters as that of Thai and Kim (2011) have been used. Results have been shown for four types of boundary conditions. Here, the two opposite edges parallel to the  $x$ -axis are simply supported and the other two edges can have any arbitrary conditions such as free, simply supported or clamped conditions as shown in the table. One may observe a close agreement of the results.

Table 4.2 Comparison of non-dimensional critical buckling load parameter for S-S-S-S nanoplate

$\frac{E_1}{E_2}$	S-S		F-C		F-S		F-F	
	Present	Ref.*	Present	Ref.*	Present	Ref.*	Present	Ref.*
10	5.5669	5.5707	1.7688	1.7733	1.0158	1.0165	1.2772	1.2745
25	11.6885	11.7003	2.8069	2.8271	1.0147	1.0148	1.2652	1.2737
40	17.7922	17.8060	3.8041	3.8804	1.0143	1.0144	1.2682	1.2735

\*Thai and Kim (2011)

## 4.2.3 Effect of length

To investigate the effect of length on the buckling load parameter, variation of buckling load ratio with length has been shown in Fig. 4.6 for F-S-C-S nanoplates with  $R = 1$ ,  $a = 10nm$  and stiffness ratio as 10. Results have been shown for different values of nonlocal parameters ( $0nm^2 - 4nm^2$ ) in the absence of elastic foundation. It is observed that buckling load ratio increases with increase in length. This observation may be explained as: Assuming  $l_{int}$  as

constant, increasing length ( $a$ ) would lead to decrease in small scale effect ( $\mu/a^2$ ). It is also noticed that buckling load ratio are highest in case of  $\mu = 0$  and goes on decreasing with increase in nonlocal parameter. From this, we may also say that nonlocal theory should be taken into account for buckling analysis of small enough nanoplates.

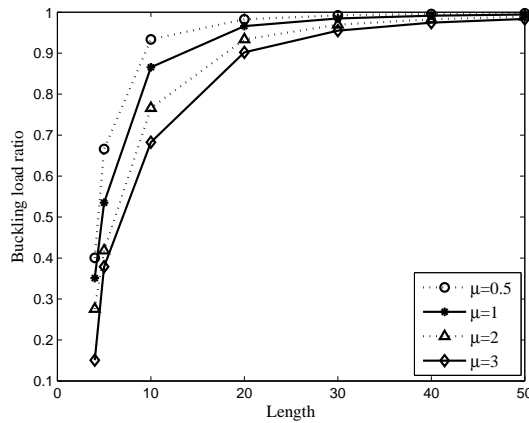


Fig. 4.6 Variation of buckling load ratio with length

#### 4.2.4 Effect of aspect ratio

In this subsection, we have considered the effect of aspect ratio on the buckling load parameter in the absence of elastic foundation. Fig. 4.7 shows the effect of buckling load ratio associated with first mode of F-S-S-S nanoplate with aspect ratio taking  $a = 10nm, \frac{E_1}{E_2} = 10$ . It is observed that buckling load ratio decreases with increase in aspect ratio. One may notice that buckling load ratio decreases with increase in nonlocal parameter. As the nonlocal parameter increases, critical buckling load ratio obtained from nonlocal plate theory become smaller than those of its local counterpart. This shows that, nonlocal theory should be considered for buckling of nanoplates.

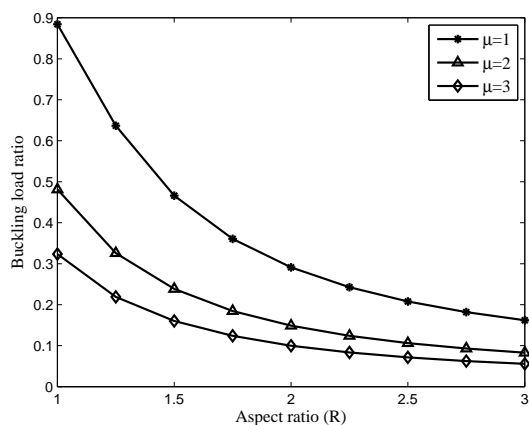


Fig. 4.7 Change of buckling load ratio with aspect ratio

### 4.2.5 Effect of stiffness ratio

Next, investigation has been performed to examine the effect of stiffness ratio on the critical buckling load parameter of nonlocal orthotropic plate model of nanoplate. As such, Fig. 4.8 illustrates variation of buckling load ratio with stiffness ratio for S-S-S-S nanoplates with  $a = 5nm$  and  $R = 1$ . Results have been shown in the absence of elastic foundation for different nonlocal parameters ( $\mu = 0.5nm^2, 1nm^2, 2nm^2$ ). It is observed from the figure that buckling load ratio decreases with increase with stiffness ratio. In other words, stiffness ratio has an increasing effect on the critical buckling load parameter.

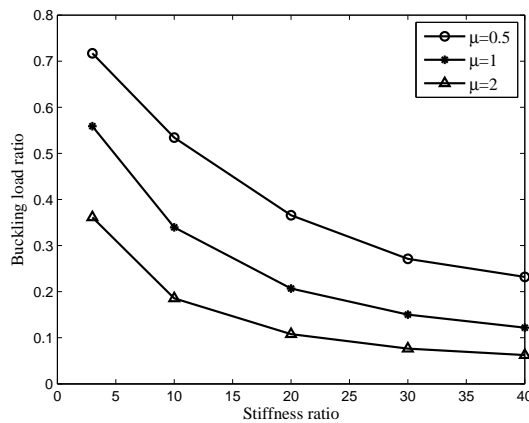


Fig. 4.8 Effect of stiffness ratio on buckling load ratio

### 4.2.6 Effect of nonlocal parameter

Here, we have examined the effect of nonlocal parameter on the buckling load parameter in the absence of elastic foundation. Variation of critical buckling load with nonlocal parameter has been illustrated in Fig. 4.9 for S-C-S-C edge condition. In this graph, we have taken  $a = 10nm, R = 2, \frac{E_1}{E_2} = 10$ . It is clearly seen from the figure that critical buckling load parameter decreases with increase in nonlocal parameter. This implies that application of local beam model for buckling analysis of graphene sheets would lead to over prediction of the buckling load. Hence, nonlocal beam theory should be used for better predictions of buckling load of nanoplates.

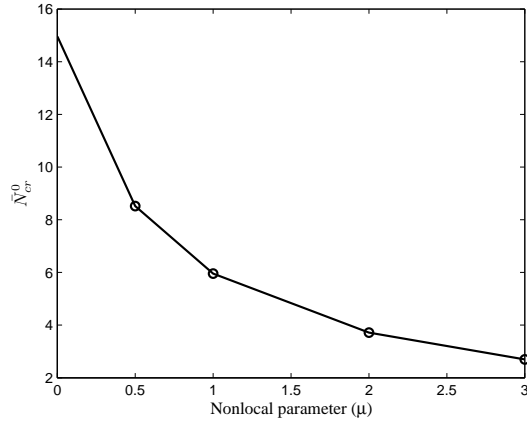


Fig. 4.9 Small scale effect on critical buckling load parameter

### 4.2.7 Effect of elastic foundation

Here, the effects of Winkler and Pasternak elastic foundations on the critical buckling load parameter have been studied. As such, Figs. 4.10-4.11 show variation of buckling load ratio with Winkler and Pasternak coefficients respectively. In these figures, we have taken  $a = 10nm$ ,  $\frac{E_1}{E_2} = 10$ ,  $R = 2$  with S-C-S-C edge condition. Effect of Winkler coefficient on the buckling load ratio has been analyzed taking  $K_p = 0$  and effect of Pasternak coefficient on the buckling load ratio has been investigated taking  $K_w = 0$ . Results have been computed for different values of nonlocal parameters ( $\mu = 0nm^2, 0.5nm^2, 1nm^2, 2nm^2, 3nm^2$ ). It is seen from the figures that buckling load ratio increases linearly by increasing the stiffness of the elastic foundation either through the springy (Winkler coefficient) or the shear effect (Pasternak coefficient). It is also noticed from these figures that the shear effect of the elastic foundation has more noticeable influence on the buckling load ratio.

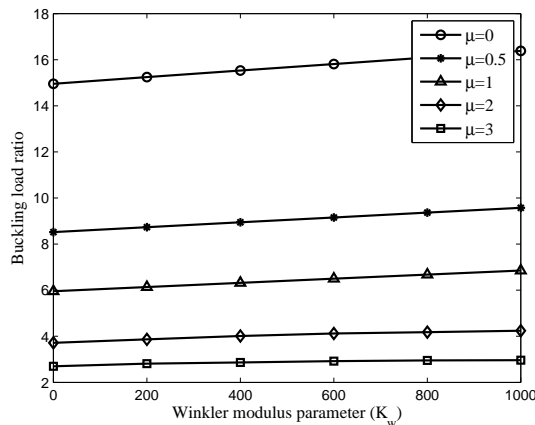


Fig. 4.10 Effect of Winkler modulus parameter on the buckling load ratio

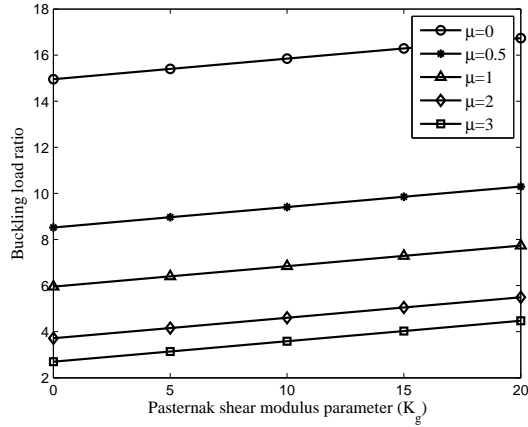


Fig. 4.11 Effect of Pasternak shear modulus parameter on buckling load ratio

### 4.3 Conclusions

Rayleigh-Ritz method with two-dimensional simple polynomials has been implemented to analyze bending and buckling of rectangular nanoplate. Bending analysis has been carried out in isotropic case while buckling study has been investigated for orthotropic nanoplate. Various parametric studies have been investigated. One may easily handle all sets of boundary conditions by the application of Rayleigh-Ritz method. Application of Rayleigh-Ritz method converts bending problem to system of linear equation and buckling problem to generalized eigen value problem.

# Chapter 5

## Vibration of nanobeams

The contents of this chapter have been published in:

1. Laxmi Behera and S. Chakraverty (2015) Application of differential quadrature method in free vibration analysis of nanobeams based on various nonlocal theories, *Computers and Mathematics with Applications*, 69, 1444-1462.
2. Laxmi Behera and S. Chakraverty (2014) Free vibration of Euler and Timoshenko nanobeams using boundary characteristic orthogonal polynomials, *Applied Nanoscience*, 4, 347-358.



# Chapter 5

## Vibration of nanobeams

In this chapter, Rayleigh-Ritz method has been applied to study vibration of nanobeams based on Euler-Bernoulli and Timoshenko beam theories. Next, differential quadrature method has been used to investigate vibration of nanobeams based on four types of beams such as Euler-Bernoulli, Timoshenko, Reddy and Levinson. In the Rayleigh-Ritz method, both one-dimensional simple polynomials and boundary characteristic orthogonal polynomials have been used as shape functions.

### Vibration of nanobeams using Rayleigh-Ritz method

In this analysis, we have used the following non-dimensional terms

$$\begin{aligned} X &= \frac{x}{L} \\ W &= \frac{w_0}{L} \\ \alpha &= \frac{e_0 a}{L} = \text{scaling effect parameter} \\ \tau &= \frac{I}{AL^2} \\ \lambda^2 &= \frac{\rho A \omega^2 L^4}{EI} = \text{frequency parameter} \\ \Omega &= \frac{EI}{k_s GAL^2} = \text{shear deformation parameter} \end{aligned}$$

Application of Rayleigh-Ritz method would convert vibration problems to generalized eigen value problems which have been discussed in section 2.1.2. In generalized eigen value equation [Eq. (2.21)], stiffness and mass matrices for EBT are given by

$$K(i, j) = \int_0^1 \varphi_i'' \varphi_j'' dX$$

$$M_a(i, j) = \int_0^1 \varphi_i \varphi_j - \frac{\alpha^2}{2} \varphi_i \varphi_j'' - \frac{\alpha^2}{2} \varphi_i'' \varphi_j dX$$

Similarly in the generalized eigen value equation for TBT nanobeams [Eq. (2.26)], matrices  $K$  and  $M_a$  are defined as

$$K = \begin{bmatrix} k_1 & k_2 \\ k_3 & k_4 \end{bmatrix} \text{ where } k_1, k_2, k_3, k_4 \text{ are submatrices and are given by}$$

$$k_1(i, j) = \int_0^1 \varphi_i' \varphi_j' dX$$

$$k_2(i, j) = \int_0^1 \varphi_i' \psi_j dX$$

$$k_3(i, j) = \int_0^1 \psi_i \varphi_j' dX$$

$$k_4(i, j) = \int_0^1 (\psi_i \psi_j + \Omega \psi_i' \psi_j') dX$$

$$M_a = \begin{bmatrix} m_1 & m_2 \\ m_3 & m_4 \end{bmatrix} \text{ where } m_1, m_2, m_3, m_4 \text{ are submatrices and are given as}$$

$$m_1(i, j) = \Omega \int_0^1 \varphi_i \varphi_j dX$$

$$m_2(i, j) = \Omega \frac{\alpha^2}{2} \int_0^1 \varphi_i \psi_j' dX$$

$$m_3(i, j) = \Omega \frac{\alpha^2}{2} \int_0^1 \psi_i' \varphi_j dX$$

$$m_4(i, j) = \Omega \int_0^1 (\tau \psi_i \psi_j + \tau \alpha^2 \psi_i' \psi_j') dX$$

## 5.1 Numerical results and discussions

Frequency parameters of SWCNT have been computed by using Rayleigh-Ritz method. In the numerical evaluations, following parameters have been used (Wang et al. 2007): diameter,  $d = 0.678nm$ ,  $L = 10d$ ,  $t = 0.066$ ,  $k_s = 0.563$ ,  $E = 5.5TPa$ ,  $G = E/[2(1 + \nu)]$ ,  $\nu = 0.19$  and  $I = \Pi d^4/64$ .

In this study, frequency parameters of both Euler-Bernoulli and Timoshenko nanobeams have been computed. Results have been investigated for different scaling effect parameters and

boundary conditions. Firstly, frequency parameters are being computed taking simple polynomials of the form  $X^{i-1}$  in the Rayleigh-Ritz method. Then the polynomials are orthogonalized by Gram-Schmidt process and are used in the Rayleigh-Ritz method to obtain frequency parameters. Table 5.1 shows the convergence studies of first three frequency parameters ( $\sqrt{\lambda}$ ) for S-S and C-S Euler-Bernoulli nanobeams taking  $\alpha = 0.5$  and  $L = 10d$ . Similarly, convergence studies of first three frequency parameters for S-S and C-S Timoshenko nanobeams are tabulated in Table 5.2 for  $\alpha = 0.5$  and  $L = 10d$ . In these tables, it is observed that the frequency parameters are close to the results of Wang et al. (2007) as the value of  $n$  increases. In Table 5.3, first four frequency parameters of Euler-Bernoulli nanobeams have been compared with results of Wang et al. (2007) and are found to be in good agreement. Similarly results of Timoshenko nanobeams subjected to various boundary conditions have been compared with Wang et al. (2007) in Table 5.4 for different scaling effect parameters. From Tables 5.3 and 5.4, it can be clearly seen that the nonlocal results are smaller than the corresponding local ones. Frequency parameters of nanobeams subjected to F-F and S-F boundary conditions have been given in Table 5.5 for different scaling effect parameters. It may be noted that the frequency parameters obtained by using orthonormalized polynomials are same as that of using simple polynomials. But here the computations become more efficient and less time is required for the execution of the program. It is due to the fact that some of the matrix elements become zero or one due to the orthonormality. One of the interesting facts in this analysis is that C-C nanobeams have highest frequency parameters than other boundary conditions. It helps the design engineers to obtain desired frequency parameters as per the application.

The behavior of scaling effect parameter on the frequency parameter is shown in Figs. 5.1-5.3 respectively for S-S, C-S and C-C Euler-Bernoulli nanobeams. Similarly, Figs. 5.4-5.6 show variation of frequency parameter with the scaling effect parameter respectively for S-S, C-S and C-C Timoshenko nanobeams. In these figures, first four frequency parameters have been shown for both Euler-Bernoulli and Timoshenko nanobeams. From these figures, it is depicted that frequency parameters are over predicted when local beam model is considered for vibration analysis of nanobeams. As the scaling effect parameter increases, frequency parameters of nonlocal nanobeams become smaller than those of its local counterpart. This reduction can be clearly seen when we consider higher vibration modes. The reduction is due to the fact that the nonlocal model may be viewed as atoms linked by elastic springs while in case of local continuum model, the spring constant is assumed to take an infinite value. So small scale effect makes the nanobeams more flexible and nonlocal impact cannot be neglected. As such, nonlocal theory should be used for better predictions of high natural frequency of nanobeams. Mode shapes are useful for engineers to design structures because they represent the shape that the structures will vibrate in free motion. Sometimes, the knowledge of higher modes is necessary before finalizing the design of an engineering system. Thus, while studying vibration problems viz. beam, plate or shell, one may always see the tabulation of the higher frequencies

in the open literature. As such, the present investigators have reported first few higher modes in Fig. 5.7 for benchmarking the results which may help the researchers of nanotechnology. In Fig. 5.7, we have given first four deflections of nonlocal C-C Euler-Bernoulli nanobeams with scaling effect parameters as 0, 0.3 and 0.6. It can be seen that mode shapes are affected by small length scale. By understanding the modes of vibration, we can better design the structures as per the need.

Table 5.1 Convergence of first three frequency parameters for Euler-Bernoulli nanobeams

$n$	S-S			C-S		
	First	Second	Third	First	Second	Third
3	2.3026	3.8475	5.0587	2.7928	3.9140	5.6488
4	2.3026	3.4688	5.0587	2.7900	3.8530	4.8090
5	2.3022	3.4688	4.3231	2.7899	3.8341	4.6708
6	2.3022	3.4604	4.3231	2.7899	3.8327	4.6194
7	2.3022	3.4604	4.2945	2.7899	3.8325	4.6122
8	2.3022	3.4604	4.2945	2.7899	3.8325	4.6106
9	2.3022	3.4604	4.2941	2.7899	3.8325	4.6105
10	2.3022	3.4604	4.2941	2.7899	3.8325	4.6105
11	2.3022	3.4604	4.2941	2.7899	3.8325	4.6105

Table 5.2 Convergence of first three frequency parameters for Timoshenko nanobeams

$n$	S-S			C-S		
	First	Second	Third	First	Second	Third
3	2.3867	3.6631	10.4677	2.7315	4.1148	6.8252
4	2.2760	3.6630	4.5482	2.7210	3.6916	4.8857
5	2.2760	3.3477	4.5481	2.7186	3.6521	4.3489
6	2.2756	3.3477	4.0425	2.7186	3.6373	4.2753
7	2.2756	3.3423	4.0425	2.7186	3.6364	4.2391
8	2.2756	3.3426	4.0212	2.7186	3.6362	4.2352
9	2.2756	3.3423	4.0212	2.7186	3.6362	4.2341
10	2.2756	3.3423	4.0209	2.7186	3.6362	4.2341
11	2.2756	3.3423	4.0209	2.7186	3.6362	4.2341

Table 5.3 Validation of first four frequency parameters of Euler-Bernoulli nanobeams

Mode no.	$\alpha = 0$		$\alpha = 0.1$		$\alpha = 0.3$	
	Present	Ref.*	Present	Ref.*	Present	Ref.*
S-S						
1	3.1416	3.1416	3.0685	3.0685	2.6800	2.6800
2	6.2832	6.2832	5.7817	5.7817	4.3013	4.3013
3	9.4248	9.4248	8.0400	8.0400	5.4423	5.4422
4	12.566	12.566	9.9162	9.9162	6.3630	6.3630
C-S						
1	3.9266	3.9266	3.8209	3.8209	3.2828	3.2828
2	7.0686	7.0686	6.4649	6.4649	4.7668	4.7668
3	10.210	10.210	8.6517	8.6517	5.8371	5.8371
4	13.252	13.352	10.469	0.469	6.7145	6.7143
C-C						
1	4.7300	4.7300	4.5945	4.5945	3.9184	3.9184
2	7.8532	7.8532	7.1402	7.1402	5.1963	5.1963
3	10.996	10.996	9.2583	9.2583	6.2317	6.2317
4	14.137	14.137	11.016	11.016	7.0482	7.0482

\*Wang et al. (2007)

Table 5.4 Validation of first four frequency parameters of Timoshenko nanobeams

Mode no.	$\alpha = 0$		$\alpha = 0.1$		$\alpha = 0.3$	
	Present	Ref.*	Present	Ref.*	Present	Ref.*
S-S						
1	3.0742	3.0929	3.0072	3.0243	2.6412	2.6538
2	5.9274	5.9399	5.4400	5.5304	4.1357	4.2058
3	8.4057	8.4444	7.3662	7.4699	5.0744	5.2444
4	10.601	10.626	8.9490	8.9874	6.0173	6.0228
C-S						
1	3.7336	3.7845	3.6476	3.6939	3.1784	3.2115
2	6.2945	6.4728	6.0015	6.0348	4.4926	4.6013
3	8.4762	8.1212	7.5816	7.8456	5.3307	5.5482
4	10.861	10.880	9.2044	9.2751	6.2286	6.2641
C-C						
1	4.3980	4.4491	4.3026	4.3471	3.7578	3.7895
2	6.7711	6.9524	6.3507	6.4952	4.8196	4.9428
3	9.1185	9.1626	8.1274	8.1969	5.6082	5.8460
4	11.014	11.113	9.1456	9.5447	6.1194	6.4762

\*Wang et al. (2007)

Table 5.5 First four frequency parameters of Timoshenko nanobeams and some new boundary conditions

Mode no.	$\alpha = 0$	$\alpha = 0.1$	$\alpha = 0.3$	$\alpha = 0.5$	$\alpha = 0.7$
S-F					
1	0.0009	0.0008	0.0001	0.0001	0.0001
2	3.8065	3.7118	3.2121	2.7378	2.3931
3	6.4684	6.0146	4.5340	3.6575	3.1302
4	8.7295	7.7276	5.3708	4.2542	3.6193
F-F					
1	0.0009	0.0008	0.0008	0.0004	0.0004
2	4.5443	4.4253	3.8029	3.2201	2.8043
3	7.0857	6.5603	4.8810	3.9150	3.3428
4	9.2673	8.1717	5.6529	4.4805	3.8132

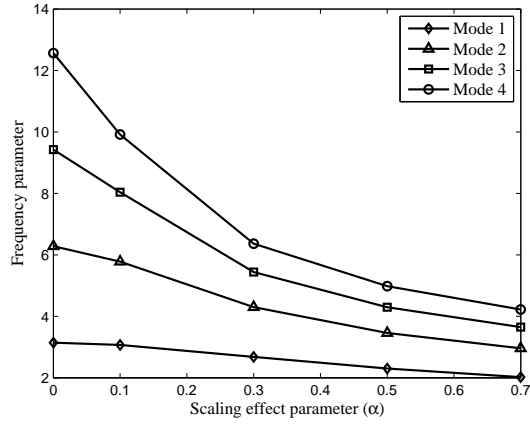


Fig. 5.1 Change of frequency parameter with  $\alpha$  (S-S)

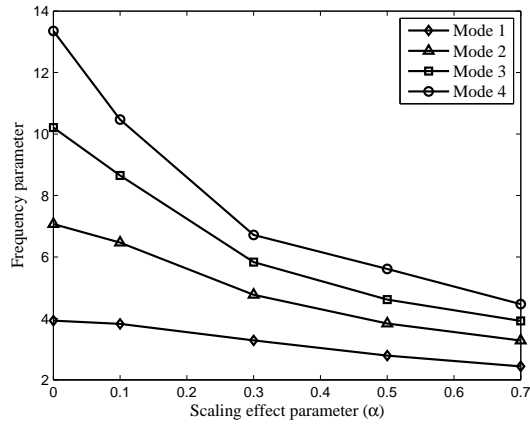


Fig. 5.2 Change of frequency parameter with  $\alpha$  (C-S)

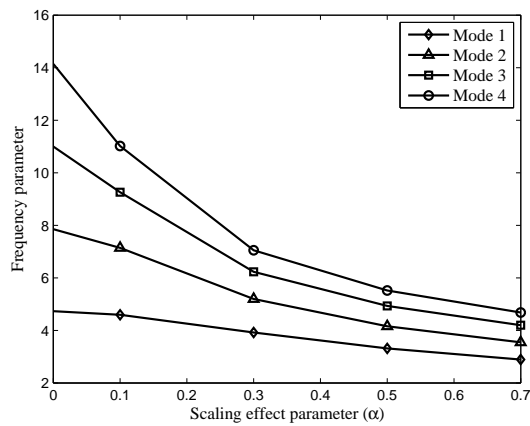


Fig. 5.3 Change of frequency parameter with  $\alpha$  (C-C)

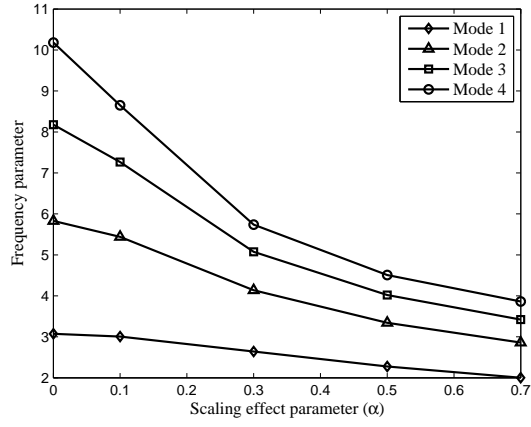


Fig. 5.4 Change of frequency parameter with  $\alpha$  (S-S)

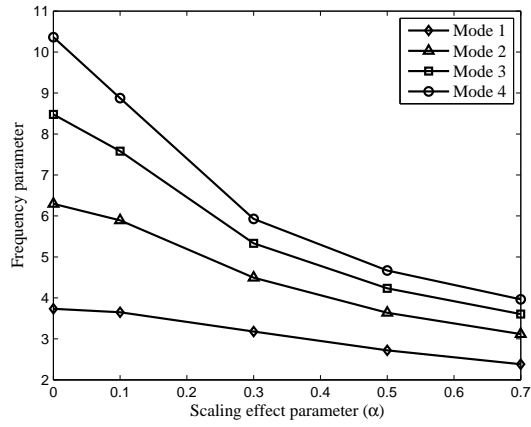


Fig. 5.5 Change of frequency parameter with  $\alpha$  (C-S)

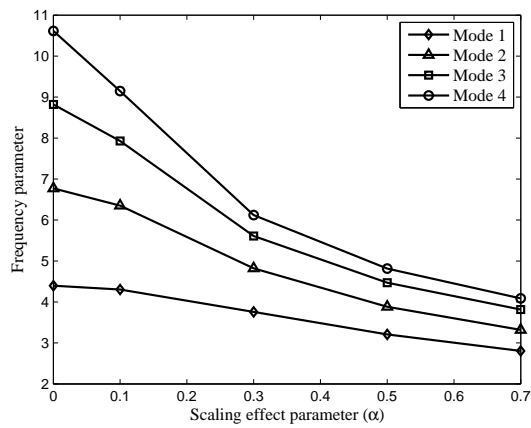


Fig. 5.6 Change of Frequency parameter with  $\alpha$  (C-C)



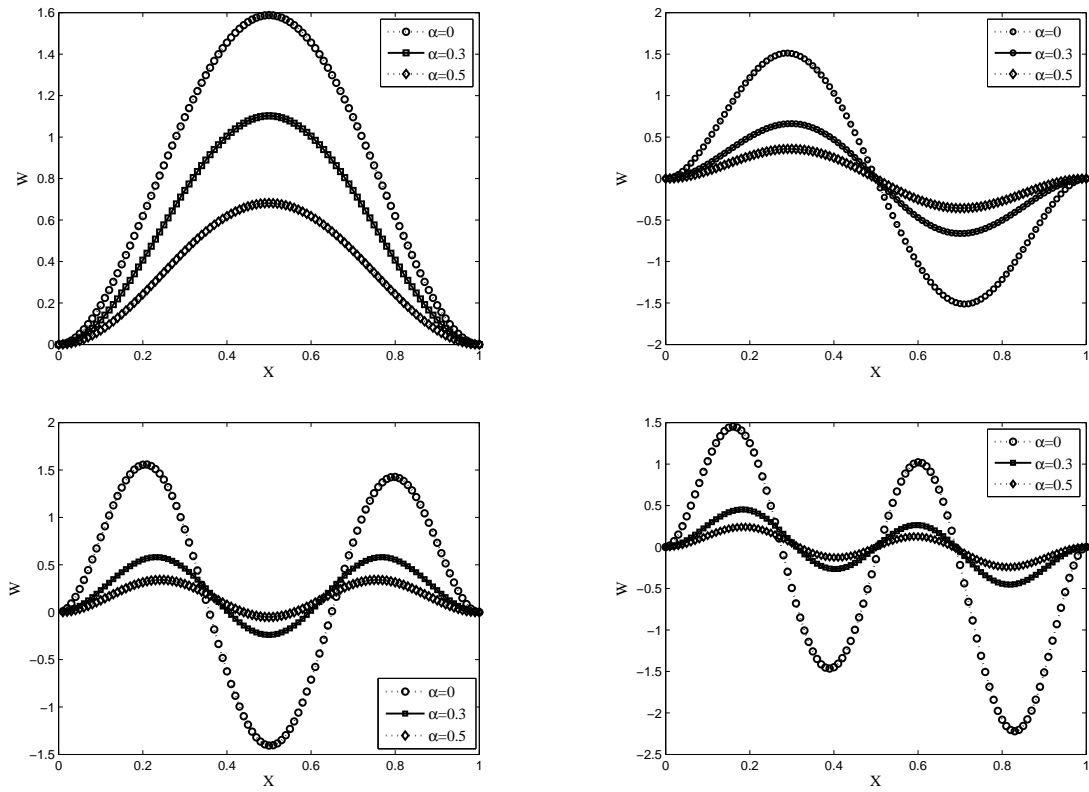


Fig. 5.7 First four deflection shapes of clamped-clamped nanobeams

## Vibration of nanobeams using differential quadrature method

In this section, differential quadrature method has been employed to study various nonlocal beam theories such as Euler-Bernoulli, Timoshenko, Reddy and Levinson. Boundary conditions have been substituted in the coefficient matrices.

In this problem, we have introduced following non-dimensional terms

$$\begin{aligned}
 X &= \frac{x}{L} \\
 W &= \frac{w_0}{L} \\
 \alpha &= \frac{e_0 a}{L} = \text{scaling effect parameter} \\
 \tau &= \frac{I}{AL^2} \\
 \lambda^2 &= \frac{\rho A \omega^2 L^4}{EI} = \text{frequency parameter} \\
 \Omega &= \frac{EI}{K_s GAL^2} = \text{shear deformation parameter} \\
 \bar{\Omega} &= \frac{G \tilde{A} L^2}{EI} \\
 \hat{\Omega} &= \frac{EI}{G \tilde{A} L^2}
 \end{aligned}$$

Below we have included the non-dimensionalized forms of the governing differential equations respectively for EBT, TBT, RBT and LBT in Eqs. (5.1-5.4).

$$\frac{d^4 W}{dX^4} = \lambda^2 \left( W - \alpha^2 \frac{d^2 W}{dX^2} \right) \quad (5.1)$$

$$\frac{d^4 W}{dX^4} = \lambda^2 \left( -\tau \frac{d^2 W}{dX^2} + \alpha^2 \tau \frac{d^4 W}{dX^4} - \Omega \frac{d^2 W}{dX^2} + \Omega \alpha^2 \frac{d^4 W}{dX^4} + W - \alpha^2 \frac{d^2 W}{dX^2} \right) \quad (5.2)$$

$$\bar{\Omega} \frac{5}{4} \frac{d^4 W}{dX^4} - \frac{1}{105} \frac{d^6 W}{dX^6} = \lambda^2 \left( -\frac{17}{21} \frac{d^2 W}{dX^2} + \frac{17}{21} \alpha^2 \frac{d^4 W}{dX^4} + \frac{105}{84} \bar{\Omega} \left( W - \alpha^2 \frac{d^2 W}{dX^2} \right) \right) \quad (5.3)$$

$$\frac{d^4 W}{dX^4} = \lambda^2 \left[ W + \left( \alpha^2 \tau + \frac{4}{5} \alpha^2 \hat{\Omega} \right) \frac{d^4 W}{dX^4} - \left( \tau + \alpha^2 + \frac{4}{5} \hat{\Omega} \right) \frac{d^2 W}{dX^2} \right] \quad (5.4)$$

By the application of differential quadrature method, one may obtain generalized eigen value problem as

$$[S] \{W\} = \lambda^2 [M_a] \{W\} \quad (5.5)$$

where  $S$  is the stiffness matrix and  $M_a$  is the mass matrix.

## 5.2 Numerical results and discussions

Frequency parameters ( $\sqrt{\lambda}$ ) have been obtained by solving Eq. (5.5) using computer code developed by the authors. Lowest four eigen values corresponding to first four frequency parameters have been reported for different boundary conditions. In this investigation, various parameters used for numerical evaluations are as follows (Reddy 2007):  $E = 30 \times 10^6$ ,  $\nu = 0.3$ ,  $L = 10nm$ ;  $G = \frac{E}{2(1+\nu)}$ ,  $k_s = \frac{5}{6}$  and unless mentioned  $\frac{L}{h} = 10$ .

### 5.2.1 Convergence

A convergence study is being carried out for finding the minimum number of grid points to obtain converged results. Lower frequency parameters converge first than successive higher frequency parameters. First three frequency parameters converge with less number of grid points than fourth one. Hence convergence of fourth frequency parameter ( $\sqrt{\lambda_4}$ ) of EBT and RBT nanobeams is shown in Fig. 5.8. In this graph,  $\mu$  is taken as  $1nm^2$  with S-S boundary condition. It is seen that fourth frequency parameter converges at sixteen grid points. Hence, sixteen grid points are taken for obtaining the converged results of first four frequency parameters of nanobeams based on four beam theories.

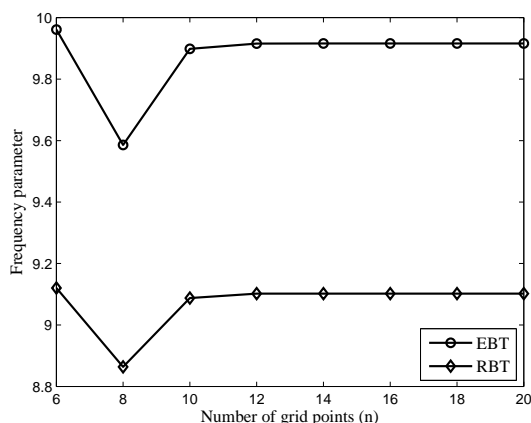


Fig. 5.8 Variation of frequency parameter with grid points

### 5.2.2 Validation

Validation of the proposed method is confirmed by comparing obtained results with those available in literature (Wang et al. 2007; Reddy 2007). For this purpose, same parameters as used in Wang et al. (2007) and Reddy (2007) are taken. Comparison of the fundamental frequency parameter has been shown in Table 5.6 for S-S edge condition. Results have been compared for all four types of beam theories. In this table,  $\mu$  is taken from  $0nm^2$  to  $4nm^2$ . Similarly, comparison of the results of Timoshenko nanobeams subjected to different boundary conditions (S-S, C-C, C-S, C-F) has been reported in Table 5.7 for different scaling effect parameters. It is observed

from the above table (Table 5.6) that fundamental frequency parameter of EBT nanobeams is higher than other types of nanobeams. One may see from Table 5.7 that no nontrivial real frequencies will exist for cantilever beams once the scaling effect parameter approaches the value 0.6138. This is due to the fact that successive odd and even vibration modes approach each other and are suppressed with the increasing value of  $\alpha$ . In addition, real frequencies can be obtained for only first few modes once value of  $\alpha$  approaches 0.6138. Similar findings are also reported in Refs. (Wang et al. 2007) and (Reddy 2007). We have also incorporated graphical comparison in Fig. 5.9 with Wang et al. (2007) for TBT nanobeams with S-S support. Similarly, Fig. 5.10 shows graphical comparison with Reddy (2007) for Reddy nanobeams with  $\frac{L}{h} = 10$ . One may observe that a close agreement of the results is achieved.

Table 5.6 Comparison of fundamental frequency parameter ( $\lambda$ ) for S-S nanobeams

$\mu$	EBT	Ref.*	TBT	Ref.*	RBT	Ref.*	LBT	Ref.*
0	9.8696	9.8696	9.7200	9.7454	9.7200	9.7454	9.7400	9.7657
0.5	9.6347	9.6347	9.4953	9.5135	9.5100	9.5135	9.5055	9.5333
1	9.4159	9.4159	9.2973	9.2973	9.3000	9.2974	9.3003	9.3168
1.5	9.2113	9.2113	9.1113	9.0953	9.1000	9.0954	9.0991	9.1144
2	9.0195	9.0195	8.9359	8.9059	8.9100	8.9060	8.9004	8.9246
2.5	8.8392	8.8392	8.7703	8.7279	8.7300	8.7279	8.7231	8.7462
3.0	8.6693	8.6693	8.6136	8.5601	8.5600	8.5602	8.5260	8.5780
3.5	8.5088	8.5088	8.4650	8.4017	8.4017	8.4017	8.3682	8.4193
4.0	8.3569	8.3569	8.2238	8.2517	8.2517	8.2517	8.2188	8.2690

\*Reddy (2007)

Table 5.7 Comparison of first three frequency parameters ( $\sqrt{\lambda}$ ) for different boundary conditions

		S-S				C-S			
$\alpha$		0.1	0.3	0.5	0.7	0.1	0.3	0.5	0.7
$\sqrt{\lambda_1}$		3.0603	2.6752	2.2994	2.0193	3.6089	3.2754	2.7857	2.4328
Ref.*		3.0243	2.6538	2.2867	2.0106	3.6939	3.2115	2.7471	2.4059
$\sqrt{\lambda_2}$		5.7309	4.2831	3.4498	2.9506	6.0430	4.7424	3.7170	3.2654
Ref.*		5.5304	4.2058	3.4037	2.9159	6.0348	4.6013	3.7312	3.2003
$\sqrt{\lambda_3}$		7.4153	5.2033	4.2693	3.5290	7.7055	5.5870	4.4767	3.8929
Ref.*		7.4699	5.2444	4.1644	3.5453	7.8456	5.5482	4.4185	3.7666
		C-C				C-F			
$\alpha$		0.1	0.3	0.5	0.7	0.1	0.3	0.5	0.7
$\sqrt{\lambda_1}$		4.3785	3.7069	3.3068	2.8823	1.8796	1.9158	2.0225	-
Ref.*		4.3471	3.7895	3.2420	2.8383	1.8650	1.8999	2.0024	-
$\sqrt{\lambda_2}$		6.4405	4.9223	3.7730	3.4473	4.4303	3.7543	2.9355	-
Ref.*		6.4952	4.9428	3.9940	3.4192	4.3506	3.6594	2.8903	-
$\sqrt{\lambda_3}$		8.0856	5.7696	4.6909	3.9600	6.5710	5.0652	-	-
Ref.*		8.1969	5.8460	4.6769	3.9961	6.6091	5.0762	-	-

\*Wang et al. (2007)

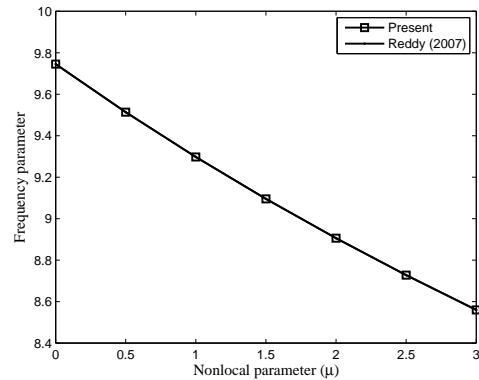
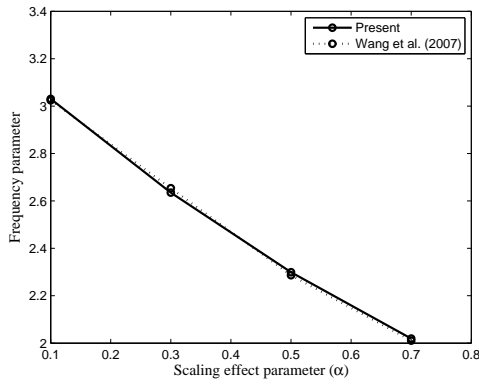


Fig. 5.9 Comparison of results with Wang et al. (2007) Fig. 5.10 Comparison of results with Reddy (2007)

### 5.2.3 Effect of nonlocal parameter

Effect of nonlocal parameter on the first four frequency parameters ( $\sqrt{\lambda}$ ) of nanobeams based on four beam theories is analyzed. In this analysis, boundary conditions such as S-S, C-S, C-C and C-F are taken into consideration. Both tabular and graphical results are presented in this context. Table 5.8 shows first four frequency parameters of S-S, C-S, C-C and C-F EBT nanobeams for different nonlocal parameters. From this table, it is seen that frequency parameters decrease with increase in nonlocal parameter except fundamental frequency param-

eter of C-F nanobeams. It is also observed that frequency parameters increase with increase in mode number. One of the interesting observation is that C-C nanobeams are having highest frequency parameters than other set of boundary conditions at the edges. Similarly Table 5.9 gives first four frequency parameters of S-S, C-S, C-C and C-F Timoshenko nanobeams subjected to various boundary conditions. Here also, it is noticed that frequency parameters decrease with nonlocal parameter except fundamental frequency parameter of C-F nanobeams. From this table also, one may see higher frequency parameters in case of C-C nanobeams. Similarly, first four frequency parameters of Reddy nanobeams subjected to S-S, C-S, C-C and C-F have been reported in Table 5.10 to illustrate the effect of nonlocal parameter on the frequency parameters. From the above table, one may conclude same observation as that of EBT and RBT nanobeams. Frequency parameters of Levison nanobeams subjected to different boundary conditions have been presented in Table 5.11. Here, one may observe that frequency parameters decrease with increase in nonlocal parameter except fundamental frequency parameter of C-F nanobeams. Next, to highlight the importance of nonlocal theory, variation of frequency ratio  $\left( \frac{\text{frequency parameter calculated using nonlocal theory}}{\text{frequency parameter calculated using local theory}} \right)$  associated with first four mode numbers with  $(e_0 a)$  has been shown in Figs 5.11-5.14 respectively for EBT, TBT, RBT and LBT. In these figures, we have taken S-S boundary condition. This frequency ratio serves as an index to estimate quantitatively the small scale effect on the vibration solution. It is clearly seen from the figures that the frequency ratios are less than unity. This implies that application of local beam model for vibration analysis of carbon nanotubes would lead to over prediction of the frequency in particular higher frequency if the small length scale effect between individual carbon atoms is neglected. Hence, nonlocal beam theory should be used for better predictions of higher frequencies of nanobeams.

One of the important observation seen in this analysis is that frequency parameters of TBT, RBT and LBT nanobeams are having approximately same results. EBT nanobeam over predicts frequency parameters than TBT, RBT and LBT nanobeams since it neglects transverse shear and stain. In all the beam theories, fundamental frequency parameter decreases with increase in nonlocal parameter in S-S, C-S, C-C boundary conditions while fundamental frequency parameter increases with nonlocal parameter in case of cantilever nanobeams. Higher frequency parameters decrease with nonlocal parameter in case of all boundary conditions. Except fundamental frequency parameter of C-F nanobeam, frequency parameter associated with nonlocal nanobeams are smaller than the corresponding local nanobeams. This reduction is clearly seen in case of higher vibration modes. This means that application of local beam models would lead to over-prediction of frequency parameters. Hence nonlocal theory should be incorporated for better prediction of higher frequencies of nanobeams.

Table 5.8 First four frequency parameters of nanobeams based on Euler-Bernoulli beam theory

		S-S				C-S			
$\mu$	$\lambda_1$	$\lambda_2$	$\lambda_3$	$\lambda_4$	$\lambda_1$	$\lambda_2$	$\lambda_3$	$\lambda_4$	
0	3.1416	6.2832	9.4248	12.5664	3.9266	7.0686	10.2102	13.3518	
1	3.0685	5.7817	8.0400	9.9161	3.8209	6.4649	8.6517	10.4688	
2	3.0032	5.4324	7.3012	8.8000	3.7278	6.0545	7.8405	9.2811	
3	2.9444	5.1683	6.8118	8.1195	3.6448	5.7488	7.3089	8.5619	
4	2.8908	4.9581	6.4520	7.6407	3.5701	5.5079	6.9204	8.0573	
5	2.8418	4.7846	6.1709	7.2764	3.5024	5.3107	6.6179	7.6740	
		C-C				C-F			
0	4.7300	7.8532	10.9956	14.1358	1.8751	4.6941	7.8548	10.9955	
1	4.5945	7.1403	9.2583	11.0138	1.8792	4.5475	7.1459	9.2569	
2	4.4758	6.6629	8.3739	9.7519	1.8833	4.4170	6.6753	8.3683	
3	4.3707	6.3108	7.8004	8.9916	1.8876	4.2994	6.3322	7.7877	
4	4.2766	6.0352	7.3840	8.4593	1.8919	4.1924	6.0674	7.3617	
5	4.1917	5.8107	7.0611	8.0551	1.8964	4.0942	5.8550	7.0272	

Table 5.9 First four frequency parameters of nanobeams based on Timoshenko beam theory

		S-S				C-S			
$\mu$	$\lambda_1$	$\lambda_2$	$\lambda_3$	$\lambda_4$	$\lambda_1$	$\lambda_2$	$\lambda_3$	$\lambda_4$	
0	3.1155	6.0867	8.8180	11.2766	3.8887	6.8298	9.5203	11.9354	
1	3.0492	5.6421	7.6300	9.0990	3.7905	6.2794	8.1477	9.5019	
2	2.9893	5.3236	6.9697	8.1207	3.7033	5.8978	7.4094	8.4532	
3	2.9349	5.0786	6.5211	7.5123	3.6252	5.6101	6.9187	7.8093	
4	2.8851	4.8813	6.1876	7.0798	3.5545	5.3815	6.5574	7.3547	
5	2.8393	4.7172	5.9251	6.7487	3.4902	5.1934	6.2747	7.0080	
		C-C				C-F			
0	4.6813	7.5696	10.2199	12.5894	1.8800	4.6400	7.5700	10.2200	
1	4.5494	6.8946	8.6377	9.8772	1.8801	4.5001	6.9012	8.6358	
2	4.4338	6.4408	7.8215	8.7567	1.8838	4.3743	6.4531	7.8164	
3	4.3312	6.1048	7.2888	8.0772	1.8875	4.2611	6.1242	7.2788	
4	4.2394	5.8412	6.9005	7.6002	1.8913	4.1584	5.8686	6.8844	
5	4.1563	5.6261	6.5987	7.7007	1.8953	4.0643	5.6624	6.5754	

Table 5.10 First four frequency parameters of nanobeams based on Reddy beam theory

		S-S				C-S			
$\mu$	$\lambda_1$	$\lambda_2$	$\lambda_3$	$\lambda_4$	$\lambda_1$	$\lambda_2$	$\lambda_3$	$\lambda_4$	
0	3.1218	6.1317	8.9488	11.5349	3.8978	6.8844	9.6685	12.2178	
1	3.0492	5.6423	7.6340	9.1022	3.7905	6.2797	8.1492	9.5063	
2	2.9843	5.3015	6.9325	8.0777	3.6963	5.8728	7.3713	8.4116	
3	2.9258	5.0437	6.4678	7.4531	3.6125	5.5714	6.8646	7.7523	
4	2.8726	4.8385	6.1262	7.0135	3.5374	5.3347	6.4955	7.2910	
5	2.8239	4.6693	5.8592	6.6791	3.4693	5.1413	6.2087	6.9413	
		C-C				C-F			
0	4.6930	7.6344	10.3861	12.8968	1.8800	4.6500	7.6400	10.3900	
1	4.5494	6.8951	8.6398	9.8831	1.8801	4.5001	6.9017	8.6380	
2	4.4250	6.4132	7.7834	8.7171	1.8841	4.3645	6.4261	7.7778	
3	4.3156	6.0626	7.2350	8.0228	1.8882	4.2434	6.0835	7.2238	
4	4.2183	5.7904	6.8394	7.5395	1.8924	4.1341	5.8205	6.8211	
5	4.1309	5.5700	6.5338	7.1741	1.8968	4.0345	5.6102	6.5071	

Table 5.11 First four frequency parameters of nanobeams based on Levinson beam theory

		S-S				C-S			
$\mu$	$\lambda_1$	$\lambda_2$	$\lambda_3$	$\lambda_4$	$\lambda_1$	$\lambda_2$	$\lambda_3$	$\lambda_4$	
0	3.1155	6.0867	8.8180	11.2766	3.8887	6.8298	9.5203	11.9354	
1	3.0431	5.6008	7.5224	8.8983	3.7810	6.2253	8.0141	9.2720	
2	2.9783	5.2625	6.8312	7.8968	3.6864	5.8197	7.2459	8.2010	
3	2.9199	5.0067	6.3732	7.2861	3.6025	5.5197	6.7461	7.5567	
4	2.8669	4.8030	6.0366	6.8566	3.5272	5.2843	6.3824	7.1062	
5	2.8183	4.6350	5.7736	6.5295	3.4590	5.0921	6.0999	6.7647	
		C-C				C-F			
0	4.6813	7.5696	10.2199	12.5894	1.8800	4.6400	7.5700	10.2200	
1	4.5354	6.8242	8.4777	9.6161	1.8804	4.4853	6.8312	8.4757	
2	4.4092	6.3417	7.6303	8.4753	1.8844	4.3482	6.3549	7.6247	
3	4.2986	5.9919	7.0893	7.7974	1.8884	4.2261	6.0128	7.0784	
4	4.2004	5.7211	6.6996	7.3262	1.8926	4.1162	5.7507	6.6821	
5	4.1123	5.5020	6.3989	6.9701	1.8969	4.0161	5.5412	6.3737	



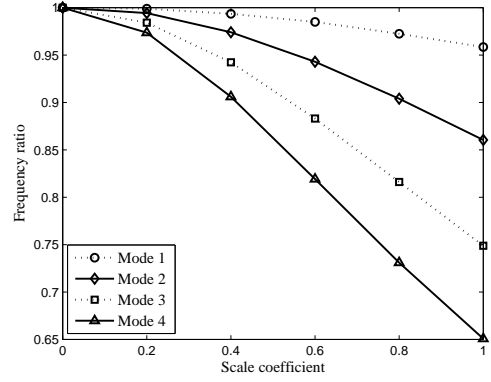
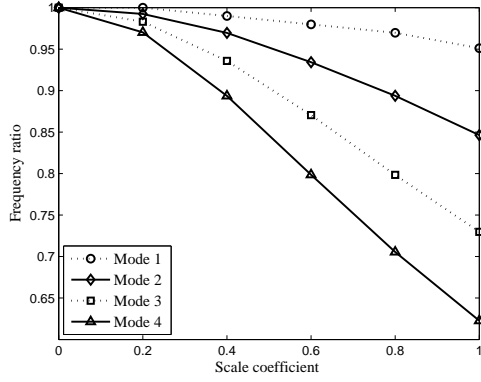


Fig. 5.11 Variation of frequency ratio with  $e_0a$  (EBT) Fig. 5.12 Variation of frequency ratio with  $e_0a$  (TBT)

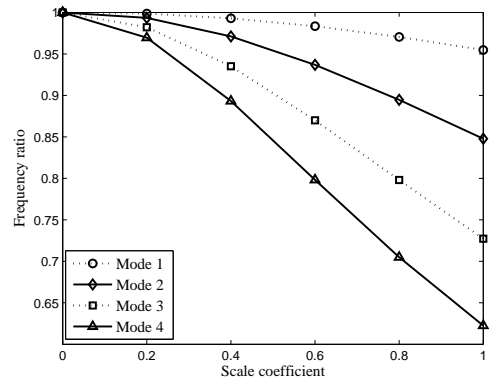
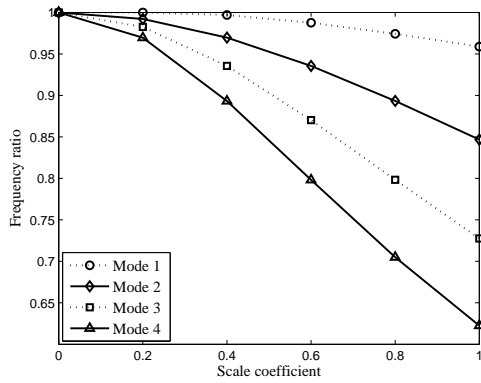


Fig. 5.13 Variation of frequency ratio with  $e_0a$  (RBT) Fig. 5.14 Variation of frequency ratio with  $e_0a$  (LBT)

## 5.2.4 Effect of various beam theories

To investigate the effect of various beam theories such as EBT, TBT, RBT and LBT on the frequency parameter, variation of fundamental frequency parameter with nonlocal parameter for nanobeams based on various beam theories is shown in Fig. 5.15. In this figure, C-C boundary condition is taken into consideration. It is seen from the figure that EBT predicts higher frequency parameter than other types of beam theories. It is due to the fact that, in EBT transverse shear stress and transverse strain are not considered. Beam theories such as TBT, RBT and LBT predict approximately closer results. Next we have compared EBT and TBT for understanding the effect of transverse shear deformation and rotary inertia on the vibration frequencies. In contrast to EBT, TBT accounts transverse shear deformation and rotary inertia. To investigate effects of transverse shear deformation and rotary inertia on the vibration analysis, Fig. 5.16 shows frequency ratio of nonlocal Timoshenko beam to that of the corresponding nonlocal Euler beam ( $\frac{\lambda_{NT}}{\lambda_{NE}}$ ) with respect to  $\frac{L}{h}$  for a given scale coefficient of  $e_0a = 0.1nm$ . In this figure, we have included first and fourth modes with S-S boundary condition. It is observed that for all value of  $L/h$ , frequency ratios are smaller than unity in these modes. This means that frequency parameter obtained by nonlocal Timoshenko beam theory is smaller than

frequency parameter obtained using nonlocal EBT. This indicates that transverse shear deformation and rotary inertia would lead to reduction of frequencies. One may find that this reduction is seen for higher modes and for small  $L/h$ . This point is discussed as: Frequency ratio associated with fundamental mode approaches unity in case of long tubes while for short tubes (for example  $L/h = 10$ ), the frequencies of nonlocal Timoshenko and nonlocal Euler beams deviate somewhat from each other. Frequency ratio associated with fourth mode is significantly smaller than unity especially at small  $L/h$ . It is also observed that at higher values of  $L/h$ , effects of transverse shear deformation and rotary inertia still have an appreciable effect on the fourth mode. Therefore, effects of transverse shear deformation and rotary inertia would lead to reduction of frequencies and the reduction is clearly seen at higher modes and also at small  $L/h$ . Hence Timoshenko beam model should be considered when  $L/h$  is small and when higher vibration modes are considered.

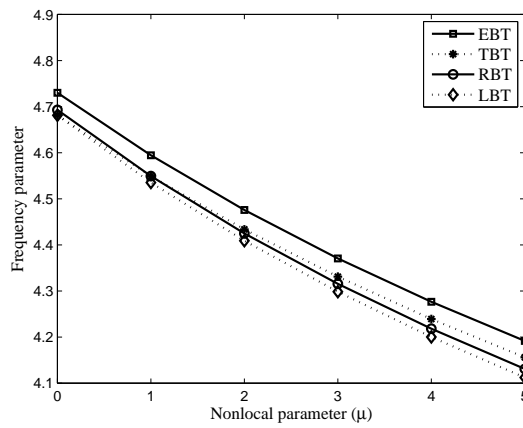


Fig. 5.15 Variation of frequency parameter with nonlocal parameter

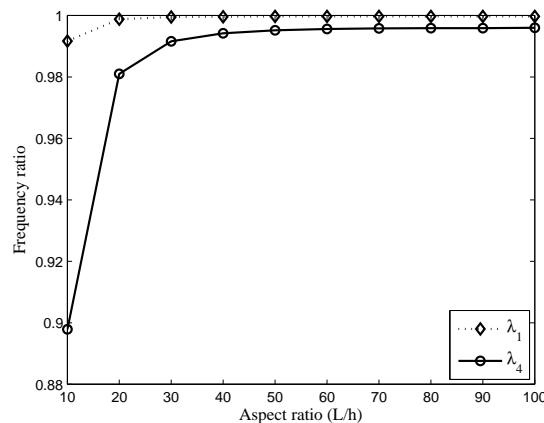


Fig. 5.16 Variation of frequency ratio with  $L/h$

### 5.2.5 Effect of boundary conditions

In this subsection, we have considered the effect of boundary condition on the frequency parameter. Fig. 5.17 depicts variation of fundamental frequency parameter of TBT nanobeam with nonlocal parameter for different boundary conditions. It is observed from the figure that C-C nanobeams are having highest frequency parameter and C-F nanobeams are having lowest frequency parameter. It is also seen that frequency parameters decrease with increase in nonlocal parameter for S-S, C-S, and C-C boundary conditions but frequency parameters increase with nonlocal parameter in case of C-F nanobeams.

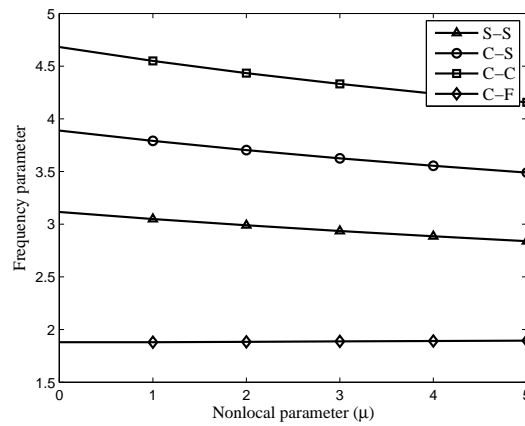


Fig. 5.17 Variation of frequency parameter with nonlocal parameter

### 5.2.6 Effect of aspect ratio

Effect of aspect ratio ( $L/h$ ) on the first four frequency parameters has been investigated. First four frequency parameters of TBT and RBT nanobeams are given in Table 5.12 for different  $L/h$  (10, 12, 14, 16, 18). In this table, we have considered S-S boundary condition. Graphical results are illustrated in Figs. 5.18 where variation of first four frequency parameter with  $L/h$  has been shown for TBT nanobeams. In these figures,  $L/h$  ranges from 10 to 20. It is noticed that frequency parameter increases with increase in  $L/h$ . It is also seen that effect of  $L/h$  is more pronounced for higher vibration modes.

Table 5.12 First four frequency parameters of TBT and RBT nanobeams for different  $L/h$

$L/h$	TBT				RBT			
	$\lambda_1$	$\lambda_2$	$\lambda_3$	$\lambda_4$	$\lambda_1$	$\lambda_2$	$\lambda_3$	$\lambda_4$
10	2.9893	5.3236	6.9697	8.1207	2.9843	5.3015	6.9325	8.0777
12	2.9951	5.3681	7.1001	8.3744	2.9936	5.3642	7.1029	8.3959
14	2.9981	5.3915	7.1713	8.5200	2.9977	5.3925	7.1833	8.5550
16	2.9998	5.4048	7.2129	8.6075	2.9997	5.4071	7.2258	8.6415
18	3.0008	5.4130	7.2386	8.6626	3.0009	5.4153	7.2501	8.6919

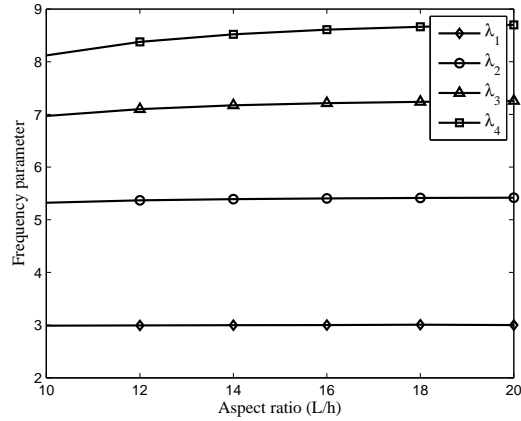


Fig. 5.18 Variation of frequency parameter with aspect ratio

### 5.3 Conclusions

Vibration characteristics of Euler-Bernoulli and Timoshenko nanobeams have been computed by using simple polynomials and orthonormal polynomials in the Rayleigh-Ritz method. Both tabular and graphical results are given for different scaling effect parameters and boundary conditions. Results are also tabulated for some new boundary conditions (S-F and F-F). Deflection shapes of nonlocal C-C Euler-Bernoulli nanobeams are presented for different scaling effect parameters.

Differential quadrature method has been applied to investigate free vibration of nanobeams based on different beam theories such as Euler-Bernoulli, Timoshenko, Reddy and Levinson in conjunction with Eringen's nonlocal elasticity theory. Boundary conditions have been implemented in the coefficient matrix which is quite easy to handle. Effects of nonlocal parameter, boundary condition, aspect ratio and beam theories on the frequency parameters have been analyzed.

# Chapter 6

## Vibration of nanobeams with complicating effects

The contents of this chapter have been published in:

1. S. Chakraverty and Laxmi Behera (2015) Free vibration of non-uniform nanobeams using Rayleigh-Ritz method, *Physica E*, 67, 38-46.
2. Laxmi Behera and S. Chakraverty (2014) Free vibration of nonhomogeneous Timoshenko nanobeams, *Meccanica*, 49, 51-67.
3. S. Chakraverty and Laxmi Behera (2015) Vibration and buckling analyses of nanobeams embedded in elastic medium, *Chinese Physics B* (Accepted).

# Chapter 6

## Vibration of nanobeams with complicating effects

### Vibration of nanobeams with non-uniform material properties

In this investigation, we have considered carbon nanotube with non-uniform material properties which is assumed as per the following relations.

$$E = E_0(1 + pX + qX^2), \quad \rho = \rho_0(1 + rX + sX^2)$$

where  $E_0$  and  $\rho_0$  denote Young's modulus and density at the left end of the carbon nanotube and  $p, q, r, s$  denote the non-uniform parameters.

Here, we have introduced the following non-dimensional parameters

$$\begin{aligned} X &= \frac{x}{L} \\ W &= \frac{w_0}{L} \\ \alpha &= \frac{e_0 a}{L} = \text{scaling effect parameter} \\ \tau &= \frac{I}{AL^2} \\ \lambda^2 &= \frac{\rho_0 A \omega^2 L^4}{E_0 I} = \text{frequency parameter} \\ \Omega &= \frac{EI_0}{k_s GAL^2} = \text{shear deformation parameter} \end{aligned}$$

To apply Raleigh-Ritz method, one needs Rayleigh quotient which is obtained by equating maximum kinetic and strain energies. As such, one may obtain Rayleigh quotient in non-dimensional form for EBT as

$$\lambda^2 = \frac{\int_0^1 (1 + pX + qX^2) \left(\frac{d^2W}{dX^2}\right)^2 dX}{\int_0^1 (1 + rX + sX^2) (W^2 - \alpha^2 W \frac{d^2W}{dX^2}) dX} \quad (6.1)$$

Similarly, Rayleigh quotient in non-dimensional form for TBT is obtained as

$$\lambda^2 = \frac{\int_0^1 (1 + pX + qX^2) \left( \left(\frac{d\phi}{dX}\right)^2 + \frac{1}{\Omega} \left(\phi + \frac{dW}{dX}\right)^2 \right) dX}{\int_0^1 (1 + rX + sX^2) \left( W^2 + \tau\phi^2 + \alpha^2 W \frac{d\phi}{dX} + \tau\alpha^2 \left(\frac{d\phi}{dX}\right)^2 \right) dX} \quad (6.2)$$

As such, matrices  $K$  and  $M_a$  for EBT are given as below:

$$K(i, j) = \int_0^1 (1 + pX + qX^2) \varphi_i'' \varphi_j'' dX$$

$$M_a(i, j) = \int_0^1 (1 + rX + sX^2) \left( \varphi_i \varphi_j - \frac{\alpha^2}{2} \varphi_i \varphi_j'' - \frac{\alpha^2}{2} \varphi_i'' \varphi_j \right) dX$$

Similarly, matrices  $K$  and  $M_a$  for TBT are given as:

$$K = \begin{bmatrix} k_1 & k_2 \\ k_3 & k_4 \end{bmatrix} \text{ where } k_1, k_2, k_3 \text{ and } k_4 \text{ are submatrices and are given by}$$

$$k_1(i, j) = \int_0^1 (1 + pX + qX^2) \varphi_i' \varphi_j dX$$

$$k_2(i, j) = \int_0^1 (1 + pX + qX^2) \varphi_i' \psi_j dX$$

$$k_3(i, j) = \int_0^1 (1 + pX + qX^2) \psi_i \varphi_j' dX$$

$$k_4(i, j) = \int_0^1 (1 + pX + qX^2) (\psi_i \psi_j + \Omega \psi_i' \psi_j') dX$$

$$M_a = \begin{bmatrix} m_1 & m_2 \\ m_3 & m_4 \end{bmatrix} \text{ where submatrices } m_1, m_2, m_3, m_4 \text{ are as follows}$$

$$m_1(i, j) = \Omega \int_0^1 (1 + rX + sX^2) \varphi_i \varphi_j dX$$

$$m_2(i, j) = \Omega \frac{\alpha^2}{2} \int_0^1 (1 + rX + sX^2) \varphi_i \psi_j' dX$$

$$m_3(i, j) = \Omega \frac{\alpha^2}{2} \int_0^1 (1 + rX + sX^2) \psi_i' \varphi_j dX$$

$$m_4(i, j) = \Omega \int_0^1 (1 + rX + sX^2) (\tau \psi_i \psi_j + \tau \alpha^2 \psi_i' \psi_j') dX$$

## 6.1 Numerical results and discussions

In the numerical evaluations, following parameters of SWCNT have been used (Wang et al. 2007): diameter,  $d = 0.678nm$ ; Length,  $L = 10d$ ; thickness,  $t = 0.066$ ; shear correction factor,  $k_s = 0.563$ ; Young's modulus,  $E_0 = 5.5TPa$ ; shear modulus,  $G = E_0/[2(1 + \nu)]$ ; Poisson's ratio  $\nu = 0.19$  and second moment of area  $I = \frac{\Pi d^4}{64}$ .

### 6.1.1 Convergence

A convergence study has been shown in Tables 6.1 and 6.2 respectively for EBT and TBT. In these tables, we have shown convergence of first three frequency parameters ( $\sqrt{\lambda}$ ). Here, we have taken non-uniform parameters as  $p = q = r = s = 0.1$  and scaling effect parameter as 0.3. Convergency has been reported for S-S and C-S edge conditions. It is clearly seen from the table that convergency is achieved as we increase the number of terms. One may notice that  $n = 11$  is sufficient for computing the results.

Table 6.1 Convergence of first three frequency parameters of EBT nanobeams

$n$	S-S			C-S		
	$\lambda_1$	$\lambda_2$	$\lambda_3$	$\lambda_1$	$\lambda_2$	$\lambda_3$
3	2.6803	4.7956	6.4334	3.2675	4.8388	7.2365
4	2.6801	4.3104	6.4307	3.2643	4.7903	6.0470
5	2.6797	4.3101	5.4811	3.2643	4.7640	5.9176
6	2.6797	4.3018	5.4807	3.2643	4.7630	5.8429
7	2.6797	4.3018	5.4432	3.2643	4.7627	5.8367
8	2.6797	4.3018	5.4432	3.2643	4.7627	5.8344
9	2.6797	4.3018	5.4426	3.2643	4.7627	5.8343
10	2.6797	4.3018	5.4426	3.2643	4.7627	5.8343
11	2.6797	4.3018	5.4426	3.2643	4.7627	5.8343



Table 6.2 Convergence of first three frequency parameters of TBT nanobeams

$n$	S-S			C-S		
	$\lambda_1$	$\lambda_2$	$\lambda_3$	$\lambda_1$	$\lambda_2$	$\lambda_3$
3	2.7683	4.5273	10.3126	3.0810	5.0918	7.7717
4	2.6394	4.5264	5.7314	3.1743	4.5316	6.1565
5	2.6394	4.1354	5.7298	3.1720	4.4990	5.4307
6	2.6390	4.1354	5.0898	3.1720	4.4814	5.3652
7	2.6390	4.1286	5.0898	3.1720	4.4807	5.3184
8	2.6390	4.1286	5.0627	3.1720	4.4805	5.3151
9	2.6390	4.1286	5.0627	3.1720	4.4805	5.3139
10	2.6390	4.1286	5.0622	3.1720	4.4805	5.3138
11	2.6390	4.1286	5.0622	3.1720	4.4805	5.3138

### 6.1.2 Validation

For the validation purpose, we have considered an uniform ( $p = q = r = s = 0$ ) nanobeam. To compare our results with that of Wang et al. (2007), we have taken same parameters as that of Wang et al. (2007). Table 6.3 shows comparison of first three frequency parameters of Euler-Bernoulli and Timoshenko nanobeams for simply-supported boundary conditions. Results have been compared with scaling effect parameters as 0, 0.3 and 0.5. It is noticed from the table that frequency parameters ( $\sqrt{\lambda}$ ) decrease with increase in scaling effect parameter. From this table, one may observe close agreement of the results with that of available literature .

Table 6.3 Comparison of frequency parameters for uniform nanobeams

EBT					
$\alpha = 0$		$\alpha = 0.3$		$\alpha = 0.5$	
Present	Ref.*	Present	Ref.*	Present	Ref.*
3.1416	3.1416	2.6800	2.6800	2.3022	2.3022
6.2832	6.2832	4.3013	4.3013	3.4604	3.4604
9.4248	9.4248	5.4422	5.4422	4.2941	4.2941
TBT					
3.0742	3.0929	2.6412	2.6538	2.2412	2.2867
5.9274	5.9399	4.1357	4.2058	3.3957	3.4037
8.4057	8.4444	5.0744	5.2444	4.1044	4.1644

\*Wang et al. (2007)

### 6.1.3 Effect of non-uniform parameter

In this sub-section, we have studied the effects of non-uniform parameters on the frequency parameters. Four cases are considered here which are discussed below.

Case 1: Density varies with space coordinate and Young's modulus as constant viz.  $\rho = \rho_0(1 + rX + sX^2)$  and  $E = E_0$ . Here following subcases may arise

(a)  $s = 0$  and  $r \neq 0$

(b)  $r = 0$  and  $s \neq 0$

(c)  $r \neq 0$  and  $s \neq 0$

Case 2: Young's modulus varies with space coordinate and density as constant viz.  $E = E_0(1 + pX + qX^2)$  and  $\rho = \rho_0$ . Here also following three subcases may arise

(a)  $p = 0$  and  $q \neq 0$

(b)  $q = 0$  and  $p \neq 0$

(c)  $p \neq 0$  and  $q \neq 0$

Case 3: Young's modulus and density both vary with space coordinate viz.  $E = E_0(1 + pX + qX^2)$  and  $\rho = \rho_0(1 + rX + sX^2)$ . Four subcases arise here are

(a) linear variations of Young's modulus and density.

(b) quadratic variations of Young's modulus and density.

(c) linear variation of Young's modulus and quadratic variation of density.

(d) linear variation of density and quadratic variation of Young's modulus.

Figs. 6.1-6.2 are the pictorial representation of case 1(a) and 1(b) respectively. Here, we have considered TBT nanobeams to show the behavior of first two frequency parameters with  $r$  and  $s$  respectively for the scaling effect parameters as 0, 0.1, 0.5. In Fig. 6.1, we have considered S-S boundary condition and in Fig. 6.2, we have taken C-S boundary condition. The solid and dotted lines represent first and second frequency parameters respectively. Also  $\alpha$  and  $\alpha^*$

depict scaling effect parameters for first and second frequency parameters respectively. Varying parameter varies from  $-0.5$  to  $0.5$ . In these figures, it can be clearly seen that frequency parameters decrease with  $r$  and  $s$ . To show the results of case 1(c), we have given the results in two ways. Firstly, keeping  $r$  constant, varying  $s$  and secondly, keeping  $s$  constant, varying  $r$ . For these two cases, the results are illustrated in Figures 6.3-6.4 respectively with S-S boundary condition. From these figures also we can conclude that, if we fix one and other vary then the frequency parameters decrease with the increase of varying parameter.

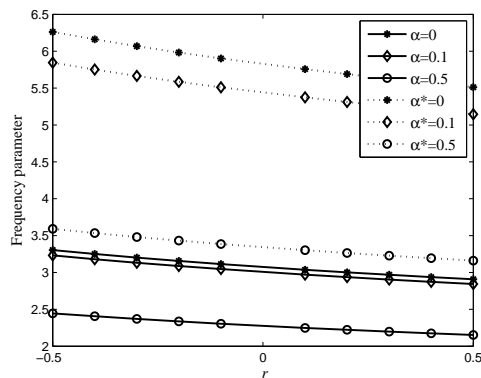


Fig. 6.1 Variation of frequency parameters with  $r$

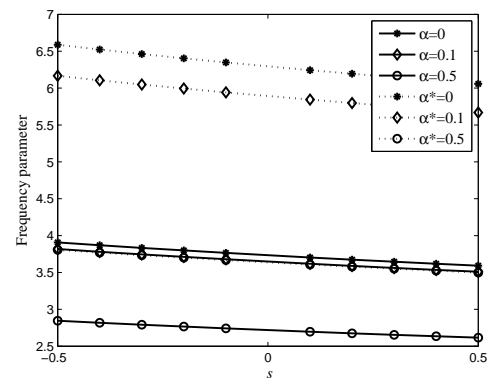


Fig. 6.2 Variation of frequency parameters with  $s$

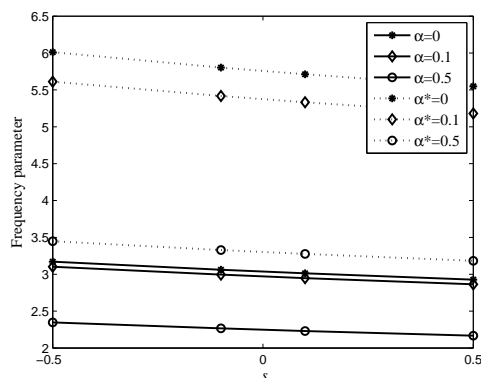


Fig. 6.3 Variation of frequency parameters with  $s$

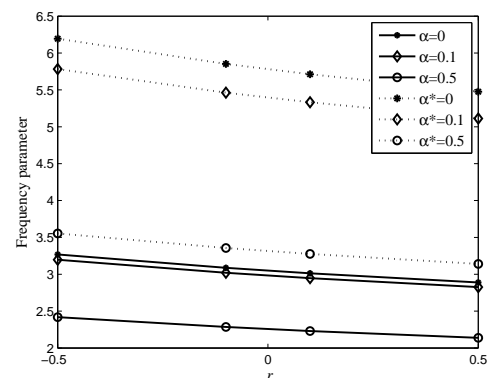


Fig. 6.4 Variation of frequency parameters with  $r$

Figs. 6.5-6.6 are the depiction of case 2(a) and case 2 (b) respectively. Graphical result have been shown for TBT nanobeams with S-S boundary condition. Varying parameter varies from  $-0.5$  to  $0.5$ . Graphs are drawn for first two frequency parameters. It is observed that frequency parameters increase with  $q$  and  $p$ . The results of case 2(c) are given in Fig. 6.7 where  $p$  is fixed,  $q$  varies and in Fig. 6.8 where  $q$  is fixed,  $p$  varies. Here we have considered C-S boundary condition. In these graphs, it is observed that the frequency parameters increase with increase of varying parameter.

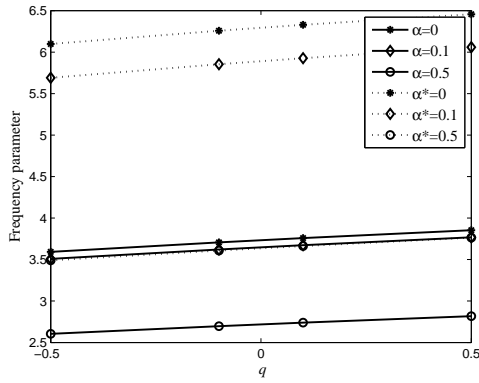


Fig. 6.5 Variation of frequency parameters with  $q$

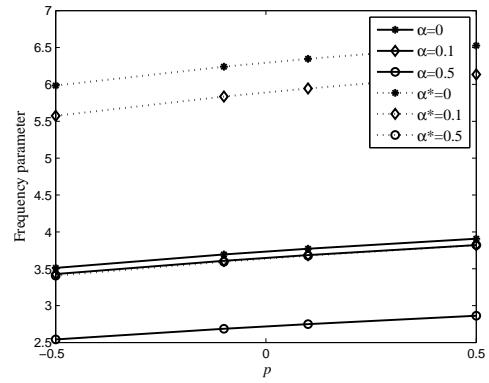


Fig. 6.6 Variation of frequency parameters with  $p$

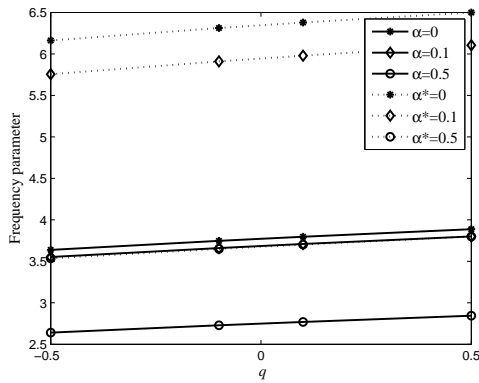


Fig. 6.7 Variation of frequency parameters with  $q$

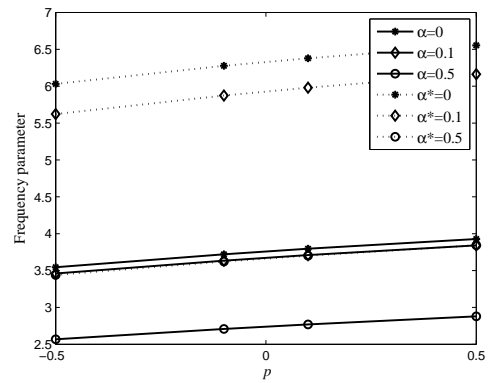


Fig. 6.8 Variation of frequency parameters with  $p$

Results of case 3 are given for EBT nanobeams and four subcases are considered. First, we have shown the effects of non-uniform parameters when density and Young's modulus vary quadratically. This case may be achieved by assigning zero to  $p$  and  $r$ . Variation of first two frequency parameters with  $s$  has been illustrated in Fig. 6.9 keeping  $q$  constant (0.1). Similarly, effect of  $q$  on the first two frequency parameters has been shown in Fig. 6.10 keeping  $s$  constant (0.1). In these graphs, varying parameters range from -0.5 to 0.5 with C-S edge condition. Results have been shown for different values of scaling effect parameters (0, 0.3 and 0.7). One may see that frequency parameters increase with  $q$  and decrease with  $s$ . It is also observed that frequency parameters decrease with increase in scaling effect parameter. This means that frequency parameters are over predicted when we consider local beam model for vibration analysis of nanobeams. It is also observed that frequency parameters increase with increase in mode number.

In this paragraph, we have presented the effects non-uniform parameters when density and Young's modulus vary linearly. This is achieved by taking  $q$  and  $s$  to zero. Graphical variation of frequency parameters with  $p$  taking  $r$  constant (0.2) has been shown in Fig. 6.11. Similarly, graphical variation of frequency parameters with  $r$  taking  $p$  constant (0.2) has been shown

in Fig. 6.12. The graphs are plotted for different values of scaling effect parameters with C-S boundary condition. It is noticed that frequency parameters increase with  $p$  and decrease with  $r$ .

Here, we have considered the effects of non-uniform parameters when Young's modulus varies linearly and density varies quadratically. This is the situation which is obtained by taking  $q$  and  $r$  as zero. Figs. 6.13 and 6.14 depict variation of frequency parameters with  $s$  and  $p$  respectively. In these graphs, we have taken S-S boundary condition with non-varying parameter as 0.1. Results have been shown for different values of scaling effect parameters. In these graphs, one may observe that frequency parameters decrease with  $s$  and increase with  $p$ .

Next, we have analyzed the effects of non-uniform parameter when Young's modulus varies quadratically and density varies linearly. For this, we have taken  $p$  and  $s$  as zero. Variations of first two frequency parameters with  $q$  and  $r$  have been given in Figs. 6.15 and 6.16. Results have been shown with the non-varying parameter as 0.1 and boundary condition as S-S. In these graphs, one may see that frequency parameters decrease with  $r$  and increase with  $q$ .

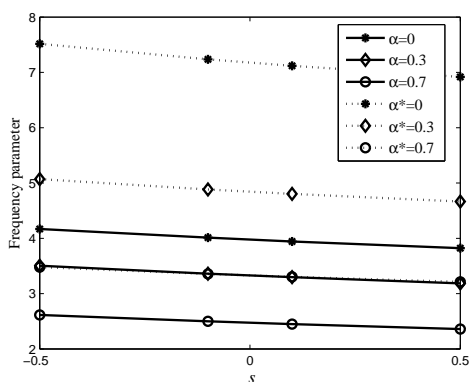


Fig. 6.9 Variation of frequency parameters with  $s$

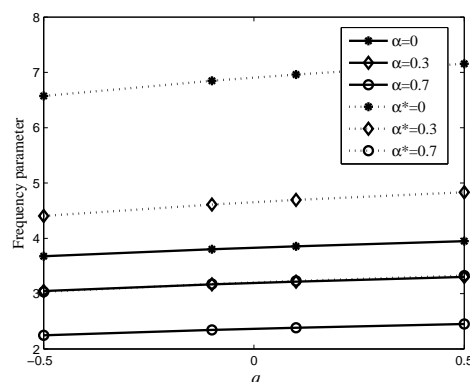


Fig. 6.10 Variation of frequency parameters with  $q$

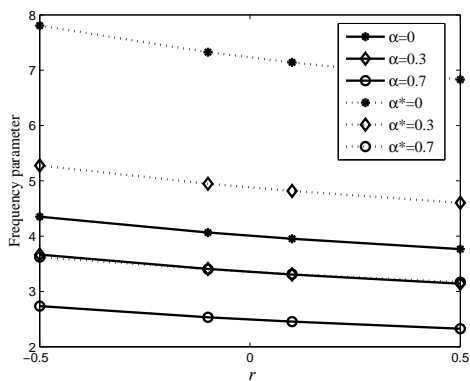


Fig. 6.11 Variation of frequency parameters with  $r$

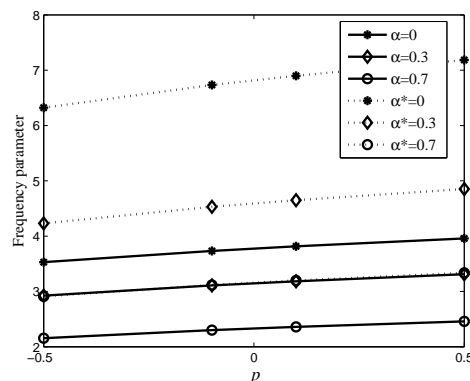


Fig. 6.12 Variation of frequency parameters with  $p$

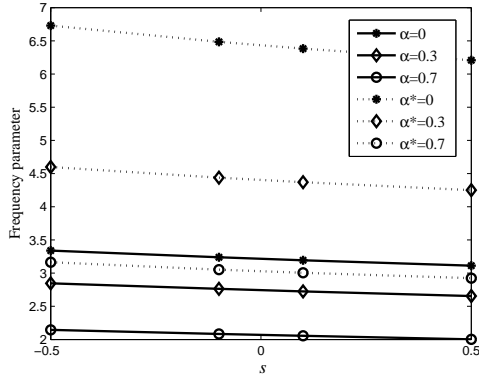


Fig. 6.13 Variation of frequency parameters with  $s$

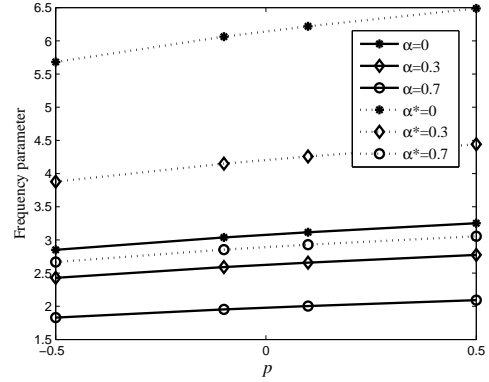


Fig. 6.14 Variation of frequency parameters with  $p$

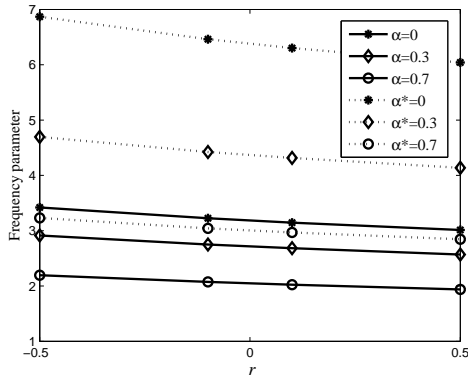


Fig. 6.15 Variation of frequency parameters with  $r$

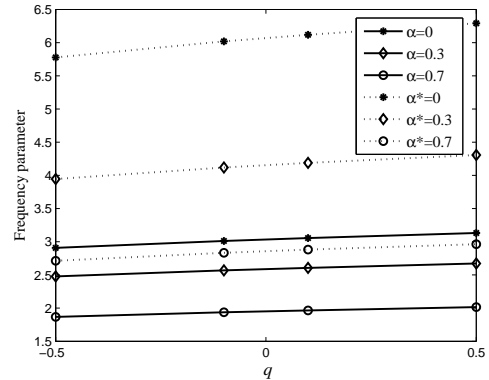


Fig. 6.16 Variation of frequency parameters with  $q$

### 6.1.4 Effect of small scale parameter

To investigate the behavior of scaling effect parameter on the frequency parameters, variation of frequency ratio for EBT nanobeams with scale coefficient ( $e_0a$ ) has been shown in Figs. 6.17-6.18 with C-F and S-F boundary conditions respectively.

Frequency ratio is calculated as  $\frac{\text{frequency parameter calculated using nonlocal theory}}{\text{frequency parameter calculated using local theory}}$ .

In these graphs, we have shown the results for the first four modes with the non-uniform parameters as  $p = 0.1, q = 0.2, r = 0.3, s = 0.4$ . It is observed from the figures that frequency ratios are less than unity. This implies that application of local beam model over predicts the frequency. It is also observed that frequency parameters decrease with increase in scale coefficient. This decrease is more pronounced in case of higher vibration modes. Thus, nonlocal theory should be employed for better predictions of higher frequencies. It is also noticed that in case of C-F nanobeams, fundamental frequency parameter obtained by nonlocal theory is more than that furnished by local beam theory. Thus, fundamental frequency parameter of cantilever nanobeams behave differently than other boundary conditions.

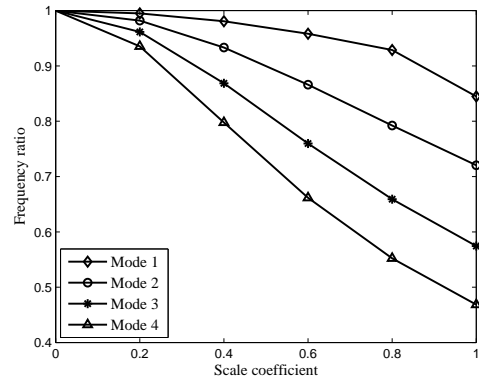
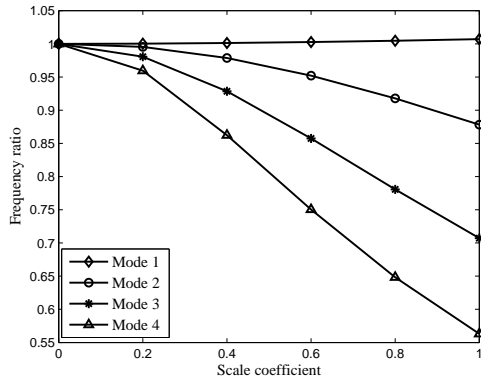


Fig. 6.17 Variation of frequency ratio with  $e_0a$  (C-F) Fig. 6.18 Variation of frequency ratio with  $e_0a$  (S-F)

### 6.1.5 Effect of boundary condition

Effect of boundary condition on the frequency parameters is investigated. Variation of fundamental frequency parameter with  $\alpha$  is shown in Fig. 6.19 for all sets of boundary conditions with  $p = 0.1, q = 0.2, r = 0.3, s = 0.4$ . One may observe that except cantilever nanobeams, frequency parameter decreases with increase in  $\alpha$ . It is also noticed that C-C nanobeams are having highest frequency parameter and C-F nanobeams are having lowest frequency parameter.

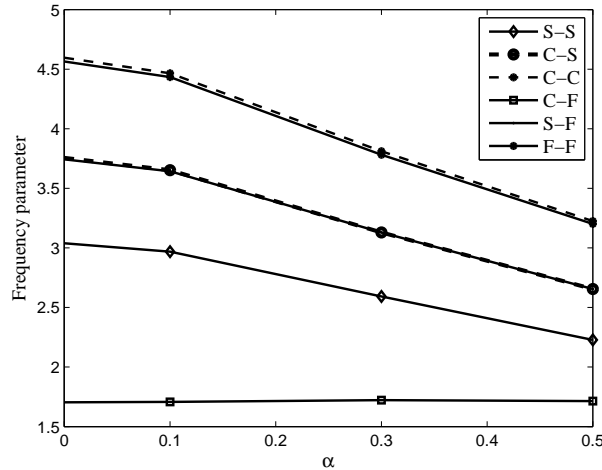


Fig. 6.19 Variation of frequency parameter with  $\alpha$

### 6.1.6 Effect of aspect ratio

To investigate the effect of aspect ratio on the frequency parameters, variation of frequency ratio with scale coefficient has been illustrated in Fig. 6.20. The graph is plotted for C-C boundary condition with  $p = 0.1, q = 0.2, r = 0.3, s = 0.4$ . Results have been shown for different values of  $\frac{L}{d}$ . It is observed that small scale effect is affected by  $\frac{L}{d}$ . This observation is explained as follows: When  $\frac{L}{d}$  increases, frequency ratio comes closer to one. This implies that frequency

parameter obtained by nonlocal beam model comes closer to that furnished by local beam model. Hence small scale effect is negligible for a very slender carbon nanotube (CNT) while it is significant for short carbon nanotubes (CNTs). This implies that if we compare magnitude of small scale effect with length of the slender tube, the small scale (internal characteristic length) is so small that it can be regarded as zero. Next, we have shown variation of first three frequency parameters with  $\frac{L}{d}$  in Fig. 6.21 with  $p = 0.1, q = 0.2, r = 0.3, s = 0.4$ . In this figure,  $\mu$  is taken as  $0.1nm^2$  and  $\frac{L}{d}$  ranges from 10-100 where  $d$  is assumed to be  $0.678nm$ . In this graph, one may notice that frequency parameter increases with  $L/d$ .

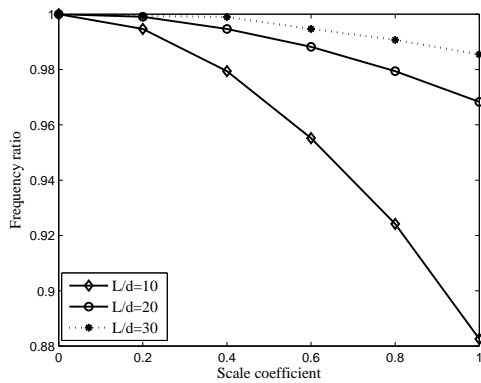


Fig. 6.20 Variation of frequency ratio with  $e_0 l_{int}$

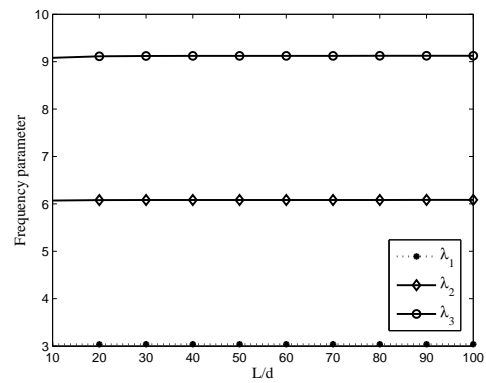


Fig. 6.21 Variation of frequency parameter with  $\frac{L}{d}$

### 6.1.7 Mode shapes

First few higher mode shapes are given in Figs. 6.22-6.23 for comparing the results which may help the researchers. Here first four mode shapes of S-S and C-S boundary conditions are given with scaling effect parameters as 0, 0.3 and non-uniform parameters as  $p = 0.1, q = 0.2, r = 0.3, s = 0.4$ . One may observe that mode shapes are affected by scaling effect parameter.



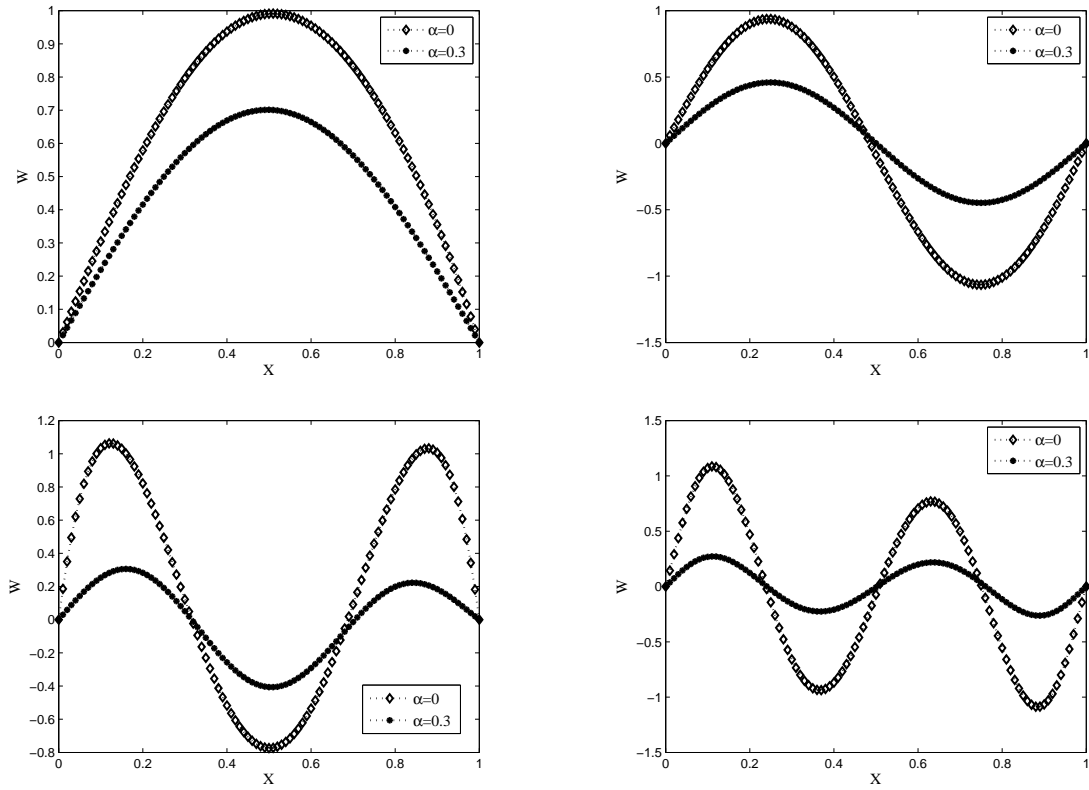


Fig. 6.22 First four deflection shapes of S-S Euler-Bernoulli nanobeams

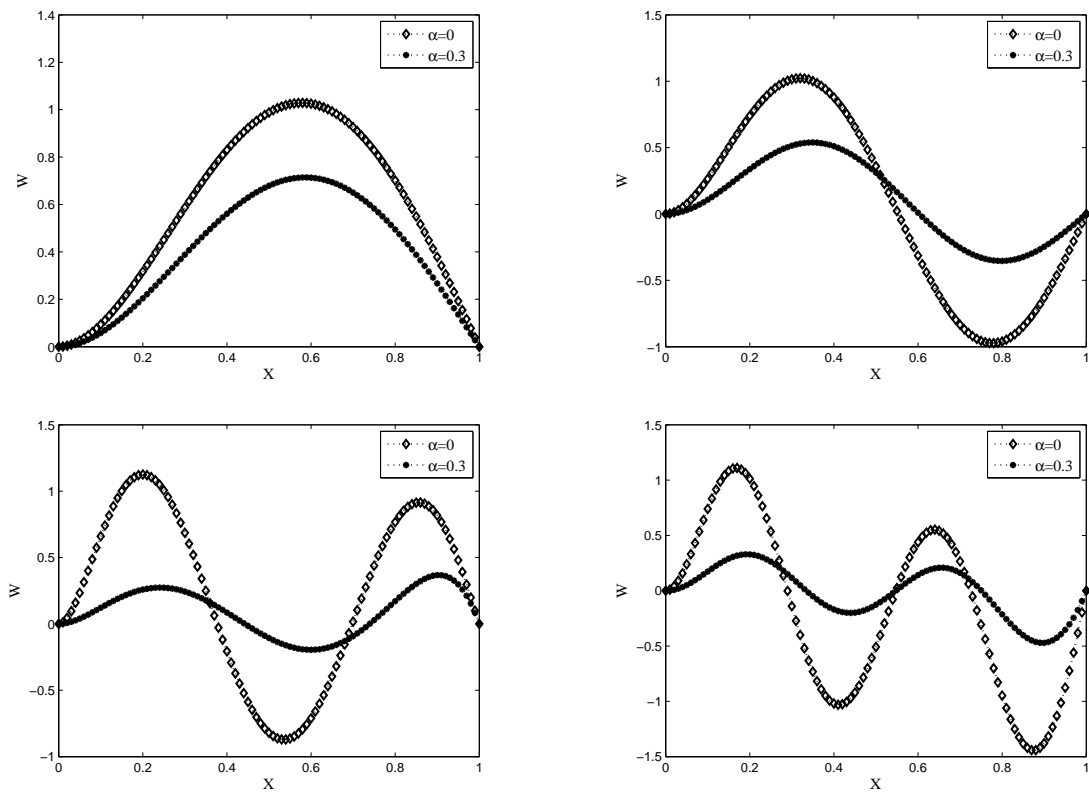


Fig. 6.23 First four deflection shapes of C-S Euler-Bernoulli nanobeams

## Vibration of nanobeams embedded in elastic foundations

Here, we have investigated vibration of embedded nanobeams in thermal environments based on EBT, TBT and RBT beam theories. The nanobeam is embedded in elastic foundations such as Winkler and Pasternak. Rayleigh-Ritz has been applied in EBT and TBT with shape functions as boundary characteristic orthogonal polynomials and Chebyshev polynomials respectively. Differential quadrature method has been employed in vibration of embedded nanobeams based on RBT.

For simplicity and convenience in mathematical formulation, the following non-dimensional parameters are introduced

$$X = \frac{x}{L}, W = \frac{w_0}{L}, \alpha = \frac{e_0 a}{L}, \tau = \frac{I}{AL^2}, \Omega = \frac{EI}{k_s GAL^2}, \bar{\Omega} = \frac{G\bar{A}L^2}{EI}, \lambda^2 = \frac{\rho A \omega^2 L^4}{EI}, K_g = \frac{k_g L^2}{EI}, K_w = \frac{k_w L^4}{EI}, \hat{N}_\theta = \frac{N_\theta L^2}{EI}$$

## 6.2 EBT

Maximum strain energy  $U_{max}$  may be given as Eq. (2.18).

Maximum kinetic energy is written as Eq. (2.20).

Maximum potential energy due to the axial force may be expressed as

$$V_a = \frac{1}{2} \int_0^L \left\{ \bar{N} \left( \frac{dw_0}{dx} \right)^2 + f_e w_0 \right\} dx \quad (6.3)$$

where the parameters have already been defined in section 3.2.7.1. Here again we have defined  $\bar{N}$  as the axial force which is expressed as  $\bar{N} = N_m + N_\theta$ . It is noted that  $N_m$  will be taken as zero for vibration analysis.

Using Hamilton's principle setting coefficient of  $\delta w_0$  to zero, we obtain following governing equation

$$\frac{d^2 M}{dx^2} + N_\theta \frac{d^2 w_0}{dx^2} - k_w w_0 + k_g \frac{d^2 w_0}{dx^2} = -\rho A \omega^2 w_0 \quad (6.4)$$

As such,  $M$  in nonlocal form may be written as

$$M = -EI \frac{d^2 w_0}{dx^2} + \mu \left[ -\rho A \omega^2 w_0 - N_\theta \frac{d^2 w_0}{dx^2} + k_w w_0 - k_g \frac{d^2 w_0}{dx^2} \right]$$

One may obtain Rayleigh Quotient from the following equation of EBT nanobeams.

$$\lambda^2 \left[ W^2 - \alpha^2 W \frac{d^2 W}{dX^2} \right] = \left( \frac{d^2 W}{dX^2} \right)^2 + \hat{N}_\theta \alpha^2 \left( \frac{d^2 W}{dX^2} \right)^2 - K_w \alpha^2 W \frac{d^2 W}{dX^2} + K_g \alpha^2 \left( \frac{d^2 W}{dX^2} \right)^2 + \hat{N}_\theta \left( \frac{d^2 W}{dX^2} \right)^2 + K_w W^2 - K_g W \frac{d^2 W}{dX^2} \quad (6.5)$$

Here, we have used orthonormal polynomials ( $\hat{\varphi}_k$ ) in Eq. (2.5). Substituting Eq. (2.5) in Eq. (6.5) and minimizing  $\lambda^2$  with respect to constant coefficients, the following eigenvalue value problem may be obtained as

$$[K] \{Z\} = \lambda^2 [M_a] \{Z\} \quad (6.6)$$

where  $Z$  is a column vector of constants and stiffness matrix  $K$  as well as mass matrix  $M_a$  are given by

$$K(i, j) = \int_0^1 \left( (2 + 2K_g \alpha^2 + 2\hat{N}_\theta \alpha^2) \hat{\varphi}_i'' \hat{\varphi}_j'' - K_w \alpha^2 \hat{\varphi}_i'' \hat{\varphi}_j - K_w \alpha^2 \hat{\varphi}_i \hat{\varphi}_j'' + 2K_w \hat{\varphi}_i \hat{\varphi}_j - K_g \hat{\varphi}_i'' \hat{\varphi}_j - K_g \hat{\varphi}_i \hat{\varphi}_j'' + 2\hat{N}_\theta \alpha^2 \hat{\varphi}_i' \hat{\varphi}_j' \right) dX$$

$$M_a(i, j) = \int_0^1 (2\hat{\varphi}_i \hat{\varphi}_j - \alpha^2 \hat{\varphi}_i'' \hat{\varphi}_j - \alpha^2 \hat{\varphi}_i \hat{\varphi}_j'') dX$$

### 6.3 TBT

Maximum strain energy  $U_{max}$  may be given as Eq. (2.22).

Maximum kinetic energy is written as Eq. (2.25).

Maximum potential energy due to work done may be written as Eq. (6.3).

Applying Hamilton's principle and setting coefficient of  $\delta w_0$  and  $\delta \phi_0$  to zero, governing equilibrium equations are obtained as

$$\frac{dM}{dx} - Q = -\rho I \omega^2 \phi_0 \quad (6.7)$$

$$\frac{dQ}{dx} + N_\theta \frac{d^2 w_0}{dx^2} - f_e = -\rho A \omega^2 w_0 \quad (6.8)$$

Using Eqs. (6.7-6.8) and Eqs. (1.13-1.14), one may obtain bending moment  $M$  and shear force  $Q$  in nonlocal form as follows

$$M = EI \frac{d\phi_0}{dx} + \mu \left[ -\rho I \omega^2 \frac{d\phi_0}{dx} - \rho A \omega^2 w_0 - N_\theta \frac{d^2 w_0}{dx^2} + f_e \right] \quad (6.9)$$

$$Q = k_s GA \left( \phi_0 + \frac{dw_0}{dx} \right) + \mu \left[ -\rho A \omega^2 \frac{dw_0}{dx} - N_\theta \frac{d^3 w_0}{dx^3} + k_w \frac{dw_0}{dx} - k_g \frac{d^3 w_0}{dx^3} \right] \quad (6.10)$$

Equating maximum energies of the system, one may obtain following expressions for TBT nanobeams

$$\begin{aligned}
\lambda^2 \left[ W^2 + \tau\phi^2 + \tau\alpha^2 \left( \frac{d\phi}{dX} \right)^2 + \alpha^2 W \frac{d\phi}{dX} + \alpha^2 \frac{dW}{dX} \left( \phi + \frac{dW}{dX} \right) \right] &= \left( \frac{d\phi}{dX} \right)^2 - \hat{N}_\theta \alpha^2 \frac{d\phi}{dX} \frac{d^2W}{dX^2} - K_w \alpha^2 W \frac{d\phi}{dX} \\
&- K_g \alpha^2 \frac{d^2W}{dX^2} \frac{d\phi}{dX} + \frac{1}{\Omega} \left( \phi + \frac{dW}{dX} \right)^2 \\
&- \hat{N}_\theta \alpha^2 \frac{d^3W}{dX^3} \left( \phi + \frac{dW}{dX} \right) + \\
&K_w \alpha^2 \frac{dW}{dX} \left( \phi + \frac{dW}{dX} \right) + \hat{N}_\theta \left( \frac{dW}{dX} \right)^2 \\
&- K_g \alpha^2 \frac{d^3W}{dX^3} \left( \phi + \frac{dW}{dX} \right) \\
&+ K_w W^2 - K_g W \frac{d^2W}{dX^2} \quad (6.11)
\end{aligned}$$

In this problem, we have used Chebyshev polynomials in the Rayleigh-Ritz method. As such, we introduce another independent variable  $\xi$  as  $\xi = 2X - 1$  which transforms the range  $0 \leq X \leq 1$  into the applicability range  $-1 \leq \xi \leq 1$ .

Now, Rayleigh Quotient may be obtained from the following equations of TBT nanobeams

$$\begin{aligned}
\lambda^2 \left[ W^2 + \tau\phi^2 + 4\tau\alpha^2 \left( \frac{d\phi}{d\xi} \right)^2 + 2\alpha^2 W \frac{d\phi}{d\xi} + 2\alpha^2 \frac{dW}{d\xi} \left( \phi + 2\frac{dW}{d\xi} \right) \right] &= 4 \left( \frac{d\phi}{d\xi} \right)^2 - 8\hat{N}_\theta \alpha^2 \frac{d\phi}{d\xi} \frac{d^2W}{d\xi^2} + \\
&2K_w \alpha^2 W \frac{d\phi}{d\xi} - 8K_g \alpha^2 \frac{d^2W}{d\xi^2} \frac{d\phi}{d\xi} + \\
&\frac{1}{\Omega} \left( \phi + 2\frac{dW}{d\xi} \right)^2 + 4\hat{N}_\theta \left( \frac{dW}{d\xi} \right)^2 \\
&- 8\hat{N}_\theta \alpha^2 \frac{d^3W}{d\xi^3} \left( \phi + 2\frac{dW}{d\xi} \right) \\
&+ 2K_w \alpha^2 \frac{dW}{d\xi} \left( \phi + 2\frac{dW}{d\xi} \right) \\
&- 8K_g \alpha^2 \frac{d^3W}{d\xi^3} \left( \phi + 2\frac{dW}{d\xi} \right) \\
&+ K_w W^2 - 4K_g W \frac{d^2W}{d\xi^2} \quad (6.12)
\end{aligned}$$

Substituting Eqs. (2.14) and (2.15) in Eq. (6.12) and minimizing  $\lambda^2$  with respect to the constant coefficients, the following eigenvalue value problem is obtained

$$[K] \{Z\} = \lambda^2 [M_a] \{Z\} \quad (6.13)$$

where  $Z$  is a column vector of constants.

Here stiffness matrix  $K$  and mass matrix  $M_a$  for TBT nanobeams are given as follows

$$K = \begin{bmatrix} k_1 & k_2 \\ k_3 & k_4 \end{bmatrix} \text{ where } k_1, k_2, k_3, k_4 \text{ are submatrices and are given as}$$

$$k_1(i, j) = \int_{-1}^1 (8(\frac{1}{\Omega} + K_w \alpha^2 + \hat{N}_\theta) \varphi_i' \varphi_j' - 16(\hat{N}_\theta \alpha^2 + K_g \alpha^2) \varphi_i''' \varphi_j' - 16(\hat{N}_\theta \alpha^2 + K_g \alpha^2) \varphi_i' \varphi_j''' + 2K_w \varphi_i \varphi_j - 4K_g \varphi_i'' \varphi_j - 4K_g \varphi_i \varphi_j'') d\xi$$

$$k_2(i, j) = \int_{-1}^1 (-8\hat{N}_\theta \alpha^2 \varphi_i'' \psi_j' + 2K_w \alpha^2 \varphi_i \psi_j' - 8K_g \alpha^2 \varphi_i'' \psi_j' + 4\frac{1}{\Omega} \varphi_i' \psi_j - (8\hat{N}_\theta \alpha^2 + 8K_g \alpha^2) \varphi_i''' \psi_j + 2K_w \alpha^2 \varphi_i' \psi_j) d\xi$$

$$k_3(i, j) = \int_{-1}^1 (-8\hat{N}_\theta \alpha^2 \psi_i' \varphi_j'' + 2K_w \alpha^2 \psi_i' \varphi_j - 8K_g \alpha^2 \psi_i' \varphi_j'' + 4\frac{1}{\Omega} \psi_i \varphi_j' - 8\hat{N}_\theta \alpha^2 \psi_i \varphi_j''' + 2K_w \alpha^2 \psi_i \varphi_j' - 8K_g \alpha^2 \psi_i \varphi_j''') d\xi$$

$$k_4(i, j) = \int_{-1}^1 (8\psi_i' \psi_j' + 2\frac{1}{\Omega} \psi_i \psi_j) d\xi$$

$$M_a = \begin{bmatrix} m_1 & m_2 \\ m_3 & m_4 \end{bmatrix} \text{ where } m_1, m_2, m_3, m_4 \text{ are submatrices and are defined as}$$

$$m_1(i, j) = \int_{-1}^1 (2\varphi_i \varphi_j + 8\alpha^2 \varphi_i' \varphi_j') d\xi$$

$$m_2(i, j) = \int_{-1}^1 (2\alpha^2 \varphi_i \psi_j' + 2\alpha^2 \varphi_i' \psi_j) d\xi$$

$$m_3(i, j) = \int_{-1}^1 (2\alpha^2 \psi_i \varphi_j' + 2\alpha^2 \psi_i' \varphi_j) d\xi$$

$$m_4(i, j) = \int_{-1}^1 (2\tau \psi_i \psi_j + 2\tau \alpha^2 \psi_i' \psi_j') d\xi$$

## 6.4 RBT

Governing equations for vibration of nanobeams embedded in elastic foundations are obtained as

$$\begin{aligned} -\rho A \omega^2 w_0 = & G\tilde{A} \left( \frac{d\phi_0}{dx} + \frac{d^2 w_0}{dx^2} \right) - \bar{N} \frac{d^2 w_0}{dx^2} - k_w w_0 + k_g \frac{d^2 w_0}{dx^2} + c_1 E J \frac{d^3 \phi_0}{dx^3} - c_1^2 E K \left( \frac{d^3 \phi_0}{dx^3} + \frac{d^4 w_0}{dx^4} \right) \\ & + \mu \left[ \bar{N} \frac{d^4 w_0}{dx^4} + k_w \frac{d^2 w_0}{dx^2} - k_g \frac{d^4 w_0}{dx^4} - \rho A \omega^2 \frac{d^2 w_0}{dx^2} \right] \end{aligned} \quad (6.14)$$

$$E\hat{I} \frac{d^2 \phi_0}{dx^2} - c_1 E J \left( \frac{d^2 \phi_0}{dx^2} + \frac{d^3 w_0}{dx^3} \right) - G\tilde{A} \left( \phi_0 + \frac{dw_0}{dx} \right) = 0 \quad (6.15)$$

Eliminating  $\phi_0$  from Eqs. (6.14) and (6.15), governing equations may be written as

$$\begin{aligned}
& -\left(\frac{68}{84}\bar{N} + \frac{105}{84EI}G\tilde{A}\mu\bar{N}\right)\frac{d^4w_0}{dx^4} + \frac{105}{84EI}G\tilde{A}\bar{N}\frac{d^2w_0}{dx^2} + \frac{68}{84}\mu\bar{N}\frac{d^6w_0}{dx^6} = \rho A\omega^2\frac{105}{84EI}G\tilde{A}w_0 - \frac{105}{84EI}G\tilde{A}k_w w_0 + \\
& \quad \left(\frac{68}{84}k_w + \frac{105}{84EI}G\tilde{A}k_g + \frac{105}{84EI}G\tilde{A}\mu k_w - \frac{68}{84}\rho A\omega^2 - \frac{105}{84EI}G\tilde{A}\mu\rho A\omega^2\right)\frac{d^2w_0}{dx^2} \\
& - \left(\frac{68}{84}k_g + \frac{68}{84}\mu k_w + \frac{105}{84EI}G\tilde{A}\mu k_g + \frac{21}{84}G\tilde{A} - \frac{68}{84}\mu\rho A\omega^2\right)\frac{d^4w_0}{dx^4} + \left(\frac{68}{84}\mu k_g + \frac{1}{105}EI\right)\frac{d^6w_0}{dx^6} \quad (6.16)
\end{aligned}$$

Eq. (6.16) may be written in non-dimensional form as

$$\begin{aligned}
\lambda^2 \left( \frac{105}{84}\bar{\Omega}W - \left( \frac{68}{84} + \frac{105}{84}\bar{\Omega}\alpha^2 \right) \frac{d^2W}{dx^2} + \frac{68}{84}\alpha^2 \frac{d^4W}{dx^4} \right) &= \left( -\frac{68}{84}\alpha^2 K_g - \frac{1}{105} + \frac{68}{84}\alpha^2 \hat{N}_\theta \right) \frac{d^6W}{dX^6} \\
&+ \left( \frac{68}{84}K_g - \frac{68}{84}\hat{N}_\theta + \frac{68}{84}\alpha^2 K_w + \frac{105}{84}\bar{\Omega}\alpha^2 K_g + \frac{105}{84}\bar{\Omega} - \frac{105}{84}\bar{\Omega}\alpha^2 \hat{N}_\theta \right) \frac{d^4W}{dX^4} \\
&+ \left( -\frac{68}{84}K_w - \frac{105}{84}\bar{\Omega}K_g - \frac{105}{84}\bar{\Omega}\alpha^2 K_w + \frac{105}{84}\bar{\Omega}\hat{N}_\theta \right) \frac{d^2W}{dX^2} + \frac{105}{84}\bar{\Omega}K_w \quad (6.17)
\end{aligned}$$

Application of differential quadrature method in Eq. (6.17), one may obtain generalized eigen value problem for RBT as

$$[K] \{W\} = \lambda^2 [M_a] \{W\} \quad (6.18)$$

where  $K$  is the stiffness matrix and  $M_a$  is the mass matrix.

## 6.5 Numerical results and discussions

Vibration of Single-Walled carbon nanotubes embedded in elastic medium under the influence of temperature has been investigated. The elastic medium is modeled as Winkler-type and Pasternak-type foundations. The effective properties of SWCNTs are taken as: (Benzair et al. 2008; Murmu and Pradhan 2009b):  $E = 1000$  GPa,  $\nu = 0.19$ ,  $\alpha_x = -1.6 \times 10^{-6}$  for room or low temperature and  $\alpha_x = 1.1 \times 10^{-6}$  for high temperature. A computer code is developed by the authors in MATLAB.

### 6.5.1 Convergence

First of all, convergence test has been performed to find minimum number of terms required for computing results. As such, Table 6.4 shows convergence of first three frequency parameters ( $\sqrt{\lambda}$ ) of EBT nanobeams with C-C support. In this table, we have taken  $K_w = 50$ ,  $K_g = 2$ ,  $\theta = 20K$ ,  $e_0a = 0.5nm$  and  $\frac{L}{h} = 10$ . Similarly, Table 6.5 shows convergence test for TBT nanobeams. In this table, we have taken  $K_w = 50$ ,  $K_g = 2$ ,  $\theta = 10K$ ,  $e_0a = 1nm$ ,  $\frac{L}{h} = 10$  with C-C edge condition. Fig. 6.24 shows convergence of fundamental frequency parameter of

nanobeams based on RBT where we have taken  $K_w = 50, K_g = 4, \theta = 20K, e_0a = 1nm, \frac{L}{h} = 10$  with S-S edge condition. Above convergence patterns show that ten grid points are sufficient to obtain results in the present analysis.

Table 6.4 Convergence of first three frequency parameters of nanobeams (EBT)

$n$	First	Second	Third
3	4.8718	7.8096	10.7781
4	4.8718	7.7285	10.7781
5	4.8718	7.7285	10.4761
6	4.8718	7.7273	10.4761
7	4.8718	7.7273	10.4657
8	4.8718	7.7273	10.4657
9	4.8718	7.7273	10.4656
10	4.8718	7.7273	10.4656
11	4.8718	7.7273	10.4656

Table 6.5 Convergence of first three frequency parameters (TBT)

$n$	First	Second	Third
3	3.6493	6.4704	13.9265
4	3.5402	6.4669	9.1435
5	3.5402	5.8616	9.1309
6	3.5399	5.8616	7.9217
7	3.5399	5.8511	7.9214
8	3.5399	5.8511	7.8697
9	3.5399	5.8511	7.8697

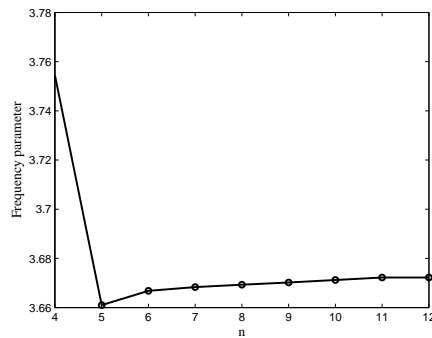


Fig. 6.24 Convergence of fundamental frequency parameter (RBT)

## 6.5.2 Validation

To validate the present results of Euler-Bernoulli, a comparison study has been carried out with the results of Wang et al. (2007). For this comparison, we have taken  $K_w = 0, K_g = 0$  and  $\theta = 0K$ . As such, Figs. 6.25-6.26 show graphical comparisons of EBT and TBT nanobeams respectively. In these figures, we have considered S-S support with  $\frac{L}{h} = 10$ . Similarly, tabular comparison study has been tabulated in Table 6.6 with that of Ansari and Sahmani (2012) for  $\frac{L}{d} = 40$ . Same parameters as that of Ansari and Sahmani (2011) have been taken for this comparison. One may find close agreement of the results. This shows the suitability and reliability of the present methods for the vibration analysis of SWCNTs.

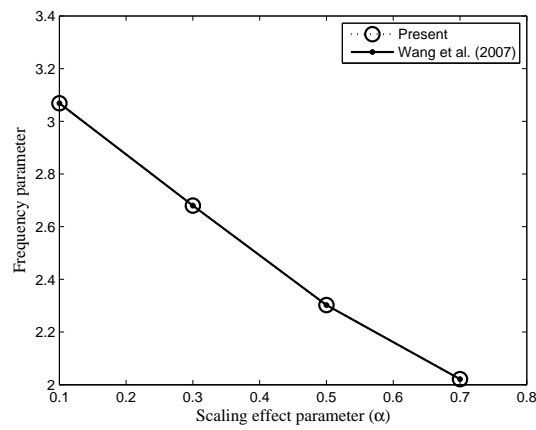


Fig. 6.25 Comparison of fundamental frequency parameter (EBT)

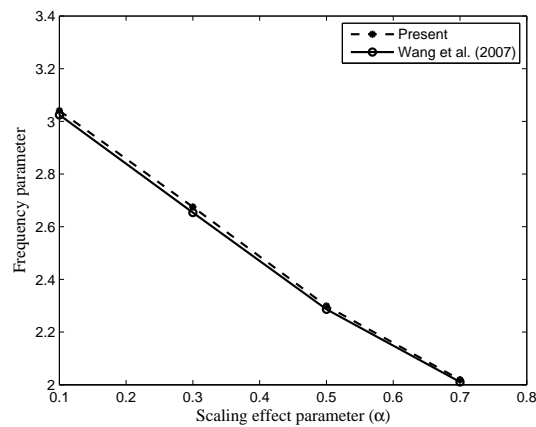


Fig. 6.26 Comparison of fundamental frequency parameter (TBT)



Table 6.6 Comparison of fundamental frequencies for various boundary conditions (RBT)

$\mu$	S-S		C-S	
	Present	Ref.*	Present	Ref.*
0.25	0.0164	0.0231	0.0321	0.0358
0.5	0.0164	0.0231	0.0320	0.0358
0.75	0.0164	0.0231	0.0320	0.0358
1	0.0164	0.0231	0.0319	0.0357

\* Ansari and Sahmani (2012)

### 6.5.3 Effect of Winkler modulus parameter

In this subsection, we have investigated the influence of surrounding medium on the vibration of SWCNTs. The elastic medium is modeled as Winkler-type and Pasternak-type foundations. Figs. 6.27-6.29 illustrate effect of Winkler modulus parameter on the vibration solutions based on EBT, TBT and RBT respectively. We have shown these graphical results in low temperature environment with  $K_g = 0$ . Numerical values taken for this computation are  $\theta = 20K, \frac{L}{h} = 10$  in Fig. 6.27 with C-S support whereas in Fig. 6.28, we have taken  $\theta = 20K, \frac{L}{h} = 10$  with C-S support and in Fig. 6.29, we have taken  $\theta = 20K, \frac{L}{h} = 20$  with C-S support. The Winkler modulus parameter is taken in the range of 0-400. It is observed from these figures that frequency parameter associated with first mode decreases with increase in scale coefficient. It may be noted that results associated with  $e_0a = 0nm$  correspond to those of local beam theory. One may observe that results obtained by local beam theory are over predicted than that of obtained by nonlocal beam theory. As the scale coefficient  $e_0a$  increases, frequency parameter obtained for nonlocal beam theory becomes smaller than those for its local counterpart. Therefore, non-local theory should be considered for vibration analysis of structures at nanoscale. It is seen that frequency parameter increases with increase in Winkler modulus parameter. This is because that the nanotube becomes stiffer when elastic medium constant is increased. This increasing trend of fundamental frequency parameter with surrounding elastic medium is influenced significantly by the small scale coefficients. In addition, it is also observed that fundamental frequency parameter show nonlinear behavior with respect to stiffness of surrounding matrix for higher  $e_0l_{int}$  values. This may be due to the fact that increase of the Winkler modulus causes CNT to be more rigid.

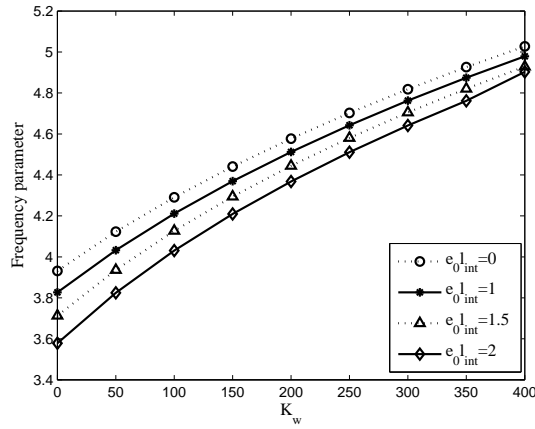


Fig. 6.27 Effect of the Winkler modulus parameter on frequency parameter (EBT)

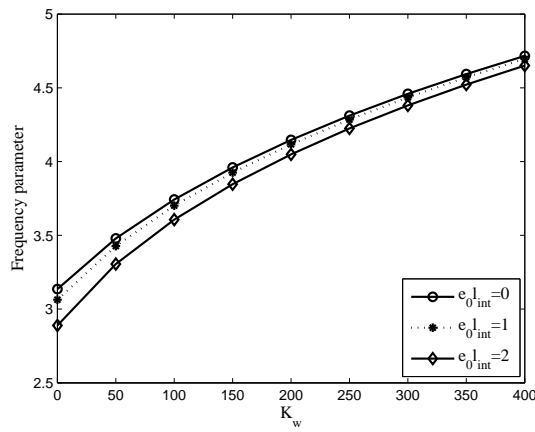


Fig. 6.28 Effect of the Winkler modulus parameter on frequency parameter (TBT)

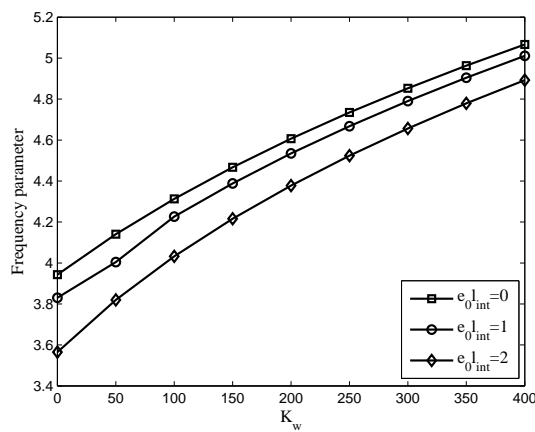


Fig. 6.29 Effect of the Winkler modulus parameter on frequency parameter (RBT)

### 6.5.4 Effect of Pasternak shear modulus parameter

In this subsection, effect of Pasternak shear modulus parameter on the vibration has been examined. Figs. 6.30-6.32 show the distribution of the fundamental frequency parameter against Pasternak shear modulus for EBT, TBT and RBT respectively in low temperature environment. Numerical values of parameters are chosen as  $K_w = 0, \theta = 20K, \frac{L}{h} = 30$  with C-C support in Fig. 6.30 whereas in Fig. 6.31, we have taken  $K_w = 200, \theta = 10K, \frac{L}{h} = 30$  with C-C support and in Fig. 6.32, we have taken  $K_w = 0, \theta = 10K, \frac{L}{h} = 10$  with C-C edge condition. Graph is plotted for various values of scale coefficients with Pasternak shear modulus parameter ranging from 0-10. It is observed from the figures that frequency parameter associated with first mode increases with Pasternak shear modulus parameter. This may be due to the effective stiffness of elastic medium. With increase in scale coefficient, frequency parameter for a particular Pasternak shear modulus parameter decreases. It is also observed that unlike Winkler foundation model, the increase of fundamental frequency parameter with Pasternak foundation is linear in nature. This is due to the domination of elastic medium modeled as the Pasternak type foundation model. Same observation has also been reported in Murmu and Pradhan (2009b). Next, we have analyzed the effect of Pasternak foundation model over Winkler foundation model. As such, Fig. 6.33 illustrates the fundamental frequency parameter of RBT nanobeams as a function of small scale coefficient in low temperature environment with  $\frac{L}{h} = 10$  and C-C edge condition. It may be observed that frequency parameter obtained from Pasternak foundation model is relatively larger than those obtained from the Winkler foundation model.

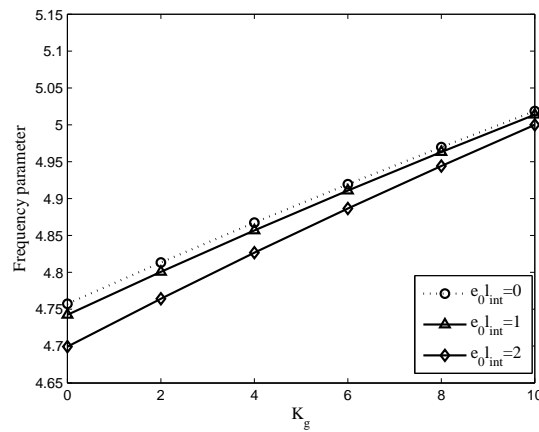


Fig. 6.30 Effect of Pasternak shear modulus parameter on frequency parameter (EBT)

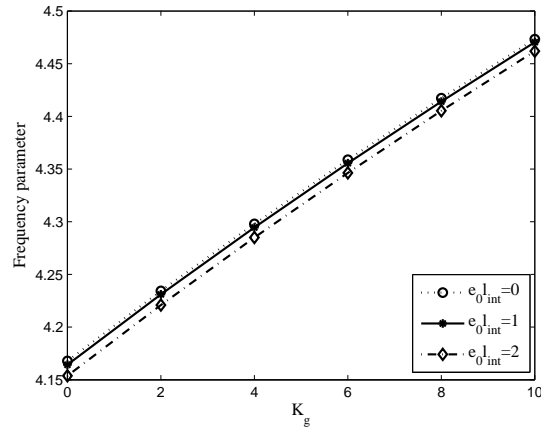


Fig. 6.31 Effect of Pasternak shear modulus parameter on frequency parameter (TBT)

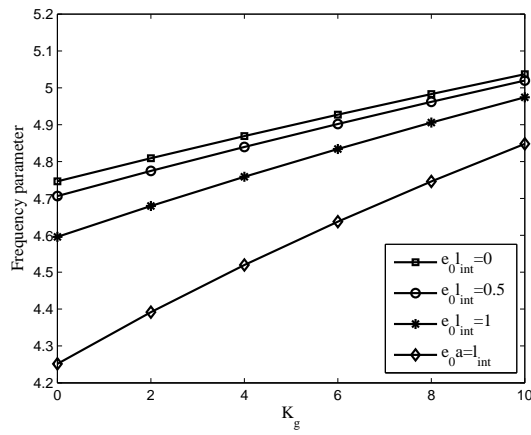


Fig. 6.32 Effect of Pasternak shear modulus parameter on frequency parameter (RBT)

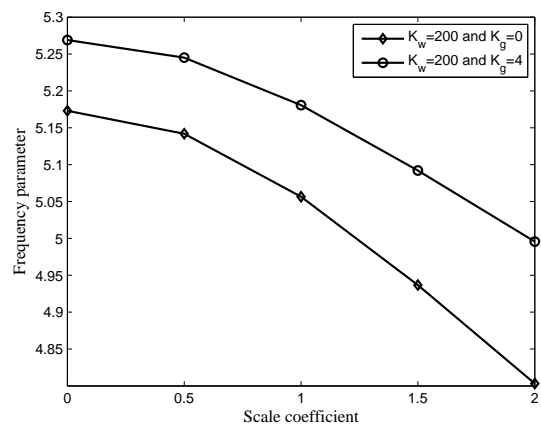


Fig. 6.33 Effect of frequency parameter with small-scale coefficients

### 6.5.5 Effect of temperature

Effect of temperature on the vibration of nanobeams embedded in elastic medium has been investigated. Effect of temperature on the vibration solutions has been illustrated in Figs. 6.34-6.36 respectively for EBT, TBT and RBT respectively. In Fig. 6.34, we have taken S-S nanobeams with  $\frac{L}{h} = 10, e_0a = 1.5nm, K_w = 10, K_g = 4$ . Similarly, we have taken  $\frac{L}{h} = 50, e_0a = 0.5nm, K_w = 50, K_g = 2$  with C-C support in Fig. 6.35 and  $\frac{L}{h} = 30, e_0a = 1nm, K_w = 50, K_g = 2$  with C-C support in Fig. 6.36. It is noticed that fundamental frequency parameter increases with increase in temperature in low temperature environment while they decrease with increase in temperature in high temperature environment. Thus, one may say that fundamental frequency parameter considering thermal effect are larger than those ignoring the influence of temperature change in low temperature environment. While in high temperature environment, fundamental frequency parameter considering thermal effect are smaller than those excluding the influence of temperature change. Same observation have also been noted in Refs. (Murmu and Pradhan 2009a; Zidour et al. 2012; Maachou et al. 2011; Murmu and Pradhan 2010).

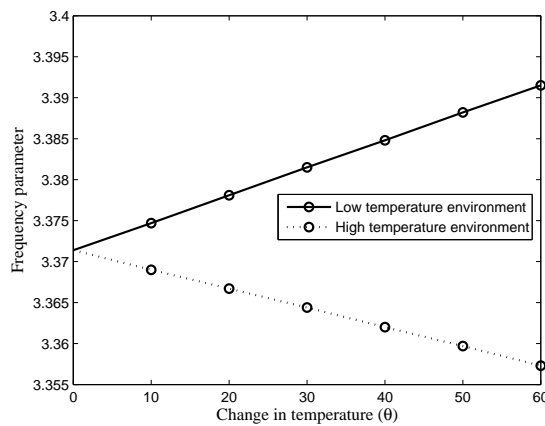


Fig. 6.34 Change of frequency parameter with temperature change (EBT)

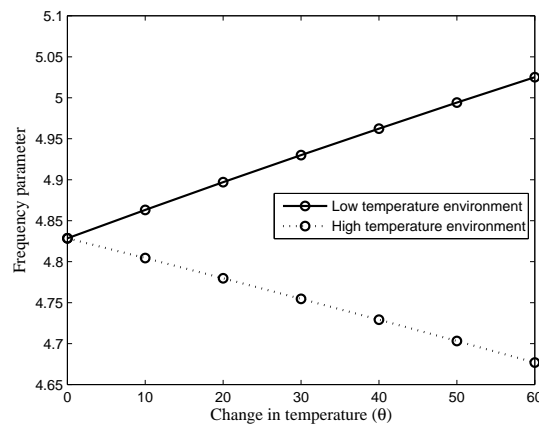


Fig. 6.35 Change of frequency parameter with temperature change (TBT)

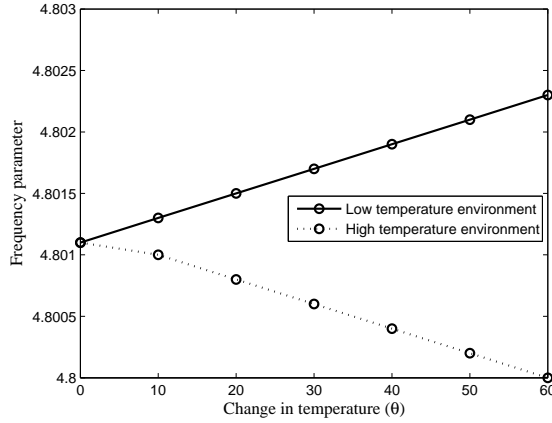


Fig. 6.36 Change of frequency parameter with temperature change (RBT)

### 6.5.6 Effect of aspect ratio

To illustrate the effect of aspect ratio on the fundamental frequency parameter, variation of frequency ratio with the aspect ratio ( $\frac{L}{h}$ ) has been shown in Fig. 6.37 for different magnitudes of temperature change. Results have been shown for EBT nanobeams with  $K_w = 50$ ,  $K_g = 2$ ,  $e_0a = 1nm^2$  and C-C support in low temperature environment. It is observed that frequency ratio increases with increase in aspect ratio. In addition, it is also seen that fundamental frequency parameter is also dependent on temperature change ( $\theta$ ). The differences in magnitudes of frequency parameter for different temperature changes are larger in low aspect ratios while the differences in magnitudes of frequency parameter for different temperature changes are smaller for large aspect ratios.

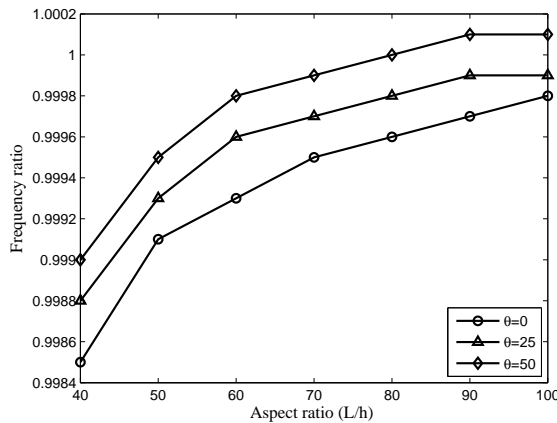


Fig. 6.37 Change of frequency ratio with aspect ratio

## 6.6 Conclusions

Present study includes vibration characteristics of free vibration of non-uniform nanobeams based on nonlocal elasticity theory. Boundary characteristic orthogonal polynomials have been generated and are applied in the Rayleigh-Ritz method to study the effect of non-uniform parameters on the frequency parameters of Euler Bernoulli and Timoshenko nanobeams. Non-uniform material properties of nanobeams are assumed by taking linear and quadratic variations of Young's modulus and density. Effects of non-uniform parameter, boundary condition, aspect ratio and scaling effect parameter on the frequency parameters have been investigated. First four deflection shapes are given for S-S and C-S boundary conditions with scaling effect parameters as 0 and 0.3.

Again, Rayleigh-Ritz method has been applied to investigate thermal effect on the vibration of nanobeams embedded in elastic medium based on EBT and TBT. While differential quadrature method has been applied to investigate thermal effect on the vibration of nanobeams embedded in elastic medium based on nonlocal Reddy beam theory. Theoretical formulations include effects of small scale, elastic medium and temperature change. It is seen that results obtained based on local beam theory are overestimated. Frequency parameter increases with increase in temperature, Winkler and Pasternak coefficients of elastic foundation.

# Chapter 7

## Vibration of nanoplates

The contents of this chapter have been published in:

1. S. Chakraverty and Laxmi Behera (2014) Free vibration of rectangular nanoplates using Rayleigh-Ritz method, *Physica E*, 56, 357-363.



# Chapter 7

## Vibration of nanoplates

Here, we have considered vibration of isotropic nanoplate. Rayleigh-Ritz method has been employed with two-dimensional simple polynomials as shape functions. Parametric studies such as effect of length, aspect ratio and nonlocal parameter have been analyzed. Three-dimensional mode shapes for some specified boundary condition have been presented.

Maximum strain energy may be obtained by setting  $k_w$  and  $k_p$  as zero in Eq. (2.35).

$$U = \frac{1}{2}D \int_0^a \int_0^b \left\{ \left( \frac{\partial^2 w_0}{\partial x^2} \right)^2 + 2\nu \left( \frac{\partial^2 w_0}{\partial x^2} \frac{\partial^2 w_0}{\partial y^2} \right) + \left( \frac{\partial^2 w_0}{\partial y^2} \right)^2 + 2(1-\nu) \left( \frac{\partial^2 w_0}{\partial x \partial y} \right)^2 \right\} dx dy \quad (7.1)$$

Maximum kinetic energy may be written as Eq. (2.36).

Equating maximum kinetic and strain energies, one may obtain the Rayleigh-quotient as

$$\frac{\rho h \omega^2}{D} = \frac{\int_0^a \int_0^b \left[ \left( \frac{\partial^2 w_0}{\partial x^2} \right)^2 + 2\nu \left( \frac{\partial^2 w_0}{\partial x^2} \frac{\partial^2 w_0}{\partial y^2} \right) + \left( \frac{\partial^2 w_0}{\partial y^2} \right)^2 + 2(1-\nu) \left( \frac{\partial^2 w_0}{\partial x \partial y} \right)^2 \right] dx dy}{\int_0^a \int_0^b \left[ w_0^2 + \mu \left( \left( \frac{\partial w_0}{\partial x} \right)^2 + \left( \frac{\partial w_0}{\partial y} \right)^2 \right) \right] dx dy} \quad (7.2)$$

where  $m_0$  is taken as  $\rho h$ .

We have introduced the non-dimensional variables  $X = \frac{x}{a}$  and  $Y = \frac{y}{b}$

As such, non-dimensional Rayleigh-quotient is obtained as

$$\frac{\rho h \omega^2 a^4}{D} = \frac{\int_0^1 \int_0^1 \left[ \left( \frac{\partial^2 W}{\partial X^2} \right)^2 + 2\nu R^2 \left( \frac{\partial^2 W}{\partial X^2} \frac{\partial^2 W}{\partial Y^2} \right) + R^4 \left( \frac{\partial^2 W}{\partial Y^2} \right)^2 + 2(1-\nu) R^2 \left( \frac{\partial^2 W}{\partial X \partial Y} \right)^2 \right] dX dY}{\int_0^1 \int_0^1 \left[ W^2 + \frac{\mu}{a^2} \left( \left( \frac{\partial W}{\partial X} \right)^2 + R^2 \left( \frac{\partial W}{\partial Y} \right)^2 \right) \right] dX dY} \quad (7.3)$$

Substituting Eq. (2.31) into Eq. (7.3), we get a generalized eigen value problem as

$$[K] \{Z\} = \lambda^2 [M_a] \{Z\} \quad (7.4)$$

where  $\lambda^2 = \frac{\rho h a^4 \omega^2}{D}$  is the non-dimensional frequency parameter,  $Z$  is a column vector of constants,  $K$  and  $M_a$  are the stiffness and mass matrices which are given as follows

$$K(ij) = \beta_{ij}^{2020} + \nu R^2 (\beta_{ij}^{2002} + \beta_{ij}^{0220}) + R^4 \beta_{ij}^{0202} + 2(1 - \nu) R^2 \beta_{ij}^{1111}$$

$$M_a(ij) = \beta_{ij}^{0000} + \mu \left(\frac{1}{a}\right)^2 (\beta_{ij}^{1010} + R^2 \beta_{ij}^{0101})$$

where  $\beta_{ij}^{klmna} = \int_0^1 \int_0^1 \left[ \frac{\partial^{k+l} \varphi_i}{\partial X^k \partial Y^l} \right] \left[ \frac{\partial^{m+n} \varphi_j}{\partial X^m \partial Y^n} \right] dX dY$

## 7.1 Numerical results and discussions

Numerical values of the frequency parameter  $\lambda$  have been obtained by solving Eq. (7.4) using a computer program developed by the authors in MATLAB which is run for different values of  $n$  to get appropriate value of the order of approximation  $n$ .

### 7.1.1 Convergence

Table 7.1 shows convergence of first three frequency parameters for S-S-S-S, S-C-S-C, F-C-F-C and F-S-F-S nanoplates with  $\nu = 0.3$ ,  $R = 2$ ,  $\mu = 2nm^2$  and  $a = 10nm$ . From this table, it can be clearly seen that the frequency parameters ( $\lambda$ ) approach to the results with the increasing value of  $n$  and further increase of  $n$  does not have any effect on the results.

Table 7.1 Convergence of first three frequency parameters of nanoplates

S-S-S-S							S-C-S-C						
$n$	First	Second	Third	First	Second	Third	$n$	First	Second	Third	First	Second	Third
10	35.0202	49.2575	80.6866	64.3936	69.6776	93.8351	10	61.8442	62.2421	64.7394	29.2401	32.9761	44.9044
15	35.0086	49.2575	68.5520	64.3898	69.6776	81.3358	15	61.8442	61.9872	64.6373	29.0358	32.9761	42.9748
20	35.0086	49.1652	68.5520	64.3898	69.6363	81.3358	20	61.8388	61.9872	64.6373	29.0358	32.7816	42.9748
25	35.0086	49.1652	67.9560	64.3898	69.6363	80.9277	25	61.8388	61.9860	64.5829	29.0261	32.7816	42.7648
30	35.0086	49.1650	67.9538	64.3898	69.6362	80.9271	30	61.8385	61.9855	64.5823	29.0260	32.7780	42.7610
35	35.0086	49.1646	67.9538	64.3898	69.6361	80.9271	35	61.8255	61.9855	64.5823	29.0260	32.7769	42.7610
40	35.0086	49.1646	67.9435	64.3898	69.6361	80.9210	40	61.8255	61.9324	64.5823	29.0259	32.7769	42.7595
45	35.0086	49.1646	67.9433	64.3898	69.6361	80.9210	45	61.7567	61.9324	64.5815	29.0259	32.7769	42.7595
47	35.0086	49.1646	67.9433	64.3898	69.6361	80.9210	47	61.7567	61.9324	64.5815	29.0259	32.7769	42.7595

### 7.1.2 Validation

For comparison of the results with analytical solutions of Aksencer and Aydogdu (2011), numerical results have been given in graphical form in Fig. 7.1 where variation of first two frequency ratios with length  $a$  is given for nanoplates with S-S-S-S boundary condition. Here aspect ratio is taken as 1 and nonlocal parameters are taken as  $0nm^2, 1nm^2, 2nm^2, 4nm^2$ . From this figure, we may say that increase in nonlocal parameter decreases frequency ratios. This decreasing behavior is clearly noticed for higher modes. This is because of the fact that increase in mode number decreases wavelength. Since nonlocal effects are more pronounced for smaller wave lengths, so there will be no nonlocal effects after a certain length of nanoplates. All these observations are expected and a close agreement of the results with Aksencer and Aydogdu (2011) are seen. Next tabular comparison has been given in Table 7.2 with Aghababaei and Reddy (2009) for the first three frequency parameters with  $R = 1$  and  $a = 10nm$ . Results have been verified for different nonlocal parameters with the consideration of S-S-S-S edge

condition.

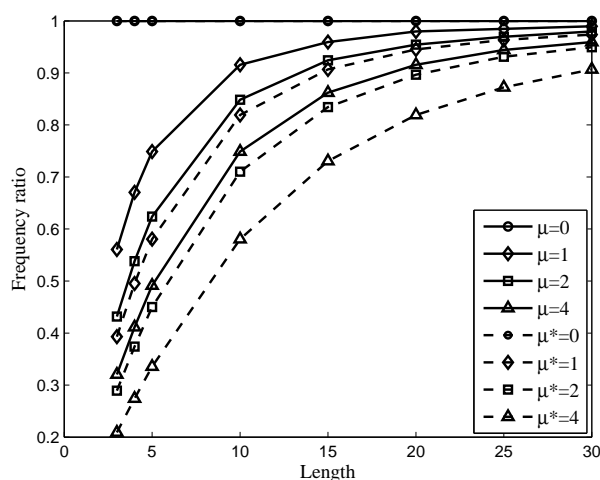


Fig. 7.1 Variation of frequency ratios with length of nanoplates

Table 7.2 Comparison of first three frequency parameters for S-S-S-S nanoplate

$\mu = 0$		$\mu = 1$		$\mu = 2$		$\mu = 3$		$\mu = 4$	
Present	Ref.*	Present	Ref.*	Present	Ref.*	Present	Ref.*	Present	Ref.*
0.0963	0.0963	0.0880	0.0880	0.0816	0.0816	0.0763	0.0763	0.0720	0.0720
0.3874	0.3853	0.2884	0.288	0.2402	0.2399	0.2102	0.2099	0.1892	0.1889
0.8608	0.8669	0.5167	0.5202	0.4045	0.4063	0.3435	0.3446	0.3037	0.3045

\*Aghababaei and Reddy (2009)

### 7.1.3 New results

First four frequency parameters are tabulated in Table 7.3 for nanoplates subjected to boundary conditions (S-S-S-S, C-C-C-C, S-C-S-C, F-C-F-C and F-S-F-S) with nonlocal parameters ( $0nm^2 - 4nm^2$ ), length ( $a = 5nm$ ) and aspect ratio as 1. From this table, it may be seen that frequency parameters are highest in C-C-C-C and lowest in F-S-F-S for a particular value of nonlocal parameter. Frequency parameters decrease with increase in nonlocal parameter in all the boundary conditions. Table 7.4 gives first four frequency parameters for nanoplates subjected to various boundary conditions having  $\mu = 2nm^2$ ,  $R = 2$  and length= $5nm$ . From Tables 7.3 ( $\mu = 2nm^2$ ) and 7.4, it is observed that frequency parameters increase with increase in aspect ratio for a particular boundary condition and nonlocal parameter. It is also seen that frequency parameters are highest in C-C-C-C than other boundary conditions. **One may also see that from Table 7.4 that frequency parameters are lowest in C-F-F-F boundary condition.**

Table 7.3 First four frequency parameters of nanoplates for  $a = 5nm$  and  $a/b = 1$

S-S-S-S				
Mode no.	$\mu = 0$	$\mu = 1$	$\mu = 2$	$\mu = 4$
1	19.7000	14.7556	12.2912	9.6800
2	49.3000	28.6157	22.1851	16.5455
3	49.3000	28.6157	22.1851	16.5455
4	79	38.7198	29.1902	21.3842
C-C-C-C				
1	36	25.6182	20.9293	16.2072
2	73.4000	40.2819	30.8650	22.8363
3	73.4000	40.2819	30.8650	22.8363
4	108.2000	50.2722	37.5982	27.4081
S-C-S-C				
1	29	21.1091	17.4090	13.5914
2	54.7000	31.3612	24.2491	18.0520
3	69.3000	38.4787	29.5537	21.9013
4	94.6000	45.1134	33.8697	24.7486
F-C-F-C				
1	22.2000	18.0585	15.2936	11.7908
2	26.5000	18.7871	15.5360	12.4295
3	43.6000	23.5071	18.0136	13.5242
4	61.2000	33.3133	24.8433	18.1651
F-S-F-S				
1	9.6000	8.1375	7.1737	5.9649
2	16.1000	11.7857	9.7195	7.5853
3	36.7000	20.0205	15.3247	11.3391
4	38.9000	24.1377	18.9747	14.2818

Table 7.4 First four frequency parameters for  $a = 5nm$ ,  $\mu = 2nm^2$  and  $a/b = 2$

B.Cs	First	Second	Third	Fourth
S-C-S-C	39.6000	40.7306	45.2329	52.5002
S-C-S-S	29.5537	33.8697	41.0402	49.9379
S-C-S-F	12.6602	21.6101	29.8275	32.1331
S-S-S-F	9.7195	20.5617	23.4617	31.2146
S-F-S-F	7.0937	11.5810	18.7576	22.7213
C-C-C-C	40.2856	43.4408	50.1693	58.9610
C-C-C-S	30.8647	37.5978	46.7047	53.5259
C-C-S-S	30.0688	35.5235	43.6951	53.1091
C-C-F-F	10.3208	16.5303	24.7089	28.6041
C-F-C-F	14.9166	15.5252	25.8441	27.5855
C-F-S-F	10.8033	13.0646	23.1535	25.2039
C-F-F-F	2.9265	6.5858	11.3837	18.3020
S-S-F-F	4.5285	12.6233	19.9921	22.1292
S-F-F-F	5.8101	8.2758	16.5722	18.8076
F-F-F-F	9.4809	11.2065	18.9165	20.3403
S-F-S-C	12.6602	21.6101	29.8275	32.1331
S-C-C-C	39.7909	41.9053	47.5163	55.5969
S-C-C-S	30.0688	35.5235	43.6951	53.1091
C-F-F-S	5.7331	14.4925	20.8909	24.3087
C-F-S-C	14.2968	24.6622	30.2733	35.5735
C-F-S-S	12.1174	23.6980	24.4128	32.6778
S-S-S-S	22.1851	29.1902	38.2287	44.1800
C-C-C-F	16.6358	28.1756	30.7702	38.0487
C-S-C-F	15.2788	24.8379	27.8202	34.5728

### 7.1.4 Effect of aspect ratio

To see the influence of aspect ratio on the frequency parameters of nanoplates, the behavior of fundamental frequency parameter of C-C-C-C nanoplates with aspect ratio is plotted in Fig. 7.2 for length=10nm. The graph is shown for different nonlocal parameters. From the above graph, it is seen that nonlocal effect on frequency parameters is more prominent in greater values of aspect ratio. This may be due to the fact that when the aspect ratio increases, nanoplates become smaller for a specified length of nanoplates. This leads to an increase in the small scale effect because size dependency plays a vital role in the nonlocal elasticity theory. Let us define the relative error percent as

$$\text{Relative Error Percent} = \frac{|\text{Local Result} - \text{Nonlocal Result}|}{|\text{Local Result}|} \times 100$$

Neglecting nonlocal effect, the relative error percents for aspect ratios 1 and 3 with  $\mu = 3nm^2$  are 23.97% and 54.09% respectively. Therefore, nonlocal theory should be considered for free vibration of small scaled rectangular nanoplates with high aspect ratios. It is also observed that for a particular nonlocal parameter, frequency parameters increase with increase in aspect ratio. When we compare all nonlocal parameters, frequency parameters are highest in case of  $\mu = 0$  i.e. local frequency parameter. This shows that frequency parameters are over predicted when local beam model is considered for vibration analysis of nanoplates. As the scaling effect parameter increases, frequency parameters for nonlocal nanoplates become smaller than those of its local counterpart. This reduction can be clearly seen when we consider higher vibration modes. The reduction is due to the fact that the nonlocal model may be viewed as atoms linked by elastic springs while in case of local continuum model, the spring constant is assumed to take an infinite value. So small scale effect makes the nanoplates more flexible and nonlocal impact cannot be neglected. As such, nonlocal theory should be used for better predictions of high natural frequency of nanoplates.

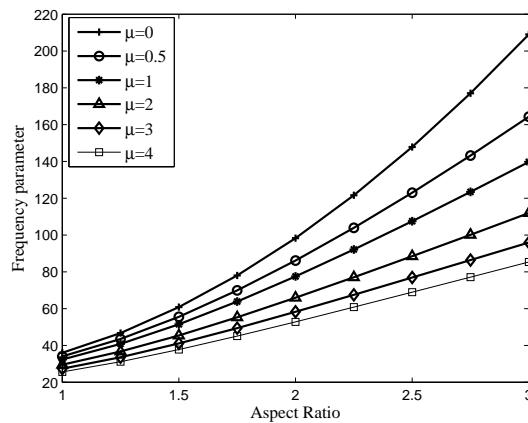


Fig. 7.2 Variation of fundamental frequency parameter with aspect ratio

### 7.1.5 Effect of nonlocal parameter

To investigate the effect of small scale in different vibration modes, non-dimensional frequency parameters associated with the first four modes are illustrated in Fig. 7.3 for different nonlocal parameters. Here we have considered F-S-F-S nanoplates with aspect ratio as 2 and length as  $10nm$ . It is noticed that frequency parameters decrease with nonlocal parameter in all the modes. It may be noted that this behavior is seen in all the boundary conditions. The nonlocal effect is more pronounced in higher vibration modes. Neglecting nonlocal effect, the relative error percents for the first and fourth mode number with  $\mu = 2nm^2$  are found to be 25.57% and 49.48% respectively. This shows noticeable influence of the nonlocal parameter on the frequency parameters in higher modes.

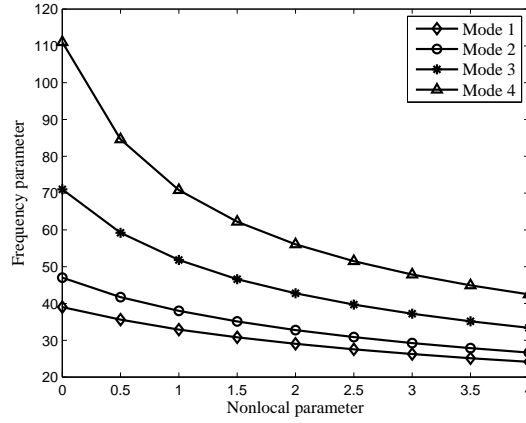


Fig. 7.3 Variation of first four frequency parameters with nonlocal parameter

### 7.1.6 Effect of length

Variation of the length of nanoplates on the fundamental frequency parameter of F-C-F-C nanoplates with  $R = 2$  is shown in Fig. 7.4 for different nonlocal parameters. From this figure, it is observed that frequency parameters obtained by local elasticity theory (with nonzero nonlocal parameter) are always larger than those obtained by nonlocal theory of elasticity. It is also noticed that for each length of nanoplates, frequency parameters decrease with increase in the nonlocal parameter. Again, one may see that as the length of nanoplates increases, frequency parameters increase. This is due to the fact that size-dependency plays a vital role in the nonlocal elasticity theory. In other words, by increasing length of the nanoplates ( $a$ ) and assuming  $l_{int}$  to be unchanged, small scale effect decreases. In this figure, it is also observed that when we increase  $a$ , nonlocal curves approach the local curves. This means for large value of  $a$ , all the results converge to those obtained from the classical theory of elasticity. Neglecting nonlocal effect, the relative error percents of fundamental frequency parameter for  $a = 10nm$  and  $a = 50nm$  with  $\mu = 2nm^2$  are 30.61% and 1.91% respectively. Hence for free vibration of large enough nanoplates, classical theory of elasticity may be used instead of nonlocal elasticity theory.



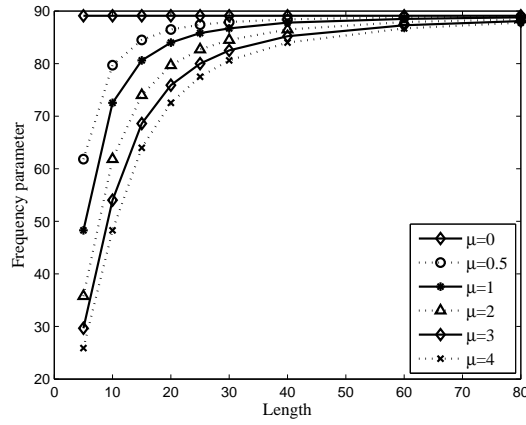


Fig. 7.4 Variation of fundamental frequency parameter with length

### 7.1.7 Mode shapes

Present investigators have reported first three modes shapes for two sets of boundary conditions such as C-C-C-C and S-C-S-C in Figs. 7.5-7.6 with  $\mu = 4nm^2$ ,  $a = 5nm$  and aspect ratio=1.

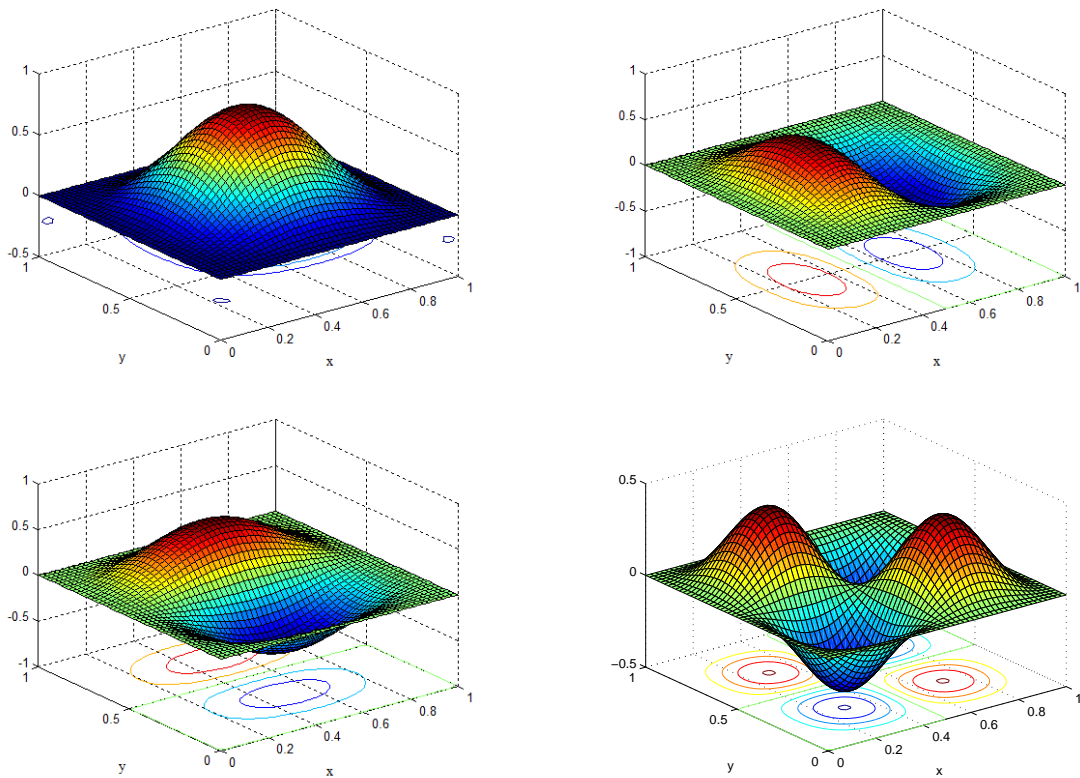


Fig. 7.5 First four deflection shapes of C-C-C-C nanoplates

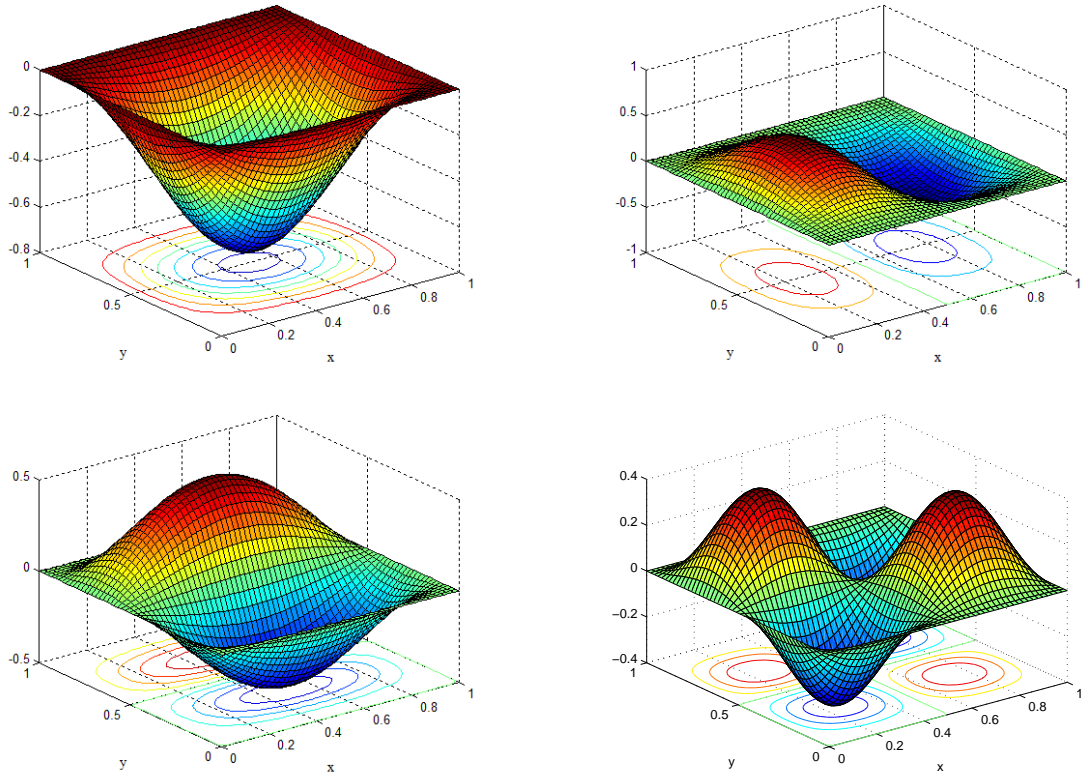


Fig. 7.6 First four deflection shapes of S-C-S-C nanoplates

## 7.2 Conclusions

Rayleigh-Ritz method has been used which can handle any classical boundary boundary conditions at the edges. Present method has been compared with available exact solutions for S-S-S-S boundary condition in graphical form and are found to be in good agreement. Results are given for different nonlocal parameters, length of the nanoplates and aspect ratios. It is observed that non locality effects should be considered for vibration nanoplates. Present analysis will be of great use to the design engineers who are designing microelectromechanical and nanoelectromechanical devices.

# Chapter 8

## Vibration of nanoplates with complicating effects

The contents of this chapter have been published in:

1. Laxmi Behera and S. Chakraverty (2014) Effect of scaling effect parameters on the vibration characteristics of nanoplates, Journal of Vibration and Control, DOI:10.1177/1077546314547376.
2. S. Chakraverty and Laxmi Behera (2015) Small scale effect on the vibration of non-uniform nanoplates, Structural Engineering and Mechanics, 55, 495-510.

## Chapter 8

# Vibration of nanoplates with complicating effects

In this chapter, we have shown vibration of nanoplates with complicating effects. Rayleigh-Ritz method with two-dimensional simple polynomials as shape functions have been implemented. Non-uniformity with elastic foundation has been taken into consideration. Parametric studies such as effect of length, aspect ratio, nonlocal parameter, non-uniform parameter and elastic foundation have been analyzed. Mode shapes for some specified boundary conditions have also been presented.

Maximum strain energy may be given as in Eq. (2.35).

Maximum kinetic energy may be written as Eq. (2.36).

In this investigation, graphene sheets with non-uniform material properties have been considered. The non-uniform material properties is assumed as per the following relations

$$E = E_0(1 + pX + qX^2), \quad \rho = \rho_0(1 + rX + sX^2)$$

Here, we have introduced the non-dimensional variables

$$X = \frac{x}{a}, Y = \frac{y}{b}, K_w = \frac{k_w a^4}{D}, K_p = \frac{k_p a^2}{D}$$

Rayleigh-Quotient in non-dimensional form may be written as

$$\lambda^2 = \frac{\int_0^1 \int_0^1 c_a \left[ \left( \frac{\partial^2 W}{\partial X^2} \right)^2 + 2\nu R^2 \left( \frac{\partial^2 W}{\partial X^2} \frac{\partial^2 W}{\partial Y^2} \right) + R^4 \left( \frac{\partial^2 W}{\partial Y^2} \right)^2 + 2(1-\nu)R^2 \left( \frac{\partial^2 W}{\partial X \partial Y} \right)^2 + c_{kw} + c_{kg} \right] dXdY}{\int_0^1 \int_0^1 c_b \left[ W^2 + \frac{\mu}{a^2} \left( \left( \frac{\partial W}{\partial X} \right)^2 + \left( \frac{\partial W}{\partial Y} \right)^2 \right) \right] dXdY} \quad (8.1)$$

where  $\lambda^2 = \frac{\rho_0 h a^4 \omega^2}{D_0}$ ,  $c_a = (1 + pX + qX^2)$ ,  $c_b = (1 + rX + sX^2)$ ,  
 $c_{kw} = K_w \left[ W^2 + \frac{\mu}{a^2} \left( \left( \frac{\partial W}{\partial X} \right)^2 + R^2 \left( \frac{\partial W}{\partial Y} \right)^2 \right) \right]$  and

$$c_{kg} = K_g \left[ \left( \frac{\partial W}{\partial X} \right)^2 + R^2 \left( \frac{\partial W}{\partial Y} \right)^2 + \frac{\mu}{a^2} \left( \left( \frac{\partial^2 W}{\partial X^2} \right)^2 + R^2 \left( \frac{\partial^2 W}{\partial X \partial Y} \right)^2 \right) + \frac{\mu}{b^2} \left( \left( \frac{\partial^2 W}{\partial X \partial Y} \right)^2 + R^2 \left( \frac{\partial^2 W}{\partial Y^2} \right)^2 \right) \right]$$

Using orthonormal polynomials ( $\hat{\varphi}_k$ ) and simple polynomials ( $\varphi_k$ ) in Eq. (2.31) and substituting in Eq. (8.1), a generalized eigen value problem obtained as

$$[K] \{Z\} = \lambda^2 [M_a] \{Z\} \quad (8.2)$$

where  $Z$  is a column vector of constants,  $K$  and  $M_a$  are the stiffness and mass matrices given as follows

$$K(ij) = c_a \left[ \beta_{ij}^{2020} + \nu R^2 (\beta_{ij}^{2002} + \beta_{ij}^{0220}) + R^4 \beta_{ij}^{0202} + 2(1 - \nu) R^2 \beta_{ij}^{1111} + K_w \left[ \beta_{ij}^{0000} + \frac{\mu}{a^2} (\beta_{ij}^{1010} + R^2 \beta_{ij}^{0101}) \right] \right] \\ + c_a \left[ K_p \left[ \beta_{ij}^{1010} + R^2 \beta_{ij}^{0101} + \frac{\mu}{a^2} (\beta_{ij}^{2020} + R^2 \beta_{ij}^{1111}) \right] + \frac{\mu}{b^2} (\beta_{ij}^{1111} + R^2 \beta_{ij}^{0202}) \right]$$

$$M_a(ij) = c_b \left[ \beta_{ij}^{0000} + \mu \left( \frac{1}{a} \right)^2 (\beta_{ij}^{1010} + R^2 \beta_{ij}^{0101}) \right]$$

$$\text{with } \beta_{ij}^{klmna} = \int_0^1 \int_0^1 \left[ \frac{\partial^{k+l} \varphi_i}{\partial X^k \partial Y^l} \right] \left[ \frac{\partial^{m+n} \varphi_j}{\partial X^m \partial Y^n} \right] dX dY$$

## 8.1 Numerical results and discussions

Generalised eigen value problem Eq. (8.2) has been solved and eigen values of Eq. (8.2) correspond to the frequency parameters. Different sets of boundary conditions (B.cs) have been considered here with Poisson's ratio as 0.3.

### 8.1.1 Convergence

Convergence of first three frequency parameters ( $\lambda$ ) of S-S-S-S and C-C-C-C nanoplates has been shown in Table 8.1 taking  $p = 0.2, q = 0.3, r = 0.4, s = 0.5$ , aspect ratio ( $R$ ) = 1, nonlocal parameter ( $\mu$ ) =  $2nm^2$  and length ( $a$ ) =  $5nm$ . Results have been shown for  $K_w = 0$  and  $K_p = 0$ . One may see that  $n = 37$  is sufficient for computing converged results for nanoplates without elastic foundation. Again, convergence of embedded nanoplates has been shown in Table 8.2 for S-S-S-S edge condition. Numerical values of parameters are taken as  $p = q = r = s = 0.1, K_w = 200, K_p = 5, \mu = 1nm^2, a = 10nm$ . It is observed that converged results for embedded nanoplates are obtained at  $n = 46$ . It is also noticed that frequency parameters increase with mode number.

Table 8.1 Convergence of first three frequency parameters of S-S-S-S and C-C-C-C nanoplates

$n$	S-S-S-S			C-C-C-C		
	$\lambda_1$	$\lambda_2$	$\lambda_3$	$\lambda_1$	$\lambda_2$	$\lambda_3$
5	11.8785	24.3785	24.4884	19.7881	29.8410	29.9750
10	11.5401	20.9273	24.2786	19.7317	29.0494	29.1283
15	11.5366	20.9013	20.9271	19.7210	29.0469	29.1277
20	11.5366	20.8621	20.8924	19.7210	29.0402	29.1049
25	11.5366	20.8404	20.8620	19.7203	29.0265	29.1048
30	11.5366	20.8404	20.8617	19.7196	29.0264	29.1047
35	11.5366	20.8403	20.8615	19.7196	29.0248	29.1030
36	11.5366	20.8400	20.8615	19.7196	29.0247	29.1030
37	11.5366	20.8400	20.8615	19.7196	29.0247	29.1030

Table 8.2 Convergence of first three frequency parameters of S-S-S-S nanoplates

$n$	$\lambda_1$	$\lambda_2$	$\lambda_3$
10	45.6173	63.9934	107.8843
15	45.6044	63.9885	90.5544
20	45.6044	63.8730	90.5418
25	45.6044	63.8729	89.7499
30	45.6044	63.8726	89.7465
35	45.6044	63.8721	89.7464
40	45.6044	63.8721	89.7328
45	45.6044	63.8721	89.7325
46	45.6044	63.8721	89.7325

### 8.1.2 Validation

Figs. 8.1 and 8.2 show graphical comparisons of S-C-S-C nanoplates with Aksencer and Aydogdu (2011). For this comparison, we have taken  $p = q = r = s = K_w = K_p = 0$  with  $R = 1$ . In these graphs, variation of frequency ratio (associated with first two modes) with length has been given for different nonlocal parameters ( $0nm^2, 1nm^2, 2nm^2, 4nm^2$ ). One may notice that increase in nonlocal parameter decreases frequency ratio. Same observation may also be seen in Aksencer and Aydogdu (2011) and we may found a close agreement of the results. Next tabular comparison has been given in Table 8.3 with Aghababaei and Reddy (2009) for the first three frequency parameters with  $R = 1$  and  $a = 10nm$ . Results have been verified for different nonlocal parameters with the consideration of S-S-S-S edge condition.

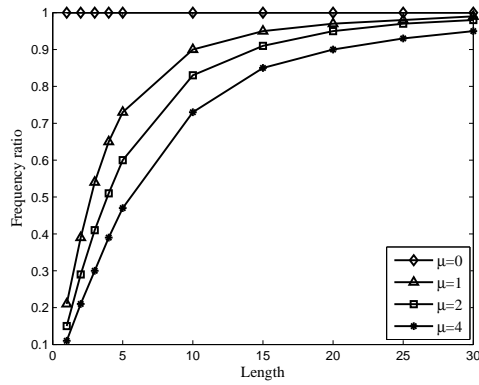


Fig. 8.1 Variation of frequency ratio with length

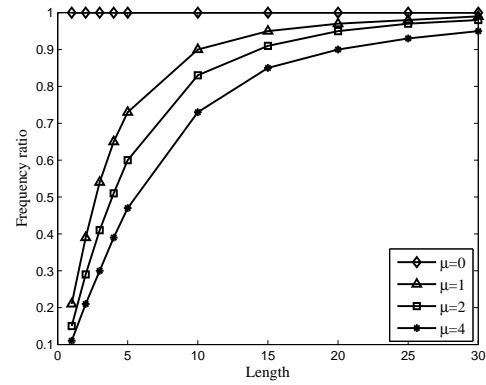


Fig. 8.2 Variation of frequency ratio with length

Table 8.3 Comparison of first three frequency parameters for S-S-S-S nanoplate

$\mu = 0$		$\mu = 1$		$\mu = 2$		$\mu = 3$		$\mu = 4$	
Present	Ref.*	Present	Ref.*	Present	Ref.*	Present	Ref.*	Present	Ref.*
0.0963	0.0963	0.0880	0.0880	0.0816	0.0816	0.0763	0.0763	0.0720	0.0720
0.3874	0.3853	0.2884	0.288	0.2402	0.2399	0.2102	0.2099	0.1892	0.1889
0.8608	0.8669	0.5167	0.5202	0.4045	0.4063	0.3435	0.3446	0.3037	0.3045

\* Aghababaei and Reddy (2009)

### 8.1.3 Effect of non-uniform parameter

In this sub-section, we have studied the effects of non-uniform parameters on the frequency parameters in the absence of elastic foundation. First, we have shown the effects of non-uniform parameters when density and Young's modulus vary quadratically. This case may be achieved by assigning zero to  $p$  and  $r$ . Variation of first three frequency parameters with  $q$  has been illustrated in Fig. 8.3 keeping  $s$  constant (0.3). Similarly, effect of  $s$  on the first three frequency parameters has been shown in Fig. 8.4 keeping  $q$  constant (0.2). In these graphs, C-C-C-C edge condition is taken into consideration and aspect ratio is taken as 2 and 3 respectively. One may see that frequency parameters decrease with  $s$  and increase with  $q$ . It is also observed that frequency parameters increase with increase in mode number.

In this paragraph, we have presented the effects non-uniform parameters when density and Young's modulus vary linearly. This is achieved by taking  $q$  and  $s$  to zero. Graphical variation of frequency parameters with  $p$  taking  $r$  constant (0.3) has been shown in Fig. 8.5. Similarly, graphical variation of frequency parameters with  $r$  taking  $p$  constant (0.2) has been shown in Fig. 8.6. In these graphs, we have considered F-F-F-F boundary condition and aspect ratio as 1. It is observed that frequency parameters decrease with  $r$  and increase with  $p$ .

Here, we have considered the effects of non-uniform parameters when Young's modulus varies linearly and density varies quadratically. This is the situation which is obtained by taking  $q$  and  $r$  as zero. Figs. 8.7 and 8.8 depict variation of frequency parameters with  $p$  and  $s$  respectively. In these graphs, C-C-C-C nanoplates with  $R = 2$  are taken into consideration. It is noticed that frequency parameters decrease with  $s$  and increase with  $p$ .

Next, we have analyzed the effects of non-uniform parameter when Young's modulus varies quadratically and density varies linearly. For this, we have taken  $p$  and  $s$  as zero. Variations of first three frequency parameters with  $q$  and  $r$  have been illustrated in Figs. 8.9 and 8.10. Results have been shown for F-F-F-F nanoplates with  $R = 1$ . In these graphs, one may see frequency parameters increase with  $q$  and decrease with  $r$ .

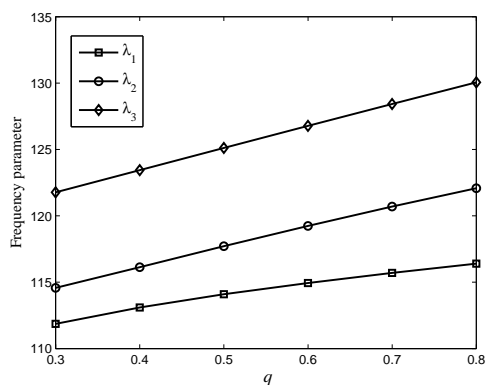


Fig. 8.3 Variation of frequency parameter with  $q$

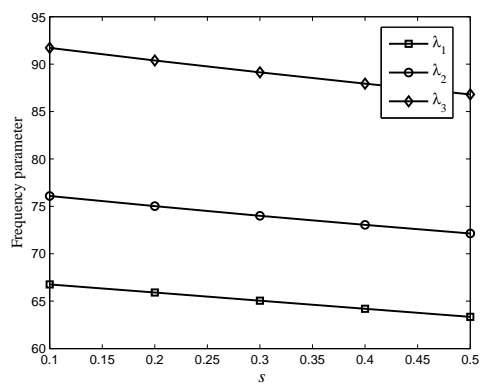


Fig. 8.4 Variation of frequency parameter with  $s$

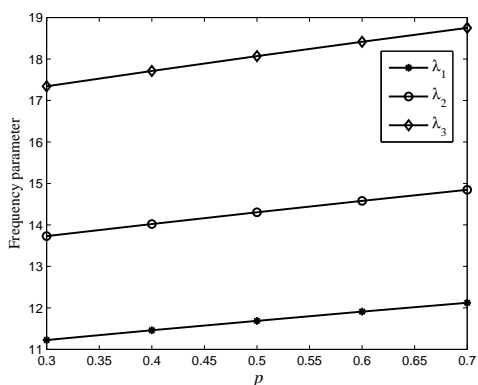


Fig. 8.5 Variation of frequency parameter with  $p$

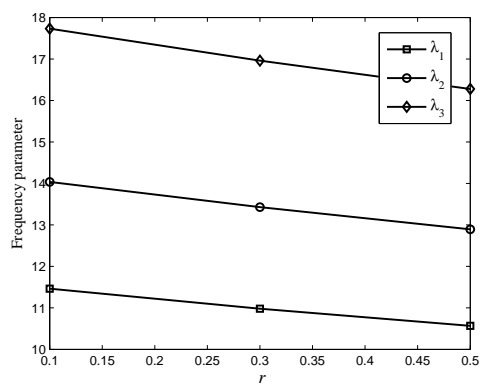


Fig. 8.6 Variation of frequency parameter with  $r$



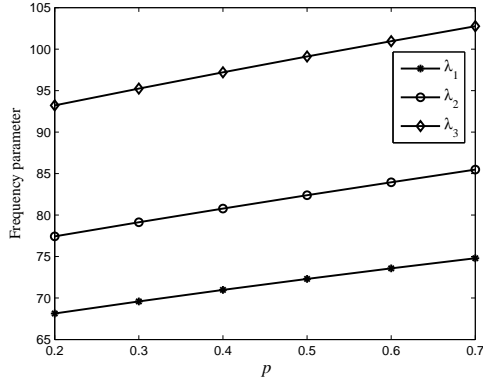


Fig. 8.7 Variation of frequency parameter with  $p$

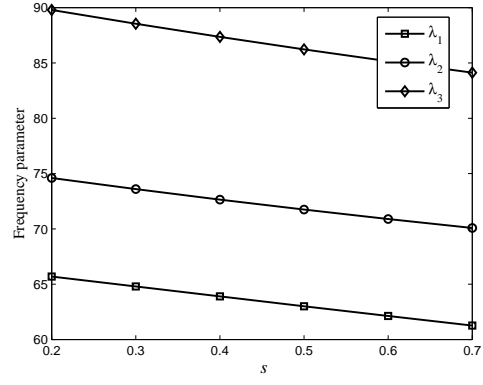


Fig. 8.8 Variation of frequency parameter with  $s$

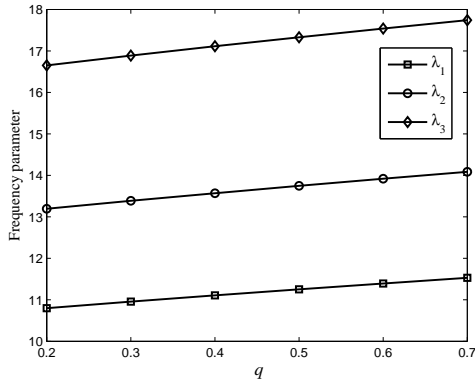


Fig. 8.9 Variation of frequency parameter with  $q$

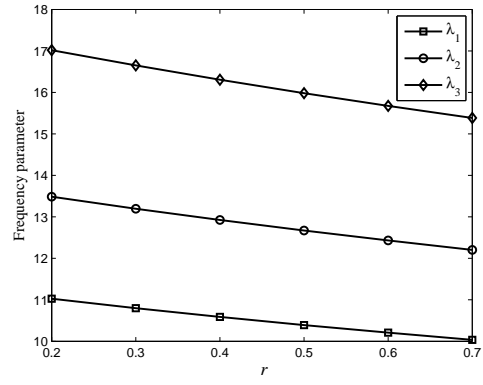


Fig. 8.10 Variation of frequency parameter with  $r$

### 8.1.4 Effect of length

To investigate the effect of length on the frequency parameters, variation of fundamental frequency parameter with length is shown in Fig. 8.11 for C-C-C-C nanoplates with  $R = 2$ ,  $p = 0.2$ ,  $q = 0.3$ ,  $r = 0.4$ ,  $s = 0.5$  in the absence of elastic foundation. Results have been shown for different values of nonlocal parameters ( $0nm^2$ ,  $0.5nm^2$ ,  $1nm^2$ ,  $2nm^2$ ,  $3nm^2$ ,  $4nm^2$ ). It is seen that frequency parameter increases with increase in length. This observation may be explained as follows. Assuming  $l_{int}$  as constant, increasing length ( $a$ ) would lead to decrease in small scale effect ( $\mu/a^2$ ). It is also noticed that frequency parameters are highest in case of  $\mu = 0$  and goes on decreasing with increase in nonlocal parameter. This fact may also be explained in terms of relative error percent. Let us define the relative error percent (REP) as

$$REP = \frac{|\text{Local Result} - \text{Nonlocal Result}|}{|\text{Local Result}|} \times 100$$

Neglecting nonlocal effect, relative error percents of fundamental frequency parameter for  $a = 3nm$  and  $a = 25nm$  with  $\mu = 3nm^2$  are 78.6753% and 12.0950% respectively. From this, we may also say that nonlocal theory should be taken into account for vibration analysis

of small nanoplates.

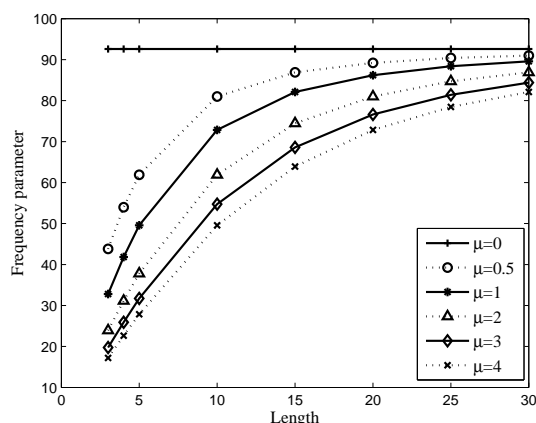


Fig. 8.11 Variation of fundamental frequency parameter with length

### 8.1.5 Effect of aspect ratio

In this subsection, we have considered effect of aspect ratio on the frequency parameters in the absence of elastic foundation. Fig. 8.12 shows the effect of fundamental frequency parameter of S-C-S-C nanoplate with aspect ratio taking  $a = 10nm$ ,  $p = 0.1$ ,  $q = 0.2$ ,  $r = 0.3$ ,  $s = 0.4$ . It is seen that nonlocal effect on the frequency parameters is more prominent in greater values of aspect ratio. This is due to the fact that for a particular length of nanoplates, increase in aspect ratio would lead to smaller nanoplates which in turn leads to increase in small scale effect. It is also observed that frequency parameter increases with aspect ratio. One may notice that frequency parameter decreases with increase in nonlocal parameter. As the nonlocal parameter increases, frequency parameters obtained from nonlocal plate theory become smaller than those of its local counterpart. This reduction is clearly seen in case of higher vibration modes. Effect of nonlocal parameter is seen more in case of higher aspect ratios. This fact may also be explained in terms of relative error percent. Neglecting nonlocal effect, the relative error percents for aspect ratios 1 and 3 with  $\mu = 3nm^2$  are 22.5041% and 54.9963% respectively. This shows that, nonlocal theory should be considered for free vibration of nanoplates with high aspect ratios.

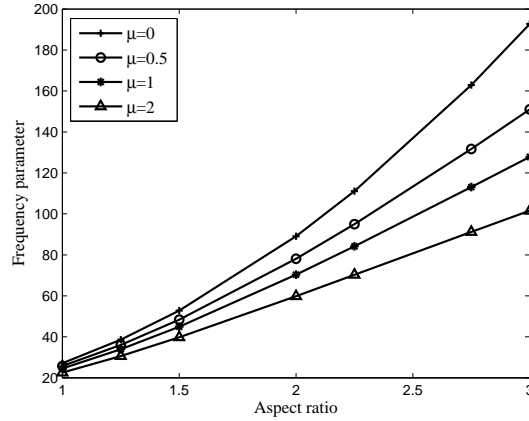


Fig. 8.12 Variation of frequency parameter with aspect ratio

### 8.1.6 Effect of nonlocal parameter

Here, we have examined the effect of nonlocal parameter on the frequency parameters in the absence of elastic foundation. Variation of frequency ratio (associated with first four mode) with nonlocal parameter has been illustrated in Fig. 8.13 for S-C-S-C edge condition. In this graph, we have taken  $a = 5nm$ ,  $R = 1$ ,  $p = 0.1$ ,  $q = 0.2$ ,  $r = 0.3$ ,  $s = 0.4$ . It is clearly seen from the figure that frequency ratio is less than unity. This implies that application of local beam model for vibration analysis of graphene sheets would lead to over prediction of the frequency. Hence, nonlocal beam theory should be used for better predictions of frequencies of nanoplates. Neglecting nonlocal effect, the relative error percents for first and fourth mode number of S-C-S-C nanoplates with  $\mu = 0.5nm^2$ ,  $R = 1$ ,  $a = 5nm$  are found to be 15.3605% and 37.8513% respectively. This shows nonlocal effect on the frequency parameters is more in higher modes.

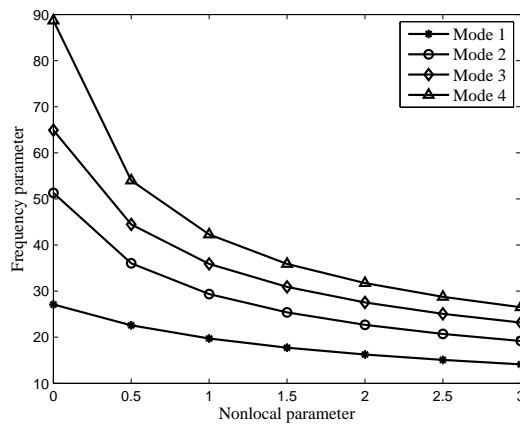


Fig. 8.13 Variation of frequency parameter with nonlocal parameter

### 8.1.7 Effect of elastic foundation

In this subsection, effect of Winkler and Pasternak elastic foundations on the fundamental frequency parameter of embedded nanoplate has been investigated. One may note from Eq. (8.2) that the effects of elastic foundation enter through the stiffness matrix of the nanoplate i.e.  $[K]$ . Therefore, total stiffness of the embedded nanoplate increases as the stiffness of the elastic foundation increases. This trend has been shown in Figs. 8.14 and 8.15 for for the springy and shear effect of the elastic foundation respectively. Numerical values of the parameters are taken as  $p = q = r = s = 0.1, a = 10nm, R = 2$ . In Fig. 8.14, we have considered  $K_p = 0$  with C-C-C-C edge condition while in Fig. 8.15, we have taken  $K_w = 0$  with S-S-S-S edge condition. Results have been given for different values of nonlocal parameters. It is observed from these figures that fundamental frequency parameter increases linearly by increasing the stiffness of the elastic foundation either through the springy (Winkler coefficient) or the shear effect (Pasternak coefficient).

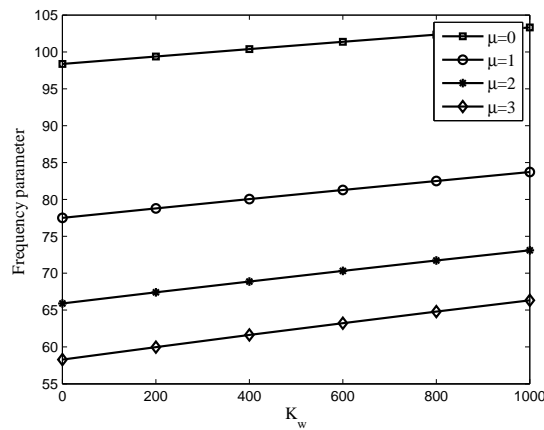


Fig. 8.14 Effect of Winkler coefficient on frequency parameter

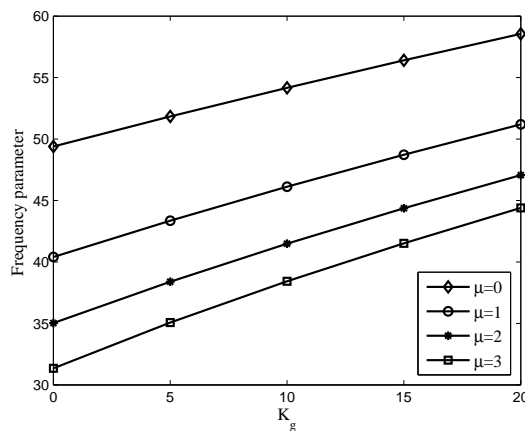


Fig. 8.15 Effect of Pasternak coefficient on frequency parameter

### 8.1.8 Mode shapes

First four mode shapes of F-C-F-C and F-S-F-S nanoplates are given respectively in Figs. 8.16-8.17 with  $\mu = 1nm^2$ ,  $a = 10nm$ ,  $R = 2$ ,  $p = q = r = s = 0.1$ .

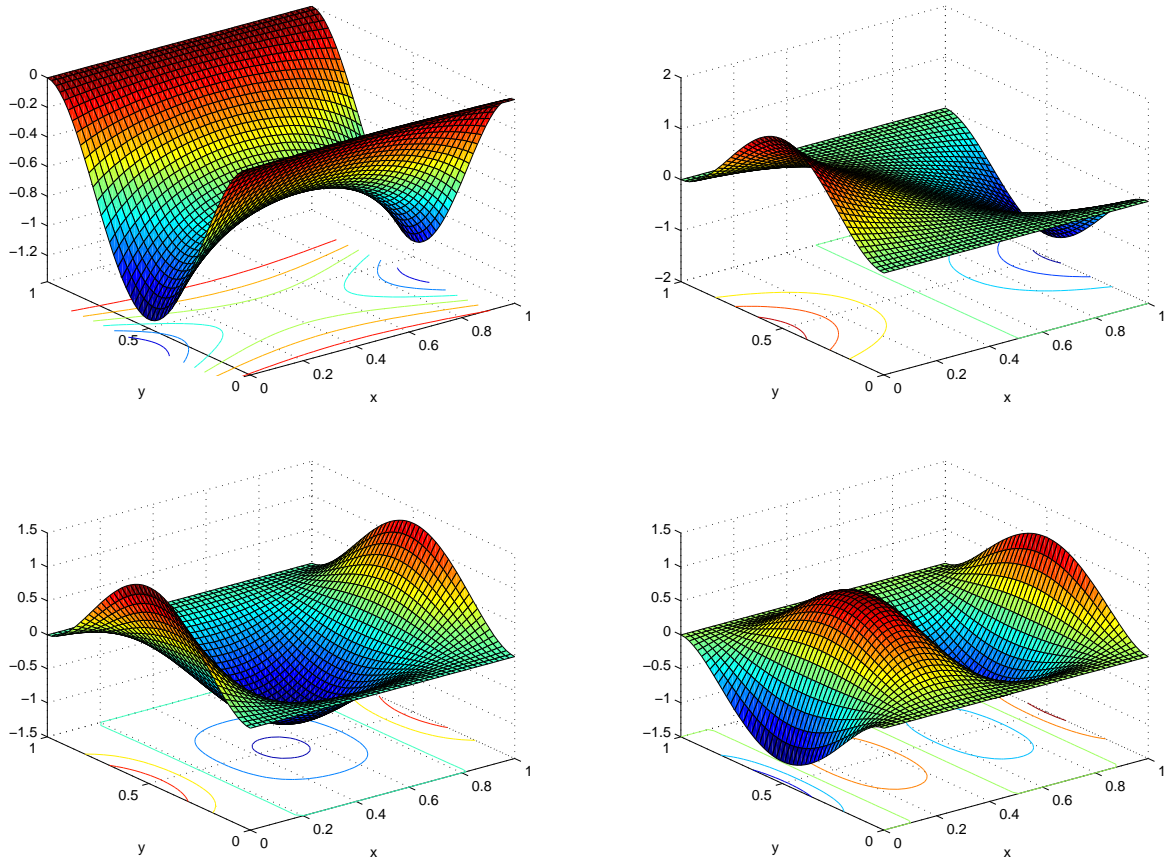


Fig. 8.16 First four deflection shapes of F-C-F-C nanoplates

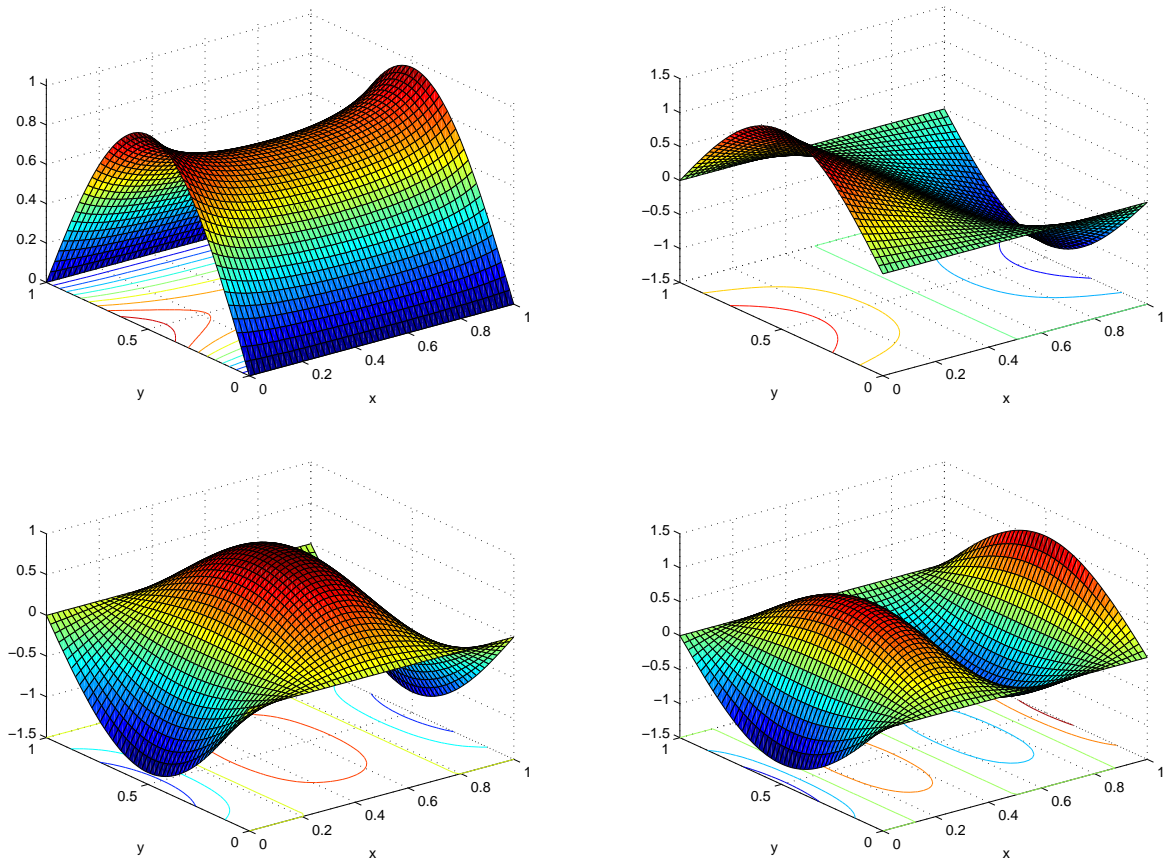


Fig. 8.17 First four deflection shapes of F-S-F-S nanoplates

## 8.2 Conclusion

Rayleigh-Ritz method has been applied to study free vibration of embedded isotropic rectangular nanoplates based on classical plate theory. It is observed that frequency parameters increase with length, Winkler and Pasternak coefficients and also with aspect ratio. Nonlocal elasticity theory should be considered for vibration of nanoplates having high aspect ratio. Similarly, nonlocal elasticity theory should also be considered for vibration of nanoplates having small length. One of the important observation seen that nonlocal effect is more in higher modes.

# **Chapter 9**

## **Conclusions and future directions**

# Chapter 9

## Conclusions and future directions

In view of the present study on bending, buckling and vibration of nanobeams and nanoplates, conclusions are drawn and finally, recommendation for future work is also incorporated here. In this investigation, nonlocal elasticity theory has been applied in all of the problems. The main purpose of this study has been to develop computationally efficient numerical methods for handling the above said problems. As such, boundary characteristic orthogonal polynomials have been used as shape functions in the Rayleigh-Ritz method to investigate bending, vibration and buckling analyses of nanobeams and nanoplates. Similarly, Chebyshev polynomials have been implemented in the Rayleigh-Ritz method to study vibration and buckling analyses of Timoshenko nanobeams embedded in elastic foundation. Next, differential quadrature method has been implemented in the buckling and vibration of nanobeams with and without elastic foundation. All the problems are computationally solved by using MATLAB.

In the following paragraphs, conclusions are drawn with respect to various methods and the application problems mentioned in previous Chapters.

### 9.1 Conclusions

- First two chapters give background of nanostructures and numerical methods such as Rayleigh-Ritz and differential quadrature. The novelty of the Rayleigh-Ritz method has been to handle any sets of boundary conditions by the chosen shape functions. Bending and buckling analyses of nanobeams have been investigated in Chapter 3. Non-dimensional maximum deflection has been obtained at the center of beam. It has been concluded that deflection is strongly dependent on the aspect ratio in case of nonlocal EBT and TBT.

Non-uniformity is assumed in the buckling analysis by taking exponential variation of flexural rigidity. New results have been presented for two types of boundary conditions such as guided and simply supported-guided. Four types of beam theories have been



considered here. Among these considered beam theories, Euler-Bernoulli beam theory would lead to over prediction of the buckling loads than other types of beam theories. Parametric studies such as effects of non-uniform parameter, nonlocal parameter, aspect ratio, boundary condition and beam theories on the critical buckling load parameter have been carried out systematically. It is found that critical buckling load decreases with increase in non-uniform as well as nonlocal parameters while critical buckling load increases with increase in aspect ratio. C-C nanobeams are found to have highest buckling loads than other types of boundary conditions. It is observed that bending responses increase with scale coefficient while buckling loads decrease with scale coefficient.

- Effects of Winkler and Pasternak coefficients of the elastic foundation on the critical buckling load and frequency parameters have been investigated under the influence of temperature in Chapter 3 and 5 respectively. It is observed that the increase of critical buckling load and frequency parameters with Pasternak foundation is linear in nature while this increasing trend is nonlinear in case of Winkler foundation. In low temperature environment, buckling load and frequency increase with increase in temperature while in high temperature environment, buckling load and frequency decrease with increase in temperature. It may also be seen that for larger temperature change, the rate of increase of buckling load ratio is less compared to smaller temperature change.
- In Chapter 4, bending analysis has been carried out for isotropic nanoplate and buckling analysis has been investigated for orthotropic nanoplate. Convergence study has been done to find minimum number of terms required to get desirable results. Effects of length, nonlocal parameter and aspect ratio on the non-dimensional maximum deflection have been systematically discussed. It is observed that deflection ratio increases with increase in aspect ratio. One of the interesting behavior may be noticed in this chapter that non-dimensional maximum deflection increases with increase in nonlocal parameter. Parametric studies are done to know the effects of length, nonlocal parameter, aspect ratio, stiffness ratio and elastic foundation on the buckling load. It may be noted from these investigations that buckling load ratio decreases with increase in stiffness ratio and elastic coefficients but buckling load ratio decreases with increase in nonlocal parameter.
- Vibration of nanobeams has been investigated in Chapter 5 to compute vibration characteristics of Euler-Bernoulli and Timoshenko nonlocal beam theories. Boundary characteristic orthogonal polynomials have been used as shape functions in the Rayleigh-Ritz method. Use of orthonormality makes computations easier. This is because of the fact that some of the entries of stiffness and mass matrices become either zero or one due to orthonormality. Results have been reported for new boundary conditions viz. S-F and F-F. Graphical results have been presented to show variation of frequency parameter with scaling effect parameter. Next, we have used differential quadrature (DQ) method

for vibration analysis of nanobeams based on four types of beam theories such as Euler-Bernoulli, Timoshenko, Reddy and Levinson. In DQ method, differential equations are converted into single unknown variable and boundary conditions have been implemented in the coefficient matrices. As such, modified coefficient matrices for different boundary conditions have been shown. Among the considered beam theories, Euler-Bernoulli nanobeams show over prediction of frequency parameters. This is due to the fact that in EBT, transverse shear stress and strain are not considered. We may conclude from this analysis that the effects of transverse shear deformation and rotary inertia would lead to reduction of frequencies. The reduction is clearly seen at higher modes and also at small aspect ratio. It is also found that the effect of nonlocal parameter is more in higher modes. Frequency parameters associated with higher mode for some of the beam theories in literatures are not reported. As such, we have computed the higher mode for Reddy and Levinson nonlocal beam theories. Another interesting observation is that fundamental frequency parameter of cantilever nanobeams do not decrease with increase in nonlocal parameter.

- The literature reveals that previous studies done in nanobeams are mostly with constant parameters like  $E$  and  $\rho$ . But in actual practice, there may be a variation in these parameters. Structural members with non-uniform material properties are frequently used in engineering applications to satisfy various requirements. As such, we have investigated non-uniform variation of Young's modulus and density in Chapter 6. Non-uniformity is assumed to arise due to linear and quadratic variations in Young's modulus and density of nanobeams with space coordinate. Possible cases of such linear and quadratic variations have been considered and discussed. Variation of non-uniform parameters on the frequency parameter is depicted in term of plots. It is noticed that frequency parameters are highest in C-C and lowest in C-F than other boundary conditions for a particular set of nonhomogeneity parameters. So it may depend upon the application where design engineers may need such desired frequency parameters.
- Vibration of rectangular nanoplate has been studied in Chapter 7 based on classical plate theory in conjunction with nonlocal elasticity theory of Eringen. Present results have been compared with available exact solutions for S-S-S-S boundary condition in graphical form and are found to be in good agreement. Variation of frequency parameters with nonlocal parameter, length and aspect ratio has been presented for different boundary conditions at the edges. Three-dimensional mode shapes have also been presented for some of the boundary conditions.
- Investigation on vibration of nanoplates with complicating effects such as non-uniformity and elastic foundation has been done in chapter 8. Non-uniformity is assumed by taking linear and quadratic variations of Young's modulus and density along space coordinate.

Various possible cases of such variations have been investigated. Comparison has been made in special cases. Effects of non-uniform parameters and Winkler as well as Pasternak coefficients have been depicted in term of plots. Various parametric studies have been carried out. It is observed that frequency parameters increase with length, Winkler as well as Pasternak coefficients and aspect ratio.

## 9.2 Future directions

Although exhaustive investigations are done related to the titled problems but there are still some gaps which are the future directions of the present research. Accordingly few of them are mentioned below:

- Nonlocal elasticity theory may be applied to other types of nanostructures such as nanorods and nanosheets with various complicating effects.
- Suitable numerical methods may also be developed for handling non-classical boundary conditions.
- It is found that most of analytical solutions have been presented for simply-supported edge condition. As such, one may also try to develop analytical solutions for other boundary conditions.
- Mostly, differential quadrature method has been applied for S-S, C-S, C-C and C-F edge conditions. Accordingly, one may develop procedures for handling other sets of boundary conditions.
- Other orthogonal polynomials such as legendre may also be used in the Rayleigh-Ritz method.
- Rayleigh-Ritz method may also be applied in vibration, bending and buckling analyses of nanoplates based on advanced plate theories such as refined plate theory .
- It may also be interesting to apply differential quadrature method in nanoplates subjected to all sets of classical boundary conditions.
- Other complicating effects such as nonlinearity, piezoelectric, electromagnetic etc. may be included in the present analysis.
- Static and vibration of nanobeams and nanoplates with some of the shapes such as elliptic, triangular, circular and annular etc. may also be done using nonlocal elasticity theory.

# References

# References

- [1] Adali, S. (2012) Variational principles for nonlocal continuum model of orthotropic graphene sheets embedded in an elastic medium, *Acta Mathematica Scientia*, 32, 325-338.
- [2] Aghababaei, R., Reddy, J. N. (2009) Nonlocal third-order shear deformation plate theory with application to bending and vibration of plates, *Journal of Sound and Vibration*, 326, 277-289.
- [3] Aksencer, T., Aydogdu, M. (2011) Levy type solution method for vibration and buckling of nanoplates using nonlocal elasticity theory, *Physica E*, 43, 954-959.
- [4] Aksencer, T., Aydogdu, M. (2012) Forced transverse vibration of nanoplates using nonlocal elasticity theory, *Physica E*, 44, 1752-1759.
- [5] Alibeigloo, A., Zanoosi, A., Pasha, A. (2013) Static analysis of rectangular nano-plate using three-dimensional theory of elasticity, *Applied Mathematical Modelling*, 37, 7016-7026.
- [6] Alshorbagy, A. E., Eltaher, M. A., Mahmoud, F. F. (2013) Static analysis of nanobeams using nonlocal FEM, *Journal of Mechanical Science and Technology*, 27, 2035-2041 .
- [7] Alzahrani, E. O., Zenkour, A. M., Sobhy, M. (2013) Small scale effect on hygro-thermo-mechanical bending of nanoplates embedded in an elastic medium, *Composite Structures*, 105, 163-172.
- [8] Amirian, B., Hosseini-Ara, R., Moosavi, H. (2013) Thermal vibration analysis of carbon nanotubes embedded in two-parameter elastic foundation based on nonlocal Timoshenko's beam theory, *Archives of Mechanics*, 64, 581-602.
- [9] Analooei, H., Azhari, M., Heidarpour, A. (2013) Elastic buckling and vibration analyses of orthotropic nanoplates using nonlocal continuum mechanics and spline finite strip method, *Applied Mathematical Modelling*, 37, 6703-6717.
- [10] Anjomshoa, A., Shahidi, A., Hassani, B., Omehzadeh, E. J. (2014) Finite element buckling analysis of multi-layered graphene sheets on elastic substrate based on nonlocal elasticity theory, *Applied Mathematical Modelling*, 38, 5934-5955.

- [11] Anjomshoa, A. (2013) Application of Ritz functions in buckling analysis of embedded orthotropic circular and elliptical micro/nano-plates based on nonlocal elasticity theory, *Meccanica*, 48, 1337-1353.
- [12] Ansari, R., Sahmani, S. (2012) Small scale effect on vibrational response of single-walled carbon nanotubes with different boundary conditions based on nonlocal beam models, *Communications in Nonlinear Science and Numerical Simulation*, 17, 1965-1979.
- [13] Ansari, R., Gholami, R., Darabi, M. (2011) Thermal buckling analysis of embedded single-walled carbon nanotubes with arbitrary boundary conditions using the nonlocal timoshenko beam theory, *Journal of Thermal Stresses*, 34, 1271-1281.
- [14] Ansari, R., Sahmani, S. (2011) Bending behavior and buckling of nanobeams including surface stress effects corresponding to different beam theories, *International Journal of Engineering Science*, 49, 1244-1255.
- [15] Ansari, R., Sahmani, S., Rouhi, H. (2011a) Axial buckling analysis of single-walled carbon nanotubes in thermal environments via the rayleigh-ritz technique, *Computational Materials Science*, 50, 3050-3055.
- [16] Ansari, R., Sahmani, S., Rouhi, H. (2011b) Rayleigh-ritz axial buckling analysis of single-walled carbon nanotubes with different boundary conditions, *Physics Letters A*, 375, 1255-1263.
- [17] Ansari, R., Ramezannezhad, H. (2011) Nonlocal Timoshenko beam model for the large-amplitude vibrations of embedded multiwalled carbon nanotubes including thermal effects, *Physica E*, 43, 1171-1178.
- [18] Ansari, R., Sahmani, S. (2013) Prediction of biaxial buckling behavior of single-layered graphene sheets based on nonlocal plate models and molecular dynamics simulations, *Applied Mathematical Modelling*, 37, 7338-7351.
- [19] Asghari, M., Kahrobaiyan, M. H., Ahmadian, M. T. (2010) A nonlinear Timoshenko beam formulation based on the modified couple stress theory. *International Journal of Engineering Science*, 48, 1749-1761.
- [20] Aydogdu, M. (2009) A general nonlocal beam theory: Its application to nanobeam bending, buckling and vibration, *Physica E*, 41, 1651-1655.
- [21] Bedroud, M., Hosseini, H. S., Nazemnezhad, R. (2013) Buckling of circular or annular Mindlin nanoplates via nonlocal elasticity, *Acta Mechanica*, 224, 2663-2676.
- [22] Behera, L., Chakraverty, S. (2014a) Free vibration of Euler and Timoshenko nanobeams using boundary characteristic orthogonal polynomials, *Applied Nanoscience*, 4, 347-358.

- [23] Behera, L., Chakraverty, S. (2014b) Free vibration of nonhomogeneous timoshenko nanobeams, *Meccanica*, 49, 51-67.
- [24] Benzair, A., Tounsi, A., Besseghier, A., Heireche, H., Moulay, N., Boumia, L. (2008) The thermal effect on vibration of single-walled carbon nanotubes using nonlocal timoshenko beam theory, *Journal of Physics D: Applied Physics*, 41, 225-404.
- [25] Bhat, R. B. (1985) Plate deflections using orthogonal polynomials, *Journal of Engineering Mechanics*, 111, 1301-1309.
- [26] Bhat, R. B. (1991) Vibration of rectangular plates on point and line supports using characteristic orthogonal polynomials in the Rayleigh-Ritz method, *Journal of Sound and Vibration*, 149, 170-172.
- [27] Chakraverty, S. (2009) *Vibration of plates*, CRC Press, Taylor and Francis Group.
- [28] Chakraverty, S., Behera, L. (2014) Free vibration of rectangular nanoplates using rayleigh-ritz method, *Physica E*, 56, 357-363.
- [29] Chakraverty, S., Petyt, M. (1997) Natural frequencies for free vibration of nonhomogeneous elliptic and circular plates using two-dimensional orthogonal polynomials, *Applied Mathematical Modelling*, 21, 399-417.
- [30] Chakraverty, S., Bhat, R. B., Stiharu, I. (1999) Recent research on vibration of structures using boundary characteristic orthogonal polynomials in the Rayleigh-Ritz method, *The Shock and Vibration Digest*, 31, 187-194.
- [31] Chakraverty, S., Jindal, R., Agarwal, V. K. (2007) Effect of non-homogeneity on natural frequencies of vibration of elliptic plates, *Meccanica*, 42, 585-599.
- [32] Civalek, Ö., Akgöz, B. (2009) Static analysis of single walled carbon nanotubes based on Eringen's nonlocal elasticity theory, *International Journal of Engineering and Applied Sciences*, 1, 47-56.
- [33] Civalek, Ö., Demir, C. (2011) Buckling and bending analyses of cantilever carbon nanotubes using the Euler-Bernoulli beam theory based on non-local continuum model, *Asian Journal of Civil Engineering (Building and Housing)*, 12, 651-661.
- [34] Danesh, M., Farajpour, A., Mohammadi, M. (2012) Axial vibration analysis of a tapered nanorod based on nonlocal elasticity theory and differential quadrature method, *Mechanics Research Communications*, 39, 23-27.
- [35] Dickinson, S. M. (1978) The buckling and frequency of flexural vibration of rectangular isotropic and orthotropic plates using Rayleigh's Method, *Journal of Sound and Vibration*, 61, 1-8.

- [36] Eltaher, M. A., Emam, S. A., Mahmoud, F. F. (2012) Free vibration analysis of functionally graded size-dependent nanobeams, *Applied Mathematics and Computation*, 218, 7406-7420.
- [37] Eltaher, M. A., Emam, S. A., Mahmoud, F. F. (2013a) Static and stability analysis of nonlocal functionally graded nanobeams, *Composite Structures*, 96, 82-88.
- [38] Eltaher, M. A., Alshorbagy, A. E., Mahmoud F. F. (2013b) Vibration analysis of Euler-Bernoulli nanobeams by using finite element method, *Applied Mathematical Modelling*, 37, 4787-4797.
- [39] Emam, S. A. (2013) A general nonlocal nonlinear model for buckling of nanobeams, *Applied Mathematical Modelling*, 37, 6929-6939.
- [40] Eringen, A. C. (1972) Nonlocal polar elastic continua, *International Journal of Engineering Science*, 10, 1-16.
- [41] Ehteshami, H., Hajabasi, M. A. (2011) Analytical approaches for vibration analysis of multi-walled carbon nanotubes modeled a smultiple nonlocal Euler beams, *Physica E*, 44, 270-285.
- [42] Farajpour, A., Danesh, M., Mohammadi, M. (2011) Buckling analysis of variable thickness nanoplates using nonlocal continuum mechanics, *Physica E*, 44, 719-727.
- [43] Ghannadpour, S. A. M., Mohammadi, B. (2010) Buckling analysis of micro and nanorods/tubes based on nonlocal Timoshenko beam theory using Chebyshev polynomials, *Advanced Materials Research*, 123, 619-622.
- [44] Ghannadpour, S. A. M., Mohammadi, B., Fazilati, J. (2013) Bending, buckling and vibration problems of nonlocal Euler beams using Ritz method, *Composite Structures*, 96, 584-589.
- [45] Hadjesfandiari, A. R., Dargush, G. F. (2011) Couple stress theory for solids, *International Journal of Solids and Structures*, 48, 2496-2510.
- [46] Hashemi, S. H., Samaei, A. T. (2011) Buckling analysis of micro/nanoscale plates via nonlocal elasticity theory, *Physica E*, 43, 1400-1404.
- [47] Janghorban, M. (2012) Static analysis of tapered nanowires based on nonlocal Euler-Bernoulli beam theory via differential quadrature method, *Latin American Journal of Solids and Structures*, 1, 1-10.
- [48] Janghorban, M., Zare, A. (2011) Free vibration analysis of functionally graded carbon nanotubes with variable thickness by differential quadrature method, *Physica E*, 43, 1602-1604.



- [49] Jomehzadeh, E., Saidi, A. R. (2012) Study of Small Scale Effect on Nonlinear Vibration of Nano-Plates, *Journal of Computational and Theoretical Nanoscience*, 9, 864-871.
- [50] Kananipour, H. (2014) Static analysis of nanoplates based on the nonlocal Kirchhoff and Mindlin plate theories using DQM, *Latin American Journal of Solids and Structures*, 11, 1709-1720.
- [51] Ke, L., Xiang, Y., Yang, J., Kitipornchai, S. (2009) Nonlinear free vibration of embedded double-walled carbon nanotubes based on nonlocal timoshenko beam theory, *Computational Materials Science*, 47, 409-417.
- [52] Kiani, K. (2011) Small-scale effect on the vibration of thin nanoplates subjected to a moving nanoparticle via nonlocal continuum theory, *Journal of Sound and Vibration*, 330, 4896-4914.
- [53] Kumar, D., Heinrich, C., Waas, A. M. (2008) Buckling analysis of carbon nanotubes modeled using nonlocal continuum theories, *Journal of Applied Physics*, 103, 073521.
- [54] Lee, H. L., Chang W.J. (2009) A closed-form solution for critical buckling temperature of a single-walled carbon nanotube, *Physica E*, 41, 1492-1494.
- [55] Liu, C., Ke, L., Wang, Y. S., Yang, J., Kitipornchai, S. (2013) Thermo-electro-mechanical vibration of piezoelectric nanoplates based on the nonlocal theory, *Composite Structures*, 106, 167-174.
- [56] Loya, J., López-Puente, J., Zaera, R., Fernández-Sáez, J. (2009) Free transverse vibrations of cracked nanobeams using a nonlocal elasticity model, *Journal of Applied Physics*, 105, 044309
- [57] Lu, P., Lee, H., Lu, C., Zhang, P. (2006) Dynamic properties of flexural beams using a nonlocal elasticity model, *Journal of Applied Physics*, 99, 073510.
- [58] Lu, P., Lee, H. P., Lu, C., Zhang, P. Q. (2007) Application of nonlocal beam models for carbon nanotubes, *International Journal of Solids and Structures*, 44, 5289-5300.
- [59] Maachou, M., Zidour, M., Baghdadi, H., Ziane, N., Tounsi, A. (2011) A nonlocal levinson beam model for free vibration analysis of zigzag single-walled carbon nanotubes including thermal effects, *Solid State Communications*, 151, 1467-1471.
- [60] Mahmoud, F. F., Eltahir, M. A., Alshorbagy, A. E., Meletis, E. I. (2012) Static analysis of nanobeams including surface effects by nonlocal finite element, *Journal of Mechanical Science and Technology*, 26, 3555-3563.

- [61] Malekzadeh, P., Setoodeh, A. R., Beni, A. A. (2011a) Small scale effect on the free vibration of orthotropic arbitrary straight-sided quadrilateral nanoplates, *Composite Structures*, 93, 1631-1639.
- [62] Malekzadeh, P., Setoodeh, A. R., Beni, A. (2011b) Small scale effect on the thermal buckling of orthotropic arbitrary straight-sided quadrilateral nanoplates embedded in an elastic medium, *Composite Structures*, 93, 2083-2089.
- [63] Malekzadeh, P., Shojaee, M. (2013) Free vibration of nanoplates based on a nonlocal two-variable refined plate theory, *Composite Structures*, 95, 443-452.
- [64] Mohammadi, B., Ghannadpour, S. (2011) Energy approach vibration analysis of nonlocal Timoshenko beam theory, *Procedia Engineering*, 10, 1766-1771.
- [65] Murmu, T., Adhikari, S. (2010a) Nonlocal transverse vibration of double-nanobeam-systems, *Journal of Applied Physics*, 108, 083514.
- [66] Murmu, T., Adhikari, S. (2010b) Scale-dependent vibration analysis of prestressed carbon nanotubes undergoing rotation, *Journal of Applied Physics*, 8, 123507.
- [67] Murmu, T., Adhikari, S. (2009) Small-scale effect on the vibration of nonuniform nanocantilever based on nonlocal elasticity theory, *Physica E*, 41, 1451-1456.
- [68] Murmu, T., Pradhan, S. C. (2009a) Thermo-mechanical vibration of a single-walled carbon nanotube embedded in an elastic medium based on nonlocal elasticity theory, *Computational Materials Science*, 46, 854-859.
- [69] Murmu, T., Pradhan, S. C. (2009b) Buckling analysis of a single-walled carbon nanotube embedded in an elastic medium based on nonlocal elasticity and timoshenko beam theory and using dqm, *Physica E*, 41, 1232-1239.
- [70] Murmu, T., Pradhan, S. C. (2009c) Vibration analysis of nanoplates under uniaxial prestressed conditions via nonlocal elasticity, *Journal of Applied Physics*, 106, 104301.
- [71] Murmu, T., Pradhan, S. C. (2009d) vibration analysis of nano-single layered graphene sheets embedded in elastic medium based on nonlocal elasticity theory, *Journal of Applied Physics*, 105, 06431
- [72] Murmu, T., Pradhan, S. C. (2010) Thermal effects on the stability of embedded carbon nanotubes, *Computational Materials Science*, 47, 721-726.
- [73] Mustapha, K. B., Zhong, Z. W. (2010) Free transverse vibration of an axially loaded non-prismatic single-walled carbon nanotube embedded in a two-parameter elastic medium, *Computational Materials Science*, 50, 742-751.

- [74] Naderi, A., Saidi, A. R. (2014) Modified nonlocal Mindlin plate theory for buckling analysis of nanoplates, *Journal of Nanomechanics and Micromechanics*, 4, 2153-5477.
- [75] Nami, M. R., Janghorban, M. (2013) Static analysis of rectangular nanoplates using trigonometric shear deformation theory based on nonlocal elasticity theory, *Beilstein Journal of Nanotechnology*, 4, 968-973.
- [76] Nami, M. R., Janghorban M. (2014) Static analysis of rectangular nanoplates using exponential shear deformation theory based on strain gradient elasticity theory, *Iranian Journal of Materials Forming*, 1, 1-13.
- [77] Narendar, S., Gopalakrishnan, S. (2011) Critical buckling temperature of single-walled carbon nanotubes embedded in a one-parameter elastic medium based on nonlocal continuum mechanics, *Physica E*, 43, 1185-1191.
- [78] Narendar, S. (2011) Buckling analysis of micro-/nano-scale plates based on two-variable refined plate theory incorporating nonlocal scale effects, *Composite Structures*, 93, 3093-3103.
- [79] Narendar, S., Gopalakrishnan, S. (2012) Scale effects on buckling analysis of orthotropic nanoplates based on nonlocal two-variable refined plate theory, *Acta Mechanica*, 223, 395-413.
- [80] Nix, W. D., Gao, H. (1998) Indentation size effects in crystalline materials: A law for strain gradient plasticity, *Journal of the Mechanics and Physics of Solids*, 46, 411-425.
- [81] Peddieson, J., Buchanan, G. R., McNitt, R. P. (2003) Application of nonlocal continuum models to nanotechnology, *International Journal of Engineering Science*, 41, 305-312.
- [82] Phadikar, J. K., Pradhan, S. C. (2010) Variational formulation and finite element analysis for nonlocal elastic nanobeams and nanoplates, *Computational Materials Science*, 49, 492-499.
- [83] Pradhan, S. C. (2012) Buckling analysis and small scale effect of biaxially compressed graphene sheets using non-local elasticity theory, *Sadhana*, 37, 461-480.
- [84] Pradhan, S. C. (2009) Buckling of single layer graphene sheet based on nonlocal elasticity and higher order shear deformation theory, *Physics Letters A*, 373, 4182-4188.
- [85] Pradhan S. C., Murmu T. (2010a) Small scale effect on the buckling analysis of single-layered graphene sheet embedded in an elastic medium based on nonlocal plate theory, *Physica E*, 42, 1293-1301.
- [86] Pradhan, S. C., Murmu, T. (2010b) Application of nonlocal elasticity and dqm in the flapwise bending vibration of a rotating nanocantilever, *Physica E*, 42, 1944-1949.

- [87] Pradhan, S. C., Phadikar, J. K. (2009a) Bending, buckling and vibration analyses of non-homogeneous nanotubes using GDQ and nonlocal elasticity theory, *Structural Engineering and Mechanics*, 33, 193-213.
- [88] Pradhan, S. C., Phadikar, J. K. (2009b) Nonlocal elasticity theory for vibration of nanoplates, *Journal of Sound and Vibration*, 325, 206-223.
- [89] Pradhan, S. C., Reddy, G. (2011) Buckling analysis of single walled carbon nanotube on winkler foundation using nonlocal elasticity theory and dtm, *Computational Materials Science*, 50, 1052-1056.
- [90] Quan, J, Chang, C. (1989) New insights in solving distributed system equations by the quadrature method-I, *Computers and Chemical Engineering*, 13, 779-788.
- [91] Rafiei, M., Mohebpour, S. R., Daneshmand, F. (2012) Small-scale effect on the vibration of non-uniform carbon nanotubes conveying fluid and embedded in viscoelastic medium, *Physica E*, 44, 1372-1379
- [92] Ravari, M. R. K., Shahidi, A. R. (2013) Axisymmetric buckling of the circular annular nanoplates using finite difference method, *Meccanica*, 48, 135-144.
- [93] Reddy, J. N. (1997) *Mechanics of Laminated Composite Plates: Theory and Analysis*, CRC Press, Boca Raton, Florida.
- [94] Reddy, J. N. (2007) Nonlocal theories for bending, buckling and vibration of beams, *International Journal of Engineering Science*, 45, 288-307.
- [95] Reddy, J. N., Pang, S. D. (2008) Nonlocal continuum theories of beams for the analysis of carbon nanotubes, *Journal of Applied Physics*, 103, 023511.
- [96] Roque, C., Ferreira, A., Reddy, J. (2011) Analysis of timoshenko nanobeams with a non-local formulation and meshless method, *International Journal of Engineering Science*, 49, 976-984.
- [97] Sahmani, S., Ansari, R. (2011) Nonlocal beam models for buckling of nanobeams using state-space method regarding different boundary conditions, *Journal of Mechanical Science and Technology*, 25, 2365-2375.
- [98] Setoodeh, A. R., Malekzadeh, P., Vosoughi, A. R. (2011) Nonlinear free vibration of orthotropic graphene sheets using nonlocal Mindlin plate theory, *Proceedings of the Institution of Mechanical Engineers, Part C: J Mechanical Engineering Science*, 226, 1896-1906.
- [99] Şimşek, M., Yurtcu, H. H. (2013) Analytical solutions for bending and buckling of functionally graded nanobeams based on the nonlocal Timoshenko beam theory, *Composite Structures*, 97, 378-386.

- [100] Singh, B., Chakraverty, S. (1992) Transverse vibration of simply supported elliptical and circular plates using boundary characteristic orthogonal polynomials in two variables, *Journal of Sound and Vibration*, 152, 149-155.
- [101] Singh, B., Chakraverty, S. (1994a) Boundary characteristic orthogonal polynomials in numerical approximation, *Communications in Numerical Methods in Engineering*, 10, 1027-1043.
- [102] Singh, B., Chakraverty, S. (1994b) Flexural vibration of skew plates using characteristic orthogonal polynomials in two variables, *Journal of Sound and Vibration*, 173, 157-178.
- [103] Thai, H. T. (2012) A nonlocal beam theory for bending, buckling, and vibration of nanobeams, *International Journal of Engineering Science*, 52, 56-64.
- [104] Thai, H. T., Vo, T. P. (2012) A nonlocal sinusoidal shear deformation beam theory with application to bending, buckling, and vibration of nanobeams, *International Journal of Engineering Science*, 54, 58-66.
- [105] Tounsi, A., Semmah, A., Bousahla, A. A. (2013) Thermal buckling behavior of nanobeams using an efficient higher-order nonlocal beam theory, *Journal of Nanomechanics and Micromechanics*, 3, 37-42.
- [106] Wang, C. M., Kitipornchai, S., Lim, C. W., Eisenberger, M. (2008) Beam Bending Solutions Based on Nonlocal Timoshenko Beam Theory, *Journal of Engineering Mechanics*, 134, 475-481.
- [107] Wang, C. M., Reddy, J. N., Lee, K. H. (2000) *Shear deformable Beams and Plates: Relationship with classical solutions*, Elsevier.
- [108] Wang, C. M., Zhang, Y. Y., He, X. Q. (2007) Vibration of nonlocal Timoshenko beams, *Nanotechnology*, 18, 105401.
- [109] Wang, C. M., Zhang, Y. Y., Ramesh, S. S., Kitipornchai, S. (2006) Buckling analysis of micro-and nano-rods/tubes based on nonlocal Timoshenko beam theory, *Journal of Physics D: Applied Physics*, 39, 3904.
- [110] Wang, C. Y., Murmu, T., Adhikari, S. (2011) Mechanisms of nonlocal effect on the vibration of nanoplates, *Applied Physics Letters*, 98, 153101.
- [111] Wang, K. F., Wang, B. L. (2011) Vibration of nanoscale plates with surface energy via nonlocal elasticity, *Physica E*, 44, 448-453.
- [112] Wang, L., Ni, Q., Li, M., Qian Q. (2008) The thermal effect on vibration and instability of carbon nanotubes conveying fluid, *Physica E*, 40, 3179-3182.

- [113] Wang, Q., Varadan, V. K. (2006) Vibration of carbon nanotubes studied using nonlocal continuum mechanics, *Smart Material Structures*, 15, 659-666.
- [114] Wang, X., Bert, C.W. (1993) A new approach in applying differential quadrature to static and free vibration analyses of beam and plates, *Journal of Sound and Vibration*, 162, 566-572.
- [115] Xu, M. (2006) Free transverse vibrations of nano-to-micron scale, *Proceedings of the Royal Society A*, 462, 2977-2995.
- [116] Yang, J., Ke, L., Kitipornchai, S. (2010) Nonlinear free vibration of single-walled carbon nanotubes using nonlocal Timoshenko beam theory, *Physica E*, 42, 1727-1735.
- [117] Yang, Y., Lim, C. (2011) A variational principle approach for buckling of carbon nanotubes based on nonlocal Timoshenko beam models, *Nano*, 6, 363-377.
- [118] Yan, Y., Wang, W., Zhang, L. (2010) Nonlocal effect on axially compressed buckling of triple-walled carbon nanotubes under temperature field, *Applied Mathematical Modelling*, 34, 3422-3429.
- [119] Zenkour, A. M., Sobhy, M. (2013) Nonlocal elasticity theory for thermal buckling of nanoplates lying on Winkler-Pasternak elastic substrate medium, *Physica E*, 53, 251-259.
- [120] Zhang, Y., Liu, X., Liu, G. (2007) Thermal effect on transverse vibrations of double-walled carbon nanotubes, *Nanotechnology*, 18, 445701.
- [121] Zhang, Y., Liu, G., Xie, X. (2005) Free transverse vibrations of double-walled carbon nanotubes using a theory of nonlocal elasticity, *Physical Review B*, 71, 195404.
- [122] Zidour, M., Benrahou, K. H., Semmah, A., Naceri, M., Belhadj, H. A., Bakhti, K., Tounsi, A. (2012) The thermal effect on vibration of zigzag single walled carbon nanotubes using nonlocal Timoshenko beam theory, *Computational Materials Science*, 51, 252-260.

# List of publications

## (a) Journals (Published/Accepted)

1. Laxmi Behera and S. Chakraverty (2015) Application of Differential Quadrature method in free vibration analysis of nanobeams based on various nonlocal theories, *Computers and Mathematics with Applications*, 69, 1444-1462.
2. S. Chakraverty and Laxmi Behera (2015) Free vibration of non-uniform nanobeams using Rayleigh-Ritz method, *Physica E*, 67, 38-46.
3. S. Chakraverty and Laxmi Behera (2015) Small scale effect on the vibration of non-uniform nanoplates, *Structural Engineering and Mechanics*, 55, 495-510.
4. S. Chakraverty and Laxmi Behera (2015) Vibration and buckling analyses of nanobeams embedded in elastic medium, *Chinese Physics B* (Accepted).
5. Laxmi Behera and S. Chakraverty (2014) Free vibration of nonhomogeneous Timoshenko nanobeams, *Meccanica*, 49, 51-67.
6. S. Chakraverty and Laxmi Behera (2014) Free vibration of rectangular nanoplates using Rayleigh-Ritz method, *Physica E*, 56, 357-363.
7. Laxmi Behera and S. Chakraverty (2014) Effect of scaling effect parameter on the vibration characteristics of nanoplates, *Journal of Vibration and Control*, DOI:10.1177/1077546314547376, 1-11.
8. Laxmi Behera and S. Chakraverty (2014) Free vibration of Euler and Timoshenko nanobeams using boundary characteristic orthogonal polynomials, *Applied Nanoscience*, 4, 347-358.

## (b) Journals (Communicated)

1. S. Chakraverty and Laxmi Behera (2015) Thermal effect on the vibration and buckling analyses of nanobeams using Rayleigh-Ritz method, *Journal of Mathematical Chemistry*.
2. Laxmi Behera and S. Chakraverty (2015) Static analysis of nanobeams using Rayleigh-Ritz method, *Journal of Nanomechanics and Micromechanics*.
3. Laxmi Behera and S. Chakraverty (2015) Buckling analysis of nanobeams with exponentially varying stiffness by differential quadrature method, *Acta Applicandae Mathematicae*.
4. Laxmi Behera and S. Chakraverty (2015) Recent research on nonlocal elasticity theory in the vibration of carbon nanotubes: A review, *The Beilstein Journal of Nanotechnology*.
5. S. Chakraverty and Laxmi Behera (2015) Vibration and buckling analyses of Reddy nanobeams embedded in elastic medium, *Latin American Journal of Solids and Structures*.

**(c) Conferences**

1. Laxmi Behera and S Chakraverty, 'Free Vibration nonlocal Euler-Bernoulli nanobeams', 40th Annual conference of Orissa Mathematical Society and National conference on Fourier Analysis and Differential equations, Sambalpur University, 29-30 December, 2012.
2. Laxmi Behera and S Chakraverty, 'Buckling analysis of Levinson nanobeams having exponentially varying stiffness', 2nd international conference on Recent Trends in Mathematics and Its Applications, Vidyasagar University, Midnapore, West Bengal ,18-19 March , 2015.



# Bio-Data

- Name** : Laxmi Behera
- Date of Birth** : 25-01-1987
- Correspondence** : C/O-Professor Snehashish Chakraverty  
Department of Mathematics  
National Institute of Technology Rourkela  
Rourkela 769008, Odisha, India  
Email:laxmibehera25@gmail.com  
Mob. No. (+91) 9861681471
- Qualification** :
  - Ph.D. Continuing (Mathematics)  
(Joined in July 2011)  
National Institute of Technology Rourkela,  
Rourkela 769008, Odisha, India
  - M.Sc. (Mathematics) (2009-2011)  
National Institute of Technology Rourkela,  
Rourkela 769008, Odisha, India
  - Int. B.Sc. B.Ed (2004-2008)  
Regional Institute of Education, (NCERT),  
Bhubaneswar, Odisha, India
- Publications** :
  - 8 Journal Articles
  - 2 Conference Articles
- Permanent Address** : Laxmi Behera  
D/O Rabindra Kumar Behera  
At-Jharanchhak, Po-Athagarh  
Dist-Cuttack, Pin-754029  
Odisha, India